The Dissertation Committee for Sean David Burns Certifies that this is the approved version of the following dissertation:

Understanding Fundamental Mechanisms of Photoresist Dissolution

Committee:

C. Grant Willson, Supervisor

Isaac C. Sanchez

Roger T. Bonnecaze

David T. Allen

William D. Hinsberg

Understanding Fundamental Mechanisms of Photoresist Dissolution

by

Sean David Burns, B.S. Ch.E.

Dissertation

Presented to the Faculty of the Graduate School of

The University of Texas at Austin

in Partial Fulfillment

of the Requirements

for the Degree of

Doctor of Philosophy

The University of Texas at Austin

May, 2003

Dedication

To My Family

Acknowledgements

The list of people who have helped with this endeavor is quite lengthy. First, I must thank my advisor, Dr. Willson for encouraging me to come to UT, join his research group, and for introducing me to microlithography. I cannot say enough about his guidance and support along the way. His desire to produce great research is second only to his desire to produce great researchers. Kathleen Sparks has also been a tremendous asset in this process - she is truly the glue that holds the Willson group together.

I would like to thank my (many) committee members - Dr. Hinsberg, Dr. Koros, Dr. Bonnecaze, Dr. Allen, and Dr. Sanchez for all of their advice and suggestions.

The graduate students in our research group have lent tremendous assistance. I must thank Gerard Schmid, Brian Trinque, Pavlos Tsiartas, Michael Stewart, Allen Gardiner, Lewis Flanagin and Chris Taylor who have all contributed directly to this work. Others have been very helpful in a variety of ways. Andrew Jamieson, Mark Somervell, Ben Rathsack, Colin Brodsky, Jason Meiring, H.V. Tran, Peter Tattersall, Brian Osborne, Charles Chambers, Heather Johnson, Steve Scheer and Matt Pinnow have all been helpful at a moments notice.

I must thank two undergraduate researchers, Jodie Lutkenhaus and James Willson, for their hard work and numerous contributions to this research.

I have also benefited from many collaborations outside our research group. I must thank Dario Goldbarb, David Medieros, and Marie Angelopoulos, who provided me with an educational internship at IBM Yorktown. During that internship, I had the chance to work with an excellent research group at NIST led by Wen-li Wu and now by Eric Lin, who taught me about neutron analysis techniques. All of the AFM data in this work was obtained from Dr. Korgel's

AFM, and I thank him and his students for their assistance. John Wind and Ryan Burns have been invaluable assets to discuss research ideas.

Outside the realm of research, I've received support from many people. My parents, both sets of grandparents, and my entire family have all been very supportive. Erin and Seth, Brian & Anne, Ward & Amy and everyone in the Willson group have been really great friends. I have to thank all the members of the 2002 IM softball team, for helping me win a T-shirt. Most importantly, I have to thank Lindsay for her constant love and support.

Understanding Fundamental Mechanisms of Photoresist Dissolution

Publication No._____________

Sean David Burns, Ph. D.
The University of Texas at Austin, 2003

Supervisor: C. Grant Willson

Fabrication of microelectronic devices relies upon the photolithographic process for patterning devices. A key step in this process is the selective, aqueous base dissolution of exposed regions of a photoresist polymer film, yet this step is not completely understood at a fundamental level. The most successful model for photoresist dissolution has been the critical ionization dissolution model. The basic premise of this model is that a critical fraction of monomer units of a given polymer chain must be deprotonated (ionized) in order to render that chain soluble.

This work is an extension of the CI model, in which subtle improvements (such as the inclusion of Coulombic forces) have been made to the lattice based

CI dissolution model. The model has been used to investigate formation of surface roughness and surface inhibition during dissolution of photoresists.

Surface inhibition has been investigated experimentally to determine the fundamental mechanisms of this phenomenon. A “Halt Development” technique was used to measure concentration gradients in resist films. It was determined that no significant concentration gradients of residual casting solvent, low molecular weight chains, photoactive compound, or polymer density were present, and thus were not responsible for surface inhibition. Several other theories were tested, including interfacial gel layer formation, surface oxidation, and roughness effects. The best explanation for surface inhibition (for the novolac polymer of interest) was derived from the CI model as a combination of roughness and pKa effects.

Real time spectroscopic interferometry and ellipsometry were used to characterize photoresist dissolution, with a focus on interfacial gel layer formation. Within the resolution limits of the techniques (10-20 nm), interfacial gel layer formation was not observed in a series of phenolic polymers, suggesting that this assumption of the CI model is valid for most phenolic polymers. Formation of surface roughness during dissolution was characterized by AFM and compared to model predictions.

Table of Contents

List of Tables

List of Figures

CHAPTER 1: INTRODUCTION TO SEMICONDUCTOR MICROLITHOGRAPHY

1.1 THE ROLE OF OPTICAL LITHOGRAPHY IN FABRICATING DEVICES

Over the past 30 years, the semiconductor industry has made tremendous improvements in device manufacturing, and device cost reduction. The benefits to industry and society are numerous, including portable computing and communications, information technology, the advent of the world wide web, *etc*. To create even greater processor speed and/or storage capacity, the size of the individual features on devices (and the distance between these features) must be reduced. This reduction in size will also reduce the cost of each device because more devices can be created per wafer, and the cost of batch producing a wafer is (nearly) constant. There is a simultaneous push to reduce the resolution of printed features while increasing the size of the wafers that are used in manufacturing.[1-3] The trend that the number of devices per wafer doubles every 2 years is known as Moore's law, shown in Figure 1.1.[4] A central goal of the semiconductor industry is to continue the pace of Moore's law for as long as possible.

A simple example of device fabrication process flow is shown in Figure 1.2 in which two resistors in series are fabricated on a silicon substrate.[5] This process involves several steps. First, an oxide insulator is deposited followed by resistor material deposition. The resistor material is patterned and then an

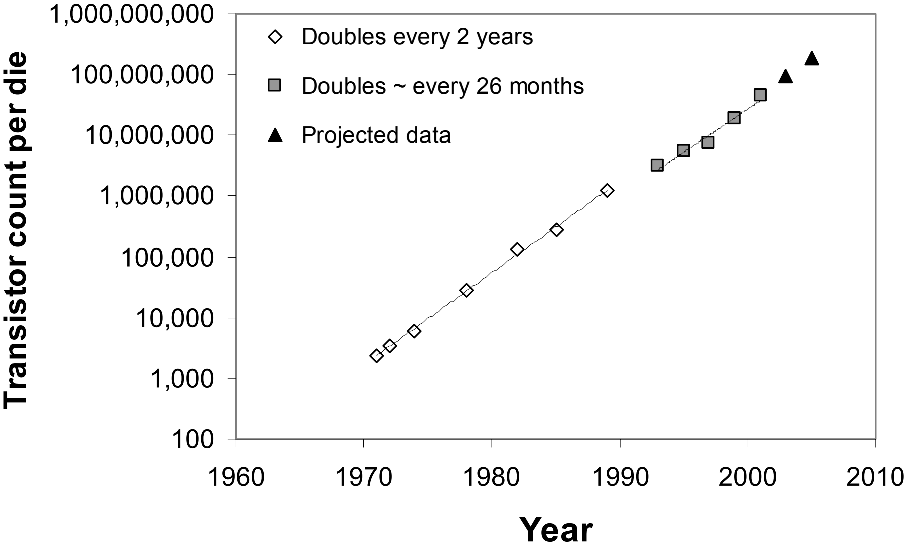

Figure 1.1 Moore's law is the trend that the number of transistors per chip doubles approximately every 2 years.

insulating layer is deposited. Another patterning step is performed on the insulating layer and then a metal layer is deposited. Finally, the metal is patterned to form the wire connecting the two resistors. The advantage of this approach is that many devices can be fabricated simultaneously on one wafer, yet the batch cost does not increase with additional devices. More complicated devices, such as transistors and memory devices, require more sophisticated processes, but the principles of batch production are the same. The only limiting factor to the number of devices that can be created is the patterning technology, which makes the patterning step one of the most important to improve in the entire process.

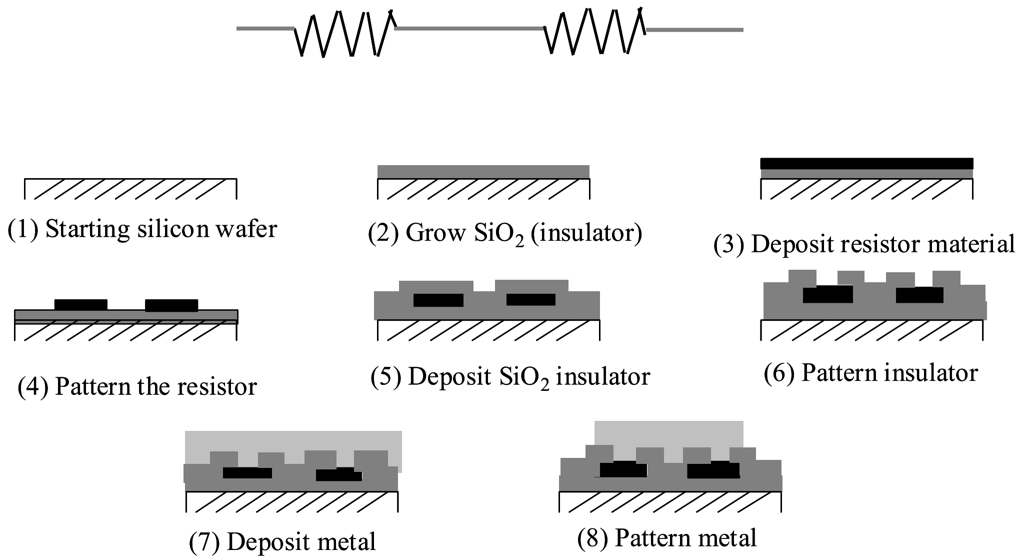
(1) Starting silicon wafer
(2) Grow SiO_2 (insulator)
(3) Deposit resistor material
(4) Pattern the resistor
(5) Deposit SiO_2 insulator
(6) Pattern insulator
(7) Deposit metal
(8) Pattern metal

Figure 1.2 A simple example of device fabrication: two resistors in series

The patterning technology that is responsible for the ultimate feature size on a device is call microlithography. Currently, the technology exists to fabricate semiconductor devices with minimum dimensions less than 130 nm in width. A diagram of the lithographic process is shown in Figure 1.3. The primary material used for this process is a sacrificial polymer solution called a photoresist. The photoresist formulation consists of a polymer resin in an organic casting solvent with a small quantity of a photoactive component, and possibly other performance improving additives. The purpose of the resist is twofold. First, it must be sensitive to exposure by light ("photo"). Second, it must act as a barrier to an etch transfer process, or an ion implantation process ("resist").[1-3]

The first step in the lithographic process is spin coating the photoresist solution onto the patterning layer. Next, a bake step is performed to drive off residual solvent and anneal the film. The wafer is then placed in a “stepper”, the purpose of which is to selectively expose the photoresist to monochromatic light through a photomask (a predetermined pattern of chrome on glass). The exposure step, combined with a post exposure bake (PEB) causes a chemical change in regions of the photoresist film. In the case of a positive tone photoresist, the exposed areas are rendered soluble to a particular solvent, usually aqueous base. (The aqueous base of choice for the semiconductor industry is 0.26 N tetramethyammonium hydroxide, primarily because it does not contain metal ions that may contaminate the underlying device.) Likewise, a negative tone

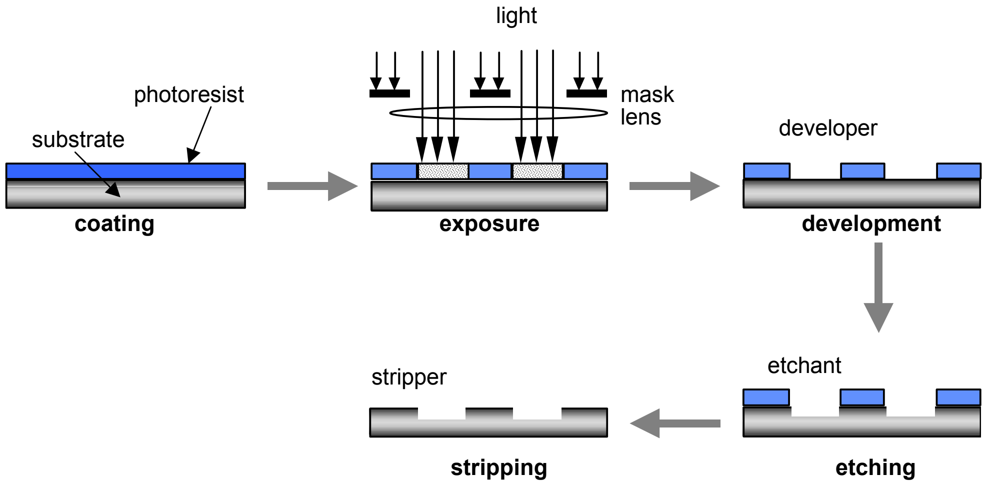

Figure 1.3 The primary steps of the microlithographic process

process renders the exposed areas insoluble to a given solvent. (Positive tone systems are the primary focus of this dissertation.) An etch step is then used to transfer the pattern into the underlying layer, and finally the photoresist is removed (stripped) with an organic solvent. The primary advantages of this process are that many relief patterns can be produced simultaneously on a given layer with high throughput. Although the purpose of the resist was stated to be twofold, the number of material requirements is actually quite numerous. For example, adhesion, thermal stability, and good mechanical properties are required.[1-3]

The resolution of the smallest features is given by the Rayleigh criterion:

$$R = k\frac{\lambda}{NA} \tag{1.1}$$

where R is the minimum feature size, λ is the wavelength of light, NA is the numerical aperture of the optical elements in the stepper, and *k* is a process dependent parameter.[5] In order to reduce the resolution and "print" smaller device features, the wavelength of light must be decreased and/or the numerical aperture must be increased. The wavelength of light used for photoresist exposure has systematically decreased from 436 to 365 to 248 to 193 nm, and now 157 nm[6] is being considered for manufacturing devices with sub 70 nm features. Each downward shift results in several challenges, both in redesigning the exposure source and lens elements as well as the photoresist. The main challenge in producing new photoresists is to develop a new polymer resin that is transparent at a given wavelength, yet possesses all of the other necessary features of a photoresist (i.e. etch resistance, solubility switching upon exposure, sensitivity, adhesion, strippability, *etc*.) The synthesis of new photoresist materials is not a direct topic of this work. However, the dissolution properties of polymer resins that are used for 365 - 157 nm photoresists will be discussed throughout the dissertation.

1.2 SUCCESSFUL PHOTORESIST FORMULATIONS - NON CHEMICALLY AMPLIFIED RESISTS

One of the first successful photoresists was a mixture of cyclized poly(cis-isoprene) rubber and a *bis*(arylazide) photoactive sensitizer (shown in Figure 1.4), and was discovered by Hepher and Wagner at Kodak. This was known as the Kodak Thin Film Resist (KTFR), and is a two component, negative-tone resist.[1,3] In the exposed areas, the photoactive sensitizer decomposes into a highly reactive nitrene compound. This photoproduct is bi-functional, and crosslinks with two polymer chains, greatly increasing the molecular weight of the resin in the exposed areas. The dissolution rate of photoresists is a strong function of molecular weight; therefore, the exposed regions of this resist are rendered insoluble and it is possible to create a negative tone relief image. The dissolution rate dependence on molecular weight (MW) will be revisited throughout this work. The main problem with this resist is that it swells upon dissolution (due also to the high MW). However, the KTFR was the mainstay of the semiconductor industry from 1957 until the early 1970s, at which point the resist could no longer resolve the micron size features in production at that time.

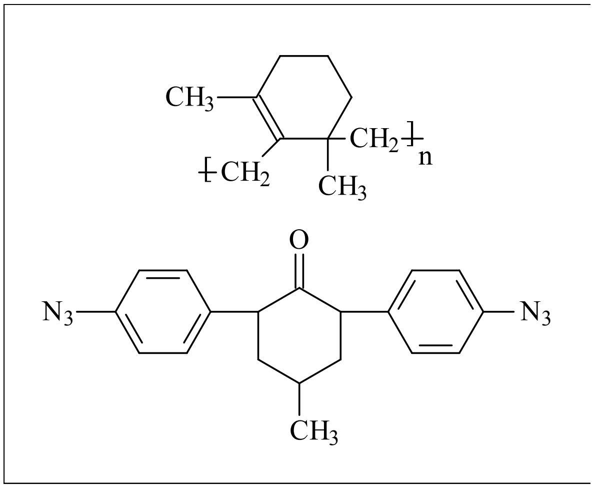

Figure 1.4 The component structures of the Kodak thin film resist (KTFR)

The next successful class of photoresists were borrowed from the printing plate industry and are known as DNQ/novolac resists.[1-3,7] These 436 and 365 nm photoresists, which were introduced in the early 1970's, are still used in manufacturing for non-critical device layers. This class of photoresist is a two component, positive-tone photoresist. The basic structures of these two components are shown in Figure 1.5. The main advantages of these resists are high contrast, good etch resistance, and limited swelling in aqueous base developer, which allows fabrication of high-aspect-ratio, high-resolution images.[7]

Novolac is a phenolic polymer with the interesting structural property that the aromatic ring is included in the backbone of the polymer. The synthesis of a novolac resin (for lithographic applications) typically consists of an acid-catalyzed condensation polymerization of formaldehyde with a mixture of *m*-cresol and *p*-cresol monomers. The *p*-cresol monomer forms linkages at the ortho (2 and 6) positions; therefore a novolac polymer made only of *p*-cresol has only ortho-ortho linkages. Conversely, *m*-cresol forms linkages at both the para and ortho positions, so a novolac polymer made from *m*-cresol can have any possible combination of ortho and para linkages. Since a mixture of these two monomers is used, novolacs typically have both linear and branched linkages, where the relative amount of each linkage is determined by stoichiometry, the catalyst and reaction conditions. For nearly all photoresist applications the novolac molecular weight is kept very low, usually between 8-20 repeat units. Perhaps the most important property is that novolac resins are transparent to 365 nm light (and

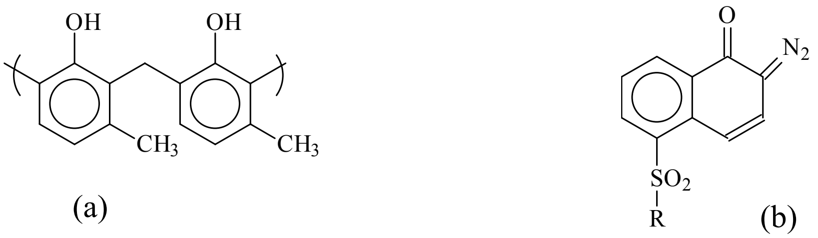

Figure 1.5 Structures of (a) novolac resin and (b) diazonapthoquinone (DNQ)

above), which is a requirement in order to produce resist features from a single layer optical process.[7]

The photoactive component (PAC) of these types of resists is diazonapthoquinone (DNQ). Many different structures can be used for the PAC in novolac/DNQ resists, but they are all derivatives of the basic DNQ molecule. Many PACs are multifunctional and have more than one photoactive component attached to the same molecule. Upon exposure to 365 nm light (in the presence of water) the DNQ forms an indene carboxylic acid photoproduct and nitrogen evolves from the film as a side product, shown in Figure 6. Some side reactions may occur. The photoproduct is much more transparent than the DNQ, a process

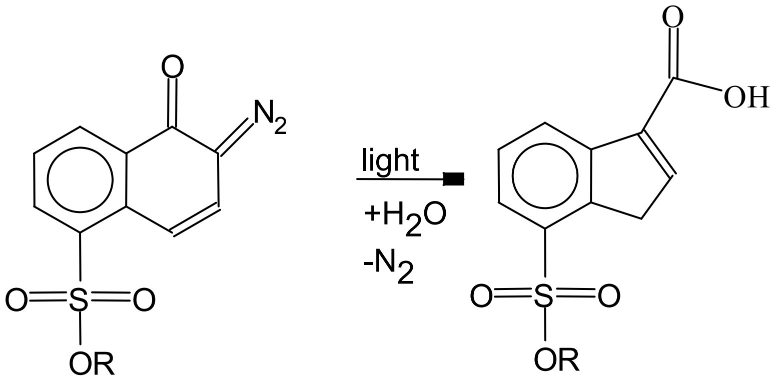

Figure 1.6 Conversion of 2-diazo-1(2H)-naphthalenone-5-sulfonate (left) to an indene carboxylic acid (right).

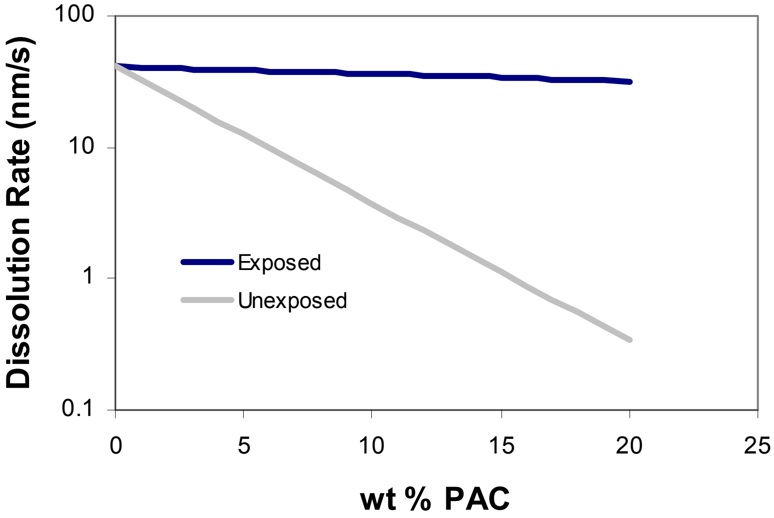

Figure 1.7 Typical Meyerhofer plot showing the dissolution rate versus wt. % added PAC for exposed and unexposed novolac films.

known as bleaching that is very beneficial in obtaining high-resolution images.[3,7]

Both the DNQ and the photoproduct have significant interactions with the matrix novolac polymer, making the exposure induced reaction (shown in Figure 1.6) a solubility switching reaction. The dissolution rate of the resin is also a strong function of the concentration of DNQ and photoproduct. Figure 1.7 shows the log of the dissolution rate of a typical novolac resin plotted against the wt% of added PAC for both unexposed and flood exposed films. This type of plot is known as a Meyerhofer plot. There is an exponential relationship in both cases. In 0.26 N TMAH, typical novolac resins dissolve quite rapidly. However, the dissolution rate can be inhibited by 2-3 orders of magnitude by addition of 5-15 wt % DNQ. Upon exposure, the dissolution rate increases slightly above that of the pure novolac resin. This fortuitous interaction allows these photoresists to be successful as 365 nm imaging materials.[3,7]

Many novolac resins exhibit surface rate inhibition upon dissolution in aqueous base.[2,7,8] Figure 1.8 shows a typical plot of the remaining thickness plotted against time for a novolac resin dissolving in 0.26 N TMAH. The initial dissolution rate is considerably slower than that of the bulk film. This phenomenon is known as surface rate inhibition or surface induction. Although surface inhibition is observed in a variety of photoresists, novolac resins are one of the only polymer *resins* in which surface inhibition is routinely observed. The phenomenon becomes quite useful for imaging, as dark loss (dissolution in unexposed areas of the resist) is minimized, and the sidewall angles of the features are improved when surface inhibition occurs. However, the fundamental mechanisms that cause surface inhibition are not agreed upon,[9] and investigation of this mechanism is a major topic of this dissertation (see Chapters 5 & 6).

DNQ/Novolac resists have been used successfully in commercial processes at 436 nm and 365 nm exposure. Features as small as 0.25 μm can be produced with these photoresists. However, at lower wavelengths in which powerful exposure sources are available (i.e. 248 nm), novolac resins absorb too much light. It is imperative that the photoresist resin is transparent so that light

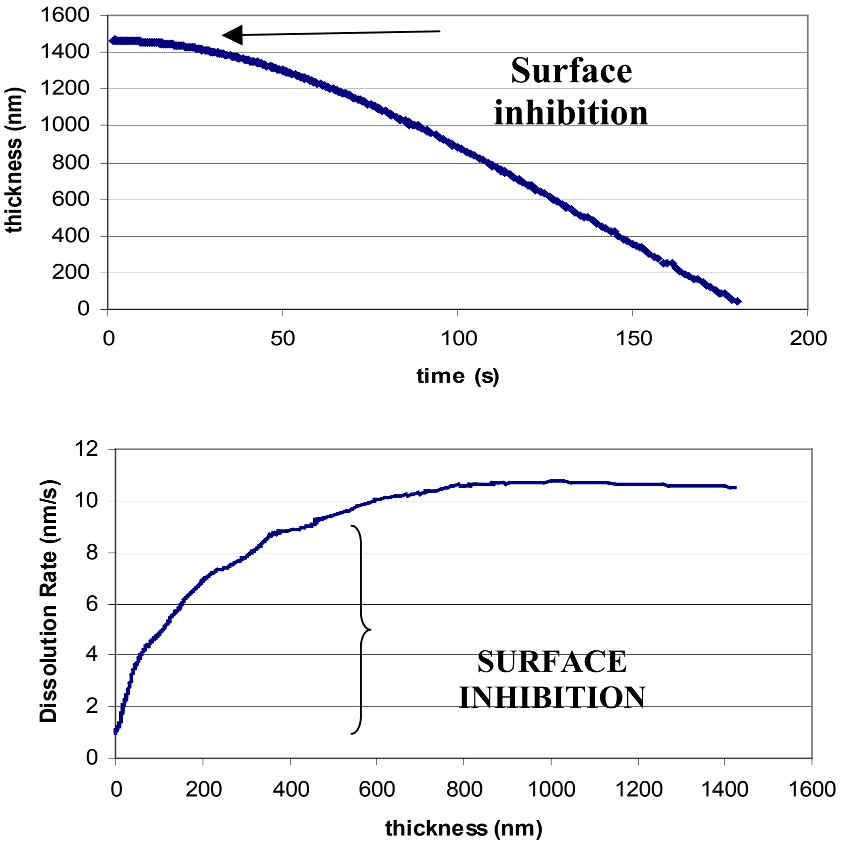

Figure 1.8 Dissolution of a typical novolac/DNQ resist in TMAH. (a) thickness versus time, and (b) dissolution rate versus distance into the film

will penetrate to the bottom of the film. Thinner films could be used, but in that case the etch resistance of the film becomes a significant issue. The trade off between transparency and etch resistance presents a constant challenge in the synthesis of new photoresist resins.[1]

It became clear to researchers that a different resin would have to be used in order to create smaller features with 248 nm light. A similar phenolic resin, polyhydroxystyrene (PHOST), shown in Figure 1.9, is transparent at 248 nm. However, the fortuitous DNQ/novolac interactions are not observed when typical PACs are added to PHOST formulations, despite the fact that the resins are so similar.[1] To date, materials have not been found that inhibit the dissolution of pure PHOST in the same manner as novolac. To compound these problems, another issue with 248 nm exposures is that, although an excimer laser is the light source and the power output is very large, the light produced is not of adequate quality to be used in the lithographic process. The light has poor spatial and temporal coherence and must be passed through numerous optical elements in order to generate illumination that is useable for lithographic imaging. This

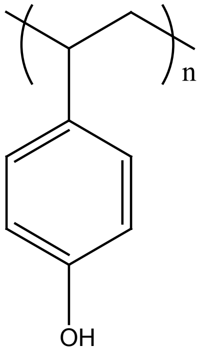

Figure 1.9 Structure of poly(p-hydroxystyrene), PHOST

results in large intensity loss such that the final power output of an excimer laser exposure tool is only marginally higher than that of a mercury arc lamp.[10] Since the exposure tool (the "stepper") is the bottleneck of any lithography process due to its large capital cost, 248 nm photoresists needed to be at least as sensitive as traditional novolac/DNQ resist systems so that the exposure time (and throughput) could remain constant. All of these problems were solved by the advent of a class of photoresists that functioned by a completely different mechanism than traditional DNQ/novolac resists.[11-13]

1.3 CHEMICALLY AMPLIFIED PHOTORESISTS

The novolac/DNQ resists discussed above, as well as other photoresists used for 365 nm or longer wavelength imaging, can all be classified as non-chemically amplified (NCA) resists. Chemically amplified (CA) photoresists can be defined as photoresists in which the photoactive component, upon exposure, becomes a catalyst for further solubility switching reactions. The photoreaction itself does not directly provide the solubility switch as in the case of the novolac/DNQ system. Rather, the photoactive component reacts with light to form a catalyst (usually an acid catalyst). During a subsequent bake step called a post exposure bake (PEB), the catalyst diffuses and reacts throughout the polymer matrix causing many reactive sites on the polymer to switch from insoluble to soluble monomer units. A conceptual diagram of this scheme is shown in Figure

1.10. While this design is slightly more complicated and involves an extra reaction step, it is actually advantageous because it minimizes the exposure dose necessary to obtain images, which increases throughput in the bottleneck step of the process. (Additionally, some low activation energy CA resists do not require a PEB, because the subsequent reaction occurs at room temperature.) The successful demonstration of CA resists[11-13] provided viable solutions to the problems stated above, and have been used as the photoresist platform for 248, 193, and now 157 nm lithography.[14]

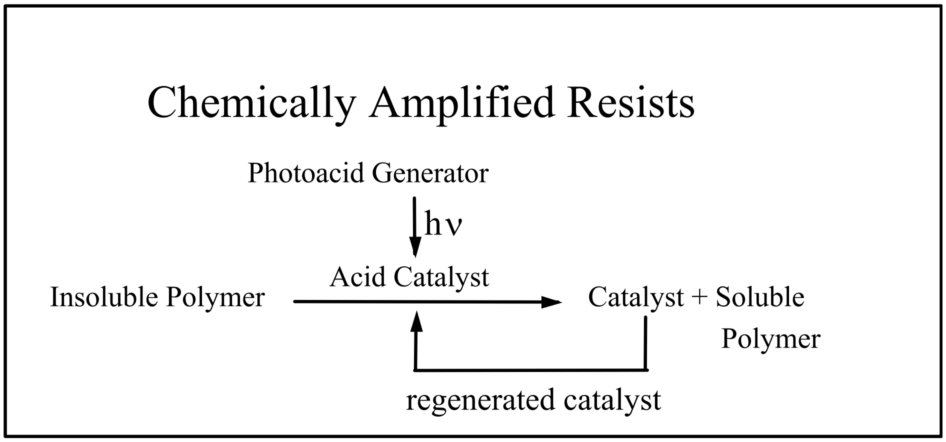

Figure 1.10 Conceptual diagram of chemically amplified photoresists

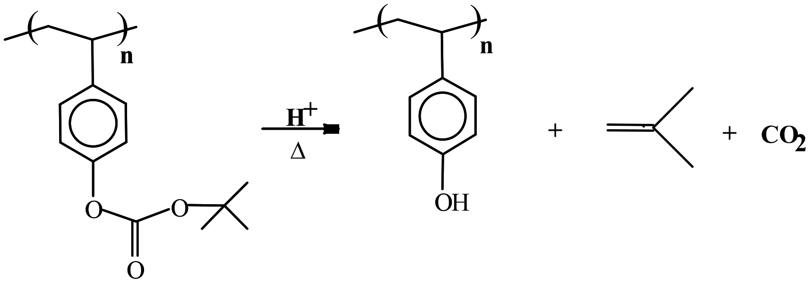

Figure 1.11 An example of a CA resist: tBOC deprotects to form PHOST in the presence of acid and moderate heat

An example of a chemically amplified photoresist is shown in Figure 1.11. The base resin is poly(*p*-*t*-butyloxycarbonyloxystryrene) (also called *t*-BOC-styrene, or simply tBOC) which consists of a t-butyl blocking group placed on a PHOST resin. This resin is nearly transparent at 248 nm. In the presence of acid and moderate heat (~ 90°C), this polymer undergoes an acid catalyzed deprotection reaction in which carbon dioxide and isobutylene are evolved from the photoresist as side products. The initial material (tBOC) is insoluble to base developer, whereas the final material (PHOST) is very soluble in base developer due to its acidic nature. This solubility switch in the exposed areas provides the imaging mechanism. In practice it is not necessary to completely block the PHOST polymer. Blocking fractions as low as 20 % are capable of rendering the unexposed photoresist essentially insoluble in aqueous base.[1,13]

A typical photoacid generator (PAG) is shown in Figure 1.12. This molecule, bis,t-butyl phenol iodonium perfluorobutane sulfonate salt, reacts with light to produce perfluorobutane sulfonate acid and by-products. A typical PAG loading for a photoresist is 2.5 wt %, which corresponds to approximately one acid molecule for every 160 blocked sites (for a completely blocked polymer). In order for the deprotection reaction to continue to completion, the catalytic chain length of the acid must be at least 160. This number may be higher due to the efficiency of the exposure reaction and the fact that low exposure areas must also be rendered insoluble.[1] McKean *et al* estimate the catalytic chain length to be ~ 1000. The high catalytic chain length provides sensitivity; low exposure doses can be used, resulting in large throughput during the bottleneck exposure step of the process. However, the large catalytic chain length also suggests that acid may migrate into areas that are unexposed, a detrimental effect that is known as acid

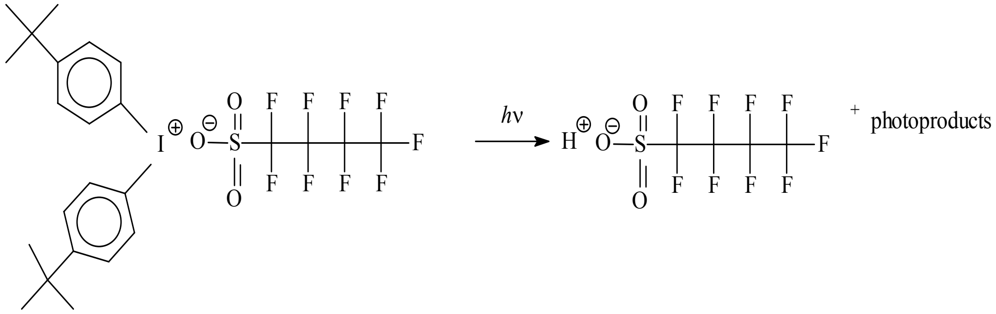

Figure 1.12 Photolysis reaction of a typical photoacidgenerator (PAG)

diffusion, image blur, linewidth spread, or CD (characteristic dimension) bias. A diagram of this effect is shown in Figure 1.13.

1.4 ACID CATALYZED DEPROTECTION AND ACID DIFFUSION

Before CA resists were introduced, it was thought that acid diffusion may cause complete image blur, rendering the entire film insoluble. However, it was determined that resist images could be resolved, albeit with a small degree of image blur.[13] This blurring effect becomes increasingly significant as feature

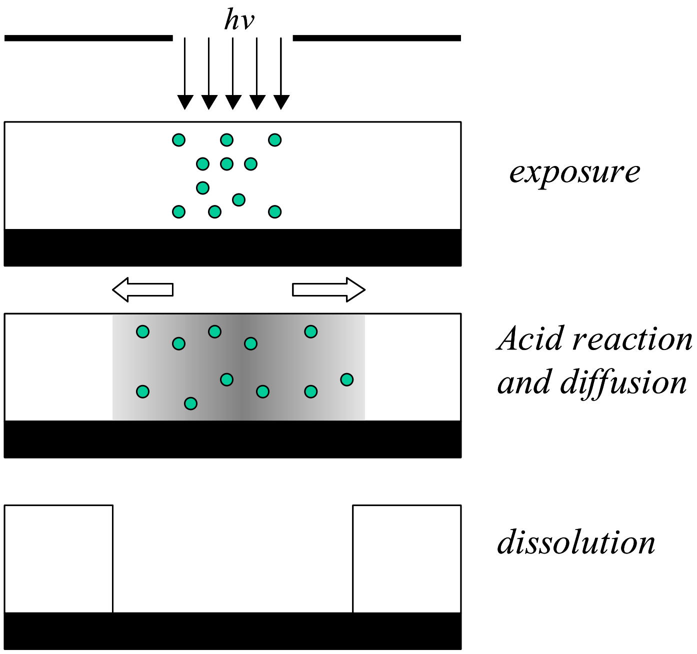

Figure 1.13 Diagram of linewidth spread due to acid reaction and transport

sizes are reduced. An experiment by Willson *et al.* with a thin (~ 2 nm) electron beam exposure resulted in a ~ 40 nm feature with tBOC.[15] However, it has been shown that (for a PEB of given temperature and time) diffusion is reduced in cases where the blocking fraction has been reduced.[16] Results of this nature indicate that acid diffusion may not be an immediately prohibitive issue in the continued use of CA photoresists, but it provides serious engineering challenges. Another related problem, caused in part by acid catalyzed deprotection and diffusion, is line edge roughness (LER), which is discussed in more detail in Chapter 8.

In summary, acid transport is an important topic for fundamental research because it poses complicated problems in semiconductor fabrication. For example, photomasks are typically reverse engineered to account for acid diffusion, CD bias, and any other effect that may change the nominal characteristic feature dimension. This process is known as optical proximity correction (OPC). If a 'perfect' photoresist were created, the OPC process would be simpler to implement and easier to model. Having a fundamental understanding of acid diffusion is potentially beneficial in the synthesis of improved photoresists, which would improve development time for a given process.

However, acid reaction/diffusion through a polymer matrix is a complicated process. The initial and final materials are quite different; the reaction itself yields small penetrant molecules that may transiently effect diffusion, and as a consequence of this outgassing the polymer film typically undergoes relaxation and densification. The reaction is also quite exothermic, which may affect the diffusivity of the acid. It is generally agreed upon that acid diffusion is initially fast, and then proceeds into a region of slow diffusion.[17,18] It is also agreed upon that, in the tBOC photoresist system, relaxation of the polymer occurs nearly concurrently with the deprotection reaction, and substantial 'extra' free volume is not observed during the PEB.[19,20] Our research group, in collaboration with IBM T.J. Watson research center and NIST (Gaithersburg, MD), has recently demonstrated the use of neutron reflectivity in exploring the fundamental mechanism of acid diffusion.[21] The interested reader is referred to the literature for an in depth discussion of acid diffusion in photoresist materials.[17-23]

1.5 193 NM PHOTORESIST PLATFORMS

The photoresists that function effectively at 248 nm are no longer useful at 193 nm.[14] Although the basic chemical amplification scheme was employed, the transition to 193 nm lithography (which has been recently introduced to manufacturing) required a complete redesign of the photoresist polymer structure. The main problem was that 248 nm photoresists are not transparent at 193 nm. Acrylic-based polymers solved the transparency requirement, but had poor plasma etch resistance.[24,25] The aromatic groups which provided this etch resistance in 248 nm photoresists were no longer transparent at the shorter, 193 nm wavelength, and it seemed very difficult to combine the two basic material requirements. The work of Goken *et al.* showed that aromaticity was not strictly needed for etch resistance.[26] Rather, it was the carbon-to-hydrogen ratio of the polymer matrix that was related to the etch rate. Fortunately, alicyclic units such as norbornane and adamantane achieve a high C:H ratio, yet are also transparent at 193 nm.[27] Many researchers developed schemes by which an alicyclic pendant group was added as one of the repeat units to an acrylic based polymer, thereby increasing the etch resistance of the photoresist. An example of this approach is IBM's V2 terpolymer system, shown in Figure 1.14(a).[28] However, these resists require increased etch resistance to be commercially attractive.

Our research group and others[29] studied methods for synthesizing polymers directly from cycloolefins with the goal that every repeat unit would contain an alicyclic, etch resistant structure. The length of this study was broad,[30-33] but an example of one of the most successful polymers is shown in Figure 1.14(b). The polymer is based on the copolymerization of tert-Butyl tetracyclo[4.4.0.1.1]dodec-3-ene-5-carboxylate with maleic anhydride, or DBNC-alt-MA. The two norbornane rings provide a large C:H ratio, and therefore adequate etch resistance. Upon exposure to acid, the t-butyl ester protecting group cleaves to produce a base soluble carboxylic acid. (Note that this acid is quite different from the phenolic acids of 365 and 248 nm lithography). This polymer, when formulated with a PAG, a dissolution inhibitor, and a small amount of base additive, has resolved features as small as 110 nm. Features as small as 80 nm have been achieved if an optical enhancement technique known as a phase shifting mask is employed.[33] This basic resist design has been refined[34,35] and it is likely that commercial 193 nm photoresists will be based upon this platform.[36]

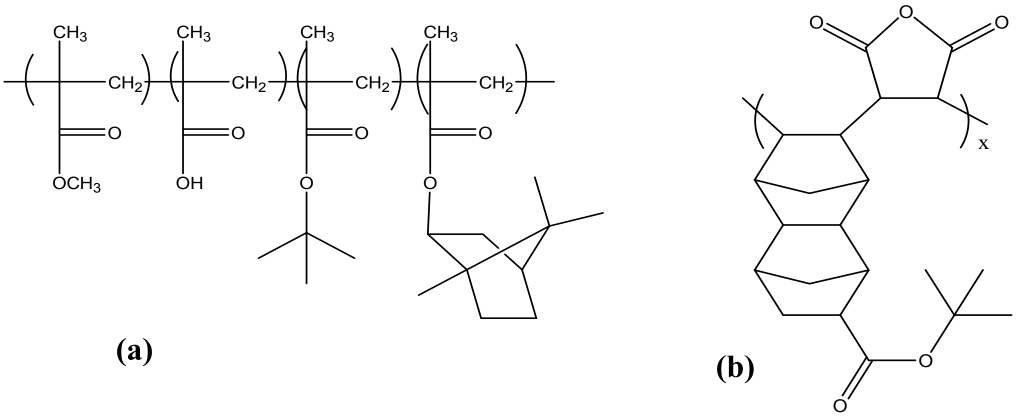

Figure 1.14 (a) IBM's V2 193 nm photoresist resin, (b) Structure of alternating copolymer DBNC-alt-MA, 193 nm photoresist

1.6 157 NM PHOTORESIST PLATFORMS

The same basic material issues arise with the transition to 157 nm lithography. That is, the photoresists that function well at 193 nm strongly absorb 157 nm photons. Unfortunately a large range of simple compounds such as oxygen, water, and poly(ethylene) all strongly absorb 157 nm light. This exposure wavelength requires new materials for the photomask substrate, the optical lenses, the pellicle[37] (a thin film screen that protects the mask from particle contamination), and of course the photoresist.[14] The first challenge was simply to identify compounds that would be transparent at 157 nm. Early work at MIT Lincoln Labs determined that the transparency of polyethylene could be improved by adding electron withdrawing groups such as fluorine and oxygen.[38,39] It was also determined that silicon based polymers are transparent at 157 nm, although in practice photoresists with silicon containing backbones have been found to have prohibitively low glass transition temperatures and therefore poor mechanical properties.[40]

The general approach by our research group has been to selectively fluorinate alicyclic polymers, in hopes that the 193 nm resist platform could be rendered transparent by the intelligent, selective addition of fluorine. The work by our group[6,41-43] and others[44-46] in this area has been extensive. A successful polymer structure is shown in Figure 1.15. This polymer, a copolymer of poly(norbornanehexafluoralcohol) and poly(norbornane t-butylester) has been able to successfully image features as small as 60 nm with 157 nm exposures.

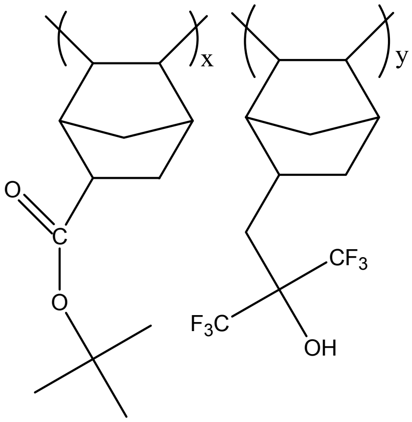

Figure 1.15 Structure of p(NHFA-co-NBTBE), a 157 nm photoresist resin synthesized at UT Austin.

1.7 NEXT GENERATION LITHOGRAPHY – WHAT'S AFTER 157 NM?

Despite the challenges of 157 nm lithography, exposure at this wavelength provides only a modest resolution improvement to 193 nm lithography. The 2001 International Semiconductor Roadmap (ISRM) states that as early as the year 2007, a next generation lithography (NGL) technology will be used to produce the 65 nm technology node.[47] At a minimum, an NGL technology will be needed by 2010 to facilitate the 45 nm technology node. (NGL typically refers to a patterning technology that is non-optical in nature. The technology node refers to the size of the DRAM half pitch, where pitch is defined as the additive width of a line and space. In lithographic terms, the 65 nm node refers to the production of dense 65 nm lines and spaces.)

Perhaps the most popular candidate for NGL is extreme ultraviolet (EUV) lithography, which is somewhat an extension of optical lithography in that photons of ~ 13 nm are used and the Rayleigh criterion applies.[47] However, it will be nearly impossible to synthesize photoresist resins that are transparent at 13 nm. Most likely, a thin film or bilayer imaging scheme will be required such as a top surface imaging process.[1,48,49] The transparency issue is even more limiting for the optical train, which will require reflective (instead of refractive) optical elements.[50,51] Despite the long development history of EUV and other NGL technologies, these technologies suffer from problems with the source, the mask, and throughput considerations. While there is still time to find solutions to these problems, it is possible that a disruptive technology, such as imprint lithography[52,53] will provide the most cost effective solution. Also, interest in immersion lithography has gained momentum.[54] This technique involves immersing the photoresist in a high index of refraction medium (i.e. water) during exposure, which increases the effective numerical aperture of the lens. In the meantime, a significant portion of our research group remains focused on improving our understanding of traditional optical lithographic processes.

1.8 DISSOLUTION OF PHOTORESIST RESINS

The discussion now turns back to the primary dissertation topic: photoresist dissolution. Selective dissolution of exposed regions of the photoresist is an important part of the lithographic process. However, the fundamental mechanism of dissolution is complicated, and not entirely understood. In general, photoresist dissolution differs from typical polymer dissolution in an organic solvent because the species that is soluble in aqueous base, a polyion, is very different from the initial polymer.[7] The process has been compared to the etching of copper by nitric acid.[55] The original polymer (for example, PHOST) undergoes an acid-base neutralization reaction with the aqueous base developer, and it is the reaction product that is soluble in developer. A simplified view of dissolution is shown in Figure 1.16 and consists of three steps: (1) transport of the base ion to the polymer film, (2) the deprotonation reaction occurs, and (3) transport of the polyion to the bulk of the developer solution. The main questions involved with this process are: (1) "Which of the 3 above steps is rate limiting?", and (2) "Does an interfacial 'gel' layer form during the dissolution process?" The goal of this dissertation is to provide insight into these questions. Note that the acidic phenolic groups of 365 and 248 nm resists are different from the carboxylic acids employed for 193 nm photoresists. These, in turn, are very different from the hexafluoroalcohol acidic groups used for 157 nm lithography.[14] Therefore, the significant changes in the dissolution behavior of these polymers is not surprising

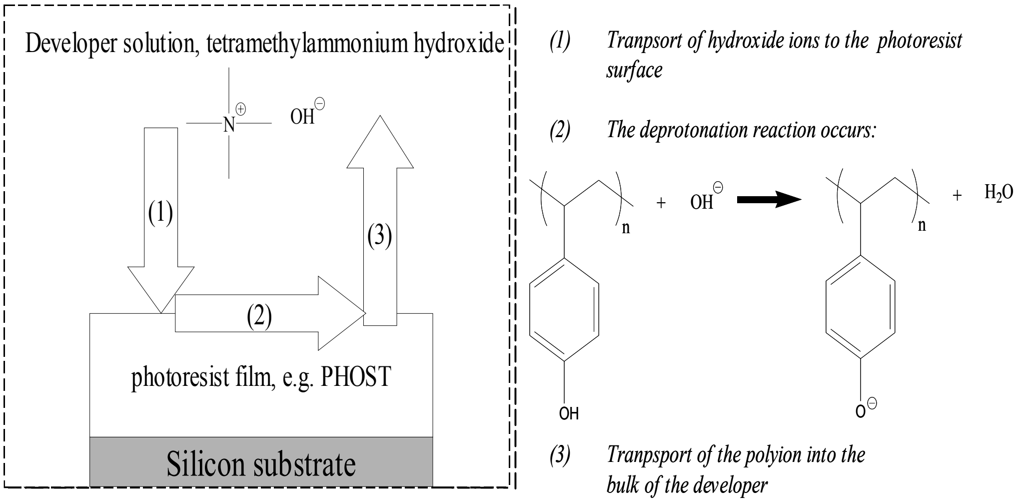

Figure 1.16 Description of phenolic polymer dissolution in aqueous base

Chapter 2 provides an in-depth review of different models for acidic polymer dissolution in aqueous base, including the critical ionization dissolution model proposed by the Willson research group. Chapter 3 provides a description of dissolution rate measurement techniques used in this work, primarily interferometry and ellipsometry. Chapter 4 presents some advancements to the CI model in which coulombic forces present during polymer dissolution are added to the model. The focus of Chapters 5 & 6 is the mechanism of surface rate inhibition in novolac resins. In Chapter 7, experimental investigation into the formation of interfacial gel layers during photoresist dissolution is discussed. Chapter 8 discusses the formation of surface roughness during dissolution, with the goal of providing insight into the formation of line edge roughness.

1.9 SIMULATING THE LITHOGRAPHIC PROCESS

The lithographic process involves many steps, each having many parameters. Thus, it is very difficult to optimize. The primary method for optimizing such a complicated process involves a rather large series of experiments, which are both time-consuming and costly. It is not possible to optimize every processing variable by response surface analysis, especially the resist formulation. In the last two decades, there has been a push to optimize lithographic processes through the use of simulation.[8] There are several notable advantages of having accurate simulation tools. They are inexpensive, (usually) less time consuming, and many "experiments" can be performed that are not possible in a clean-room facility. There exist several software packages that allow the exposure step to be rigorously modeled, but the kinetics and transport processes during the bake steps and dissolution step are not fully understood.[8] In the best case, the models currently used for these steps are empirical. In the worst cases they are inaccurate. Furthermore, in many software packages the photoresist is considered to be a “black box” with certain optical properties and diffusion/dissolution parameters that are usually acquired experimentally. A complete model does not exist in which it is possible to change the photoresist formulation (i.e. the polymer molecular weight, or the concentration of PAG) and determine the outcome on the lithographic performance. The 2001 ISRM states that “there is a growing need for resist studies based on computational molecular modeling.”[47]

A major goal of our research group is to improve the understanding of the bake steps and the dissolution step, and to use that understanding to investigate molecular level simulation tools. An intended consequence of this understanding is that the rational design of resin polymers and photoresist formulations can also be improved. Our research group has been investigating mesoscopic simulation tools for lithography in which film formation, PAB, exposure, PEB, and dissolution steps are carried out in sequence. (For an in depth discussion of this topic, the reader is referred to the works of Flanagin[55-58] and Schmid.[59-61]) The approach has been an on-lattice simulation, in which each lattice site is considered to be a monomer unit of a polymer chain. Nominally, the side of a lattice cube is considered to be ~ 0.7 nm. The polymer chain length and polydispersity can be varied and the polymer chains are equilibrated by a reptation method. Lattice sites can also be filled with other species, most notably blocking groups, free volume, residual solvent, and photoactive species. Other resist additives, such as dissolution inhibitors and base quenchers, can also be employed. In this manner it is possible to simulate variations in the photoresist formulation and the effect on the lithographic performance.

As previously stated, an understanding of the fundamental mechanism of photoresist dissolution is the main topic of this work. However, the underlying goal is to include this fundamental model in the mesoscale simulation tool that is being developed on a broad level by our research group. To this end, many experiments have been performed in order to compare the results to model predictions, or to verify assumptions used in the model. The satisfying aspects of this work are the many cases in which the model compares well with experimental results. The particularly rewarding respects are those in which the model provides insight into the experimentally observed dissolution behavior. The mesoscopic lattice model, as it applies to dissolution, will be primarily discussed in chapters 4 and 8.

1.10 REFERENCES

(1) Thompson, L. F.; Willson, C. G.; Bowden, M. J. *Introduction to Microlithography*; 2nd ed.; American Chemical Society: Washington D.C., 1994.

(2) Moreau, W. M. *Semiconductor Lithography: Principles, Practices, and Materials*; Plenum Publishing: New York, 1988.

(3) Reiser, A. *Photoreactive Polymers*; John Wiley & Sons: New York, 1989.

(4) <*http://www.intel.com/pressroom/kits/quickrefyr.htm>; 2003-05- International Technology Roadmap for Semiconductors, available at <http://public.itrs.net/Files/2000UpdateFinal/ORTC2000final.pdf>*. **2002**.

(5) Campbell, S. A. *The Science and Engineering of Microelectronic Fabrication*; Oxford University Press: New York, 2001.

(6) Patterson, K.; Somervell, M.; Willson, C. G. *Solid State Technol.* **2000**, *43*, 41-+.

(7) Dammel, R. *Diazonapthoquinone-based Resists*; SPIE Optical Engineering Press: Bellingham, Washington, 1993.

(8) Mack, C. A. *Inside Prolith: A Comprehensive Guide to Optical Lithography Simulation*; FINLE Technologies: Austin, TX, 1997.

(9) Burns, S. D.; Gardiner, A.; Krukonis, V.; Wetmore, P.; Schmid, G. M.; Lutkenhaus, J.; Flanagin, L. W.; Willson, C. G. *Proc. SPIE* **2001**, *4345*, 37-49.

(10) Pol, V.; Bennewitz, J. H.; Escher, G. C.; Feldman, M.; Firtion, V.; Jewell, T. E.; Wilcomb, B. E.; Clemens, J. T. *Proc. SPIE* **1986**, *633*, 6.

(11) Ito, H.; Willson, C. G. *Polym. Eng. Sci.* **1983**, *23*, 1012-1018.

(12) Frechet, J. M. J.; Eichler, E.; Ito, H.; Willson, C. G. *Polymer* **1983**, *24*, 995-1000.

(13) Willson, C. G. *Acs Symposium Series* **1983**, *219*, 87-159.

(14) Stewart, M. D.; Patterson, K.; Somervell, M.; Willson, C. G. *J. Physical Organic Chemistry* **2000**, *13*, 767-764.

(15) Umbach, C. P.; Broers, A. N.; Willson, C. G.; Koch, R.; Laibowitz, R. B. *J. Vac. Sci. Technol. B* **1988**, *6*, 319-322.

(16) Stewart, M. D.; Schmid, G. M.; Postnikov, S.; Willson, C. G. *Proc. SPIE* **2001**, *4345*, 10-18.

(17) Houle, F. A.; Hinsberg, W. D.; Morrison, M.; Sanchez, M. I.; Wallraff, G. M.; Larson, C. E.; Hoffnagle, J. *J. Vac. Sci. & Tech. B* **2000**, *18*, 1874.

(18) Postnikov, S.; Stewart, M. D.; Tran, H. V.; Nierode, M.; Medeiros, D.; Cao, T.; Byers, J.; Webber, S.; Willson, C. G. *J. Vac. Sci. & Tech. B* **1999**, *17*, 2965-2969.

(19) Burns, S. D.; Stewart, M. D.; Hilfiker, J. N.; Synowicki, R. A.; Schmid, G. M.; Brodsky, C.; Willson, C. G. *Forefront of Lithographic Materials Research, Proc. of the 12th International Conference on Photopolymers* **2000**, 232-334.

(20) Hinsberg, W. D.; Houle, F. A.; Poliskie, G. M.; Pearson, D.; Sanchez, M. I.; Ito, H. *Journal of Physical Chemistry A* **2002**, *106*, 9776-9787.

(21) Lin, E. K.; Soles, C. L.; Goldfarb, D. L.; Trinque, B.; Burns, S. D.; Jones, R. L.; Lenhart, J. L.; Angelopoulos, M.; Willson, C. G.; Satija, S. K.; Wu, W.-l. *Science* **2002**, *297*, 372.

(22) Stewart, M. D.; Tran, H. V.; Schmid, G. M.; Stachowiak, T.; Becker, D. J.; Willson, C. G. *J. Vac. Sci. & Tech. B* **2002**, *20*, 2946.

(23) Hinsberg, W. D.; Houle, F. A.; Sanchez, M. I.; Wallraff, G. M. *Ibm Journal of Research and Development* **2001**, *45*, 667-682.

(24) Kunz, R. R.; Allen, R. D.; Hinsberg, W. D.; Wallraff, G. M. *Proc. SPIE* **1993**, *1672*, 66.

(25) Allen, R. D.; Wallraff, G. M.; Hinsberg, W. D.; Conley, W. E.; Kunz, R. R. *J. Photopolymer Sci. Tech.* **1993**, *6*, 575.

(26) Goken, H.; Esho, S.; Ohnishi, Y. *J. Electrochem. Soc.* **1983**, *130*, 143.

(27) Kaimoto, Y.; Nozaki, K.; Takechi, S.; Abe, N. *Proc. SPIE* **1992**, *1672*.

(28) Allen, R. D.; Wallraff, G. M.; Hofer, D. C.; Kunz, R. R. *IBM J. Res. Dev.* **1997**, *41*, 95.

(29) Houlihan, F. M. J.; TI, W.; Nalamasu, O.; Reichmanis, E. *Macromolecules* **1997**, *30*, 6517.

(30) Okoroanyanwu, U.; Shimokawa, T.; Medeiros, D.; Willson, C. G.; Frechet, J. M. J.; J.Q., N.; Byers, J.; Allen, R. D. *Proc. SPIE* **1997**, *3049*, 92.

(31) Okoroanyanwu, U.; Shimokawa, T.; Byers, J.; Willson, C. G. *Chem. Mat.* **1998**, *10*, 3319-3327.

(32) Okoroanyanwu, U.; Byers, J.; Shimokawa, T.; Willson, C. G. *Chem. Mat.* **1998**, *10*, 3328-3333.

(33) Patterson, K.; Okoroanyanwu, U.; Shimokawa, T.; Cho, S.; Byers, J.; Willson, C. G. *Proc. SPIE* **1998**, *3333*, 425-437.

(34) Byers, J.; Patterson, K.; Cho, S.; McMallum, M.; Willson, C. G. *J. Photopolymer Sci. Tech.* **1998**, *11*, 465.

(35) Yamachika, M.; Patterson, K.; Cho, S.; Rager, T.; Yamada, S.; Byers, J.; Paniez, P. J.; Mortini, B.; Gally, S.; Sassoulas, P.; Willson, C. G. *J. Photopolymer Sci. Tech.* **1999**, *12*, 553.

(36) Amblard, G.; Byers, J.; Domke, W.-D.; Rich, G.; Graffenburg, V.; Patel, S.; Miller, D.; Perez, G. *Proc. SPIE* **2000**, *3999*, 32.

(37) Burns, R. L.; Punsalan, D.; Towidjaja, M. C.; Koros, W. J. *J. Vac. Sci. & Tech. B* **2001**, *20*, 1954.

(38) Kunz, R. R.; Bloomstein, T. M.; Hardy, D. E.; Goodman, R. B.; Downs, D. K.; Curtin, J. E. *Proc. SPIE* **1009**, *3768*, 13.

(39) Bloomstein, T. M.; Horn, M. W.; Rothschild, M.; Kunz, R. R.; Palmacci, S. T.; Goodman, R. B. *J. Vac. Sci. & Tech. B* **1997**, *13*, 2112.

(40) Tran, H. V.; Hung, R.; Loy, D. A.; Wheeler, D. R.; Byers, J.; Conley, W.; Willson, C. G. *Polymeric Materials: Science and Engineering* **2001**, *84*.

(41) Patterson, K.; Yamachika, M.; Hung, R.; Brodsky, C.; Yamada, S.; Somervell, M.; Osborn, B.; Hall, D.; Dukovic, G.; Byers, J.; Conley, W.; Willson, C. G. *Proc. SPIE* **2000**, *3999*.

(42) Brodsky, C.; Byers, J.; Conley, W.; Hung, R.; Yamada, S.; Patterson, K.; Somervell, M.; Trinque, B.; Tran, H. V.; Cho, S.; Chiba, T.; Lin, S. H.; Jamieson, A.; Johnson, H.; Vander Heyden, T.; Willson, C. G. *J. Vac. Sci. Technol. B* **2000**, *18*, 3396-3401.

(43) Trinque, B.; Chiba, T.; Hung, R.; Chambers, C.; Pinnow, M.; Tran, H. V.; Wunderlich, J.; Hsieh, Y.; Thomas, B.; Shafer, G.; Shafer, D.;

DesMartequ, D.; Conley, W.; Willson, C. G. *J. Vac. Sci. & Tech. B* **2002**, *20*, 531-536.

(44) Ito, H.; Allen, R. D.; Opitz, J.; Wallow, T. I.; Truong, H. D.; Hofer, D. C.; Varanasi, P. R.; Jordhamo, G. M.; Jayaraman, S.; Vicari, R. *Proc. SPIE* **2000**, *3999*, 2-12.

(45) Toriumi, M.; Yamazaki, T.; Furukawa, S.; Irie, S.; Ishikawa, S.; Itani, T. *J. Vac. Sci. & Tech. B* **2002**, *20*, 2909.

(46) Ito, H.; Wallraff, G. M.; Fender, N.; Brock, P. J.; Hinsberg, W. D.; Mahorwala, A.; Larson, C. E.; Truong, H. D.; Breyta, G.; Allen, R. D. *J. Vac. Sci. & Tech. B* **2001**, *19*, 2678.

(47) *International Roadmap for Semiconductors, available at: http://public.itrs.net/Files/2002Update/2001ITRS/Home.htm* **2001**.

(48) Somervell, M.; Fryer, D.; Osborn, B.; Patterson, K.; Byers, J.; Willson, C. G. *J. Vac. Sci. & Tech. B* **2000**, *18*, 2251-2559.

(49) Brodsky, C.; Trinque, B.; Johnson, H.; Willson, C. G. *Proc. SPIE* **2001**, *4343*, 415-420.

(50) Gwyn, C. W.; Stulen, R.; Sweeney, D.; Attwood, D. *J. Vac. Sci. & Tech. B* **1998**, *16*, 3142.

(51) Champman, H. N. e. a. *J. Vac. Sci. & Tech. B* **2001**, *19*, 2389.

(52) Colburn, M.; Grot, A.; Amistoso, M.; Choi, B.; Bailey, T. C.; Ekerdt, J. G.; Sreenivasan, S. V.; Hollenhorst, J.; Willson, C. G. *Proc. SPIE* **2000**, *3999*, 453-457.

(53) Bailey, T. C.; Johnson, S. J.; Sreenivasan, S. V.; Ekerdt, J. G.; Willson, C. G. *J. Photopolymer Sci. Tech.* **2002**, *15*, 481.

(54) Switkes, M.; Rothschild, M. *J. Vac. Sci. & Tech. B* **2001**, *19*, 2353.

(55) Tsiartas, P. C.; Flanagin, L. W.; Henderson, C. L.; Hinsberg, W. D.; Sanchez, I. C.; Bonnecaze, R. T.; Willson, C. G. *Macromolecules* **1997**, *30*, 4656-4664.

(56) Flanagin, L. W. *Ph.D. Dissertation, University of Texas at Austin*, 1999.

(57) Flanagin, L. W.; Singh, V. K.; Willson, C. G. *J. Polym. Sci. Pt. B-Polym. Phys.* **1999**, *37*, 2103-2113.

(58) Flanagin, L. W.; Singh, V. K.; Willson, C. G. *J. Vac. Sci. Technol. B* **1999**, *17*, 1371-1379.

(59) Schmid, G. M.; M.S., S.; Singh, V. K.; Willson, C. G. *J. Vac. Sci. & Tech. B* **2002**, *20*, 185-190.

(60) Schmid, G. M.; Burns, S. D.; Tsiartas, P. C.; Willson, C. G. *J. Vac. Sci. & Tech. B* **2002**, *20*, 2913.

(61) Burns, S. D.; Schmid, G. M.; Tsiartas, P. C.; Flanagin, L. W.; Willson, C. G. *J. Vac. Sci. & Tech. B* **2002**, *20*, 537.

CHAPTER 2: MODELS FOR PHENOLIC POLYMER DISSOLUTION*

2.1 GENERAL DESCRIPTION OF PHOTORESIST RESIN DISSOLUTION

The semiconductor microlithographic process is based on photo-induced reactions in polymer films that change the rate of dissolution in aqueous base. It is somewhat surprising that the aqueous base dissolution step, which is necessary in order for the multibillion dollar microelectronics industry to thrive, is not well understood at a mechanistic level. Recall the two questions posed in Chapter 1: (1) What is the rate-limiting step for dissolution? and (2) Does a gel layer form during dissolution? As recently as the past year, studies have appeared in the literature in which somewhat conflicting answers to the two questions have been provided with regards to phenolic polymers.[1,2] Even though this topic has been studied for many years by a variety of researchers, the general mechanism of phenolic polymer dissolution in aqueous base is not yet completely agreed upon. Most researchers agree that the dissolution mechanism of 193 nm and 157 nm photoresist resins (which are based upon carboxylic acids and hexafluoroalcohols, respectively) are more complicated than that of phenolic polymer dissolution.[3] These systems will be mentioned throughout this work, although the focus is

---

*Reproduced in part with permission from S.D. Burns, G.M. Schmid, P. Tsiartas, C.G. Willson, *J. Vac. Sci. Tech. B*. Copyright 2001 phenolic polymer dissolution. This chapter is primarily a review of models that have been used to describe phenolic polymer dissolution. These models are numerous, and there are multiple reviews.[3-6] This chapter focuses more upon recent models of phenolic polymer dissolution, namely the critical ionization (CI) dissolution model,[7] kinetic extensions of the CI model,[1] and the "string of buoys" model.[2] As a prologue to that discussion, the acidity of common photoresist resins is discussed.

2.2 THE ACIDITY OF PHOTORESIST RESINS

The deprotonation reaction described in Figure 1.16 is an acid-base neutralization reaction. Thus, one might expect that the dissolution behavior of a photoresist may be related to the relative acidity of the functional moiety that takes part in this reaction. Phenolic acid groups are used in 365 nm and 248 nm materials, whereas carboxylic acids and hexafluoroalcohols are used in 193 and 157 nm materials, respectively.[3] Table 2.1 shows the pKa of several compounds in aqueous solution at 25°C.[8] Carboxylic acids have a pKa of ~5, hexafluoroalcohol has a pKa of 9.3, and phenol has a lower pKa than that of substituted cresol (9.99 compared to ~ 10.3). In general, it has been observed that 193 nm resins (that are based on carboxylic acids) dissolve at a faster rate than 157 nm resins (based on hexafluoroalcohols), which dissolve faster than 248 nm resins (based on PHOST), which in turn dissolve faster than 365 nm resins (based on novolac).[3,4] Thus, resins with a lower pKa have faster dissolution rates. From this general observation, the acid-base neutralization reaction is expected to play a large role in the dissolution mechanism.

Flanagin *et al.* discuss the importance of pKa and acid-base equilibrium with regards to the dissolution mechanism.[5,9] An important result of this analysis was that the overall degree of ionization, α, of an acidic polymer dissolving in aqueous base is given by:

$$\alpha = \frac{10^{\mathrm{pH}-\mathrm{p}\overline{K_a}}}{1+10^{\mathrm{pH}-\mathrm{p}\overline{K_a}}} \tag{2.1}$$

in which pH represents the hydroxide concentration of the developer, and the $\mathrm{pK_a}$ refers to the acidity of the polymer. α is considered to be the overall fraction of ionized surface sites. The function given by Equation 2.1 is shown in Figure 2.1, in which α is plotted as a function of $\mathrm{pH}-\mathrm{pK_a}$.[9] It is clear that for a significant amount of sites to be ionized (>0.5), it is necessary to have pH>pKa. The semiconductor industry standard aqueous base developer is 0.26 N tetramethylammonium hydroxide (TMAH) with pH=13.4. Given the range of pKa's shown in Table 2.1 it is clear that a significant fraction of monomer sites are ionized at equilibrium during aqueous base dissolution of photoresist films. The critical ionization model, described in detail at the end of this chapter, postulates that the dissolution rate of a photoresist film is related to the fraction of ionized sites described by equation 2.1. Some methods for decreasing α (and, in turn, lowering the dissolution rate) include lowering the developer concentration,

Table 2.1 pKa of common photoresist acidic functional groups

acid	pK_1	pK_2	acid	pK_1	
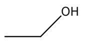 ethanol	15.93		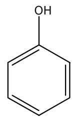 phenol	9.994	
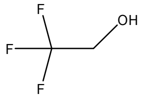 2,2,2-trifluoroethanol	12.37				
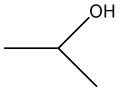 2-propanol	17.1		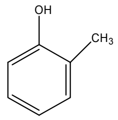 o-cresol	10.333	
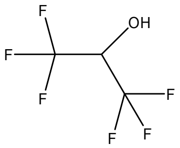 1,1,1,3,3,3-hexafluro-2-propanol	9.3		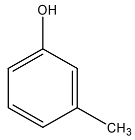 m-cresol	10.098	
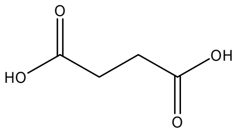 butanedioic (succinic)	4.2	5.7	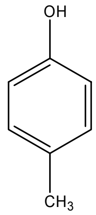 p-cresol	10.276	
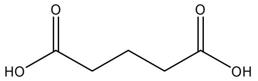 pentanedioic (glutaric)	4.4	5.4			
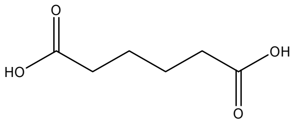 hexanedioic (adipic)	4.4	5.4	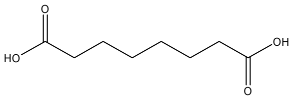 octanedioic	4.5	5.5

(dissolution inhibitors), and blocking acidic monomer sites with non acidic moieties (i.e. chemically amplified resists). It will be shown in Chapter 4 that the geometry of the interface may also contribute to an overall decrease in the fraction of ionized sites (α) due to the Coulombic forces acting at the reactive interface.

The purpose of the above discussion is to illustrate that empirical observations suggest the pKa of a photoresist resin has a large influence on the dissolution rate. This idea is a prelude to the introduction of the critical ionization model at the end of this chapter.

2.3 MODELING THE DISSOLUTION OF PHOTORESIST RESINS

In this section, an overview is presented of the many models for photoresist dissolution described in the literature. They range from empirical to quite physical. There are 5 basic models, termed the "Stone wall" model, the "Octopus pot" model, the Percolation (membrane) model, the "String of Buoys" model, and the Critical Ionization (CI) model. The section begins with a brief overview of general mechanisms of polymer dissolution in organic solvents.

2.3.1 GENERAL MECHANISMS OF POLYMER DISSOLUTION

This work does not intend to summarize the large, general topic of polymer film dissolution in organic solvents. The topic will be briefly discussed

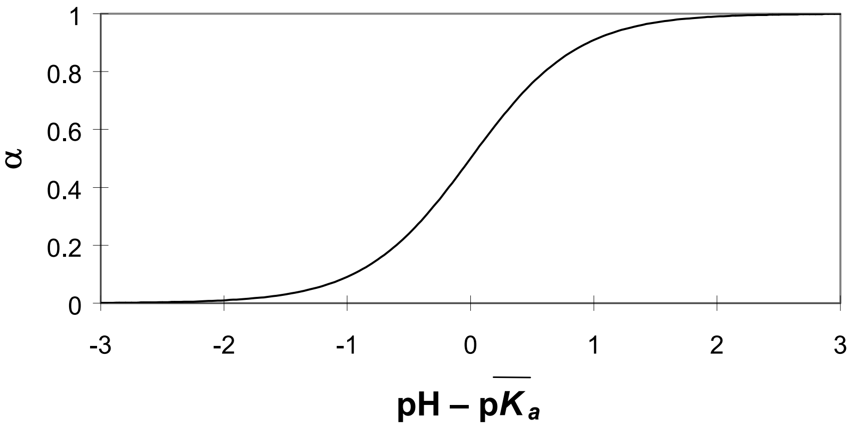

Figure 2.1 Degree of ionization versus pH-pKa

as it applies to the more complicated case of an acidic photoresist resin dissolving in aqueous base. The reader is referred to review articles[10-12] and the general literature for a more thorough discussion.[13-28]

The dissolution of polymer films in organic solvents (or inert solvents) can be viewed as a multistep process, similar to Figure 1.16. The difference between these cases and that of photoresist dissolution is that no chemical reactions are necessary. Transport of the solvent to (and perhaps through) the polymer film, and transport of the dissolved chains into the bulk of the solution are the only steps required. General theories for polymer dissolution postulate either that solvent penetration is rate limiting, or that polymer disentanglement and diffusion are the rate limiting steps. The salient points of these theories are that the systems are unreactive, and the polymers are high molecular weight (above the entanglement molecular weight of the polymer). Conversely, photoresists are reactive systems, requiring a number of deprotonation reaction events for the polymer to become soluble in the aqueous base solvent. Also, photoresists are typically low molecular weight systems, usually below the entanglement molecular weight. Therefore, it is expected that the mechanism that governs photoresist dissolution may be significantly different than other polymer-solvent systems.

In many cases of polymer-solvent dissolution, there is clear evidence of the formation of an intermediate phase (or intermediate gel layer). Peppas *et al.* demonstrate a thick (~0.5 mm) gel layer for the dissolution of polystyrene in methyl ethyl ketone (MEK).[15] Ouano and Carrothers showed evidence of a gel layer in the same polymer-solvent system, as well as poly(α-methylstyrene) dissolving in MEK.[19] Both works reported that poly(methyl methacrylate) (PMMA) dissolved in a variety of organic solvents by crack propagation, without the formation of any significant gel layer.[15,19] In contrast, Rodriguez *et al.*[25] and Winnick *et al.*[29] report thin gel layers (on the order of 45 nm) for PMMA dissolving in MEK and a 2:1 mixture of MEK and isopropyl alcohol. It is generally accepted that the thickness of the gel layer increases with increasing polymer molecular weight.[15,25] However, there are a few distinct mechanistic explanations for gel layer formation, and these will be discussed in more detail in Chapter 7.

2.3.2 NOVOLAC-DNQ DISSOLUTION MODELS

Initial models of photoresist dissolution focused on novolac-DNQ systems, since this was the primary resist platform available at that time.[4] These models sought only to explain the poorly understood interaction between novolac and DNQ. That is, the purpose of these models was to explain the mechanism of dissolution inhibition and dissolution enhancement observed with unexposed and exposed films, respectively. The most prominent of these models were the "stonewall" model and the "octopus pot" model. These models did not explicitly seek an answer to the question "What is the mechanism of pure novolac dissolution in aqueous base?" This question was addressed by later models, such as the Percolation and Critical Ionization models.

2.3.2.1 THE STONE WALL MODEL

Recall the novolac-DNQ dissolution phenomenon discussed in section 1.2. The "Stone wall" model is a contribution by Hanabata *et al.* to explain the observed dissolution inhibition and dissolution enhancement by the DNQ additives.[30-34] The model was the first to consider the azocoupling reaction that may occur between intact DNQ, novolac, and hydroxide ions during dissolution. For a multifunctional DNQ, the azocoupling reaction could lead to crosslinking of novolac chains, which increases the molecular weight and therefore decreases the dissolution rate. Hannabata *et al.* called this model a "stone wall" model. In the exposed regions, the low molecular weight and the UV exposed (reacted) DNQ (the mortar) do not undergo azo-coupling and dissolve rapidly. Any high molecular weight novolac "stones" in this region will be exposed to developer, increasing the surface area and solubility of these chains and leading to a breakup of the "stone wall". In the unexposed region, crosslinking due to azo-coupling will severely increase molecular weight and cause these areas to be insoluble.[30-34] This model describes many aspects of photoresist dissolution, but there are many compounds that act as powerful dissolution inhibitors that do not undergo azo-coupling. Therefore, this model is not a comprehensive model, even for novolac-DNQ dissolution.

2.3.2.2 THE OCTOPUS POT MODEL

Honda *et al.* proposed a model which describes the inhibition of novolac by DNQ in terms of static and dynamic inhibition.[35-37] The dynamic inhibition describes processes such as the azo-coupling described by Hanabata *et al*. Other processes may also result in dynamic inhibition, such as azoxy-coupling or diffusion of inhibitors to form an inhibitor rich layer during the development process. In general, any inhibition process that occurs *during* the dissolution step is referred to as dynamic inhibition.

Static inhibition refers to molecular interactions between phenolic groups of the polymer resin and structural components of the inhibitor. Due to IR hydroxyl shifting with added DNQ, Honda *et al.* proposed the existence of macromolecular complexes. Each of these complexes was thought to consist of six molecules of p-cresol trimer, and a single inhibitor DNQ molecule. The inhibitor molecule was thought to block or "cap" a region of phenolic groups, keeping them together by hydrogen bonding. The macromolecular complex was nicknamed an "octopus pot". It was proposed that steric hindrance of the complex blocked absorption or diffusion of developer hydroxide ions, which thus led to reduced dissolution rates of the polymer film.[35-37] The "Octopus pot" model is more complete in its observations than the "Stone wall" model. However, it still only applies to the case of novolac-DNQ photoresists, and also does not offer a quantitative, predictive description of photoresist dissolution.[4,5]

2.4 PHENOLIC POLYMER DISSOLUTION MODELS

2.4.1 THE MEMBRANE MODEL

In 1986, Arcus proposed a membrane model for novolac photoresist dissolution.[38] This was the first of many models to propose that a transition or gel layer formed during phenolic polymer dissolution. This work was very important because it focused attention on the 'forgotten' reaction of Fig 1.16. That is, the reaction of phenol with hydroxide ion to form a soluble phenolate anion. Arcus reasoned that the polymer chain occupies a three dimensional volume, and for solubility to occur "phenolate [must] exist at all possible chain locations." For all monomer sites to be ionized (including monomers buried within the film) the rate limiting step was reasoned to be diffusion of hydroxide ions to these sites.[38] This diffusion creates a developer concentration gradient that can be described as a transition zone or gel layer similar to that described by Peppas *et al.*[22] and Pappanu *et al.*[11]

One common complaint of Arcus' work was that the material for which a gel layer was observed (via interferometry) was a high molecular weight phenolic material, and not representative of low molecular weight phenolic polymers commonly used for lithographic purposes. There are some other minor drawbacks to this model, but perhaps the largest drawback is the recent discovery that the interpretation of the interferometry data upon which the model is based is *highly* questionable. Modeling of gel layer formation performed by Rodriguez *et al.*,[24-26] Winnik *et al.*,[29] Hinsberg *et al.*,[39] and recently by our research group suggests that Arcus' data is not even qualitatively consistent with the presence of a gel layer. In Chapter 7, this data is discussed in much more detail.

2.4.2 THE PERCOLATION MODEL

Arnost Reiser and his students have developed the percolation model,[40,41] which was based on the experimental work of Arcus.[38] The percolation model uses the basic concept of a gel or transition layer, and percolation theory is adapted to describe the diffusion behavior through the gel layer (or penetration zone). Percolation theory is a lattice-based theory that deals with the probability of finding connected channels ("percolation clusters") of randomly distributed sites on a grid. In the case of phenolic polymer dissolution, hydrophilic sites within the penetration zone are thought to be favorable to the diffusion of aqueous base hydroxide ion. The issue is whether or not enough sites are connected into a continuous channel in order for diffusion to occur through the transition zone. This concept is shown schematically in Figure 2.2.[4] The percolation parameter (*p*) is the number of randomly distributed percolation sites on the lattice. These can be considered hydrophilic or free volume regions of the polymer lattice – sites that would be favorable to hydroxide diffusion. Figure 2.2(a) shows the case of $p = 0.5$. In this case, individual clusters may form, but percolation cannot occur throughout the entire lattice. In Fig 2.2(b), the percolation parameter has been arbitrarily increased to $p = 0.625$. In this case, percolation channels are present throughout the entire lattice and the clusters are infinite in size. Between these two values of *p* is a critical percolation value, p_c, which is the minimum fraction of percolation sites necessary for continuous clusters to form.[4] For a 2-D lattice, $p_c \sim 0.6$. For a 3-D lattice, $p_c \sim 0.2$. The dissolution rate (*R*) can be related to the percolation parameters by:

$$R = k(p - p_c)^2 \tag{2.2}$$

This general model has been used by Reiser *et al*. to describe many factors

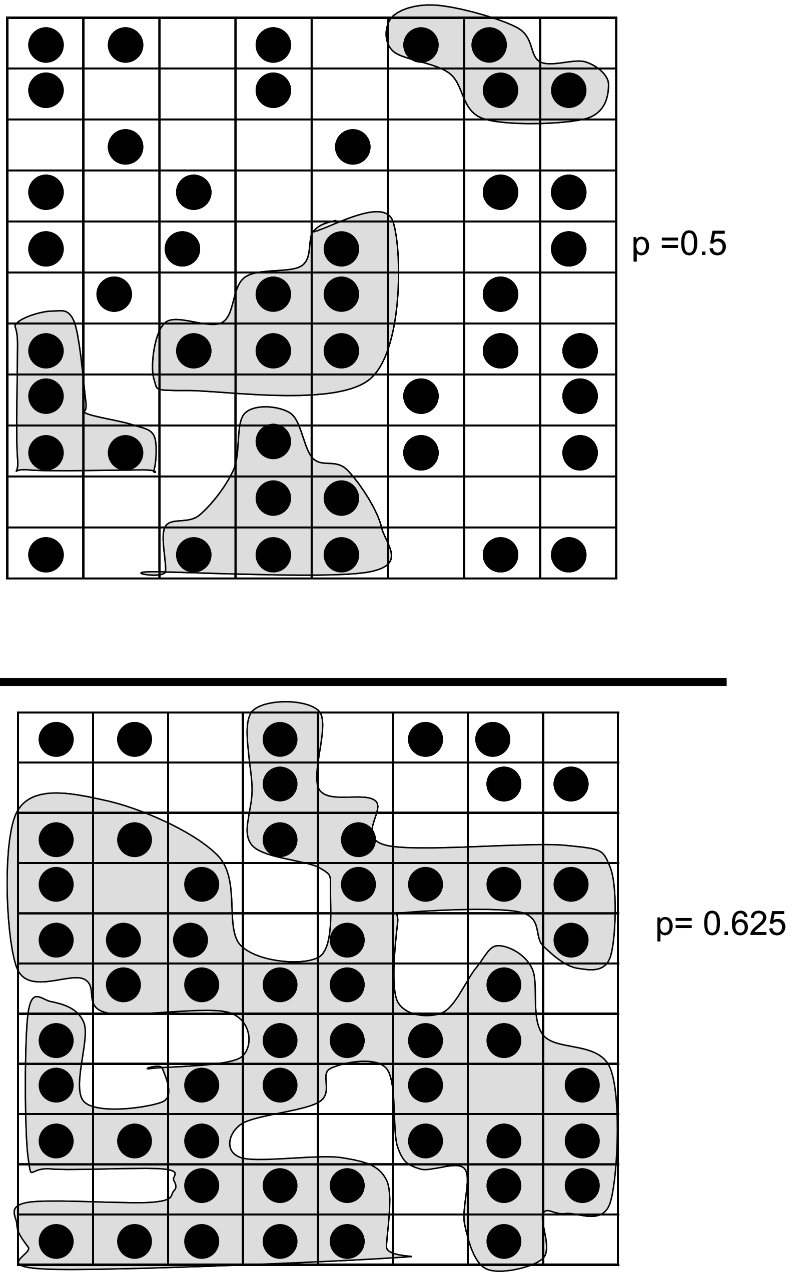

Figure 2.2 Percolation on a 2-D lattice. (a) $p<p_c$, and all clusters are finite in size. (b) $p>pc$, and the clusters are infinite in size (assuming periodic boundary conditions of the lattice). In the latter case, diffusion can occur through the entire lattice.

affecting the dissolution rate of novolac, including the base cation[42], added salts[43], dissolution inhibitors[44,45], dissolution promoters[46], isotopic substitution[47] and resin molecular weight.[48] The main concerns with the model are the explanations offered for the added salts and molecular weight effects on dissolution. For example, to explain the added salt effect with the percolation theory, it was necessary to conclude that hydroxide ions have a diffusivity 5 times higher than alkali ions of comparable size. This was explained in terms of a Grotthuss hopping mechanism,[49] as opposed to simple free volume diffusion, but this explanation has been unconfirmed. In terms of molecular weight effects, the basic premise of the Percolation model (that the dissolution rate depends only on the density of hydrophilic sites) cannot explain variations in dissolution rate with molecular weight. Reiser *et al*. have suggested that all sites of a percolation channel must receive a simultaneous thermal activation to allow diffusion of the hydroxide ions, and that the probability of this occurrence is inversely proportional to chain length.[48] Again, this assumption is unconfirmed, and does not provide a simple, experimentally verifiable explanation for phenolic polymer dissolution. While the Percolation model is capable of explaining several dissolution trends, and has been very useful for generating ideas regarding dissolution, it does not provide a complete explanation of phenolic polymer dissolution. Perhaps the biggest drawback of this model is that the assumption of gel layer (percolation zone or penetration zone) formation rests entirely on the now highly questionable experimental work of Arcus.[38] Flanagin also provides a detailed review of the Percolation model.[5]

2.4.3 THE 'STRING OF BUOYS' MODEL

Hunek and Cussler have presented a relatively new model for phenolic polymer dissolution.[2] Their model is based on experimental dissolution results involving a thick (~ 0.5 cm) film of phenolic, novolac resin coated onto a spinning disk and dissolved in sodium hydroxide. The dissolution rate was monitored by UV spectroscopy of the developer solution, and the speed of the spinning disk was varied. They found that the dissolution rate varied by a factor of ~ 2 in the laminar flow regime. Hunek and Cussler matched their data to a model that suggests the rate controlling step for dissolution is a combination of 'solute release' and transport of the poly ion into the bulk of developer. They used a 'string of buoys' (SOB) analogy to describe their model, which they compared to a large group of lane markers (a buoy on a string, that represents a polymer molecule) that have collapsed at the bottom of a dry pool (representing a dry film). Three features are incorporated to extend the analogy to phenolic polymer dissolution. First, the unionized phenolic polymer is insoluble, so the 'buoyancy' is zero. Gel layer formation is not expected because the initial 'string of buoys' is not soluble. The acid-base reactions quickly make some buoys ‘buoyant’, but unreacted sites are still trapped, and the dissolution of the polyion is hindered due to solute-solute interaction (as opposed to polymer entanglement). After a sufficient fraction of buoys (monomer sites) are reacted on the same ‘string’, the polymer is slowly transported into the bulk solvent by diffusion. The conclusion of Hunek and Cussler was that “the dissolution of low molecular weight phenolic resin is controlled by a combination of solute release and solute mass transfer, without the formation of any significant gel phase”. In other words, the rate by which the final deprotonation reaction necessary to reach f_{crit} occurs (solute release) is comparable to the rate at which the polymer is transported into solution (solute mass transfer), and both rates can be considered limiting in the dissolution mechanism. Their results are “consistent with [Willson] *et al.* in highlighting the key role chemical reaction plays in phenolic resin dissolution.”

The SOB analogy is the first model to consider the effect of developer flow rate on the dissolution rate of the film. In this regard, it is important because it suggests that mass transfer must play a role in order for the flow rate of developer to influence the dissolution rate. It is thus far unknown how well this model might explain other commonly observed dissolution trends. One drawback of the model can be found in the overall mathematical description of the dissolution rate:

$$\frac{d[R]}{dt}=\frac{[OH]-\frac{1}{K_2'K_3}[R]}{\frac{1+K'_2[OH]}{k_3K'_2[RH_s]_o}+\frac{1}{k_4a}\frac{1}{K'_2K_3}} \tag{2.3}$$

where [R] is the concentration of phenolate (polyion), [OH] represents the developer concentration, *a* is dependent on the geometry of the experiment, and all other variables are constants, representing either mass transfer coefficients are equilibrium constants. (These are defined by Cussler *et al.*[2], and identical notation has been used). K'_2 is determined from the pKa. The value of pK_a used was 12.4, which yields $K'_2=3.98 \times 10^{-13}$. It follows that the K'_2[OH] term will be small compared to unity and this term can be neglected. The resulting equation states that the dissolution rate is *linearly* related to hydroxide concentration:

$$\frac{d[R]}{dt}=A[OH]+B[R] \tag{2.4}$$

where A and B are constants. However, a well established experimental trend is that the *log* of the dissolution rate is linear related to the hydroxide concentration, or

$$\frac{d[R]}{dt}=10^{\alpha[OH]} \tag{2.5}$$

which is inconsistent with equation 2.4. Thus, the model of Hunek and Cussler has at least one obvious drawback, in that it fails to properly describe the change in dissolution rate with concentration of aqueous base.

2.4.4 THE CRITICAL IONIZATION DISSOLUTION MODEL

The critical ionization (CI) dissolution model has been presented previously by our research group through the works of Pavlos Tsiartas[6,7] and Lewis Flanagin.[5] The model is based upon the assumption that the deprotonation reaction is rate limiting to phenolic polymer dissolution. Simply stated, the CI model proposes that an individual polymer molecule becomes soluble when a critical fraction of its monomer sites (f_{crit}) have become ionized, or deprotonated. This last ionization reaction to reach f_{crit} is proposed to be the rate-limiting step in the dissolution process. The transport of hydroxide ion to the surface and the transport of the polyion away from the surface are considered to be fast in comparison to this reaction step. This process has been compared to the etching of copper by nitric acid, in that a surface reaction creates a soluble species which may then dissolve. It is expected that this model is only valid for polymer chain lengths below the entanglement molecular weight. The reaction step may not be rate limiting if dissolution involves significant disentanglement of chains. If this picture of dissolution is valid, it is expected that an interfacial gel layer would not form during dissolution, because this process is usually associated with mass transfer as the rate-limiting step. (Note that Hunek and Cussler propose a mechanism based in part on mass transfer, but also conclude that a gel phase does not form.) Our research group has implemented the CI model into dissolution simulations with the assumption that a gel layer does not form. The validity of this assumption is discussed in Chapter 7.

The work of Flanagin *et al.* presents the CI model in various degrees of complexity. In its simplest form the CI model states that the dissolution rate, R, is proportional to the number of ionized sites divided by the number of total sites:

$$R = \quad \frac{[A^-]}{[HA]} = \frac{K[\mathrm{OH}^-]\gamma_{\mathrm{OH}^-}}{\gamma_{\mathrm{A}^-}} \quad R = k \cdot 10^{Ac^{1/3} - Bc} \tag{2.6}$$

$$\log \gamma_{\pm} = -Ac^{1/3} + Bc \tag{2.7}$$

where γ represents the activity coefficient in solution. This simple form of the CI model has been used to describe the rather unintuitive result that the dissolution rate increases, reaches a maximum, and then decreases as the concentration of inert salts is increased in an aqueous base developer solution. A plot of this effect is shown in Figure 2.3, in which experimental results are shown for a NaOH-NaCl solution, and a TMAH-TMACl solution. Although the peak position is different, the dissolution model derived from Equation 2.6 provides a good description of the phenomenon with few adjustable parameters.

Flanagin *et al.* then improved upon the simple dissolution description of equation 2.6. A continuum model description of dissolution was developed with the following assumptions. For an acidic polymer film with X ionizable protons per molecule in contact with a reservoir of hydroxide ion (i.e. aqueous developer,

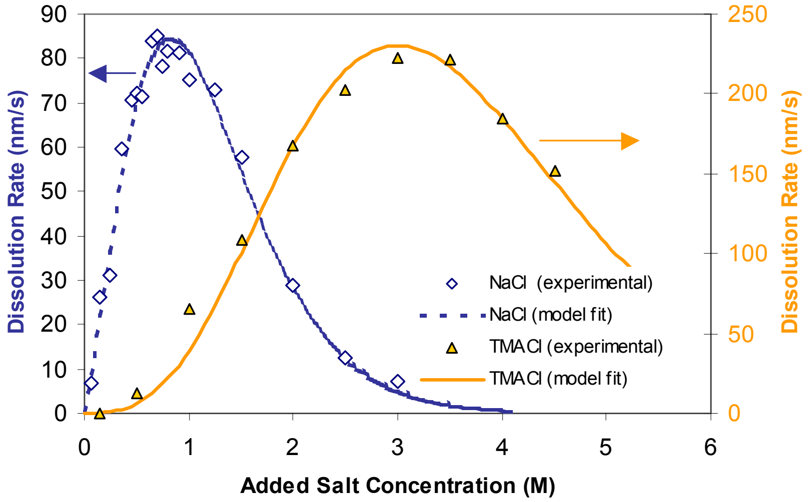

Figure 2.3 Dissolution rate of a novolac resin as a function of added chloride concentration for NaOH-NaCl and TMAH-TMACl solutions.

TMAH), the following set of reaction (deprotonation) steps occur at the liquid-solid interface:

$$\mathrm{OH}^- + \mathrm{P}_X\mathrm{H}_X \overset{K_1}{\rightleftharpoons} \mathrm{P}_X\mathrm{H}_{X-1}{}^- + \mathrm{H_2O}$$

$$\mathrm{OH}^- + \mathrm{P}_X\mathrm{H}_{X-1}{}^- \overset{K_2}{\rightleftharpoons} \mathrm{P}_X\mathrm{H}_{X-2}{}^{2-} + \mathrm{H_2O}$$

$$\vdots$$

$$\mathrm{OH}^- + \mathrm{P}_X\mathrm{H}_{X-i+1}{}^{(i-1)-} \overset{K_i}{\rightleftharpoons} \mathrm{P}_X\mathrm{H}_{X-i}{}^{i-} + \mathrm{H_2O}$$

$$\vdots$$

$$\mathrm{OH}^- + \mathrm{P}_X\mathrm{H}_1{}^{(X-1)-} \overset{K_X}{\rightleftharpoons} \mathrm{P}_X\mathrm{H}_0{}^{X-} + \mathrm{H_2O}$$

Where $P_xH_{x-i}{}^{i-}$ is the polymer chain, which started with *X* ionizable sites, but now has only *X-i* reactive protons remaining on the chain. K_i represents the equilibrium constant for each step. Having a single constant for each step implies that the value of K_i is not dependent upon the arrangement of ionized sites. (This assumption is thought to be true for PHOST resins, but not for novolac resins.[5] The structural reason for this is discussed in Chapter 6.) The concentration of OH^- is considered to be constant because the supply is large compared to the amount of polymer, and the transport of OH^- to the film surface is considered to be rapid. Flanagin stated that the equilibrium constants ($K_1 \ldots K_x$) are related to one another by a statistical factor that arises from a difference in the number of pathways for deprotonation and protonation for each set of reactions. The equilibrium constants are related by the following expression:

$$K_i = \left(X - i + 1\right) K_{GM} / i \tag{2.8}$$

where K_{GM} is the geometric mean of all the equilibrium constants. Then, the assumption is made that the transfer of each ionized chain, $P_xH_{x-i}{}^{i-}$, from the solid state to the aqueous solution is assumed to be an irreversible first order process characterized by a rate constant, $k_{d,i}$:

$$\mathrm{P}_X\mathrm{H}_{X-i}{}^{i-} \xrightarrow{k_{\mathrm{d},i}} \mathrm{P}_X\mathrm{H}_{X-i(aq)}{}^{i-};\, r_i = \frac{\mathrm{d}\left[\mathrm{P}_X\mathrm{H}_{X-i(aq)}{}^{i-}\right]}{\mathrm{d}t} = k_{\mathrm{d},i}\left[\mathrm{P}_X\mathrm{H}_{X-i}{}^{i-}\right] \tag{2.9}$$

The film dissolves on a molecular basis at a rate R, given by:

$$R = \sum_{i=0}^{X} k_{\mathrm{d},i}[\mathrm{P}_X\mathrm{H}_{X-i}{}^{i-}] \tag{2.10}$$

However, the key assumption of the CI model is that only chains that have reached a critical ionization fraction, F, may dissolve. (Note that the variable F is identical to f_{crit}. The variable F was used in this section to maintain consistency with the notation of Flanagin.[5]) Thus, Flanagin *et al.* assumed that $k_{d,i}$ is zero for chains whose ionization fraction is less than F. For chains with an ionization fraction equal or above F, $k_{d,i}$ is assumed to have a singular, nonzero value, k_d. Equation 2.10 then becomes:

$$R = k_\mathrm{d} \sum_{i=FX}^{X} \left[\mathrm{P}_X \mathrm{H}_{X-i}{}^{i-} \right] \tag{2.11}$$

This equation was further derived (using equation 2.1 for the fraction of ionized surface sites) to:

$$R = \frac{k_\mathrm{d} \left[\mathrm{P}_X \mathrm{H}_X \right]_0}{\left(1 + 10^{\mathrm{pH}\text{-}\mathrm{p}\overline{K_a}}\right)^X} \sum_{i=FX}^{X} \binom{X}{i} \left(10^{\mathrm{pH}\text{-}\mathrm{p}\overline{K_a}}\right)^i \tag{2.12}$$

where

$$\binom{X}{i} = \frac{X!}{i!\,(X-i)!} \tag{2.13}$$

This continuum form of the dissolution rate model qualitatively explained many experimental observations, such as PHOST dissolving faster than novolac, the affect of additive dissolution inhibitors to both novolac and PHOST, and the difference in dissolution rate between protonated and deuterated novolac.[5]

Flanagin went on to incorporate the CI model into a statistically based, mesoscopic lattice model. The model was described briefly in Chapter 1 as a lattice based simulation in which each lattice site nominally represents a monomer unit, and the dimension of each site edge is 0.7 nm, based on the volume of a PHOST monomer. However, lattice sites may also represent void volume, blocking moieties, and resist additives (such as PAC, PAG, dissolution inhibitors, or added base). The monomer units are strung together to form an equilibrated array of polymer chains by random walks, reptation, or a combination of reptation with various Monte Carlo equilibration "moves".[5] In this manner, the resist formulation (molecular weight, polydispersity, concentration of additives) is a user defined input variable.[5] This is a very unique capability for a lithography simulation tool.

Dissolution occurs in the model by incorporating the basic assumption of the CI model into a simple algorithm. At t=0, developer is brought into contact with the upper surface of the film. In the work of Flanagin,[5] hydroxide ions are not considered explicity. Rather, the developer concentration and pKa of the resin were predetermined, and a value of α, the fraction of ionized surface sites, was either calculated or assumed (Equation 2.1). A fraction (α) of surface sites are randomly ionized during the first simulation time step. Then, the algorithm searches for individual polymer chains in which the fraction of ionized sites was equal to or exceeded the critical fraction, f_{crit}, and those polymer chains are

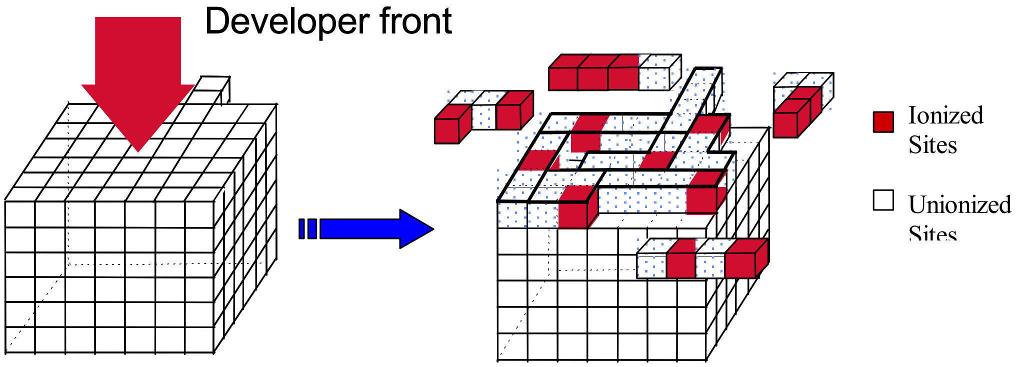

Figure 2.4 Description of the lattice based CI model

allowed to dissolve. The transport into solution is assumed to be rapid, and the identity of the lattice site is changed to void (developer) sites. The dissolution of some chains exposes other chains to the developer interface for subsequent ionization. In the next time step, the new surface is again randomly ionized to meet the equilibrium state, α. The process ends when the dissolution of all chains is complete, or when a user defined time step is reached.

The main inputs to this model are the photoresist formulation, the fraction of ionized surface sites, α, and the critical ionization fraction, f_{crit}. For a given resist system, the formulation parameters are known (except, perhaps, for the void fraction). Also, α can be calculated based upon the developer concentration and the pKa of the polymer system. The input parameter that is most ambiguous to correctly determine is f_{crit}, because it is a microscopic quantity and difficult to measure. Estimates of f_{crit} are discussed at the end of this chapter. The output of the simulation is film thickness and roughness versus simulation time, which does not provide a physically meaningful dissolution rate. In the current form of the model, it is necessary to calibrate the simulation time to real time by comparing a simulation of a known resist system to experimentally determined dissolution rates.

While this lattice model is simple, it was successful as a tool for modeling image formation and correctly predicted a number of experimentally observed dissolution trends. The qualitative trends of the continuum model discussed above are correctly captured, and the simulation correctly captured dissolution rate trends with changes in void fraction, residual casting solvent, polydispersity, and blocking fraction. Perhaps the most useful function of the lattice-based model over a continuum based model is the ability to model surface and line edge roughness (LER). As feature sizes of photoresists become smaller, the variation in line width over the entire line (LER) becomes an increasingly important problem, and it becomes necessary to have models that can yield quantitative, mechanistic predictions of roughness with changes in the resist formulation and other parameters. Flanagin demonstrated that the CI lattice model could qualitatively predict changes in surface roughness with changes in time, molecular weight, and exposure dose (blocking fraction). This study is extended in Chapter 8, in which the lattice model is compared with quantitative AFM measurements of surface roughness in a variety of photoresist resins.

2.4.5 KINETIC EXTENSIONS OF THE CI MODEL

Houle, Hinsberg and Sanchez at IBM Almaden have recently presented an extension of the CI model.[1] Their model considers the general assumption of the CI model to be valid. That is, the deprotonation reaction is rate limiting, and once a critical fraction of ionized sites on a polymer is reached, the chain becomes soluble. Their model considers the reaction rates of every forward and reverse ionization step leading up to dissolution, which is a more detailed approach than the equilibrium approach described above. Their model differs in another respect. All the chains in a surface (gel) layer (of arbitrary size) are considered to have equal access to the base ions in developer solution. The thickness of the gel layer is an input parameter to the model, and must be determined from experiment or a value must be assumed.

An example is provid to describe their model.[1] Consider a PHOST chain with 10 monomer units, and assume f_{crit} is 0.5. The kinetic reaction sequence leading up to dissolution is shown in Figure 2.5. It is necessary to know 6 forward and 5 reverse rate constants (11 total) in order to properly model the reaction sequence for that chain. The assumption used by Houle *et al*. to determine the rate constants is that statistical factors (σ_i) can be used to relate the

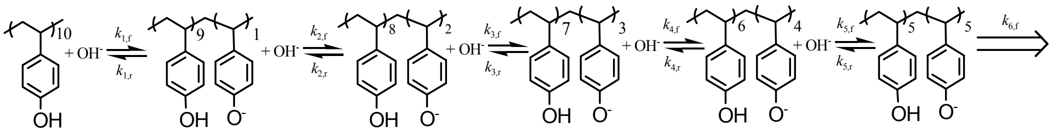

Figure 2.5 Deprotonation reaction sequence leading to dissolution of a PHOST 10 mer for f_{crit} =0.5.

rate constants to one global rate constant, *k*, where the subscript *i* represents a particular reaction. The statistical factors are determined by the number of pathways available for a given reaction step. For example, any one of 10 monomer units can initially be ionized, so the statistical factor for the first forward ionization step is 10 ($\sigma_{f,1}$=10). Likewise, there is only one equivalent pathway available for the reverse reaction, so $\sigma_{r,1} = 1$. In the next step, $\sigma_{f,1}$=9 and $\sigma_{f,2}$=2, and so on…the reaction rate constant for each step is then $k_{f,i} = \sigma_{f,i}k$, and $k_{r,i} = \sigma_{r,i}k$, where *k* is constant for each reaction in the scheme.

If one considers the equilibrium constant of each step and relates it to a general expression for the statistical factors:

$$K_i = \frac{k_{i,f}}{k_{i,r}} = \frac{\sigma_{i,f}k}{\sigma_{i,r}k} = \frac{(X - i + 1)}{i} \tag{2.14}$$

where X is the number of monomer units on a particular chain, it is evident that the statistical factors used by Houle *et al.* are identical in form to the statistical factors presented by Flanagin *et al*. (equation 2.8). However, the treatment of Houle *et al.* in implementing the model was different than the lattice model used by Flanagin. Flanagin used Equation 2.14 only to determine the equilibrium ionization condition. In retrospect, equation 2.9 describes the transport of ionized polymer chains into the bulk as the rate limiting step for dissolution with a rate constant k_d, which was not the original intent of the model. However, the CI lattice model does not use equation 2.9, and the original intent of the model is well captured in the form and results of the simulations.[5]

However, the CI lattice model (by Flanagin) considers the final equilibrium of the ionized surface, rather than the kinetics of each individual reaction. For example, if f_{crit}=0.5, and α=1.0, one may envision many cases in which the critical fraction of ionized sites on a chain has been temporarily exceeded, if only for a single time step. Since the time step is extremely small and ultimately calibrated to experimental data, it is not necessarily expected that this slightly nonphysical approach would lead to significant errors in simulating dissolution. But, the approach of Houle *et al*. is more rigorous to the strict definition of the CI model on this point. That is, a polymer chain is dissolved immediately upon reaching f_{crit}. The distinction is subtle, and it is currently unknown what change it might have on overall simulation results.

A saliet feature of the approach by Houle *et al*. is in simulating polymers of various blocking fractions. Consider the reaction scheme shown in Figure 2.6, in which a 50% blocked PHOST 10-mer dissolves by a series of deprotonation reactions, identical to those described above. Again, 11 forward and reverse rate constants are needed, but can be estimated by considering statistical factors. Table 2.1 shows the difference in absolute value of the statistical factors for the case of completely deprotected PHOST, and the case of 50% protected PHOST. It is clear that the 100% deprotected PHOST will dissolve much faster based upon

Table 2.1 Statistical factors for the examples of Fig 2.5 and 2.6

	Case 1. 10 mer, completely deprotected PHOST	Case 2. 10 mer, partially protected PHOST
σ_1	10	5
σ_2	4.2	2
σ_3	2.6	1
σ_4	1.75	0.5
σ_5	1.2	0.2

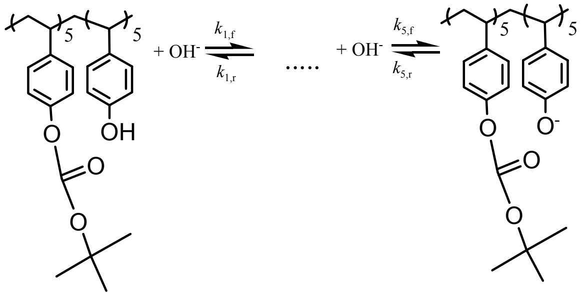

Figure 2.6 Deprotonation reaction sequence leading to dissolution of partially protected PHOST 10-mer for f_{crit} =0.5.

the kinetic criterion, which is consistent with experimentally observed trends. A similar trend is observed with the current form of the CI lattice model.[5]

There are some disadvantages of the current approach by Houle *et al*. For example, the current form of the model is not a lattice-based model, and does not consider the position of polymers in terms of cartesian coordinates. That is, polymer morphology is not considered. (In terms of computation time, this may be considered an advantage.) For determining surface roughness, this is may be considered less ideal because polymer morphology contributions are not considered. Also, the current form of this model does not capture the molecular weight effects that are inherent to the original CI lattice model. The author's interpretation is that if polymer resins of different molecular weights and polydispersities are to be simulated, it is necessary to run at least the same number of calibration experiments in order to simulate the correct experimental dissolution trend. The assumption of gel layer formation in the kinetic model is considered in Chapter 7. It is envisioned that a hybrid version of the kinetic model and the lattice CI model may be a useful research tool for investigating dissolution trends in phenolic polymers and other photoresist resins.

Houle *et al*. stated that "We propose that the critical ionization threshold corresponds to a state in which the energy of the ionized and solvated state in the polymer film has become very close to the energy of an ionized molecule in solution".[1] The author agrees with this statement. Ultimately, dissolution of an individual chain will occur when the energy change corresponding to dissolution is more favorable than remaining within the polymer film. A lattice model of this type was proposed by Ralph Dammel, in which an each type of lattice cell (i.e. unionized monomer, ionized monomer, and developer) have a unique interaction parameter with other types of lattice cells. A schematic of this proposed model is shown in Figure 2.7. This model was investigated by our research group and although it was a useful conceptual approach, it did not yield any significant advantage over the current form of the lattice based CI model. In fact, it was very difficult to estimate the relative values of the relative interaction parameters, so

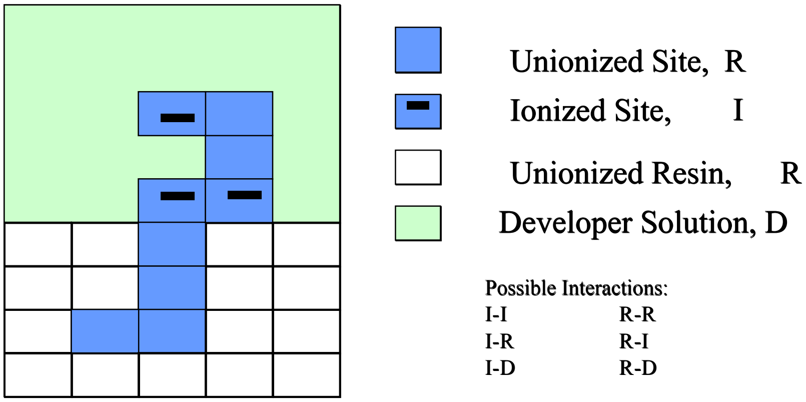

Figure 2.7 Schematic of interaction energy dissolution lattice model proposed by Dr. Ralph Dammel.

this approach was not continued. The CI model can be considered a simplified version of this approach, in which the sum of the energetic interactions are convolved into a single parameter, f_{crit}. Thus, the author is in agreement with the proposal by Houle *et al*. that the critical ionization threshold corresponds to a state that is energetically favorable for dissolution, which is a fundamental thermodynamic requirement for solubility.

The f_{crit} parameter is, in principle, easier to measure than the individual interaction energies proposed by Dammel. Both the CI lattice model and the kinetic extension of the CI model require that the critical fraction of ionized sites, f_{crit}, is known in order to rigorously simulate photoresist dissolution. This chapter concludes with a discussion of methods that have been used to measure or estimate f_{crit} for a given polymer system.

2.5 ESTIMATES OF F_{CRIT} FOR PHENOLIC POLYMERS

Flanagin also discussed methods for determining f_{crit} in detail.[5] Perhaps the best estimates of this value have been determined by examining the dissolution rate of copolymers of hydroxystyrene, and blocked or inert monomer units, such as polystyrene, or poly(*p*-methoxystyrene). These copolymers are shown in Figure 2.9. Such studies have been undertaken by Yeh *et al.*,[50] Long *et al.*,[51] and Barclay *et al.*[52] A similar study has also been taken within our research group through the work of Wunderlich and Schmid.[53] The goal of such a study in terms of f_{crit} is to determine the blocking fraction needed in order to render the polymer insoluble (having a dissolution rate that is immeasurably small) in aqueous base developer. A common result of these studies is that the "critical" blocking fraction depends upon the concentration of the aqueous base developer solution. As the developer concentration is increased, the critical blocking fraction decreases. For example, at 0.26 N base concentration Wunderlich and Schmid found that a blocking fraction between 0.3-0.47 was necessary to render the film insoluble. However, at base concentrations of ~3 N, a blocking fraction as high as 0.85 still had a finite dissolution rate. This latter value suggests that f_{crit} < 0.1, which is an unreasonably low value. These results imply that f_{crit} changes with varying developer concentration. This result can be understood by considering the discussion above concerning the energetic factors affecting dissolution. A high developer concentration can significantly change the interaction parameters, and make dissolution of polymers much more energetically favorable, even for a polymer with only a few ionized sites. Thus f_{crit}, which can be thought of as a convolution of the interaction parameters, may be expected to change with developer concentration. The important value for lithographic applications is the value of f_{crit} that corresponds to the industry standard 0.26 N developer concentration. In Table 2.2, the review of Flanagin is reexamined, considering only the critical blocking fraction that occurs at 0.26 N hydroxide concentration. From these previous studies, one concludes that f_{crit} (at 0.26 N) for PHOST resides between 0.55-0.7.

Table 2.2 Estimation of f_{crit} based upon copolymer dissolution rate experiments

Research Group	Copolymer	Mw	Pd	Bake Conditions	Developer Concentration	estimated f_{crit}
Reiser[49]	PHOST-co-PMOS	22k	_____	1 hr/90 C	0.26 N	0.65-0.70
Rodriguez[50]	PHOST-co-PS	75-99k	3.8-5.3	1 hr/160 C	< 0.26 N	< 0.70
Barclay[51]	PHOST-co-PS	7-10k	1.12-1.27	60 s/130 C	0.26 N	0.55-0.7
Willson[52]	PHOST-co-PMOS	4k	~1.1	90 s/90 C	0.26 N	0.47-0.71

Another method for determining f_{crit} was examined in this work. This method involved fitting simulated data to experimental dissolution rate data in a unique way. Before describing the technique, it should be noted that equilibrium ionization was an affect that was added to the CI lattice model in this work. The previous version of the model randomly ionized surface sites, but the ionization distribution did not change unless polymer dissolution occurred. That is, no consideration was made for the fact that ionized sites could reprotonate based upon statistical equilibration effects. In the new version of the model, new sites are ionized in each time step at random, keeping α constant in each step. This new approach allows for the simulation of "slower" dissolution rates, because more ionization states can be probed in a given simulation. In previous versions of the model, if α was approximately equal to f_{crit}, the simulation would often become “stuck” with no means of becoming “unstuck”. In the newer version, equilibrium ionization allows sampling of other energetic configurations, which is a more physically realistic picture of the dissolution process.

Some results of this new version of the CI lattice model are shown in Figure 2.8. The log of the dissolution rate (in units of thickness change per time step) is plotted against the log of the degree of polymerization. Simulation results are shown for various values of f_{crit}, using $\alpha = 0.9$, and a void fraction of 0.1. The polydispersity was kept constant at unity.

The experimentally determined relationship between dissolution rate and molecular weight is an exponential function:

$$R = MW^n \tag{2.15}$$

where R is dissolution rate, MW is the molecular weight of the polymer, and the exponent, n, varies between -0.3 to -3 for a variety of novolac and PHOST fractions.[7,50-52,54,55] Our research group has found that for monodisperse polyhydroxystyrene, n ~ -2.3.[7] In the simulation results of Figure 2.8, a value of $f_{crit} = 0.69$ results in a slope of ~ -2.3.

These results indicate significant advancements to the model. First, the molecular weight dependence of the dissolution rate can be captured quantitatively with only one variable (which was not possible in previous versions[5]). Second, this technique provides a unique method for determining f_{crit} for any given polymer system. Figure 2.9 shows the experimentally determined dissolution rate of poly(p-hydroxystyrene),[7] 4-bistrifluoromethylcarbinol substituted polystyrene (HFPS),[54] and novolac.[55] All three polymers show a linear change in dissolution rate with molecular weight on a log-log scale (Equation 2.15). However, the slope of each line differs considerably. Novolac has a slope of -2.6, PHOST has a slope of -2.3, while HFPS has a slope of -0.54. Comparing these experimental data to the simulation

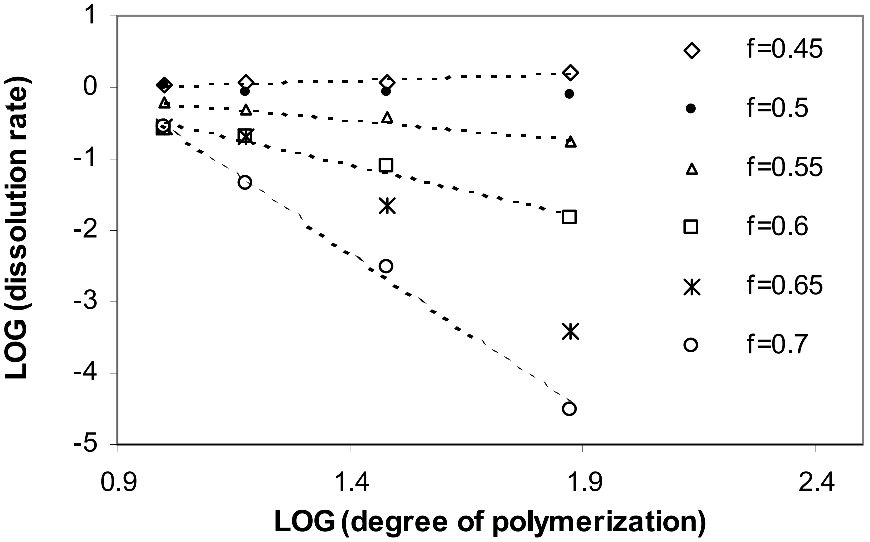

Figure 2.8 Results of CI lattice model simulations, showing the log of the dissolution rate versus the log of degree of polymerization. fcrit is varied between 0.45 and 0.7.

as shown in Figure 2.8 indicates that the best fit value of f_{crit} for novolac is ~ 0.71, for PHOST is ~ 0.69, and for HFPS is ~ 0.6. The molecular weight dependence of the dissolution rate of each polymer is correctly captured by the CI model by using the appropriate value of f_{crit}. Thus, if the value of n in equation 2.15 is known for a given polymer platform, then f_{crit} can be determined by comparing

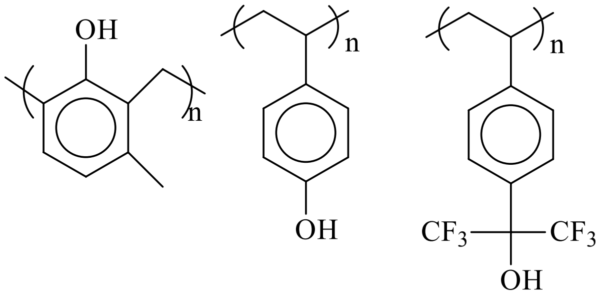

Novolac PHOST HFPS

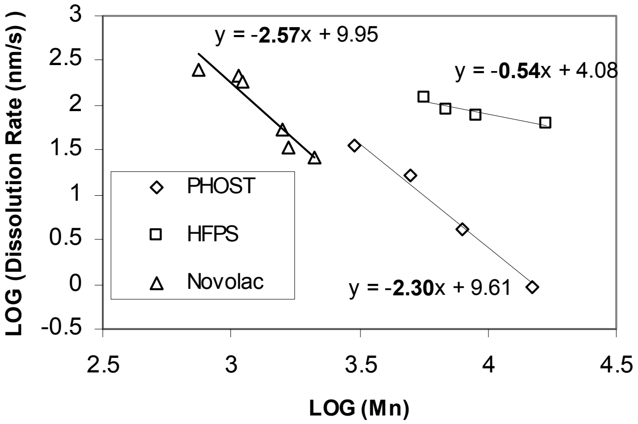

Figure 2.9 Experimental data showing the log of dissolution rate versus the log of degree of polymerization for three common photoresist resins.

the simulation data with experimental data.

Also note that the best-fit value of f_{crit} decreases with decreasing pKa of the polymer resin. This observation, in terms of the interaction parameter discussion above, suggests that the dissolution of resins with lower pKa is more energetically favorable over resins with a higher pKa. At this point, this is merely a qualitative trend, but intuition suggests that this should be correct and lends additional credibility to this approach for determining f_{crit}.

2.6 SUMMARY

In this chapter, several models for phenolic polymer dissolution in aqueous base were considered. The primary models considered were the Percolation model, the String of Buoys model, the Critical Ionization model, and a kinetic extension of the CI model. The CI model was presented in both a continuum and lattice form, and compared to the other models. Both the SOB model and the kinetic extension of the CI model have certain benefits in their approach, however the CI model was shown to provide a good overall description of phenolic polymer dissolution. Specific aspects of this dissolution model will now be considered throughout the remainder of this work. Specifically, coulombic forces are added to the model (Chapter 4), theories for surface rate inhibition are tested (Chapter 5 and 6), the assumption of gel layer formation is experimentally tested (Chapter 7) and finally the CI lattice model is used as a technique to study the formation of surface roughness during dissolution (Chapter 8).

2.7 REFERENCES

(1) Houle, F. A.; Hinsberg, W. D.; Sanchez, M. I. *Macromolecules* **2002**, *35*, 8591-8600.

(2) Hunek, B.; Cussler, E. L. *AIChE Journal: Fluid Mechanics and Transport Phenomena* **2002**, *48*, 661.

(3) Ito, H. *IBM Journal of Research and Development* **2001**, *45*, 683.

(4) Dammel, R. *Diazonapthoquinone-based Resists*; SPIE Optical Engineering Press: Bellingham, Washington, 1993.

(5) Flanagin, L. W. *Ph.D. Dissertation, University of Texas at Austin*, 1999.

(6) Tsiartas, P. C. *Ph. D. Thesis, The University of Texas at Austin* **1998**.

(7) Tsiartas, P. C.; Flanagin, L. W.; Henderson, C. L.; Hinsberg, W. D.; Sanchez, I. C.; Bonnecaze, R. T.; Willson, C. G. *Macromolecules* **1997**, *30*, 4656-4664.

(8) Serjeant, E. P.; Dempsey, B. *Ionisation Constants of Organic Acids in Aqueous Solution* Pergamon: Oxford, 1979.

(9) Flanagin, L. W.; McAdams, C. L.; Hinsberg, W. D.; Sanchez, I. C.; Willson, C. G. *Abstr. Pap. Am. Chem. Soc.* **1999**, *218*, 112-PMSE.

(10) Narasimhan, B.; Peppas, N. A. *Advances in Polymer Science* **1997**, *128*, 157-207.

(11) Papanu, J. S.; Soane, D. S.; Bell, A. T.; Hess, D. W. *J. Applied Polymer Science* **1989**, *38*, 859-885.

(12) Vrentas, J. S.; Vrentas, C. M. *J. Polym. Sci. Pt. B-Polym. Phys.* **1998**, *36*, 2607-2614.

(13) Ueberreiter, K.; Asmussen, F. *Journal of Polymer Science* **1957**, *23*, 75-81.

(14) Reinhardt, M.; Pfeiffer, K.; Lorkowski, H. J. *J. Appl. Polym. Sci.* **1994**, *51*, 297-301.

(15) Peppas, N. A.; Wu, J. C.; Vonmeerwall, E. D. *Macromolecules* **1994**, *27*, 5626-5638.

(16) Papanu, J. S.; Hess, D. W.; Soane, D. S.; Bell, A. T. *J. Appl. Polym. Sci.* **1990**, *39*, 803-823.

(17) Papanu, J. S.; Hess, D. W.; Bell, A. T.; Soane, D. S. *J. Electrochem. Soc.* **1989**, *136*, 1195-1200.

(18) Papanu, J. S.; Hess, D. W.; Soane, D. S.; Bell, A. T. *J. Electrochem. Soc.* **1989**, *136*, 3077-3083.

(19) Ouana, A. C.; Carothers, J. A. *Polym. Eng. Sci.* **1980**, *20*, 160-166.

(20) Narasimhan, B. *Adv. Drug Deliv. Rev.* **2001**, *48*, 195-210.

(21) Narasimhan, B.; Peppas, N. A. In *Polymer Analysis - Polymer Physics*, 1997; Vol. 128, pp 157-207.

(22) Narasimhan, B.; Peppas, N. A. *Macromolecules* **1996**, *29*, 3283-3291.

(23) Kong, B. S.; Kim, D. *Polym.-Korea* **1997**, *21*, 270-281.

(24) Krasicky, P. D.; Groele, R. J.; Rodriguez, F. *Chem. Eng. Commun.* **1987**, *54*, 279-299.

(25) Krasicky, P. D.; Groele, R. J.; Jubinsky, J. A.; Rodriguez, F.; Namaste, Y. M. N.; Obendorf, S. K. *Polymer Engineering and Science* **1987**, *27*, 282-285.

(26) Krasicky, P. D.; Groele, R. J.; Rodriguez, F. *J. Appl. Polym. Sci.* **1988**, *35*, 641-651.

(27) Herman, M. F.; Edwards, S. F. *Macromolecules* **1990**, *23*, 3662-3671.

(28) Brochard, F.; Degennes, P. G. *Physicochemical Hydrodynamics* **1983**, *4*, 313-322.

(29) Nivaggioli, T.; Winnik, M. A. *Chem. Mat.* **1993**, *5*, 658-660.

(30) Hanabata, M.; Furata, A.; Uemura, Y. *Proc. SPIE* **1986**, *631*, 76-82.

(31) Furata, A.; Hanabata, M.; Uemura, Y. *J. Vac. Sci. Technol. B* **1986**, *4*, 430-436.

(32) Hanabata, M.; Furata, A.; Uemura, Y. *Proc. SPIE* **1987**, *771*, 85-92.

(33) Hanabata, M.; Uetani, Y.; Furata, A. *Proc. SPIE* **1988**, *920*, 349-354.

(34) Hanabata, M.; Furata, A. *Proc. SPIE* **1990**, *1262*, 476-482.

(35) Honda, K.; Beauchemin, B. T., Jr.; Hurditch, R. J.; Blakeney, A. J.; Kawabe, Y.; Kokubo, T. *Proc. SPIE* **1990**, *1262*, 493-500.

(36) Honda, K.; Beauchemin, B. T., Jr.; Fitzgerald, E. A.; Jeffries, A. T. I.; Tadros, S. P.; Blakeney, A. J. *Proc. SPIE* **1991**, *1466*, 141-148.

(37) Honda, K.; Beauchemin, B. T., Jr.; Hurditch, R. J.; Blakeney, A. J.; Kokubo, T. *Proc. SPIE* **1992**, *1672*, 297-304.

(38) Arcus, R. A. *Proc. SPIE* **1986**, *631*, 124-131.

(39) Hinsberg, W. D., et. al. *Presented at EIPBN, 2002; private communications with Dr. W.D. Hinsberg* **August, 2002**.

(40) Reiser, A.; Yan, Z. L.; Han, Y. K.; Kim, M. S. *J. Vac. Sci. Technol. B* **2000**, *18*, 1288-1293.

(41) Reiser, A.; Huang, J. P.; He, X.; Yeh, T. F.; Jha, S.; Shih, H. Y.; Kim, M. S.; Han, Y. K.; Yan, K. *Eur. Polym. J.* **2002**, *38*, 619-629.

(42) Shih, H. Y.; Reiser, A. *Macromolecules* **1997**, *30*, 4353-4356.

(43) Kim, M. S.; Reiser, A. *Macromolecules* **1997**, *30*, 3860-3866.

(44) Shih, H. Y.; Reiser, A. *Macromolecules* **1994**, *27*, 3330-3336.

(45) Shih, H. Y.; Reiser, A. *Macromolecules* **1995**, *28*, 5595-5600.

(46) Shih, H. Y.; Reiser, A. *Macromolecules* **1997**, *30*, 3855-3859.

(47) Kim, M. S.; Reiser, A. *Macromolecules* **1997**, *30*, 4652-4655.

(48) Shih, H. Y.; Zhuang, H.; Reiser, A.; Teraoka, I.; Goodman, J.; Gallagher-Wetmore, P. M. *Macromolecules* **1998**, *31*, 1208-1213.

(49) Huggins, M. L. *J. Am. Chem. Soc.* **1931**, *53*, 3190-3191.

(50) Yeh, T. F.; Shih, H. Y.; Reiser, A. *Macromolecules* **1992**, *25*, 5345-5352.

(51) Long, T.; Rodriguez, F. *Proc. SPIE* **1991**, *1466*, 188-198.

(52) Barclay, G. G.; Hawker, C. J.; Ito, H.; Orellana, A.; Malefant, P. R. L.; Sinta, R. F. *Proc. SPIE* **1996**, *2724*, 249-260.

(53) Wunderlich, J.; Schmid, G. M. *Unpublished data - available on request from C. Grant Willson, willson@che.utexas.edu* **2002**.

(54) Hall, D.; Osborne, B.; Patterson, K.; Burns, S. D. *Proc. SPIE* **2001**, *4345*.

(55) Tsiartas, P. C.; Simpson, L. L.; Qin, A.; Allen, R. D.; Krukonis, V. J.; Wetmore, P. M.; Willson, C. G. *Proc. SPIE* **1995**, *2438*, 261.

CHAPTER 3: EXPERIMENTAL MEASUREMENT TECHNIQUES

3.1 INTRODUCTION

The purpose of this chapter is to provide a description of the more complex measurement techniques used throughout this work. The intent is to provide background and descriptions of the techniques, as well as references for the interested reader. Later chapters focus on results, analysis, and conclusions, for which a basic understanding of the measurement techniques is beneficial. The three measurement techniques discussed in this chapter are reflectance interferometry, spectroscopic ellipsometry, and ^{14}C radio-labeling techniques (scintillation counting). The first two techniques are used to measure the thickness and/or index of refraction of thin films, and can be used in both static and dynamic modes. ^{14}C radio-labeling was used to determine the concentration gradient of residual casting solvent and low molecular weight polymer chains (Chapter 5 & 6) throughout a photoresist film.

3.2 REFLECTANCE INTERFEROMETRY

Historically, reflectance interferometry has been the technique most commonly used to measure the thickness and dissolution rate of thin films.[1-6] Interferometry can be used in a single wavelength or multiwavelength (spectroscopic) mode, and the latter is used throughout this work. Several commercial thin film characterization tools are available that are based upon reflectance interferometry. The reader is referred to some selected literature on the subject.[1-10] In order to understand the advantages and limitations of this technique, this section begins with a brief review of thin film interference effects.

3.2.1 Thin Film Interference Effects: A Single Film

Consider the case of a thin film (e.g. a photoresist film) supported by a reflective substrate (e.g. a silicon wafer), shown in Figure 3.1. The film has an index of refraction, $\boldsymbol{n_2}$, and the substrate has an index of refraction, $\boldsymbol{n_3}$. The film is surrounded by a medium with index of refraction, $\boldsymbol{n_1}$. In the case of photoresist dissolution, the surrounding medium is aqueous base developer. In each case, the index of refraction is a complex number, defined as $\boldsymbol{n} = n\text{-}ik$, where n represents the real index of refraction and k is the extinction coefficient, which is a measure of the absorption (attenuation) of the light wave as it propagates through a film. For this discussion and the interferometry experiments in this work, only films for which k=0 over the relevant wavelength range are considered. That is, the films are transparent and only the real part of the refractive index is important in determining the thickness.[9]

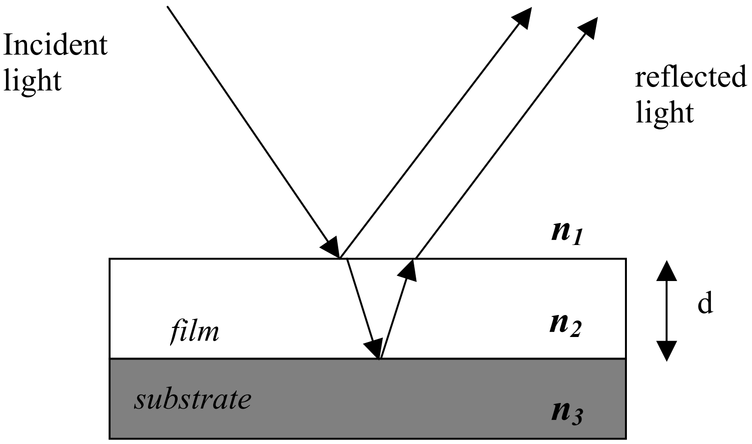

Figure 3.1 Schematic and diagram of a typical reflectance interferometry experiment

Also shown in Figure 3.1 is a beam of light striking the film that is reflected from both the substrate-film interface as well as the film-ambient interface. (Although this beam can be directed at any angle, the analysis presented here assumes that the light beam is normal to the surface. Note that the discussion of ellipsometry in section 3.3 does not utilize the same assumption.) The two reflections result in either constructive or destructive interference that is quantitatively related to the film thickness and optical constants. The electric field, E_I, associated with this incident light wave is represented by the time independent equation for propagation of an electromagnetic wave in one direction:[9]

$$E_I = E(x) = E_o e^{-i2\pi x/\lambda} \tag{3.1}$$

where E_o is the amplitude of the wave and the exponential term represents the phase variation of the wave along an axis of propagation, x. When the wave strikes the film, it is split into a reflected wave and a refracted (transmitted) wave, both of which have an amplitude that is a fraction of the amplitude of the incident wave. These fractions are given by the Fresnel equations:

$$r_{ij} = \frac{\boldsymbol{n}_i - \boldsymbol{n}_j}{\boldsymbol{n}_i + \boldsymbol{n}_j} \quad \text{and} \quad t_{ij} = \frac{2\boldsymbol{n}_i}{\boldsymbol{n}_i + \boldsymbol{n}_j} \tag{3.2}$$

where r_{ij} and t_{ij} are the reflection and transmission coefficients for a light wave transmitted from layer i to j. Note that there are many reflections and transmissions, as the light wave reflected off the substrate is partially reflected back into the film, resulting in an infinite series of reflections and transmissions. Using the Fresnel equations, and employing a converging infinite series, it can be shown that the total reflected amplitude is:

$$R = \frac{r_{12} + r_{23}e^{-i4\pi \mathbf{n} x/\lambda}}{1 + r_{12}r_{23}e^{-i4\pi \mathbf{n} x/\lambda}} = \frac{r_{12} + r_{23}e^{-i2\delta}}{1 + r_{12}r_{23}e^{-i2\delta}} \tag{3.3}$$

where $\delta = 2\pi nd/\lambda$ is known as the phase thickness.[9] This describes the phase change that occurs every time a wave traverses the full thickness of the film. The expression in equation (3.3) represents a complex value. The physical reflectance (or reflectivity) is the complex conjugate of this value:[9]

$$\boldsymbol{R}\,(\lambda, d) = |R|^2 = \frac{r_{12}^2 + 2r_{12}r_{23}\cos 2\delta + r_{23}^2}{1 + 2r_{12}r_{23}\cos 2\delta + r_{12}^2 r_{23}^2} \qquad (3.4)$$

Equation (3.4) describes the reflectivity spectrum for a film stack. In Figure 3.2, this value is plotted as a function of wavelength and film thickness, which produces a three dimensional sinusoidal surface with periodic maxima and minima in both λ and d. It is clear from Figure 3.2 that a given inteference spectra corresponds to a unique film thickness (if the optical constants are known). In this manner the film thickness can be rigorously determined from analysis of the interference spectra.[9,10]

A convenient method for calculating the film thickness is to determine the number of peaks and their locations in the interferogram (as opposed to rigorously fitting the entire spectrum). At the local extrema of equation (3.4), the reflectance reaches a maximum that corresponds to the cosine term of equation (3.4) having a value of +/- 1 (depending on whether the extrema is a maximum or a minimum). This is equivalent to seeking the solution to the equation cos (2δ) = +/- 1, for which the solution is $2\delta = f\pi$, where f is any integer. Substituting into the equation for the phase thickness:

$$d = \frac{f \cdot \lambda}{4n_2} \qquad (3.5)$$

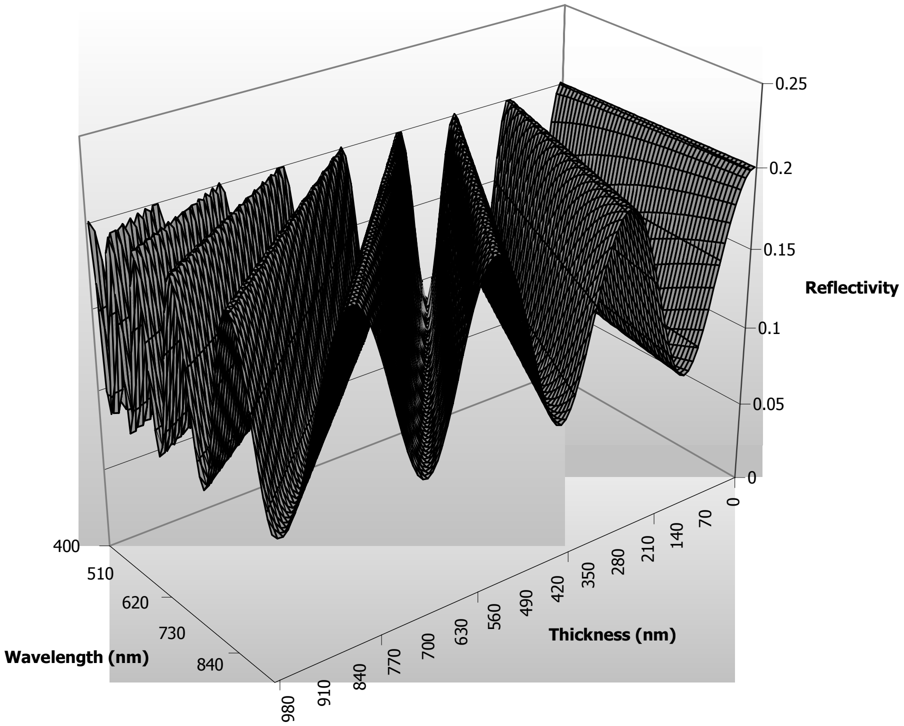

Figure 3.2 3-D plot of Equation 3.4, showing reflectivity plotted against film thickness and wavelength of the incident light

where the integer f is labeled the fringe order for each peak (node) in the interference spectrum.[7,10]

To this point in the discussion, it has been assumed that the index of refraction of the film does not vary with wavelength. This assumption is not usually valid. The index of refraction of many materials in transparent regions ($k = 0$) is well described by the three parameter Cauchy model:[9]

$$n(\lambda) = A + \frac{B}{\lambda^2} + \frac{C}{\lambda^4} \qquad (3.6)$$

where A, B, and C are empirical parameters known as the Cauchy coefficients. These coefficients can be measured by spectroscopic ellipsometry, and the details of this measurement are discussed in Section 3.3.

3.2.2 Extension to a case of multiple layers

Many applications require the use of multiple layers of films. For characterization purposes it is beneficial to extend the calculations presented above to the case of a film stack of two or more layers. The procedure for this analysis is known as Rouard's treatment, and is described in many reviews. A computationally convenient method for implementing this treatment is known as the characteristic matrix method, developed by Abeles, and also described in detail by many sources.[2,3,11] For this work, analysis of a multilayer stack by the methods described above has been useful for investigating the existence of interfacial gel layers, and is discussed further in Chapter 7.

3.2.3 Single Wavelength Interferometry

The simplest form of interferometry is single wavelength interferometry, in which a monochromatic light source is used to measure the dissolution rate of polymer films. The films (coated onto a substrate, usually silicon) can be immersed in a bath of the developer solution, or a puddle of the developer can be poured onto the film. These processes are known as immersion and puddle development, respectively. The light source (for example, a He-Ne laser, with λ=633 nm) is reflected off of the substrate, and the reflected intensity is measured. For a static film, this value is a single data point, and it is not possible to determine the film thickness. However, for a dissolving film the reflected intensity changes in a sinusoidal manner as the film thickness decreases, and the reflected intensity oscillates through a series of constructive and destructive interference effects. The change in thickness from one peak to another (maximum to minimum, or node to node) can be calculated as:

$$\Delta d = \frac{\lambda}{4 \cdot n_2} = \frac{633nm}{4 \cdot 1.6} \approx 100\,nm = 0.1\,\mu m \qquad (3.7)$$

For incident light of 633 nm, and a film of n = 1.6, the change in film thickness between adjacent nodes is approximately 100 nm. A theoretical curve of reflectivity plotted against film thickness is shown in Figure 3.3. Since the time between the nodes is also easily recorded, the change in film thickness over time (the dissolution rate) is easily calculated. Also, the reflectivity will remain constant after the entire film has dissolved. At the point when the reflectivity stops changing, the film thickness is assigned d = 0, and each node is then assigned an absolute film thickness, a so-called "bottom up" analysis. A schematic of this analysis is shown in Figure 3.4.[1,2,9]

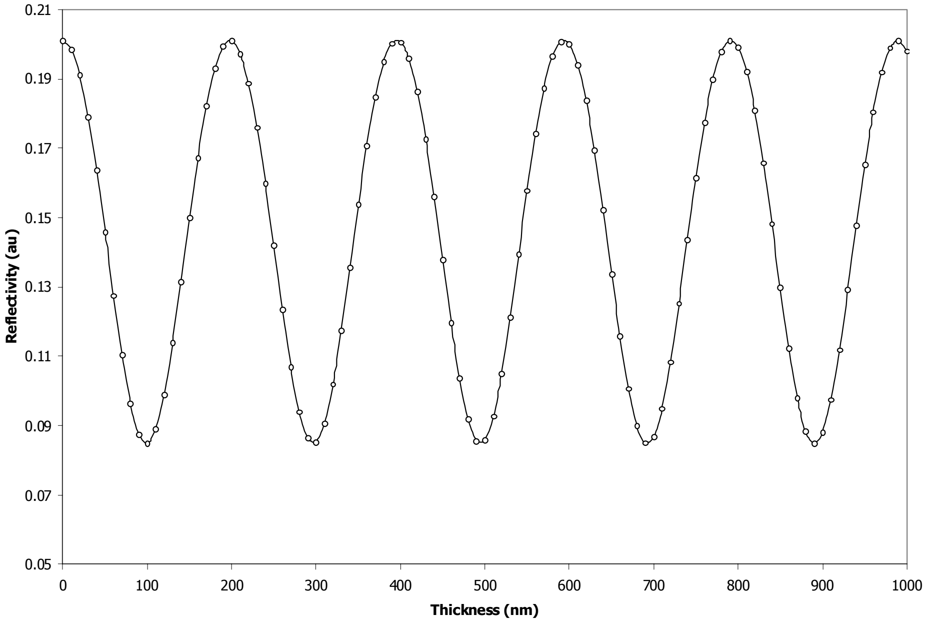

Figure 3.3 A theoretical single wavelength reflectance curve for a hypothetical dissolution rate experiment. (assuming n_1~1.6)

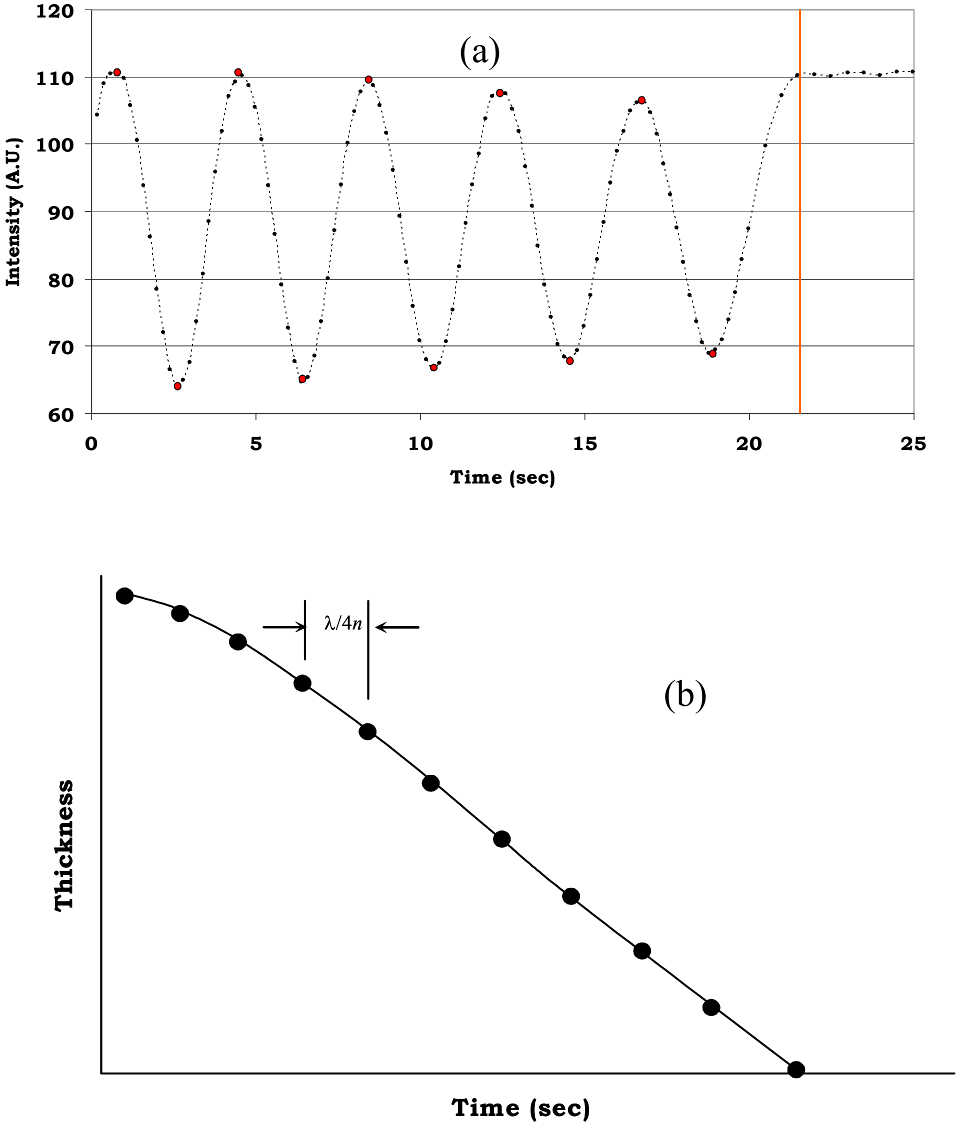

Figure 3.4. (a) An experimental interferogram of a novolac film dissolved in aqueous base. The results of the single wavelength data analysis are shown in (b).

However, a single wavelength experiment (with no other experimental characterization) has some limitations. First, ideal dissolution behavior is already assumed, which can lead to misinterpretation of data in some cases. For example, suppose a film swelled slightly and then equilibrated at a constant thickness. The change in reflectivity would be very similar to the case of a dissolving film, yet the physical process is significantly different. Also, films may lose adhesion from the substrate in the process of dissolution, which results in a "false zero" point and inaccurate thickness calculations. For these reasons, multiwavelength interferometry is a preferred technique.

3.2.4 Multiwavelength Interferometry

A multiwavelength interferometry analysis exploits the advantage of the additional information available in the third dimension in Figure 3.2.[1,2,9] A white light source (typically a halogen light source) is used to produce the visible spectrum of light which is reflected from a resist coated wafer. With each data set acquired, a unique thickness can be determined by matching the shape of the reflectivity spectrum to that predicted by Equation 3.4. There are two methods for analyzing the experimental data. The first is to rigorously fit the entire curve to a model calculation. One drawback of this technique is that it is computationally intensive. Another drawback is that the experimental reflectivity is sometimes offset slightly from the theoretical prediction due to sample nonideality, focusing errors, signal attenuation, or other unforeseen experimental errors. However, the positions of the peaks are insensitive to these types of *dc* offset errors. Thus, the second technique is a peak finding method in which (similar to the single wavelength data) the number and position of peaks in the spectrum is determined, and the thickness is calculated. The exact methods for peak finding and for computing the thickness have been well reported[1,7,9,10] and will not be reviewed here. Finally, multiwavelength interferometry is advantageous because in addition to rigorously determining the film thickness at each data point, the data can also be analyzed as multiple single wavelength experiments. This is especially useful near the end of dissolution, when the film is too thin for a substantial number of peaks to be found in the spectral data. All of the dissolution rates measured in this work are the result of a combination of both multiwavelength and singlewavelength analysis, a technique that provides very accurate dissolution rate data.[1,2,9,10]

Figure 3.5 shows a diagram of a multiwavelength interferometer used in this work. A fiber optic bundle transmits white light from a halogen source to the sample. The central fiber transmits the detected light to an Ocean optics spectrometer, with a maximum data acquisition rate of 12 Hz. A labview program records the spectra as a function of time, and separate labview and Visual Basic programs are used for data analysis.[1]

Finally, multiwavelength interferometry has been used throughout this work to measure the dissolution rates of photoresist films as a function of thickness, molecular weight, developer concentration, etc. It is an invaluable tool for evaluating new photoresist materials and determining dissolution behavior. However, the analysis presented here relies on the assumption that the index of refraction of the film (as a function of wavelength) is known prior to the measurement. In theory, it may be possible to calculate the Cauchy coefficients and the thickness of the film from multiwavelength interferometry data alone. Again, this requires an ideal experiment, and the uniqueness of this four parameter fit becomes significantly worse with decreasing film thickness. No commercial tool exists which provides thickness and index without some *a priori* knowledge of the optical constants. Therefore, variable angle spectroscopic ellipsometry (VASE) has been used to determine the index of refraction before measuring the dissolution rate. Recent advances in spectroscopic ellipsometry have allowed rapid data acquisition and it is now possible to use ellipsometers to measure dynamic thin film processes, such as photoresist dissolution. A demonstration of the utility of a spectroscopic ellipsometer in measuring dissolution rates of photoresists is presented in Chapter 7. A review and description of spectroscopic ellipsometry is now presented in the following section.

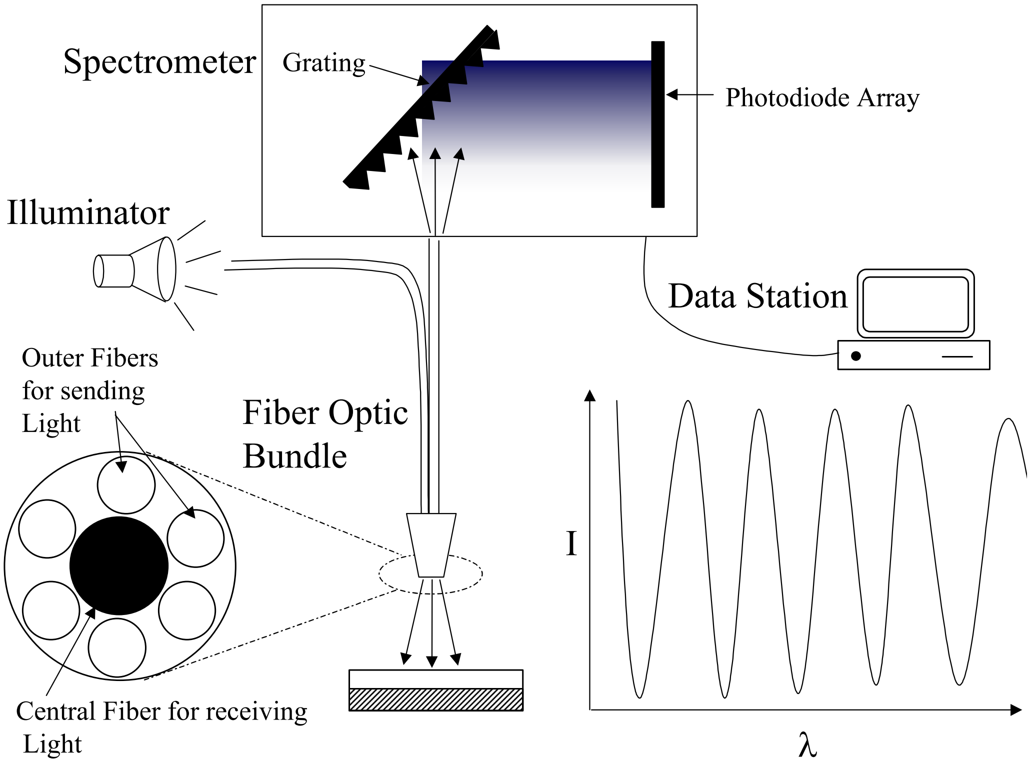

Figure 3.5 Diagram of a multiwavelength interferometer

3.3 SPECTROSCOPIC ELLIPSOMETRY

Spectroscopic ellipsometry is similar to interferometry in many ways and the two techniques are often confused. In both cases, a beam of white light is reflected from a resist coated substrate and changes in the reflected beam are measured and analyzed to determine the structure of the film (film thickness and/or optical properties). The primary difference is that in the case of ellipsometry the light is purposely polarized before striking the sample. Changes in the polarization states are measured by the ellipsometer, and this information is used to determine film optical constants and film thickness.[9,12,13]

3.3.1 The Fundamental Equation of Ellipsometry – Defining ψ and Δ

The mathematical description of light given in Equation 3.1 is inadequate to describe the function of an ellipsometer. This is because the wave of light is described as a two dimensional structure in which the entire wave is contained in a single plane. For many applications, this is both a convenient picture of a light wave as well as a convenient mathematical analysis. However, light actually travels as a three-dimensional wave, much like an elongated spring. If one were to look directly down the path of an individual photon, there are three general cases that properly describe the wave, shown schematically in Figure 3.6. First, the light could be traveling as a perfectly cylindrical wave. That is, the magnitude of the electric vector in the plane normal to the direction of propagation is constant in any direction. In this case the light is said to be *circularly polarized*. The other extreme case is that the light could be traveling such that this vector oscillates in a single plane, and this case is termed *linearly polarized*. Intermediate cases are known as *elliptically* polarized light, which is the origin of

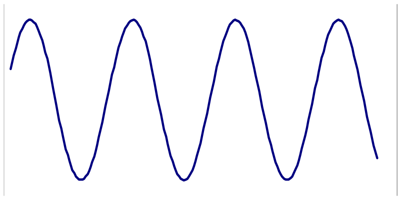

2-D light wave

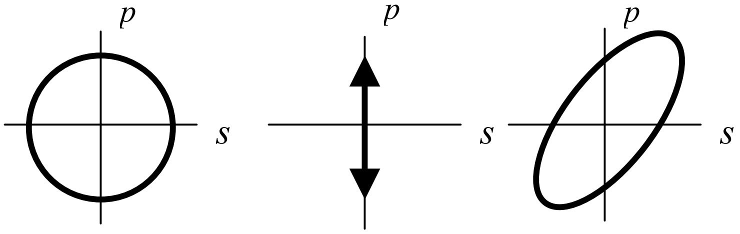

Circularly polarized light

Linearly polarized light

Elliptically polarized light

Figure 3.6 Description of the time averaged position of the electric vector during propagation of various polarization states of light.

the term “ellipsometer”. An ellipsometer measures changes in the ellipticity of the polarized light.[9]

Figure 3.7 shows the geometry of a typical ellipsometer measurement. Light of known polarization is projected onto a sample with an angle of incidence, θ. The incident beam and the reflected beam define a plane known as the plane of incidence or the *p* plane. The plane perpendicular to the “*p*” plane (and also normal to the sample) is called the *s* plane. The light wave has a unique amplitude, *A*, in both the *p* and *s* plane (A_p and A_s, respectively). Similarly the light wave has a unique phase, δ, in both the *p* and *s* plane (δ_p and δ_s, respectively). All of these values undergo predictable changes as a result of their interaction with the sample, such that the incident value is different from the reflected value. It is now possible to define two values, Δ and ψ, which described the change in amplitude and phase of the light upon reflection:

$$\varphi = \frac{A_p^r / A_s^r}{A_p^i / A_s^i} \tag{3.8}$$

$$\Delta = \left(\delta_p^r - \delta_s^r\right) - \left(\delta_p^i - \delta_s^i\right) \tag{3.9}$$

where the superscripts *i* and *r* refer to the incident and reflected light beams, respectively. Another value, ρ, called the "ellipticity", is defined as the complex ratio of the total reflection coefficients (in the *p* and *s* plane), and is related to ψ and Δ:

$$\rho = \frac{R_p}{R_s} = \tan\varphi e^{i\Delta} \tag{3.10}$$

Equation 3.10 is known as the fundamental equation of ellipsometry. An ellipsometer measures only the quantities ψ and Δ, and is not capable of directly measuring either a film thickness or optical constants. Once the values for ψ and

Δ have been obtained, an ellipsometer is very much like a reflectometer. Both are model based techniques in which the experimental behavior of light is compared to predicted behavior of light, based upon a guessed film thickness and/or optical constants. If there is a sufficient match (based on a predetermined merit function) between the experimental and predicted behavior, then the model parameters are considered to be correct.[9,13]

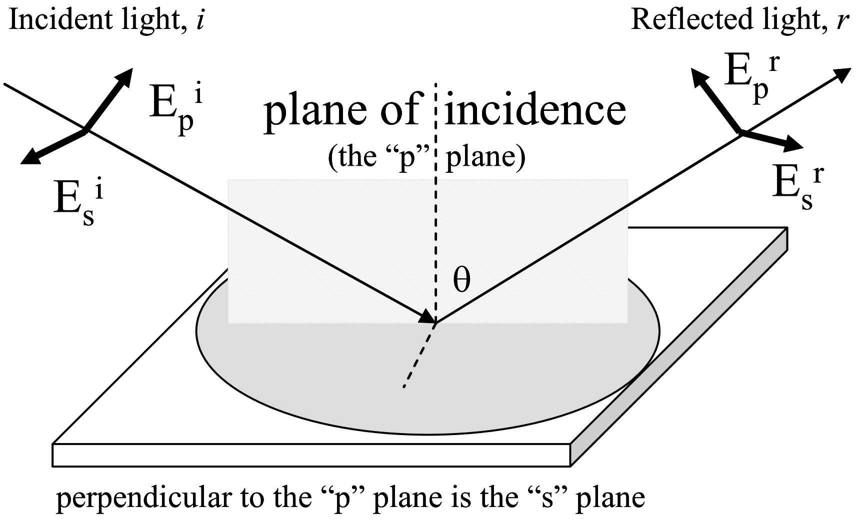

Figure 3.7 Geometry of a typical ellipsometry experiment

The equations that describe ψ and Δ as a function of film thickness, optical constants, wavelength, and incident angle are rather complicated and available elsewhere.[9] Furthermore, several software packages exist that are capable of performing these calculations, as well as regression fitting the model data to experimental data. The WVASE32 software package available from J.A. Woollam was used for the data analysis in this work.

3.3.2 Representative Data

Figure 3.8 shows the measured ψ and Δ parameters for a common photoresist coated onto a silicon substrate. Spectroscopic data were taken from a range of 400-1000 nm at three incident angles (65, 70 and 75°). Also shown is the model fit to the data, with a mean squared error (MSE) of 22.8. (MSE is the merit function used by WVASE32 to determine the quality of the fit to the experimental data. It is defined elsewhere.[9]) A four parameter model was used, with the thickness (*d*) and three Cauchy coefficients (*A*,*B*, and *C*) allowed to vary. The best-fit parameters are listed in Table 3.1. There are several salient features of this example data set that are explained below.

First, note that the data is acquired with a light beam at an incident angle of 65-75°. (In contrast, reflectometry almost always involves a normal incident angle.) The reason is that the best signal to noise ratio is obtained if the difference between the intensities of the *p*-wave and *s*-wave are maximized. This maximum usually occurs at the Brewster angle, which is defined as the angle for which the reflectance of the *p*-wave is zero. For a bare silicon wafer, the Brewster angle is ~70°. As films are added, the Brewster angle may shift to a

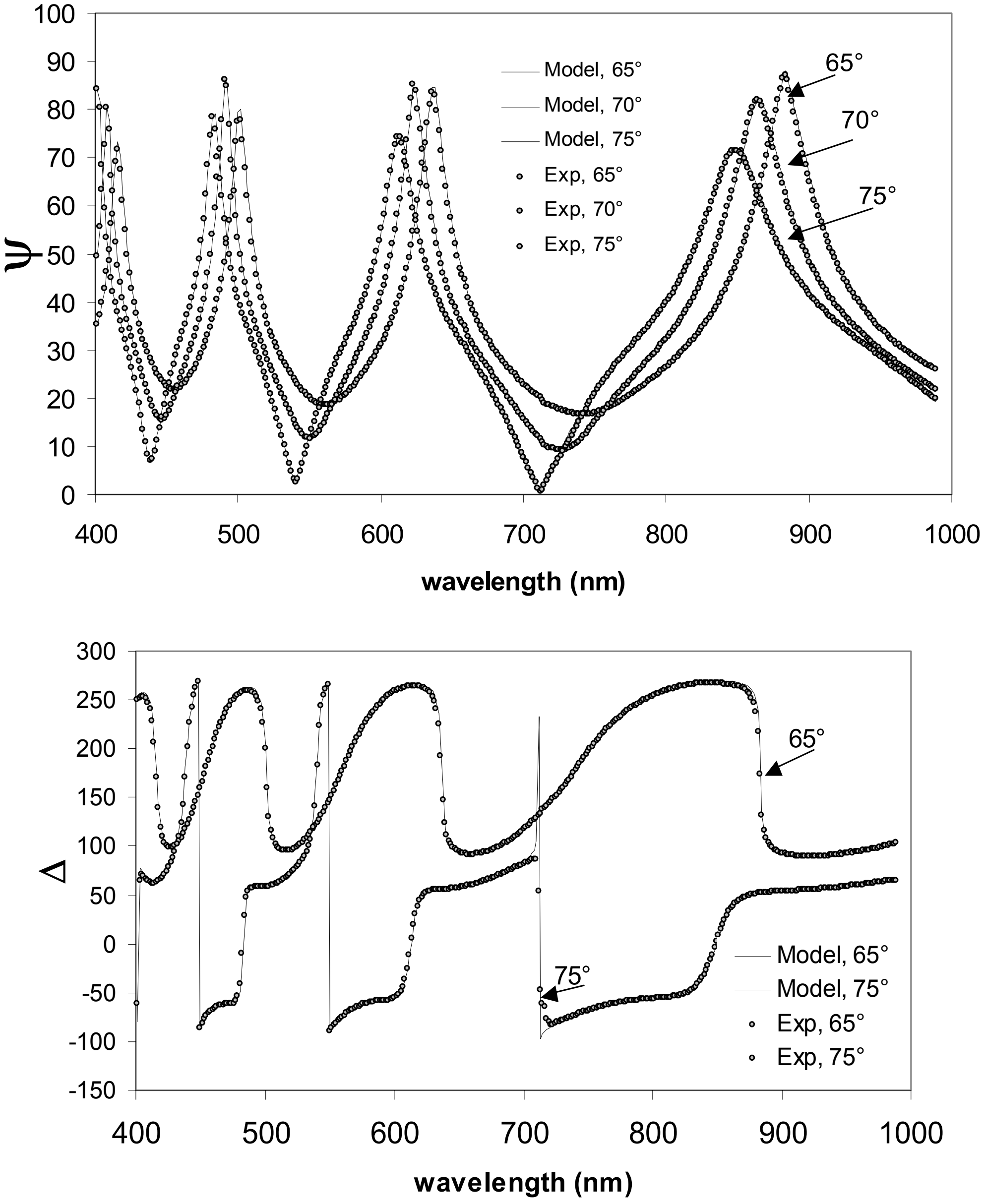

Figure 3.8 Typical spectroscopy ellipsometry data for a common photoresist film coated on an Si substrate. Model fits to the experimental data are also shown.

Table 3.1 Model parameters, by fitting the experimental data of Fig. 3.8

Model parameter	Value
thickness, *d*	916.68±0.27
A	1.4964±0.0002
B	0.00695±0.0001
C	7.62e-005±1.7e-005
MSE	22.79

"pseudo" Brewster angle, but the shift is usually not large.[9] Therefore, when characterizing films on a silicon substrate, it is beneficial to obtain ellipsometric data with an incident angle near 70°. However, it is also beneficial to obtain experimental data over a range of incident angles.

Second, the model parameters are determined by fitting the entire non-linear spectrum of ψ and Δ experimental data to a generated model. In contrast, interferometry analysis typically involves fitting only the peak locations. The reason is the absolute intensity of the reflected beam does not affect the measurement of ψ or Δ, because ψ is a measure of the ratio of the reflectance in the *p* and *s* plane. In contrast, interferometry does rely upon the absolute reflectance, but this value can be altered by many factors such as sample roughness, sample tilt, *etc*., that cannot necessarily be controlled in every experiment. Thus, it is often not practical to rigorously fit the entire curve from a reflectance interferometry experiment.[7]

Third, note that it is possible to obtain four parameters from the model fit. The general explanation is that two parameters (ψ and Δ) are measured, therefore two parameters can be determined (thickness and index). However, that argument is valid at every wavelength, so it is possible to determine both the film thickness, and the index of refraction at each wavelength measured. The Cauchy equation (Eq 3.6) provides a convenient relation to reduce the total number of parameters. The determination of four parameters is therefore straightforward.[9]

Fourth, it is important to restate that both ellipsometry and interferometry are model based techniques. *The models used to determine fit parameters always contain important assumptions, and it is necessary to validate these assumptions*. The two primary assumptions used throughout this work are that the film is (a) homogeneous and uniform, and (b) that the film is transparent in the spectral region under consideration (k=0). If the film is slightly absorbing, the Cauchy relation is not valid. The first assumption can usually be tested by profilometry and/or AFM in certain cases. The second assumption (k=0) may require *a priori* knowledge of the absorption spectrum of the polymer under consideration. However, poor data fits near the UV region of the spectrum usually indicate slight absorption, but this problem is easily solved by analyzing a higher wavelength region. These assumptions will also be discussed in Chapter 7.

In summary, spectroscopic ellipsometry is very useful for determining the film thickness and optical constants of thin films, and thin film stacks. Recent advances in ellipsometry hardware have allowed rapid data acquisition. The newest version of the J.A. Woollam M-2000 has a maximum data rate of 47 Hz, over a wavelength range of 366-1000 nm. This capability allows for experimental study of films that are changing dynamically, which is extremely beneficial for studying almost every step of the lithographic process, as well as thin film thermal properties. Our research group has recently demonstrated the usefulness of dynamic ellipsometry in studying post exposure bake kinetics, photoresist dissolution, water sorption, and fundamental studies of top surface image processing. Throughout this work, ellipsometry is used to determine Cauchy coefficients for inteferometry analysis of photoresist dissolution.

3.4 ^{14}C RADIOLABELLING OF RESIDUAL CASTING SOLVENT

Radioisotope labeling of molecules has been used extensively as a “tracer” technique to monitor position and quantity of a given molecular species in complicated systems.[14-17] Two main advantages of radiolabeling techniques are the labeling does not change the chemistry of the system and the techniques are extremely sensitive to low concentrations. For these reasons, radiolabeling has been used as a method to determine the concentrations of individual photoresist components after processing, primarily to measure the amount of residual casting solvent.[14] Radiolabeling was also used to measure the concentration gradient of a specific molecular weight polymer in a photoresist film, as demonstrated in Chapters 5 & 6.

In this work, ^{14}C was chosen as the radioisotope (as opposed to ^{3}H) because it has a higher detection signal, is very similar to ^{12}C, and is not likely to exchange with non labeled atoms.[14] The two radiolabeled casting solvents used in this work were propylene glycol methyl ether acetate (PGMEA) and methoxyethylether (diglyme). The radiolabeled polymer was various fractions of low molecular weight novolac. The structures of these molecules are shown in Figure 3.10. The synthesis and characterization of these molecules has been reported elsewhere.[14] The remainder of this section provides a brief description of radioactive decay and liquid scintillation counting, which was the method used to detect the radiolabeled molecules. Detailed descriptions of liquid scintillation counting are available[15-18], and the PhD dissertation of Gardiner[14] discusses some specific issues directly relevant to the measurements made in this work.

3.5.1 Radioactive Decay

Many elements have naturally occurring, unstable isotopes that are radioactive because the nuclei of these isotopes undergo random disintegration, or nuclear decay. The rate of decay is called the activity, and the SI unit for activity is the curie (Ci), which is defined as 3.7×10^{10} nuclear disintegrations per second. (Note that the activity is sometimes confused with specific activity, which is the rate of decay per unit mass, typically expressed in units of Ci/g. It is necessary to measure the specific activity of a tracer prior to performing an experiment, if the

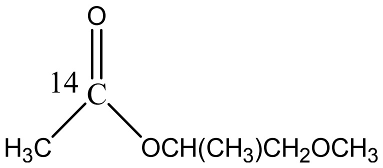

PGMEA (casting solvent)

$CH_3OCH_2CH_2OCH_2CH_2O^{14}CH_3$

diglyme (casting solvent)

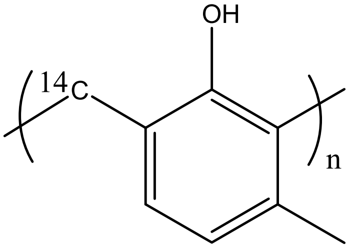

labeled novolac polymer

Figure 3.10 Chemical structure of radiolabeled molecules used in this work

mass of the radiotracer is to be determined quantitatively.) Nuclear decay produces three types of radiation: alpha, beta, and gamma. ^{14}C undergoes beta decay, which is ejection of an electron. ^{14}C produces electrons with a maximum kinetic energy of 156 keV, and a the isotope has a half-life of 5730 years. The long half-life adds to the convenience of this radiolabel, because half-life corrections are not needed on the time scale of the experiment.

3.5.2 Detection of Radioactive Decay: Liquid Scintillation Counting

There are a few known methods for detecting radiation, but scintillation counting has the highest sensitivity and is applicable for a wide range of materials. This technique utilizes a fluorescent material known as a scintillator to convert radiation energy into photons. The photon signal is measured by a photomultiplier tube and converted to an electronic signal. There are two types of scintillation counters: liquid and solid. Liquid scintillation counting (LSC) involves immersing the radioactive sample and the scintillator in a common solvent. This allows intimate contact between the radiation and scintillators, so the transport distance of the radiation is short,[15-18] which is ideal for types of radiation that do not have large penetration depths. ^{14}C beta decay, for example, has a maximum range of 24 cm in air and 1 cm in plexiglass. Liquid scintillation counting has been used in this work and others to determine the concentration of residual casting solvent in photoresist films.[14]

The calibration of an LSC machine requires a detailed understanding of the detection process. Figure 3.11 shows a diagram of the general LSC process. First, the sample with an unknown amount of radiolabeled tracer is dissolved into a solution known as a scintillation cocktail, which contains (at least) one solvent and one scintillator. Most cocktails have additional solvents and scintillators. Typical solvents used are toluene, xylenes, or naphthalene, and a typical secondary solvent is cellosolve (2-ethoxy-ethanol). A typical scintillator is PPO (2,5-diphenyl oxazole).

The purpose of the scintillator is to convert the radiation energy into photons within the visible range. Often, a second scintillator is used to shift the photo energy to a wavelength that can be detected more efficiently by the photomultiplier tube. The secondary scintillator also improves the efficiency of the cocktail solution.

In the detection process, the first step is the nuclear decay of a radiolabeled tracer element. The emitted radiation comes into contact with scintillation cocktail components, primarily the solvent molecules. The kinetic energy of the radiation is transferred to the cocktail producing excited solvent molecules, solvent ions and electrons, molecular fragments, etc. The excited solvent molecules may transfer energy between other solvent molecules, and the primary scintillator. The primary scintillator is raised to an electronic excited state and then emits a photon. Often, a secondary scintillator absorbs this photon and reemits a photon at a longer wavelength, where the detector has higher efficiency. The detector is usually a photomultiplier tube.

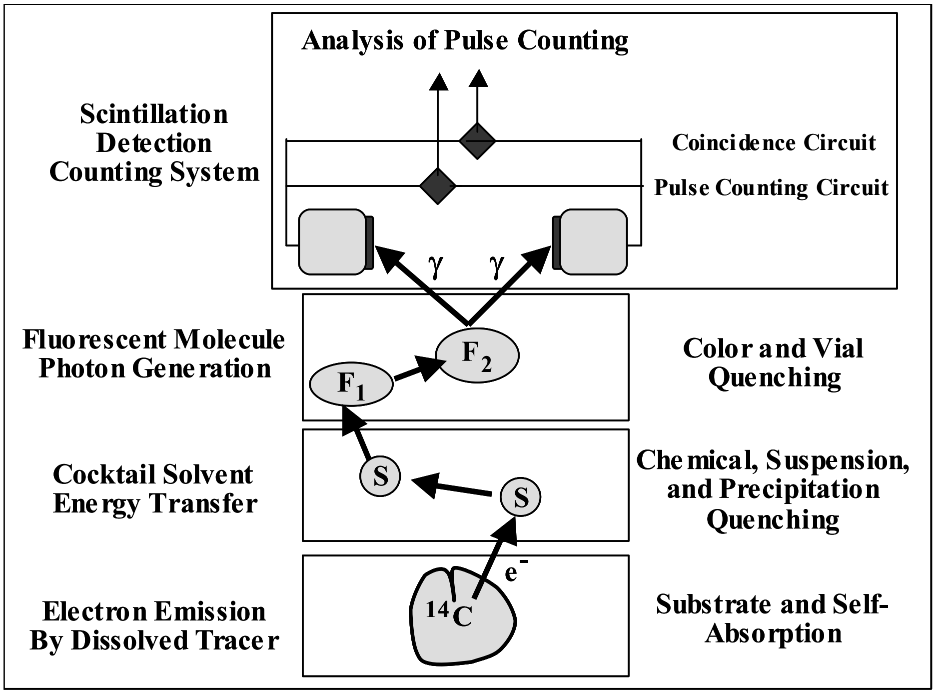

Figure 3.11 Diagram of scintillation counting, along with typical quenching mechanisms that may occur

In theory, each nuclear decay (disintegration) should result in exactly one detected photon (one count). However, many processes occur that can decrease the expected photon signal, and these are referred to as “quenching”. The factor by which the counts per minute (CPM) are decreased compared to the disintegrations per minute (DPM) is the efficiency of the sample:

$$Efficiency = \frac{CPM_{total}}{DPM} \tag{3.13}$$

The efficiency can be decreased by various quenching mechanisms: self-absorption, chemical, suspension, precipitation, vial, and color quenching are all possible ways to the lower the efficiency. It is not necessary to know exactly which mechanism is causing the efficiency loss, so long as the efficiency can be accurately measured for each sample. However, it is helpful to have a general knowledge of what chemical species (that may be present in the sample) cause significant quenching, because it is desirable to maximize the efficiency when possible.

The efficiency is measured by a method known as the "H-number" technique developed by Horrocks.[16,17] This technique involves placing a gamma-ray radiation source close to the sample, and a fraction of the gamma photons undergo Compton scattering. This process results in a photon of lower energy and an electron with energy approximately equal to the difference in energy of the two photons. The Compton scattering produces electrons with a spectrum of energies equal to that of beta particle decay, and thus these electrons are quenched in the same manner. In this case, however, it is possible to quantify the amount of quenching. The $H^{\#}$ is defined as:

$$H^{\#} = b \ln\left(\frac{E_o}{E_q}\right) \tag{3.14}$$

where E_o is the unquenched Compton edge at the inflection point, E_q is the quenched Compton edge at the inflection point, and b is a machine factor determined by the LSC manufacturer. Equation 3.14 allows for an $H^{\#}$ determination for a given sample, but does not provide a direct method for determining the efficiency. A calibration curve must be measured to determine the relationship between $H^{\#}$ and efficiency. The calibration curve is made by preparing samples with known amounts of radioactive tracer, but otherwise very similar to other samples. For example, varying amounts of dissolved photoresist material are mixed with known amounts of radioactive casting solvent and scintillation cocktail. Because the samples have a known amount of radiation, the efficiency can be calculated, and the $H^{\#}$ can be independently measured. Thus, a calibration curve of the form:

$$\ln(Efficiency) = f\left(H^{\#}\right) \tag{3.15}$$

where $f(H^{\#})$ is typically a 3rd order polynomial, is obtained. The specific procedure and calibrations curves for the radio-labeled residual casting solvent data presented in Chapter 5 and 6 have been reported in the dissertation of Gardiner.[14]

Ultimately, a measure of the mass of tracer in a given sample is the desired result. This quantity is determined by the following set of relations:

$$mass_{tracer} = \frac{DPM_{sample}}{SA_{tracer}} \tag{3.16}$$

$$DPM_{sample} = \frac{CPM_{sample} - CPM_{background}}{Efficiency} \tag{3.17}$$

where SA_{tracer} is the specific activity of the tracer (units of Ci/gram, or disintegrations per time per mass), and $CPM_{background}$ is the measured counts per minute due to background radiation. Both of these quantities can be easily measured. The background signal is determined by monitoring the CPM of a vial with only scintillation cocktail present. The specific activity can be measured by LSC with a pure sample of radioactive tracer.[17,18]

In summary, to make accurate measurements of the mass of radiolabeled tracers, it is necessary to quantify the background radiation, the specific activity of the pure radiolabeled substance, and the amount of quenching (signal loss) created by each sample. In this manner, it is possible to quantify the amount of residual casting solvent remaining in photoresist films under a variety of processing conditions, as well as the amount of low molecular weight polymer fractions. Using a separation technique, it has also been possible to determine the concentration gradient of residual casting solvent and low molecular weight polymer species throughout a photoresist film. These results are presented in Chapters 5 & 6.

3.6 REFERENCES

(1) Tsiartas, P. C. *Ph. D. Thesis, The University of Texas at Austin* **1998**.

(2) Scheer, S. A.; Brodsky, C. J.; Robertson, S. A.; Kang, D. *Proc SPIE* **2002**, *4689*, 937-948.

(3) Nivaggioli, T.; Winnik, M. A. *Chem. Mat.* **1993**, *5*, 658-660.

(4) Krasicky, P. D.; Groele, R. J.; Rodriguez, F. *Chem. Eng. Commun.* **1987**, *54*, 279-299.

(5) Arcus, R. A. *Proc. SPIE* **1986**, *631*, 124-131.

(6) Thompson, L. F.; Willson, C. G.; Bowden, M. J. *Introduction to Microlithography*; 2nd ed.; American Chemical Society: Washington D.C., 1994.

(7) Scheer, S. A. *MS Thesis: Design of Development Rate Monitoring Software and Measurement of Photoacid Concentration in Chemically Amplified Resists*; The University of Texas at Austin, 2001.

(8) Robertson, S. A.; Kang, D.; Scheer, S. A.; Brodsky, C. J. *Proc. SPIE* **2002**, *4689*, 213-222.

(9) Tompkins, H. G.; McGahan, W. A. *Spectroscopic Ellipsometry and Reflectometry: A User's Guide*; Wiley: New York, 1999.

(10) Henderson, C. L. *PhD Dissertation, The University of Texas at Austin* **1998**.

(11) Heavens, O. S. *Optical Properties of Thin Solid Films*; Dover Publications: New York, 1965.

(12) Azzam, R. M. A.; Bashara, N. M. *Ellipsometry and Polarized Light* North-Holland, Amsterdam, 1988.

(13) Styrkas, D.; Doran, S. J.; Gilchrist, V.; Keddie, J. L.; Lu, J. R.; Murphy, E.; Sackin, R.; Su, T.-J.; Tzitzinou, A. *Application of Ellipsometry to Polymers at Interfaces and Thin Films*; John Wiley & Sons: New York, 1999; Vol. III.

(14) Gardiner, A. B. *PhD Dissertation*; The University of Texas at Austin: Austin TX, 1999.

(15) Gibson, J. A. B. *Liquid Scintillation Counting Recent Applications and Developments*; Academic Press: New York, 1980.

(16) Horrocks, D. L. *Applications of Liquid Scintillation Counting*; Academic Press: New York, 1974.

(17) Horrocks, D. L. *Liquid Scintillation Science and Technology*; Academic Press: New York, 1976.

(18) Howard, P. L. *Basic Liquid Scintillation Counting*; American Society of Clinical Pathologists: Chicago, 1976.

CHAPTER 4: THEORETICAL CALCULATION OF ELECTROSTATIC DOUBLE LAYER DURING PHOTORESIST DISSOLUTION*

4.1 COULOMBIC EFFECTS DURING PHOTORESIST DISSOLUTION

In Chapter 2, it was stated that the critical ionization (CI) lattice model did not explicitly consider the hydroxide ions in the developer solution. The fraction of ionized surface sites (α) was calculated, but coulombic interaction between the ionized polymer chains and the developer solution had not yet been considered. More importantly, α was calculated by considering an equilibrium, homogeneous solution, as opposed to a heterogeneous flat film. In this chapter, the dissolving photoresist film is envisioned as a planar, charged surface, which contributes a coulombic force to the adjacent developer ions. This "electrostatic double layer" may influence the local hydroxide ion concentration near the film surface, and thus change the dissolution rate of the polymer film. More importantly, the model parameters (such as the fraction of ionized sites, α) are altered by this effect. A continuum model is demonstrated that can be used to calculate corrected parameter values, and a recent stochastic approach to this problem is discussed at

*Reproduced in part with permission from S.D. Burns, G.M. Schmid, P. Tsiartas, C.G. Willson, *J. Vac. Sci. Tech. B*. Copyright 2001 the close of the chapter. The stochastic approach allows for consideration of finite ion size effects, film roughness and feature topography.

4.2 INCLUDING COULOMBIC EFFECTS IN THE CI MODEL

Consider a charged, flat plate that is adjacent to an electrolyte solution. Near the plate, ions of opposite charge will be attracted to the charged plate. This effect is known as an electrostatic "double layer", shown in Figure 4.1. The "double layer" refers to a layer of, in this case, negative charges fixed to the surface and the adjacent layer of positive ions that form due to coulombic forces.[1] Similarly, negative ions will be repelled from the surface. This situation has been studied for many systems, most commonly in the area of electrochemistry, in which a charged electrode surface is in contact with an electrolyte solution.[2] Here,

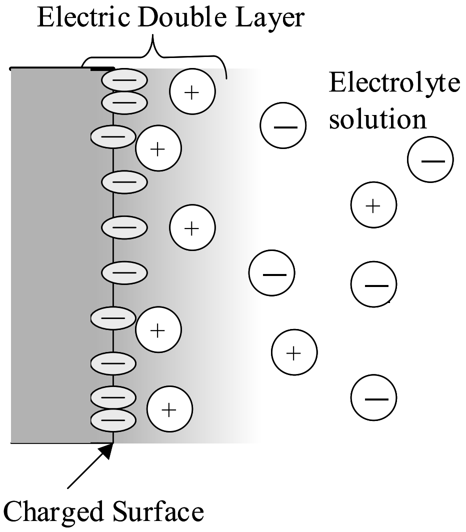

Figure 4.1 A charged surface next to an electrolyte solution forms an electrostatic double layer.

we apply this problem to the dissolution of a photoresist film, shown in Figure 4.1. In order to use a similar continuum approach, it is necessary to assume that the surface of the film is flat and that significant ion penetration does not occur into the film. The validity of these assumptions will be discussed at the end of the chapter, as well as in Chapters 7 and 8. The goal of this analysis is to quantitatively determine how the CI model parameters (specifically, the fraction of ionized sites, α) are altered by consideration of the electrostatic double layer.

4.3 SOLUTION OF THE POISSON-BOLTZMANN EQUATION

Israelachvili[1] provides an excellent discussion and many examples that quantify electrostatic surface charges on flat surfaces in contact with electrolyte solutions. These examples have been applied to a polymer film dissolving in aqueous base. The governing equation for this system is the Poisson-Boltzmann equation:[1]

$$\frac{d^2\psi}{dx^2} = -\left(\frac{ze\rho_\infty}{\varepsilon\varepsilon_o}\right)\exp\left(\frac{-ze\psi}{kT}\right) \qquad (4.1)$$

in which ψ is the electrostatic potential, x is the distance from the film surface, e is the charge of an electron, z is the valency of the electrolyte ions, ρ is the number density of ions in the bulk, ε is the dielectric constant of the medium, ε_o is the permittivity of free space (8.854 x 10^{-12} $C^2/J\text{-}m$), k is Boltzmann's constant, and T is the temperature. Solving this equation yields the electrostatic potential and ion concentration as a function of the distance from the film surface into the developer solution.[1]

In order to calculate the ion concentration at the surface of the film (x=0), the surface charge (σ) of the film (which is directly proportional to α) must be known. However, the ion concentration affects α, so an initial guess must be made. First, the relationship between σ and α must be determined. In the lattice simulations, the volume of a monomer unit is approximated by a cube that is 0.7 nm on a side. The corresponding area for an ionizable site is therefore 0.49 nm^2, with one possible electronic charge per site. Thus, for a fully ionized film surface, σ is approximately equal to 0.326 C/m^2. The relationship between surface charge, σ, and the fraction of ionized sites, α, is approximated as:

$$\sigma = 0.326\alpha \tag{4.2}$$

The ion concentrations away from the surface of a generic base developer solution (ROH) are given by the Boltzmann distribution[1]:

$$\left[R^+\right](x) = \left[R^+\right]_\infty e^{\frac{e\psi(x)}{kT}} \tag{4.3}$$

$$\left[OH^-\right](x) = \left[OH^-\right]_\infty e^{\frac{-e\psi(x)}{kT}} \tag{4.4}$$

By considering the PB equation and charge neutrality (the total charge of counterions near the surface must equal the charge on the surface), the surface potential and the surface concentration of ions can be calculated (see Appendix A):

$$\psi_o = \frac{2kT}{e}\left[\sinh^{-1}\left(\frac{\sigma^2}{8\varepsilon\varepsilon_o kT\{[ROH]_\infty + [AS]_\infty\}}\right) + 1\right] \tag{4.5}$$

$$\left[R^+\right]_o = \left[R^+\right]_\infty e^{\frac{e\psi_o}{kT}} \tag{4.6}$$

$$\left[OH^-\right]_o = \left[OH^-\right]_\infty e^{\frac{-e\psi_o}{kT}} \tag{4.7}$$

where the subscript *o* indicates the surface of the film, and [AS] is the concentration of any added salts to the developer solution. Note that the double layer analysis predicts a change in α (and thus dissolution rate) with added salts and with temperature.

A parameter typically used to describe a double layer system is the Debye length, which is the characteristic length of the electrostatic potential.[1] The Debye

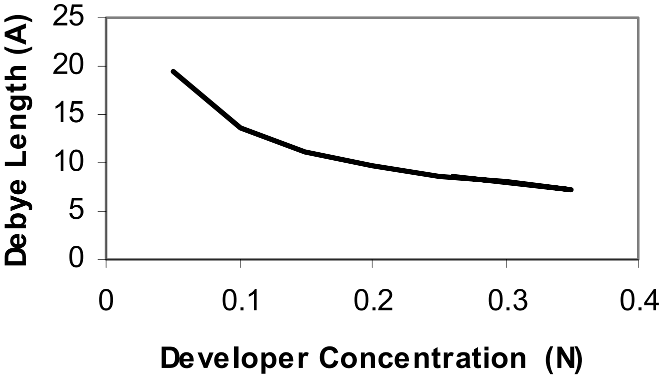

Figure 4.2 Calculated Debye length as a function of developer concentration

length (K^{-1}) is defined as:

$$K^{-1} = \left[\frac{\varepsilon\varepsilon_o kT}{1000e^2 N_A \sum z_i^2 [C_i]} \right] = [\mathrm{m}] \tag{4.8}$$

where N_A is Avogadro's number, and C_i is the concentration of ionic species i. For the case of a monovalent aqueous base at room temperature, the Debye length (K^{-1}) is related to the developer concentration as:

$$K^{-1} = \frac{0.43}{[ROH]_\infty^{0.5}} = [\mathrm{nm}] \tag{4.9}$$

Note that the Debye length is dependent only on the developer concentration, and not the surface charge or other properties of the film. The Debye length is plotted against developer concentration in Figure 4.2. There is an inverse square root dependence on developer concentration. Therefore, the Debye length is ~1 nm for typical lithographic applications.

Equations 4.2, 4.5, and 4.7 can be combined into a function that relates the pH at the surface of the film to the pH in the bulk of the developer:

$$pH_o = 0.8686\left[\sinh^{-1}\left(\frac{0.0133\alpha^2}{\varepsilon\varepsilon_o kT\left(10^{pH_{bulk}-14} + [AS]_\infty\right)} \right) + 1 \right]\left(14 - pH_{bulk}\right) + 14 \tag{4.10}$$

It is useful to also determine the electrostatic potential gradient, $\psi(x)$, although it is not strictly necessary in order to calculate the model parameters (α).

However, it is useful to visualize the concentration gradient from the surface to determine the length scale of the double layer effect. The potential as a function of distance from the surface is (derived by Israelachvili):

$$\varphi(x) = \frac{2kT}{e}\ln\left[\frac{\left(1+\gamma e^{-Kx}\right)}{1-\gamma e^{-Kx}}\right] \tag{4.11}$$

where
$$\gamma = \tanh\left(\frac{e\varphi_o}{4kT}\right) \tag{4.12}$$

The concentration gradient of ions away from the surface is found by substituting $\psi(x)$ into equations 4.3 and 4.4. Figure 4.3 shows the potential gradient and ion gradient for a developer concentration of 0.26 N and $\alpha = 0.3$. Note the log scale

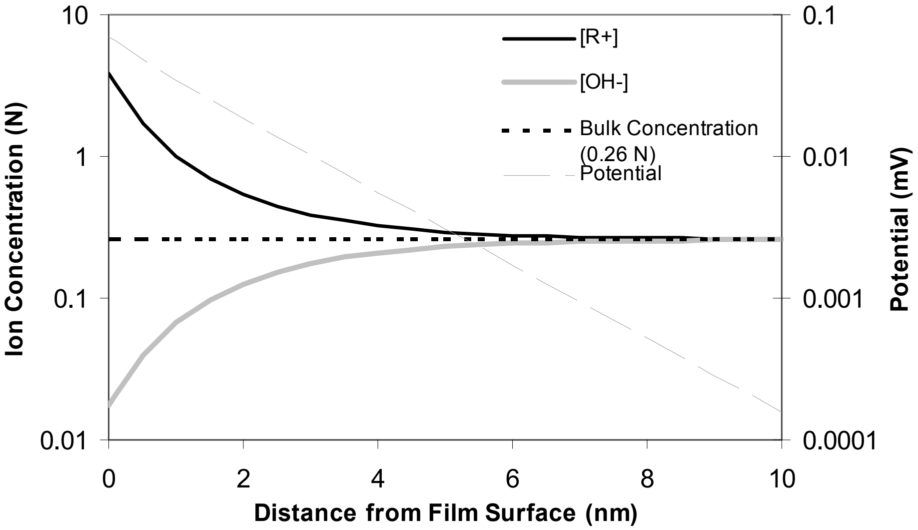

Figure 4.3 Concentration gradient and potential gradient away from a charged photoresist surface, assuming 0.26 N developer concentration and α = 0.3. (Note the log scale on both axes.)

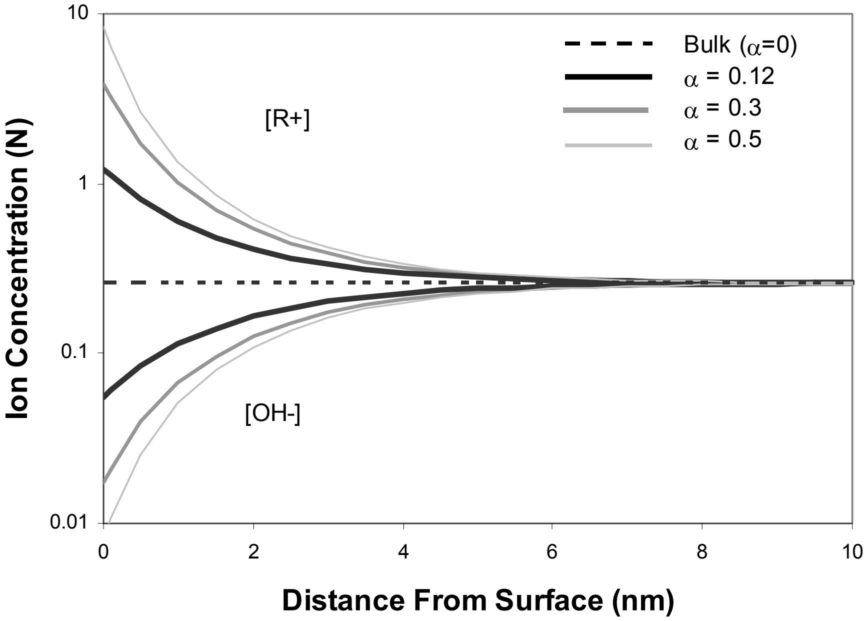

Figure 4.4 Concentration gradient of ions from a charged photoresist surface over a range of α, assuming the developer concentration is 0.26 N.

on the graphs, and that the potential gradient is linear when plotted on a log scale. Note also that the fraction of positive surface ions increases by a factor of ~30 over that of the bulk. The hydroxide ion concentration decreases by an identical value.

Figure 4.4 shows the concentration gradient of ions for varying fractions of ionized sites. The distance over which the concentration gradient acts is ~5 nm. Note that the graphs shown in Figures 4.3 and 4.4 represent hypothetical situations. That is, the fraction of ionized surface sites (α) is a predetermined, assumed value. The goal of this analysis was to determine how the double layer might influence the fraction of ionized surface sites. Qualitatively, it is clear that the electrostatic repulsion of the surface will lower the local concentration of hydroxide ions, which in turn will lower the amount of deprotonations occurring, and thus lower the surface charge. To analyze these multiple effects quantitatively, it is necessary to combine the double layer analysis above with the equilibrium expression for the deprotonation reaction equilibrium presented in Chapter 2.

4.4 EFFECT OF DOUBLE LAYER ON CI MODEL PARAMETERS

At this point, the general relationship between the bulk hydroxide ion concentration and the surface hydroxide ion concentration is known (Equation 4.10). This can be used in conjunction with equation 2.1:

$$\alpha = \frac{10^{\mathrm{pH}-\mathrm{p}\overline{K_a}}}{1+10^{\mathrm{pH}-\mathrm{p}\overline{K_a}}} \tag{4.11}$$

to determine the change in α considering the Coulombic effects. However, one caveat is that the pKa of the polymer is also a function of α:

$$\mathrm{p}K_a = f(\alpha) \tag{4.12}$$

Equation 4.10 defines the acidity function of the polymer, which has been estimated for both PHOST and novolac[3,4] based on literature data for the pKa of phenolic oligomers.[5] Figure 4.5 shows the estimated pK_a of both PHOST and novolac as a function of the degree of ionization, α.[3,4] The subtle differences in the structure of the phenolic polymers result in large differences in their acidity functions. The fraction of ionized sites (α) was first calculated by solving

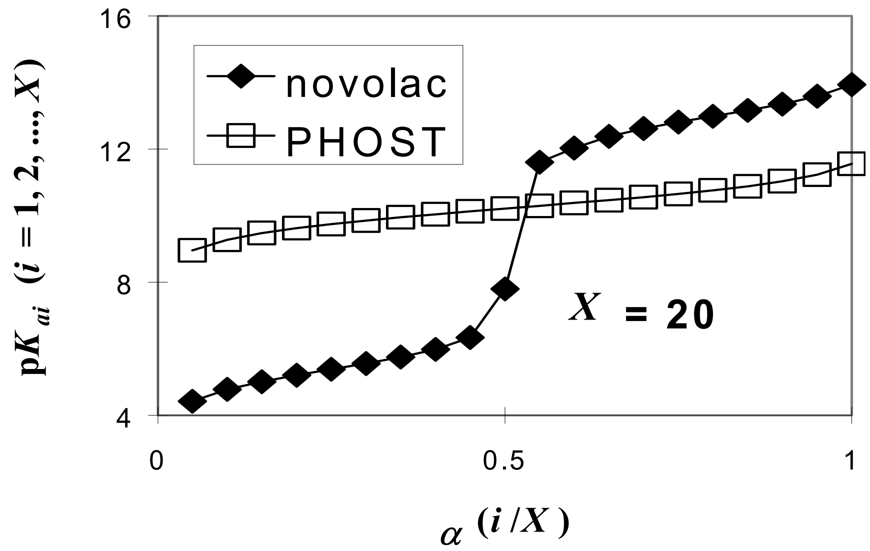

Figure 4.5 Estimated pKa of PHOST and novolac as a function of the degree of ionization, α.

equations (4.10) and (4.11), assuming that the hydroxide ion concentration at the surface of the film was the same as the bulk. At a developer concentration of 0.26

N, the calculated value of α for PHOST is greater than that for novolac (0.99 compared to 0.80), and this result may explain the high dissolution rate of PHOST films compared to novolac films.[3,4] This may also contribute to observed surface rate inhibition in novolac films, which is addressed in Chapter 6.

However, it is not necessary to assume that the surface hydroxide concentration is equal to that of the bulk. Incorporating the analysis above, Equation 4.10 along with Equations 4.12 and 4.12 constitute a system of 3 equations and 3 unknowns that can be solved simultaneously to yield pH_o, pK_a, and α. The solution to these equations is shown in both Figures 4.6 and 4.7 for PHOST and novolac, respectively. The calculated value of α is also shown without considering electrostatic surface forces. That is, α was also calculated using only Equations (4.10) and (4.11). In each case, the calculated value of α drops considerably when electrostatic surface forces are considered.

There are several assumptions implicit in the above analysis. Most notably, the assumption is made that the charged surface is impenetrable to the base ions and that the surface is flat. Also, the Poisson Boltzmann equation does not consider finite ion size (steric) effects or the discreteness of surface charges. Thus far, the critical ionization model has been successful without considering diffusion of ions into the polymer matrix. The assumption has been that for typical photoresist polymers and processing conditions (0.26 N TMAH), the film

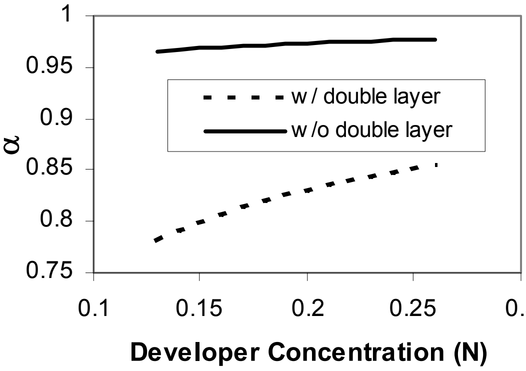

Figure 4.6 Calculated fraction of ionized sites (α) for a PHOST film at various developer concentrations with and without considering the double layer effect.

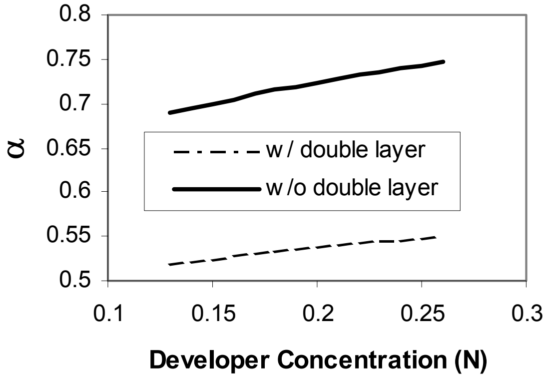

Figure 4.7 Calculated fraction of ionized sites (α) for a novolac film at various developer concentrations with and without considering the double layer effect

dissolves faster than ions can penetrate the film. For this analysis, it is assumed that gel layer formation is negligible. The validity of this assumption is discussed further in Chapter 7.

The flat surface assumption is definitely a poor assumption for real photoresist systems. At high degrees of polymerization (dp = 75), the surface roughness during development is on the order of 3-7 nm (see Chapter 8).[6-11] Depending upon the imaging conditions and other factors, the roughness near a line edge may be larger than 5 nm.[9,10] Since the Debye length is on the order of 1 nm, the double layer will not be flat, but take on the topography of the photoresist. For such cases, the assumption of a flat surface is no longer valid. However, the flat surface assumption is not necessary if the double layer is considered from a stochastic point of view. An added benefit of a stochastic approach is that finite ion size effects can be investigated. A simple technique has initially been used to incorporate this effect directly into the CI lattice simulations. A more rigorous approach will be described at the end of the chapter, and has been included in a parallel work by our research group.[12]

4.5 STOCHASTIC APPROACH TO THE DOUBLE LAYER ANALYSIS

A stochastic method for incorporating the double layer effect into the lattice simulations is shown in Figure 4.8. As a site becomes ionized, an adjacent site is chosen at random and filled with a positive counterion (R^+). The double layer then exists as discrete positive charges directly adjacent to ionized sites. (This layer is more accurately described as the Stern layer, which defines the immobile ions in direct contact with the ionized surface.[1] Note that the following analysis assumes a monovalent developer cation.) This simple approach includes the cation as an excluded volume element on the resist lattice. However, no other interactions (such as coulombic interactions) were initially considered. The effect of adding the countercation is to block ionization of adjacent sites, which leads to lower fraction of ionized surface sites (just as the continuum model predicts). In Figure 4.8b, the size of the counterion is assumed to be identical to the size of the monomer repeat unit. This assumption is an overestimation for a tetramethylammonium cation (or smaller cations), so a probabilistic approach was taken to account for ions of varying size. Hydration of the cations has not explicitly been considered.

For a given cation site, the volume of the cation (not the site) was used to calculate a probability that the developer site may be capable of housing another cation and ionizing another adjacent polymer site. For example, if the cation is half the size of a monomer site, then the probability, P_{cation}, that the site may ionize another adjacent site is 0.5. Simply stated:

$$P_{cation} = \frac{V_{cation}}{V_{monomersite}} \tag{4.13}$$

For each cation site, a random number is generated, and if this number is greater than P_{cation}, another adjacent site (chosen at random) is ionized. In other words, if a monomer site is twice the size of a cation, a single developer site is capable of housing two cations (Figure 4.8c). This approach is practical if the cation size is less than the size of the monomer unit. For typical applications, this is always true unless the developer consists of tetraethylammonium (TEA^+) or a larger cation. Figure 4.9 demonstrates the decrease in dissolution rate with increasing cation size.

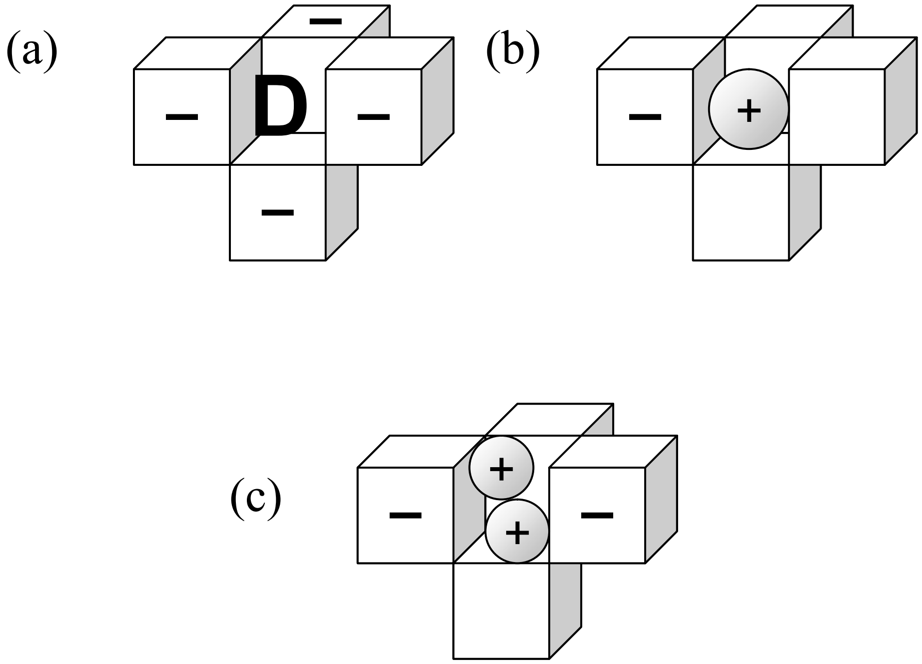

Figure 4.8 Implementation of the stochastic double layer (a) No double layer: a developer site is capable of ionizing 5 adjacent sites (b) P_{cation} =1.0: a developer site is capable of ionizing only 1 adjacent site (c) P_{cation}= 0.5: a developer site is capable of ionizing 2 adjacent sites

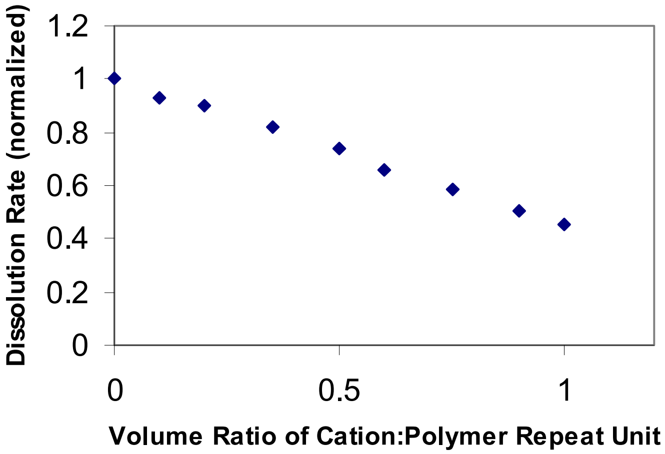

Figure 4.9 Change in simulated dissolution rate with size of the developer counterion.

The predicted decrease in dissolution rate with increasing counterion size agrees with experimental observations.[13] Note that the double layer stochastic analysis predicts a decrease in dissolution rate with increasing ion size without any penetration of the counterion into the film. The experimental trend that dissolution rate is inversely proportional to ion size is usually interpreted to mean that mass transfer must influence the dissolution process.[13,14] The simulation data in Figure 4.9 qualitatively predict the correct experimental trend, without invoking mass transport steps as the rate-limiting factor for dissolution.

4.6 MONTE CARLO APPROACH TO THE DOUBLE LAYER ANALYSIS

Our research group has improved upon the above analysis through the recent work of Schmid *et al.*[12] The approach taken was also a stochastic approach that alleviated the need for flat surface and point charge assumptions. The following is a brief description of that work, and the reader is referred elsewhere for additional details.[12]

Like the stochastic analysis above, the polymer chains are modeled on-lattice, with the same properties described in Chapters 1 & 2. However, the developer ions are modeled off lattice, using the so-called primitive model of electrolytes. This model considers discrete, hard sphere ions in a continuum of structureless dielectric ambient (in this case, water). There are two types of interactions between charged species (ions and ionized monomer sites) which are hard sphere, excluded volume repulsions and Debye-Huckel interactions. Thus, the excluded volume interactions and Coulombic interactions of each ion are individually responsible for the formation of the overall electric double layer.

There are two types of dynamic, Monte Carlo moves allowed in order to reach an equilibrium state. The first is random hops (diffusion) of the ions within a specified radius (<1 nm) of the present location. The energy difference between the initial and final location is calculated by summing all interactions with neighboring ions. Based upon the Metropolis criterion,[15] the move is accepted if the energy change is favorable. This type of move allows the ions to equilibrate into a random distribution, governed by Coulombic forces.

The second type of move (or equilibrium) considered is reaction equilibrium with the polymer surface. When a hydroxide ion is within a certain distance of the polymer site, a trial ionization move is attempted. The critical distance occurs when the Gibbs free energy change of ionization is equivalent to the unscreened Coulombic interaction between the ion and a positive proton located at the surface of the film. Within this distance, the Metropolis criterion[15] is again used to determine whether ionization occurs. When a hydroxide ion is consumed at the surface due to acid-base reaction, another is added randomly into the simulation volume (as a salt pair), to prevent the bulk concentration from being lowered. This approximation is valid based on the assumption of rapid ion diffusion from the bulk, an assumption that is already implicit in the CI dissolution model.

4.7 SUMMARY

Several techniques for incorporating Coulombic forces into the CI model have been presented. A solution to the Poisson-Boltzman equation resulted in a continuum model for calculating the decrease in surface hydroxide concentration, and the subsequent decrease in the fraction of ionized surface sites, α. Previous methods for calculating α assumed polymer chains in a dilute solution, but this recent model has succesfully incorporated the interfacial structure of a thin polymer film, and the calculated values of α are more consistent with expected values. However, it was determined that the assumptions of a flat profile and infinitely small ions were not valid, and that a stochastic approach to the problem provides a more accurate solution. Two stochastic models were discussed. The first considered only excluded volume interactions, and the second considered both excluded volume and Debye-Huckel (Coulombic) interactions. The latter approach, in combination with the mesoscale lattice model already developed, provides a rigorous photoresist dissolution simulation tool that can be used to investigate the effect of fundamental resist/developer properties on dissolution behavior and roughness formation. It is very satisfying to report that the CI model captures nearly all of the qualitative aspects of the dissolution process, and that incorporation of Coulombic forces adds a quantitative, physical aspect to the model.

4.8 REFERENCES

(1) Israelachvili, J. *Intermolecular and Surface Forces, 2nd Ed*; Harcourt Brace & Company: London, 1992.

(2) *The Electrochemical Double Layer*; The Electrochemical Society, Inc.: Pennington, N.J., 1997.

(3) Flanagin, L. W.; McAdams, C. L.; Hinsberg, W. D.; Sanchez, I. C.; Willson, C. G. *Abstracts of Papers of the American Chemical Society* **1999**, *218*, 112-PMSE.

(4) Flanagin, L. W. *Ph.D. Dissertation, University of Texas at Austin*, 1999.

(5) Perrin, D. D.; Dempsey, B.; Serjeant, E. P.; Chapman and Hall: London, 1981.

(6) He, D.; Cerrina, F. *J. Vac. Sci. & Tech. B* **1998**, *16*, 3748.

(7) Burns, S. D.; Schmid, G. M.; Flanagin, L. W.; Tsiartas, P. C.; Willson, C. G. *J. Vac. Sci. & Tech. B* **2002**, *20*, 527.

(8) Flanagin, L. W.; Singh, V. K.; Willson, C. G. *Journal of Vacuum Science & Technology B* **1999**, *17*, 1371-1379.

(9) Lin, Q.; Sooriyakumaran, R.; Huang, W.-S. *Proc SPIE* **2000**, *3999*, 230.

(10) Sanchez, M. I.; Hinsberg, W. D.; Houle, F. A.; Hoffnagle, J. A.; Ito, H.; Nguyen, C. *Proc SPIE* **1999**, *3678*, 160.

(11) Schmid, G. M.; M.S., S.; Singh, V. K.; Willson, C. G. *J. Vac. Sci. & Tech. B* **2002**, *20*, 185-190.

(12) Schmid, G. M.; Burns, S. D.; Tsiartas, P. C.; Willson, C. G. *J. Vac. Sci. & Tech. B* **2002**, *20*, 2193-2199.

(13) Dammel, R. *Diazonapthoquinone-based Resists*; SPIE Optical Engineering Press: Bellingham, Washington, 1993.

(14) Shih, H. Y.; Reiser, A. *Macromolecules* **1997**, *30*, 4353-4356.

(15) Metropolis, N.; Rosenbluth, A. W.; Rosenbluth, M. N.; Teller, A. H.; Teller, E. *J. Chem. Phys.* **1953**, *21*, 1087.

CHAPTER 5: MEASURING RESIDUAL SOLVENT CONCENTRATION GRADIENTS IN PHOTORESIST FILMS*

5.1 EFFECT OF RESIDUAL CASTING SOLVENT UPON DISSOLUTION

The choice of casting solvent in the photoresist formulation is very important. The solvent must be inert, volatile, non-toxic, compatible with the resin, *etc*. It was stated in Chapter 1 that one purpose of the post apply bake was to remove solvent from the film. In practice, some solvent remains in the film, unless the photoresist is annealed for a significant period of time above the glass transition (T_g) temperature. Figure 5.1 shows the amount of residual casting solvent (RCS) versus post apply bake temperature (PAB), at bake temperatures above and below the glass transition (~115°C) of a novolac film. This plot demonstrates that at bake temperatures below T_g, a significant amount of solvent is retained. Usually, the post apply bake temperature is below the glass transition of the polymer, so it is expected that some solvent remains in the film, and may affect the performance of the photoresist. In the case of Figure 5.1, the casting solvent was diglyme (methoxyethyl ether). For the case of propylene glycol methyl ether acetate (PGMEA) casting solvent, as much as 15-20 wt% may remain in a novolac film. In general, residual solvent acts as a plasticizer,

---

*Reproduced in part with permission from A.B. Gardiner, S.D. Burns, A. Qin, C.G. Willson, *J. Vac. Sci. Tech.*, Copyright 2001 increasing the dissolution rate of the resist, as well as changing the transport behavior of resist additives.[1-4] As expected, higher PAB temperatures result in lower concentrations of residual casting solvent and slower dissolution rates.

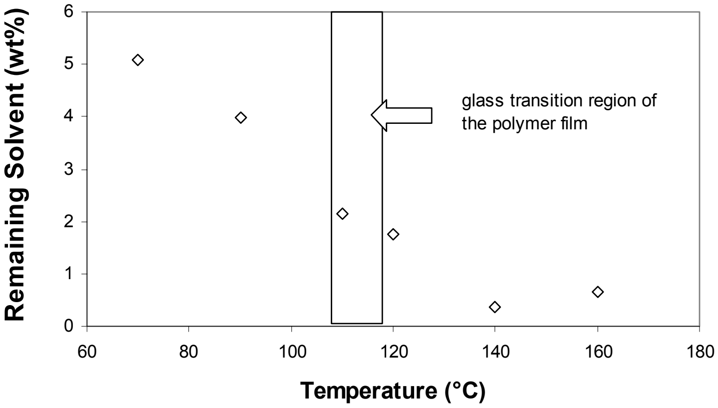

Figure 5.1 Amount of retained residual solvent for a novolac film baked above and below the glass transition temperature. (Diglyme solvent, PAB time of 3 min)

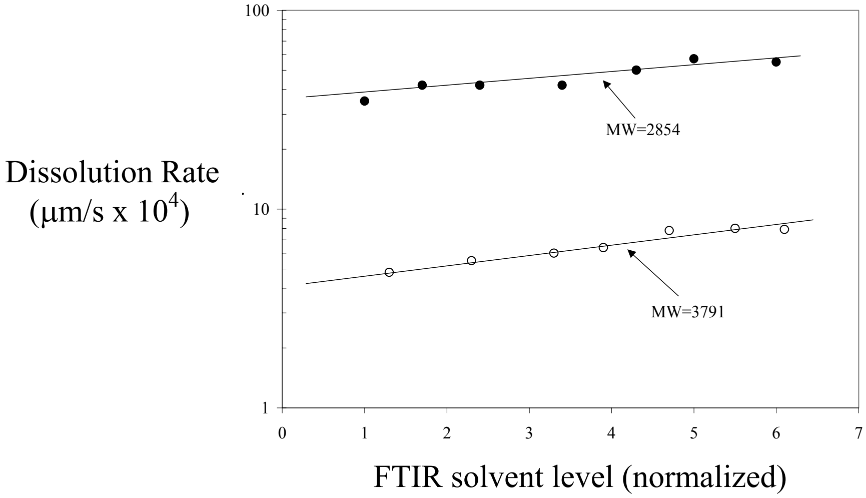

Figure 5.2 Effect of residual casting solvent concentration on dissolution rate of a novolac film.[5] (Data provided by Beauchemin *et al.*)

Figure 5.2 shows the effect of residual casting solvent concentration (a relative measurement by FTIR) upon dissolution rate.[5] The polymer resin was novolac and the casting solvent was PGMEA. This casting solvent has found widespread use in the semiconductor industry for photoresist solutions. In this chapter, the goal was to measure the concentration gradient of the solvent in the film, and the effect of the gradient upon dissolution rate profile of the photoresist.

5.2 A THEORY FOR SURFACE INHIBITION: RCS CONCENTRATION GRADIENTS

One important aspect of the dissolution process that remains a mystery is the phenomenon of surface rate inhibition. The term "surface inhibition" describes the slower development rate near the surface of a resist film (or at the beginning of dissolution). The plots of the thickness of resist remaining versus time in developer for resist films cast from diglyme (bis(2-^{14}C-methoxy ethyl)ether) and PGMEA are shown in Figure 5.3. The resists are a homemade novolac/DNQ formulation. The dissolution rate versus thickness of these two different resists are shown in Figure 5.4. When cast from diglyme, films of this resist show little surface inhibition. If PGMEA is used as the casting solvent, there is a noticeable amount of surface inhibition. This dissolution inhibition at the film surface has a powerful and beneficial influence on the lithographic process. Specifically, surface inhibition leads to reduced dark loss (dissolution in unexposed areas) and improved sidewall angles. This is shown quantitatively in

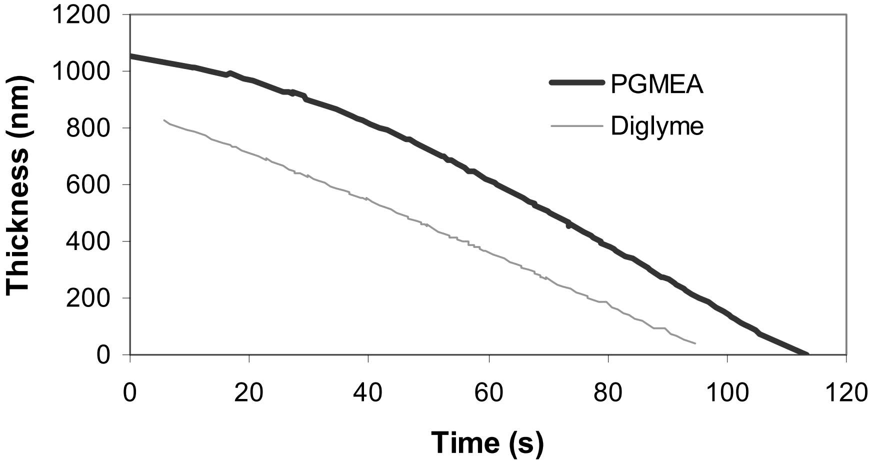

Figure 5.3 Aqueous base dissolution of novolac resist cast with diglyme and PGMEA

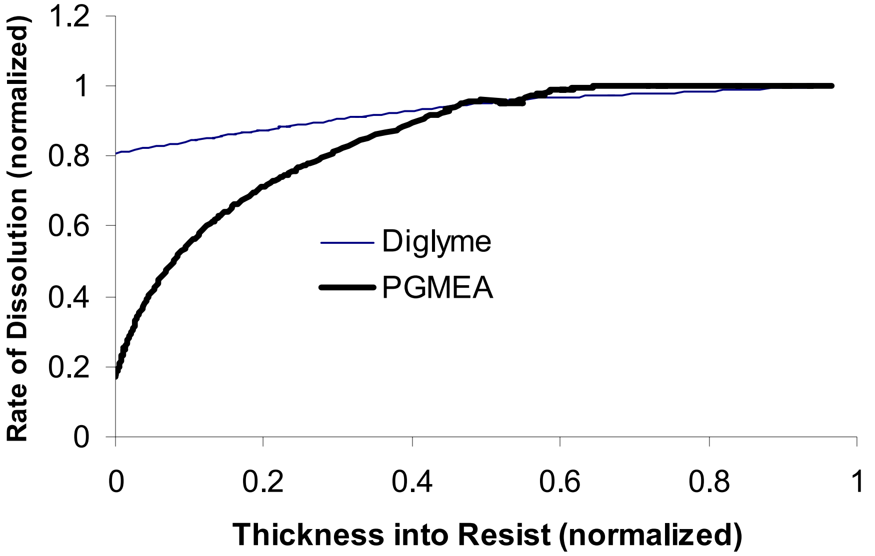

Figure 5.4 Rate of dissolution versus film thickness for a novolac resist cast from diglyme and PGMEA solvents

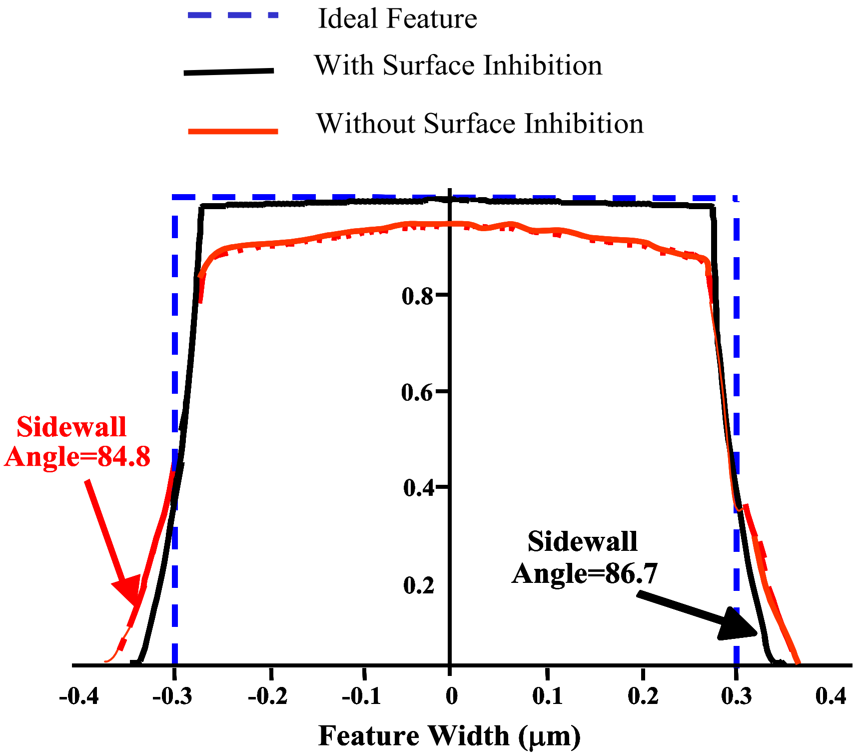

Figure 5.5 A ProLith simulation of a photoresist feature with and without surface inhibition effects. Surface rate inhibition improves the profile of photoresist features

in Figure 5.5 by a ProLith simulation[6] of a photoresist feature with and without surface inhibition effects.

It has been suggested that surface inhibition may be explained by the presence of concentration gradients in residual casting solvent.[5,6,7] It has been shown that films with lower RCS concentration have lower dissolution rates.[5] It follows that the dissolution rate at the surface of a baked photoresist film may be lower than the bulk dissolution rate because the RCS concentration is higher in the bulk. The RCS concentration gradient in a photoresist film has been measured by others using FTIR methods and it has been proposed that the gradient may be responsible for surface inhibition.[5] However, the resolution of these experiments was not adequate (0.1-0.25 μm), nor was the measured concentration gradient compared to the dissolution rate profile to determine the relationship between the solvent and dissolution gradient.

5.3 INTRODUCTION OF THE 'HALT DEVELOPMENT' TECHNIQUE

A "Halt Development" (HD) technique has been developed to test this relationship. The HD technique provides a simple method for quantitatively separating different layers of the resist film for chemical analysis. The analysis method chosen for detection of trace quantities of RCS was ^{14}C isotope labeling and liquid scintillation counting (LSC). The LSC method is used extensively in studies of molecular diffusion, and it has been used previously for measuring RCS in a variety of photoresist systems.[8,9] The mass of RCS in the top layer (one tenth) of a 1 μm film on a 2 inch wafer is less than 0.05 mg, so gravimetric techniques are challenging. This measurement is further complicated by the variety of other compounds in photoresist samples. The advantages of the LSC method include high sensitivity and no chemical or physical change in the system. The specific advantages of LSC over other conventional methods for RCS measurement in photoresist systems are described in more detail in Chapter 3 and in the Ph.D. dissertation of Gardiner.[1]

The dissolution rate of the resist films was measured using a multiwavelength dissolution rate monitor (DRM). The instrument and its operation are described in Chapter 3 and elsewhere.[10-13] This technique provides accurate information about the absolute thickness of the resist film as a function of development time. The derivative of the thickness versus time curve results in the dissolution rate as a function of time (which can be easily converted to rate versus thickness). This rate profile was then correlated with the RCS concentration at the thickness that was determined from the LSC data. The combination of these two techniques allowed for the direct measurement of the residual solvent concentration throughout the depth of the resist film. Thus, a quantitative relationship between dissolution rate and the local RCS concentration was established.

5.4 MATERIALS: RESIST FORMULATIONS AND RADIO-TRACER PREPARATION

The photoresist systems used for the study were novolac/diazonaphthoquinone (DNQ) positive-tone resists. The resists were made using cresol novolac (Mn=9370, Pd=4.9) from Schenectady International, and a bis-(1-oxo-2-diazonaphthoquinone sulfonate) (DNQ) from IBM Corp. The resists consisted of 77 wt% solvent and the DNQ loading was 12 wt% relative to the solids. Two developer solutions were prepared using AZ 300 MIF tetramethylammonium hydroxide (TMAH) developer from Clariant Corp. The resists were developed with the first solution, which contained 90% by volume of the AZ 300 MIF and 10% distilled water. The HD cell was then washed with the second solution, of 70% AZ300 MIF and 30% distilled water (by volume). The 70% solution was strong enough to act as a washing solution without causing the developed resist to precipitate, yet it was weak enough not to cause significant resist development.

The ^{14}C radio-labeling synthesis routes for PGMEA (propylene glycol methyl ether acetate-carbonyl-^{14}C) and diglyme have been previously described.[1] A Beckman 1801 liquid scintillation counter was used to measure the activity of each sample. The specific activity of the diglyme and PGMEA based resists were measured to be 8.21 and 9.9 μCi/g, respectively. Scintiverse II from Fisher Scientific Inc. was used as the scintillation cocktail for the developer/resist solution samples. An H-Number quenching calibration as defined by Beckman-Coulter, Inc. was performed using a developer/resist solution as the quenching material. The H-number calibration of these aqueous samples has been previously documented.[1]

5.5 FILM COATING AND HALT DEVELOPMENT CELL DESCRIPTION

The resists were spun cast on 2 inch wafers for 40 seconds using 0.35 mL of resist solution. The spin speed was adjusted to obtain a 1 μm resist film for the diglyme resists. The films cast from PGMEA were 1.5 μm thick. The wafers were baked on a Thermolyne hotplate with a vacuum chuck for 90 seconds at bake temperatures of 70°C, 90°C, and 110°C. A diagram of the HD cell is shown in Figure 5.6. A schematic of the HD experiment is shown in Figure 5.7. The plastic backing of the HD cell has a recess that holds films coated on 2-inch (in diameter) silicon wafers. A 2 mm Viton™ gasket rests between the glass plate and the backing. The gasket was designed to provide an inlet for the developer at the top of the cell. The tapered area at the bottom of the inlet was designed to allow trapped air to rise into this space and prevent bubble formation over developing

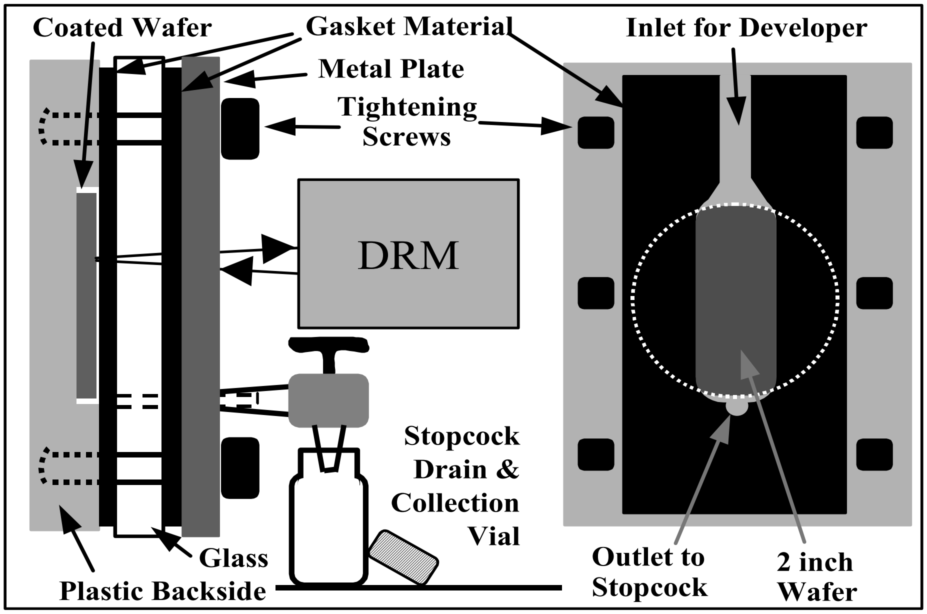

Figure 5.6 Halt development cell apparatus (profile and front view)

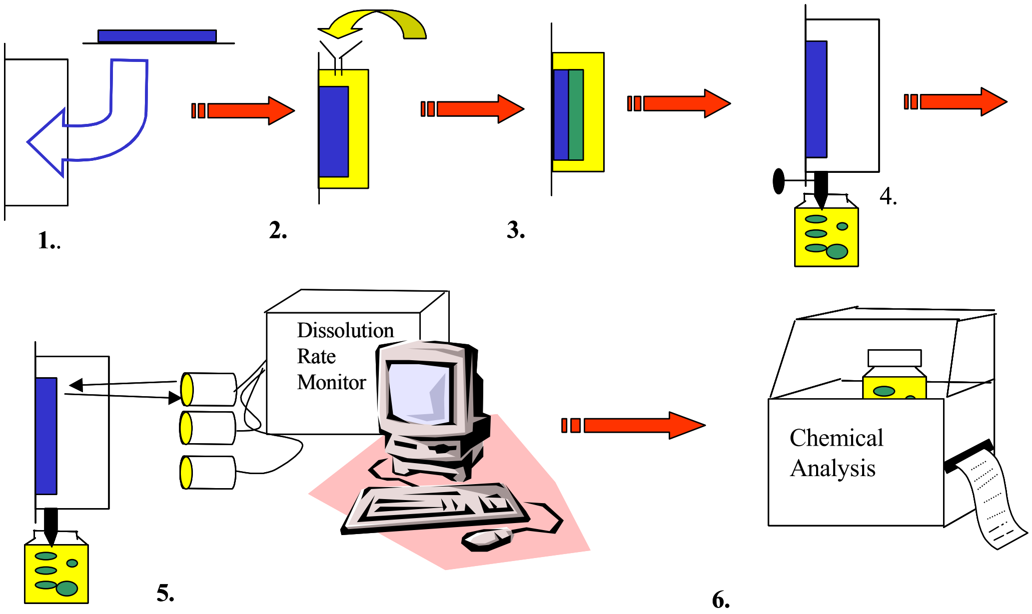

Figure 5.7 Diagram of Halt Development Technique. 1) A coated wafer is loaded into the cell. 2) Dilute developer is poured into the cell. 3) The resist is allowed to partially dissolve. 4) The dissolved resist is drained from the cell. 5) The intermediate thickness is determined. 6) The top layer is analyzed. The process is repeated for the bottom layer of resist.

resist areas. The gasket covers some of the resist film. Experiments have shown that a negligible amount of resist under the gasket dissolves. The open cell has a total liquid volume of 2.5 ml. This cell volume allows for two 2.5 mL aliquots of aqueous solutions to dissolve and collect the different layers of the resist film. One cell volume of developer was used to dissolve the resist film, and another 2.5 mL volume was used to wash the cell to ensure adequate transfer of resist components into the scintillation vial.

After assembling the HD cell with the resist film inside, the DRM beam was aligned with the wafer for optimal signal and the DRM data collection was started. The 90% developer solution was added quickly to the cell. (In all experiments, the cell was completely full in less than 2 seconds.) The resist was allowed to develop for a specified time interval. The stopcock valve was then opened and the contents of the cell flowed into a 20 ml scintillation vial. The cell was then washed with the 70% solution. The solution was held in the cell for 8 seconds, and the cell was then drained again. The scintillation vial, with ~ 5 mL of developer/resist solution was sealed. This vial contained the top layer of the resist. The cell was filled again with 90% developer solution, and the remaining resist was dissolved and then transferred into a second scintillation vial for measurement.

This procedure was repeated for different resist films at varying halt times to measure the relative concentration of residual casting solvent throughout the thickness of the resist film. Scintillation cocktail (14.5 mL) was added to both vials, and the solutions were shaken until an emulsion formed. The total volume of sample was less than 80% of the total vial volume. This volume of sample did not show any significant amount of vial quenching due to large sample volumes. (Refer to Chapter 3 for discussion and references concerning sample quenching.) The samples were counted and the activity was calculated. The ratio of activity in the top layer to that in the total film was combined with the DRM thickness data to obtain the RCS concentration gradient. The concentration gradient was then correlated with the dissolution rate data to establish the relationship between the RCS gradient and surface inhibition.

5.6 DISCUSSION AND VERIFICATION OF THE TECHNIQUE

5.6.1 Advantages and Limitations of the Halt Development Technique

The HD cell concept provides benefits over other methods[5] used for the analysis of concentration gradients in photoresists and the quantitative establishment of the relationship between the gradients and the dissolution rate. The HD cell allows the film to be interrogated by a light source through a transparent window. The thickness of this film can then be monitored using interference techniques. This monitoring is accomplished simultaneously with the collection of different resist layers dissolving from the film by placing the wafer vertically into the cell and draining the developer solution. This design provides a simple method for quickly removing and collecting the developer solution in order to “halt development” quickly and easily.

Another advantage of this method is that the volume of developer can be controlled. The control of the sample size is important for accurate concentration analysis. LSC requires samples to be placed into a liquid scintillation solution (see Chapter 3) to convert the radiation from the radioisotope to a light signal for the photo-multiplier tube in LSC instruments. Unfortunately, the instruments have sample size limits and the scintillation cocktails have sample loading limitations. Therefore, the control over the sample volume is critical for liquid scintillation counting and this design facilitated minimizing the sample size to volumes compatible with LSC.

The scintillation cocktail used forms an emulsion when the cocktail is mixed with aqueous samples and is cited as being capable of providing accurate counting statistics for aqueous samples with less than 25% loading (i.e. 25 % aqueous sample, and 75 % cocktail). This loading limitation was confirmed during LSC instrument calibrations with solutions characteristic of the resist/developer samples expected in the study. The emulsion formation prevents phase separation of the aqueous sample and the cocktail, which causes counting losses due to decreased sample stability.

5.6.2 Verification of the Halt Development Technique

Experiments with non-labeled resist formulations were performed to establish the ability of the HD method to quantitatively separate resist layers and prove that one washing was sufficient to remove the developer/resist solution from the cell. The DRM data was analyzed for each dissolved film. Figure 5.8 shows the interference intensity signal of the DRM versus time for the three monitoring beams directed at three different areas on the wafer during a halt-development experiment. The data become noisy as the cell was drained, washed and refilled. The data demonstrates that the development rate is uniform across the wafer. Thickness non-uniformities are negligible, and they do not cause unwanted mixing of resist layers. Figure 5.8 shows an example of the halted development of a resist film. A very slight amount of development continues to occur during the halted development period. This plot demonstrates the ability to stop development while the developer solution is changed, and cleanly separate layers of a photoresist.

Another set of experiments was conducted to demonstrate that dissolved layers of the film were being separated and that the DRM thickness data could be correlated with the chemical analysis of the dissolved resist samples. These were performed using non-labeled resist films at different halt times. The relative polymer concentration of the dissolved and remaining portions of the resist film were established by measuring the UV absorbance of the solutions with a Hewlett

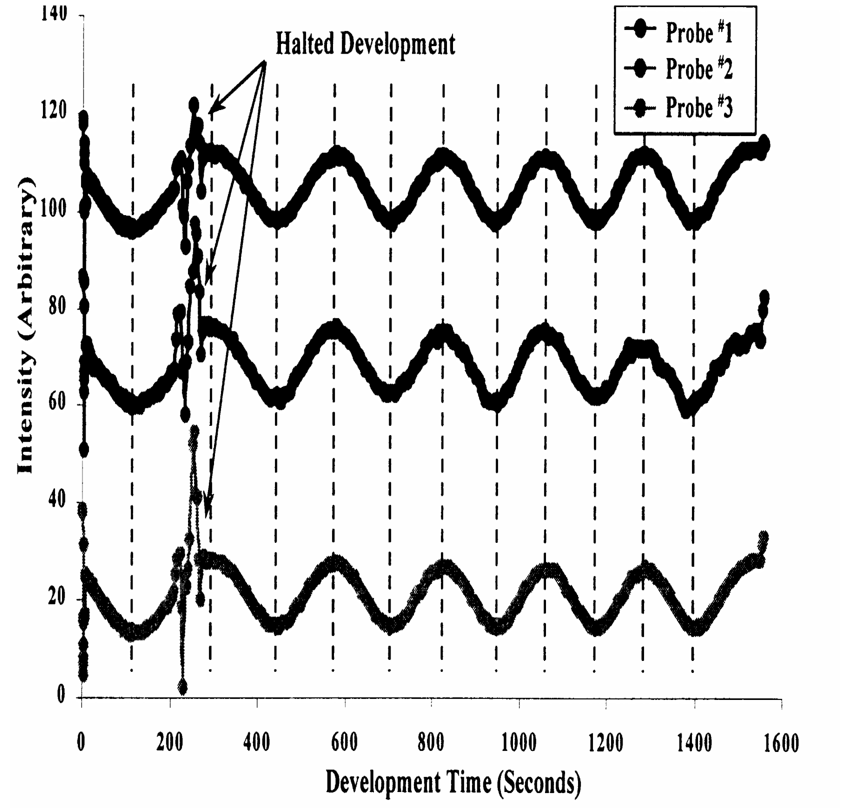

Figure 5.8 Intensity versus time curves of three regions on the wafer demonstrating uniform film development across the wafer

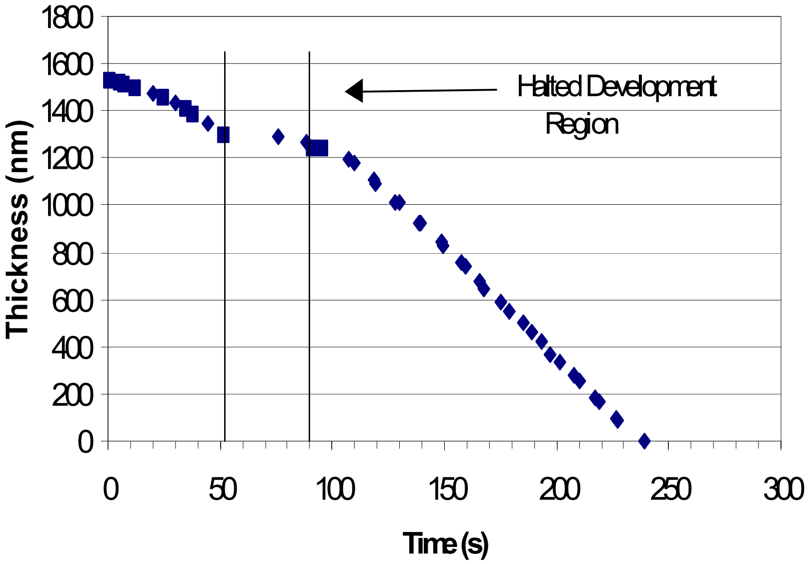

Figure 5.9 An example of the halted development region of a resist film.

Packard 8452A UV-Vis spectrophotometer. The novolac solution had a strong and easily isolated absorbance at 298 nm. The relative concentration in the top layer of the film was determined by dividing the absorbance (at 298 nm) of the top effluent by the total absorbance (the sum of both effluents). Figure 5.10 shows a strong linear correlation between the extent of resist dissolved measured by the DRM and the UV absorbance of the developer solution. This linear correlation (the slope of one and near zero intercept) indicates successful separation of discrete layers of the resist film. In this analysis, it is assumed that there is no gradient in the polymer density across the thickness of the resist film.

A test was performed to determine if one washing was adequate using the radio-labeled resist cast from diglyme. Employing the HD method, a film was coated and developed half way. The top layer, as well as the first and second washings were placed into separate scintillation vials. The amount of radioactivity removed from the HD cell with the first washing was on the order of 5% of the amount of radioactivity removed in the main solution. The amount of radioactivity removed with further 2.5ml washing solutions was below the background levels of the LSC instrument. Therefore, one washing was considered to be adequate to remove radiolabeled material from the cell.

Another potential problem is that solvent molecules diffuse out of the polymer film and into the developer at a rate *faster* than the polymer film dissolves. Ito *et al.* have reported a large transport of residual solvent out of resists in a humid environment.[14] They have suggested that water molecules are able to diffuse into and plasticize the resist, allowing solvent molecules to diffuse out of the resist into the surrounding environment. In this case, the surrounding environment is the developer solution. If this type of solvent transport does occur quickly, it would have an appreciable effect on the interpretation of the HD experimental results. In light of this issue, an experiment was devised to quantify the "leaching" of RCS from the polymer film into the aqueous phase.

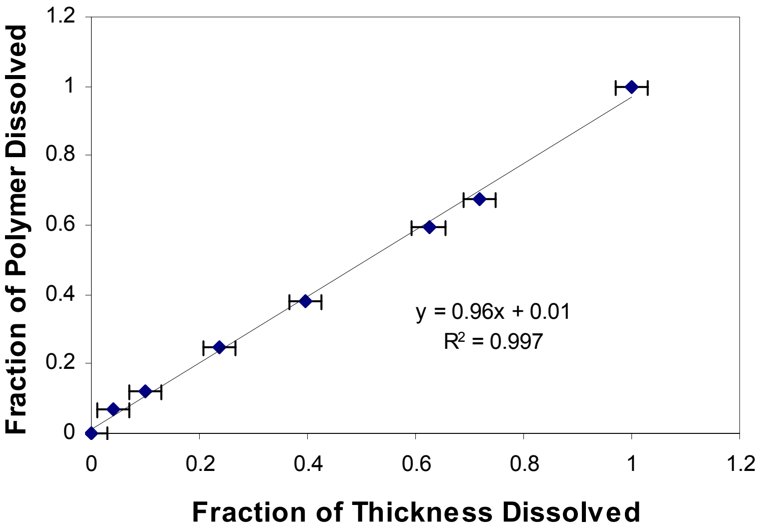

Figure 5.10 Feasibility experiment: relationship between the extent of development measured by the DRM and UV-Vis chemical analysis of the collected effluent developer solution (novolac cast with diglyme solvent)

5.6.3 Radio-labeled HD Experiments: "Leaching" of Residual Casting Solvent

The first set of leaching experiments were performed with the radio-labeled diglyme resist. The standard HD procedure was used with one change. Instead of using developer, pure distilled water was poured into the cell. The water was allowed to contact the resist for a specified time, and then the cell was drained and washed with distilled water. The water did not cause any dissolution of the resist film. The remaining resist was dissolved using the standard developer, and washed with the standard washing solution. The experiment was repeated with different films, allowing the water to contact the resist for varying amounts of time. The amount of solvent that was transported into the water was measured with the liquid scintillation counter. The results of this experiment are shown in Figure 5.11.

At long contact times (~25 min) as much as 5 % of the residual casting solvent diffuses into the water. Only 1% of the residual solvent diffuses out of the film in 5 minutes. Note that the total time used for the HD experiments were all less than 5 minutes. A second "leaching" experiment was conducted with the PGMEA labeled resist (Figure 5.10). Less than 2% of the residual PGMEA leaches out of the resist during 5 minutes of contact with water. Therefore, the rate of solvent transport into developer is too low to give significantly inaccurate RCS gradient results.

This type of "leaching" experiment may also be useful in characterizing photoresists for immersion lithography (see Section 9.4.3 for a brief description of this process). Small amounts of resist components that leach into the ambient fluid may alter the resist performance, as well as causing subtle (but important) changes in the optical constants of the fluid medium.

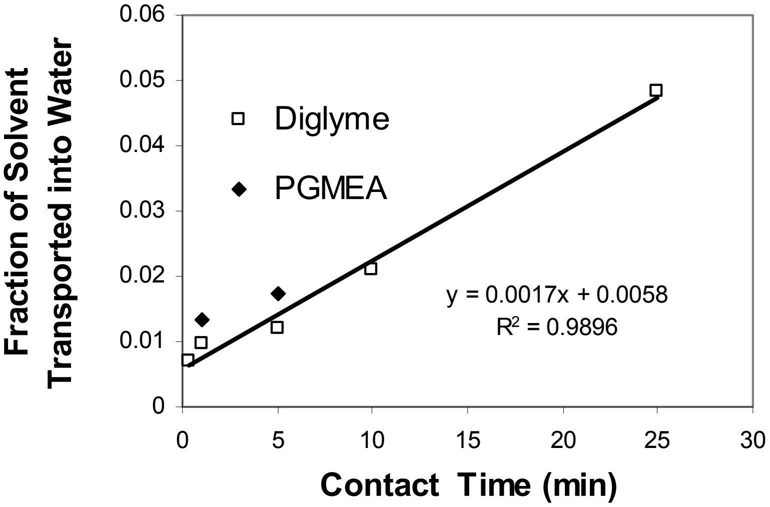

Figure 5.11 Relative amount of residual diglyme and PGMEA "leached" out of a novolac resist for varying contact times

5.7 RADIO-LABELED HD EXPERIMENTS – MEASURING RESIDUAL CASTING SOLVENT CONCENTRATION GRADIENTS

The HD/LSC method was used to determine the RCS concentration gradient in the resist cast from diglyme. Six resist films were spin coated with a 90^{o}C, 90s PAB and developed for various lengths of time. The thickness and RCS concentration was determined in each individual resist layer and RCS concentration was plotted against depth into the film (Figure 5.12). Films cast from diglyme show no significant depletion of RCS at the surface of the film. The experiment was repeated with films baked at different temperatures (70 and 110^{o}C) to create films with (perhaps) different degrees of depletion in the surface region. The results of these additional experiments are also shown in Figure 5.12. There were not any observable RCS concentration gradients in the films. Only a slight amount of surface inhibition was observed at each bake temperature (similar to Figure 5.4). The bulk RCS concentration corresponded well with measurements made previously.[1] Thus, the experimental results are believed to be accurate, and the conclusion is that a measurable concentration gradient of diglyme is not present in this film. However, because the surface rate inhibition was not significant, a large concentration gradient of solvent was not expected in this case.

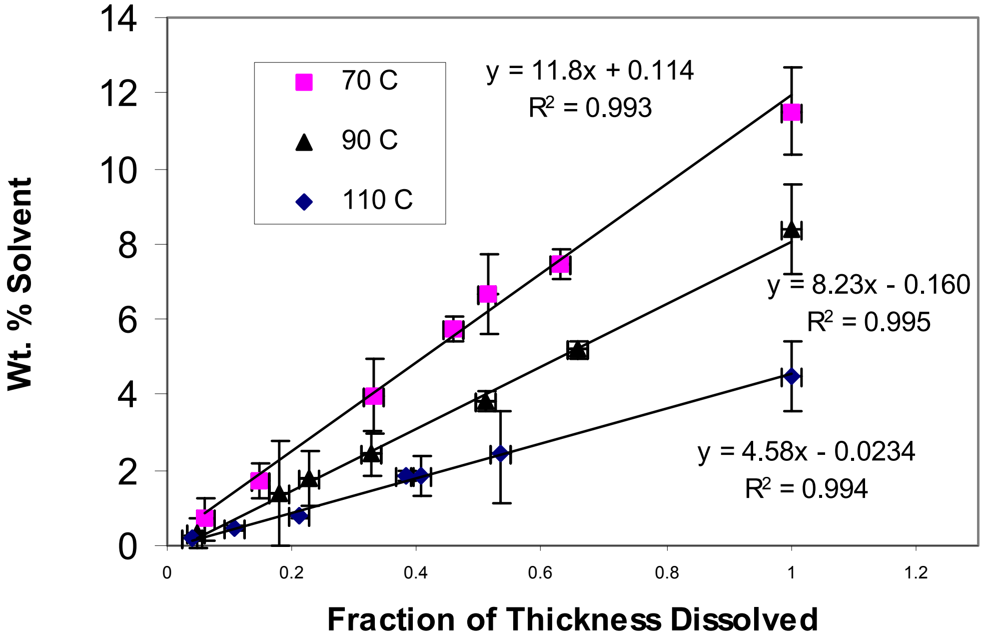

Figure 5.12 Measured concentration of residual diglyme casting solvent versus thickness of resist using the HD procedure at bake temperatures of 70,90, and 110°C.

Identical experiments were performed using the PGMEA labeled resist baked at temperatures of 70 and 110°C, and the results are plotted in Figure 5.13. A minor difference in the experiment is that the average film thickness was 1.5 μm. The resist cast from PGMEA had a much higher viscosity than the diglyme resist and required a much higher spin speed to coat a 1μm film. The higher spin speed also resulted in poor film uniformity. The nature of the HD experiment requires a very uniform film to keep the dissolution uniform across the wafer. The lowest spin speed which would provide uniform coatings resulted in a film thickness of 1.5 μm. It has been shown that the RCS overall concentration was the same for 1μm films and 1.5 μm films.[1] Therefore, the RCS gradients of these films with two different thicknesses and the same overall RCS concentration was assumed to be roughly the same. It is expected that the RCS gradient is controlled primarily by the influence of the bake conditions and the solvent-film interactions. It should also be noted that 1 μm PGMEA films showed similar dissolution profiles to the 1.5 μm films.

No observable RCS gradient was measured for either set of films using the HD method. (It is assumed that there are no concentration gradients within the thickness segments measured. Other than the surface region of the resist, there is not expected to be any large deviations in residual solvent concentration.) From these results it can be concluded that a RCS gradient is not the primary cause of surface inhibition in this photoresist. The PGMEA cast resists have surface inhibition that persists through more than one third of the film thickness (Figure 5.4), but the concentration of the RCS is constant throughout the film.

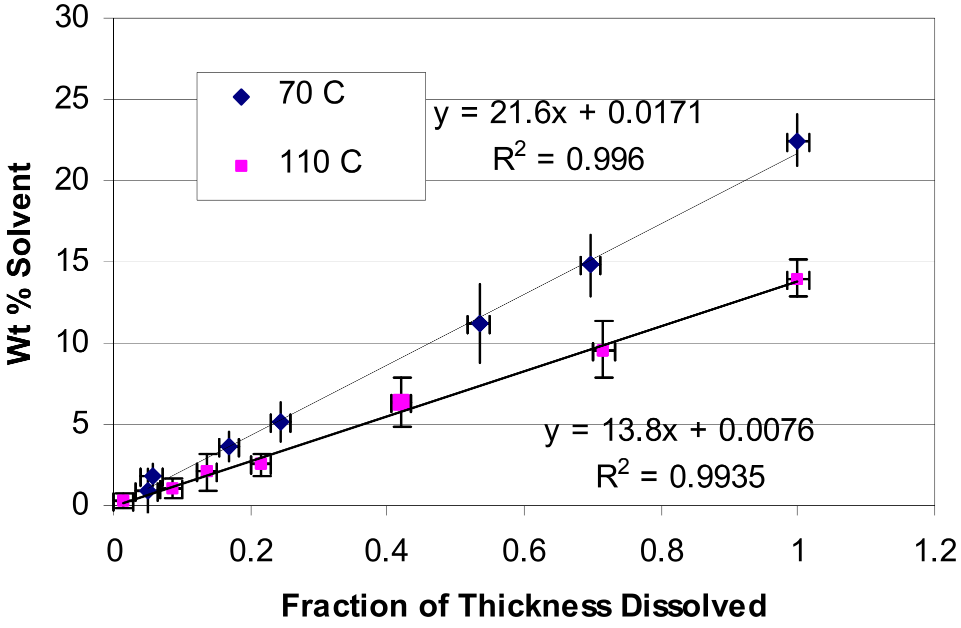

Figure 5.13 Measured concentration of residual PGMEA casting solvent versus thickness of resist using HD procedure at bake temperatures of 70 and 110°C

5.7 COMPARISON OF HD DATA WITH A CASTING SOLVENT DIFFUSION MODEL

Further evidence demonstrating that there is no relationship between RCS distribution and surface inhibition comes from the correlation of this HD data with simulation data from a solvent diffusion model by Mack.[3] The RCS distribution for this resist cast from PGMEA was simulated using this model. The calculated distribution was integrated to simulate the data from the HD experiments. Figure 5.14 shows the simulated distribution, the simulated integral of the distribution, and the HD experimental data. The simulated integral data corresponds well with the measured data. These results show the majority of the RCS gradient exists in the very top layer of the resist, and the HD data confirms the results of the model. This steep concentration gradient produces a fairly smooth curve. The experimental technique does not have the resolution necessary to detect a concentration profile as steep as the gradient predicted by the model.

Figure 5.15 shows the simulated RCS gradient plotted with the measured dissolution rate versus thickness (also shown in Figure 5.4). The residual solvent concentration rises steeply and nearly reaches a bulk concentration within the first 10% of the resist thickness. Conversely, the dissolution rate does not reach a bulk rate until one half of the film is developed. While the residual solvent may be responsible for slower development rates *very* close to the surface, it cannot be entirely responsible for the change in development rate observed for this particular resist system. Since small changes in RCS have been shown to produce large changes in dissolution rates, all these data together suggest that the presence of RCS gradients alone does not explain surface inhibition in the novolac/DNQ photoresist studied.

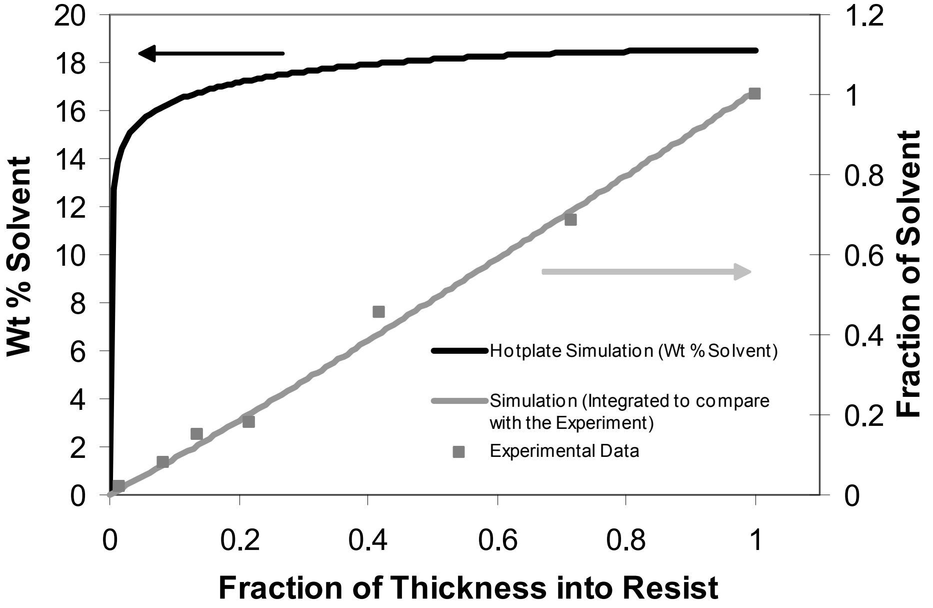

Figure 5.14 Measured and simulated concentration of residual PGMEA casting solvent versus thickness of resist for a bake temperature of 110oC. The simulated concentration profile has been integrated to compare with experiment.

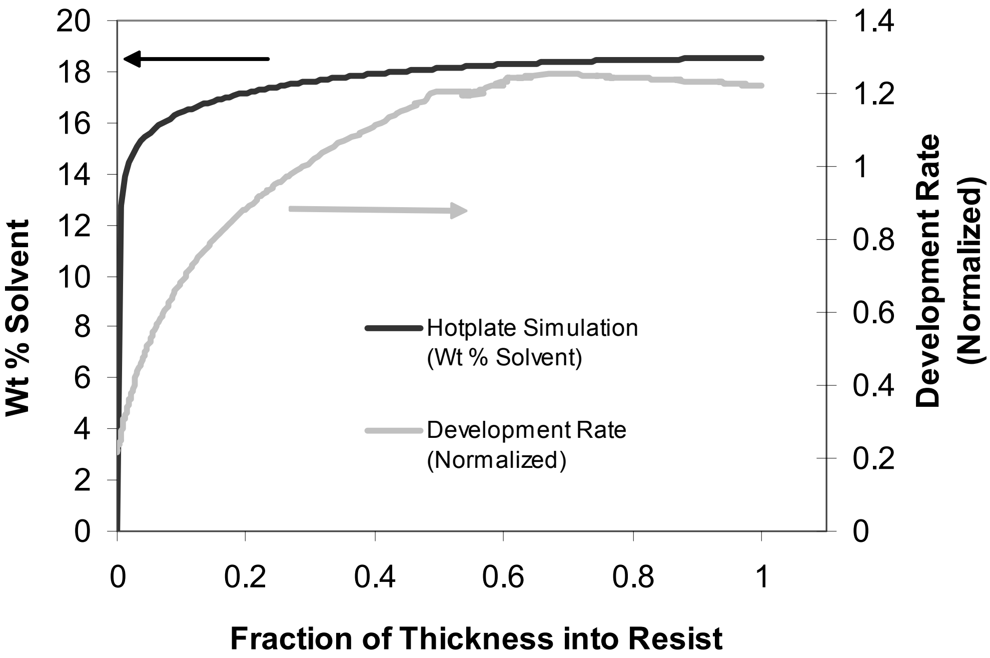

Figure 5.15 Dissolution rate and simulated concentration of residual PGMEA versus thickness of resist for a PAB temperature of 110oC. The dissolution rate has been normalized.

5. 9 SUMMARY

A technique has been presented which allows for layer by layer chemical analysis of resist films. This technique has been used in conjunction with liquid scintillation to determine the concentration profile of residual casting solvent in a DNQ/novolac resist system cast with PGMEA and diglyme solvents. The experiments show no observable concentration gradient for films cast with either diglyme and PGMEA over a range of bake temperatures from 70-110^{o}C. The experiments were compared with the solvent diffusion model for resist films by Mack.[3,4] The measured and simulated concentration profile of residual casting solvent was consistent. Furthermore, the dissolution rate profile of both photoresists were measured in conjunction with the chemical analysis of RCS distribution to test the theory that the residual solvent profile was responsible for observed surface induction. The resist cast from diglyme was essentially a control experiment: a linear solvent profile and a linear dissolution profile were observed. However, the resist cast from PGMEA showed a linear solvent profile (within the resolution of the experiment), and a very non-linear dissolution rate profile. For this resist system, another mechanism must be responsible for the observed surface inhibition. Other mechanisms for surface rate inhibition are considered in Chapters 6 and 7.

5.10 REFERENCES

(1) Gardiner, A. *PhD Dissertation*; The University of Texas at Austin: Austin TX, 1999.

(2) Hinsberg, W. D.; MacDonald, S. A.; Snyder, C. D.; Ito, H.; Allen, R. D. *Polym. Mater. Sci. Eng.* **1992**, *66*, 52-53.

(3) Mack, C. A. *Ph.D. Dissertation*; University of Texas at Austin: Austin, TX, 1998.

(4) Mueller, K. *Ph.D. Disseration*; The University of Texas at Austin: Austin, TX, 1998.

(5) Beauchemin, B. T.; Ebersole, C. E.; Daraktchiev, I. *Proc. SPIE* **1994**, *2195*, 610.

(6) Mack, C. A. *Inside Prolith: A Comprehensive Guide to Optical Lithography Simulation*; FINLE Technologies: Austin, TX, 1997.

(7) Shih, H.-Y.; Reiser, A. *Macromolecules* **1996**, *29*, 2082-2087.

(8) Hinsberg, W. D. e. a. *Chem. Mater.* **1994**, *6*, 481-488.

(9) Rao, V.; Hinsberg, W. D.; Frank, C. W.; Pease, R. F. W. *Proc. SPIE* **1993**, *1925*, 538.

(10) Henderson, C. L. *Ph.D Dissertation*; The University of Texas at Austin: Austin, TX, 1998.

(11) Scheer, S. A.; Brodsky, C. J.; Robertson, S. A.; Kang, D. *Proc SPIE* **2002**, *4689*, 937-948.

(12) Scheer, S. A. *MS Thesis: Design of Development Rate Monitoring Software and Measurement of Photoacid Concentration in Chemically Amplified Resists*; The University of Texas at Austin, 2001.

(13) Tsiartas, P. C. *Ph. D. Thesis, The University of Texas at Austin* **1998**.

(14) Ito, H.; Sherwood, M. *Proc. SPIE* **1999**, *3678*, 104.

CHAPTER 6: TESTING THEORIES FOR SURFACE RATE INHIBITION*

6.1 HYPOTHESES FOR SURFACE RATE INHIBITION

In the previous chapter, it was proposed that surface rate inhibition may be caused by concentration gradients of residual casting solvent (RCS) throughout the thickness of the photoresist. However, the main conclusion of Chapter 5 was that the films tested had an even distribution of residual solvent and that the observed inhibition could not be quantitatively linked to a RCS gradient. Therefore, other theories were explored to explain the phenomenon of surface inhibition. This chapter begins by describing several theories that have been proposed in the literature for surface inhibition (see Figure 6.1).

6.1.1 A Concentration Gradient of Varying Molecular Weight Species

Each and every component of the photoresist has an effect upon its dissolution rate. It is logical to suggest that a concentration gradient of *any* resist component could lead to observed surface rate inhibition. It is well known that an inverse relationship exists between the polymer molecular weight and the

---

*Reproduced in part with permission from S.D. Burns, A.B. Gardiner, J. Lutkenhaus, V.J. Krukonis, P.J. Wetmore, C. G. Willson, Proc. SPIE, Copyright 2001

Theories for Surface Rate Inhibition

Concentration Gradient Theories:

- Residual casting solvent concentration gradient
- Low MW chains concentration gradient
- Polymer density concentration gradient
- Photoactive compound concentration gradient

Other Theories:

- Oxidation of novolac surface
- Surface roughness
- Auto-dissolution enhancement
- Gel layer formation
- Combination of roughness/pKa effects

Figure 6.1 Summary of proposed theories for the mechanism of surface inhibition

dissolution rate, resulting in slower dissolution rates for higher molecular weight polymers.[1,2] Also, photoresist resins typically consist of polydisperse polymers. If longer chains migrated towards the surface or shorter chains migrated away from the surface, this would result in surface rate inhibition during dissolution. Presumably, low molecular weight chains would be more mobile, and may migrate away from the non-polar resist surface during PAB due to their polar end groups.[3] In film blends of polystyrene and deuterated polystyrene, it has been observed that preferential surface migration can occur based on relative molecular weights.[4,5] In this work, this theory was tested by doping a novolac resist with low molecular weight, radio-labeled polymer chains. Using the HD technique, it was possible to determine the concentration gradient of low MW chains in the photoresist film.

6.1.2 A Concentration Gradient of Polymer Density

Another theory involves a gradient of a photoresist component: polymer density. It is well known that as solvent is baked off during the PAB, densification of the film occurs. It has been suggested that the film densifies to a greater extent near the surface where the solvent is escaping.[6] A thicker "skin" is thought to form on the top layer of the resist. Dissolution of the film's surface is not slower if considered on a mass per time basis, but if measured as thickness per time, the large concentration of mass at the top of the film appears to dissolve slower than the bulk. This theory can also be tested using the HD technique. In this case, polymer concentration can be measured via the characteristic UV absorbance of the polymer in solution, and then correlated to the dissolution rate profile of the film.

6.1.3 A Concentration Gradient of Photoactive Compound (PAC)

Yet another theory also involves a concentration gradient of the most obvious resist component: the photoactive compound (PAC). This is by far the weakest theory for surface inhibition, since the phenomenon is known to occur in pure novolac resin with no added PAC.[7] Also, if PAC segregated to the surface causing surface inhibition in unexposed areas, heavily exposed areas would inevitably show surface enhancement. To the knowledge of the author, that effect has not been observed in the literature, and it is not observed with the novolac resin studied in this work. In order to confirm that the PAC gradient is indeed an incorrect hypothesis, the concentration gradient of a common PAC was measured in this work with the HD technique.

6.1.4 Oxidation of the novolac surface

The next theory is that the surface of the photoresist is oxidized during the PAB. In the presence of heat or UV light, oxygen is known to cause crosslinking of the methylene bridges in *ortho-ortho* novolac. The reaction is reported by Dammel[8] and Moreau[9] and is shown in Figure 6.2. A tacit assumption of this theory is that oxygen is more highly concentrated at the surface of the resist, resulting in a higher MW at the surface of the resist film as the polymer chains undergo crosslinking. Bowden *et al.*[7] report that with N64C novolac resin, considerable surface inhibition is observed with a PAB under ambient conditions, whereas a PAB in vacuum resulted in very little surface inhibition and faster bulk dissolution rates. An IR study confirmed the growth of the carbonyl peak (indicating crosslinking) in the open air bake, whereas crosslinking was not observed during the vacuum bake. In the work of Bowden *et al.*, slower dissolution rates and a longer induction period are clearly linked to the presence of oxygen during the PAB.[7] Empirical evidence for the oxidation theory is that the bake temperature has a large effect on the shape and extent of surface inhibition.[7,10] In this work, the oxidation theory was examined by confirming the effect of bake temperature on dissolution rate and measuring the sorption and permeability (and thus, diffusivity) of oxygen through a novolac film. Additionally, resists were baked with and without a nitrogen purge, and the effect upon the dissolution rate was compared.

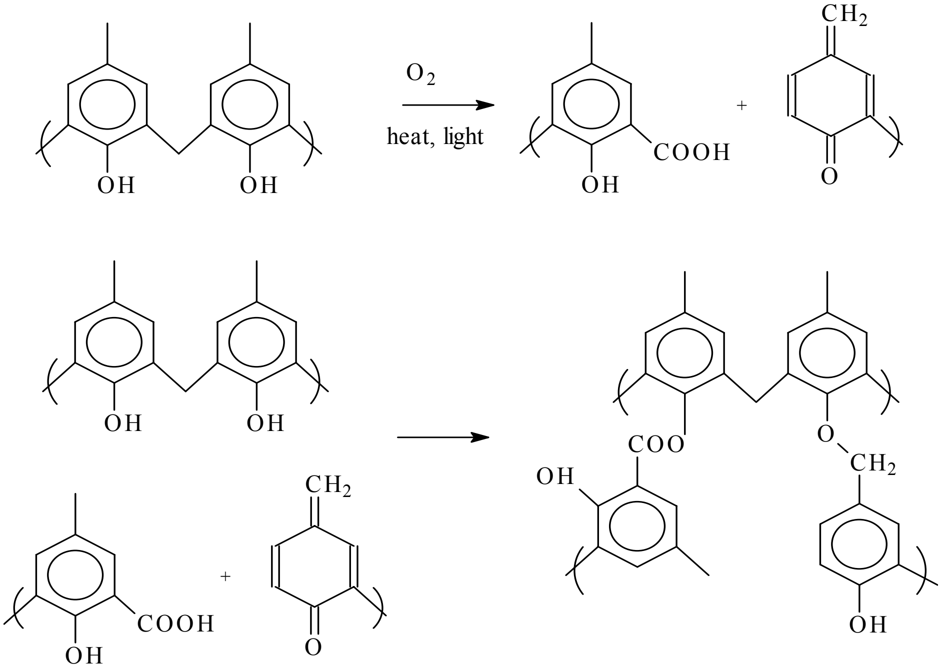

Figure 6.2 Oxidation and crosslinking reaction of *ortho-ortho* novolac at high temperatures or under UV light.[8,9]

6.1.5 Novolac Auto-Dissolution Enhancement

An interesting explanation for surface inhibition is discussed by Dammel.[8] He notes that for tank (immersion) development systems, it has been found that the first few wafers dissolved have slightly slower dissolution rates. The implication is that some dissolved novolac contaminates the developer, functioning as a surfactant that acts as an auto-dissolution enhancer. Novolac is often added to developer to keep processing conditions constant over time. This idea may explain surface inhibition because at the beginning of dissolution the concentration of dissolved novolac in the developer is low. As dissolution proceeds, the concentration of dissolved novolac in the developer near the resist increases, and may act as a surfactant that increases the dissolution rate for the bulk of the film. This theory was tested empirically in this work by adding small amounts of novolac resin to the developer, and measuring the bulk dissolution rate of the polymer films with various concentration of novolac in the developer.

6.1.6 Surface Roughness Evolution

The next hypothesis is that the dissolution rate is strongly dependent on the surface roughness, and that the surface roughness increases as dissolution proceeds. The origin of this theory stems from lattice simulations of dissolution that predict surface inhibition based upon an increase in surface roughness as the film dissolves.[11,12] The underlying mechanism is based on the fact that as the surface area available to the developer increases (due to increasing roughness), the dissolution rate increases. Reynolds and Taylor have shown that for APEX-E, the surface roughness does increase as dissolution proceeds with the same functional form observed for the dissolution rate in novolac materials.[13] The shape of the roughness plot strongly suggests a link to surface inhibition. However, the dissolution rate as a function of thickness has not been previously compared with the surface roughness as a function of thickness. In this work, that direct comparison is made for a novolac polymer film and a poly(hydroxystyrene) (PHOST) film by using the experiment technique of Reynold's and Taylor[13], and comparing the result to the measured dissolution rate profile.

6.1.7 Interfacial Gel Layer Formation

Another theory for surface inhibition stems from the "gel layer" theory for dissolution, which was introduced in Chapter 2. The assumption of this theory is that base transport into the film is (at least initially) the rate limiting step for dissolution. The "gel" is a separate phase between the developer and the bulk of the film with an intermediate composition. Peppas *et al.* discuss this theory for the general dissoluton of glassy polymers.[14] This theory has been studied extensively as the percolation model for phenolic polymer dissolution by Reiser,[15-23] and is also discussed in detail by Dammel.[8] The question of interfacial gel layer formation is addressed throughout Chapter 7 and will not be discussed explicitly in this chapter. (However, it should be noted that the main conclusion of Chapter 7 is that gel layer formation is not observed in a variety of phenolic polymers within the resolution (<15 nm) of the techniques used.) The relationship of this theory to surface inhibition is thought to be as follows: at the beginning of development, no gel layer exists and the dissolution is slow. As the gel layer forms, the dissolution accelerates. The gel layer eventually reaches a constant thickness and the dissolution rate reaches a steady state value. The surface inhibition period is thought to correspond with the formation of a gel layer. Hinsberg *et al*. have presented data showing gel layer formation in a Varcum novolac (phenolic resin) and a 157 nm resin (poly(norbornanehexafluoroalcohol) (pNHFA), in which the gel layer formation is concurrent with the observed surface rate inhibition.[24] This theory is revisited in Chapter 7.

6.2 USING THE ‘HALT DEVELOPMENT’ TECHNIQUE TO MEASURE CONCENTRATION GRADIENTS OF VARIOUS PHOTORESIST COMPONENTS

6.2.1 Investigating Low Molecular Weight Concentration Gradients by Halt Development

Radio-labeled novolac was synthesized from metacresol and ^{14}C labeled formaldehyde. The details of the synthesis are described elsewhere.[3] The separation of narrow MW fractions was accomplished by supercritical fluid fractionation at Phasex Corp. The details of this separation and analysis are described elsewhere.[3,25] The two samples of low molecular novolac "tracers" used to dope the resist had an Mn = 2130 and Pd = 1.26 (^{14}C-Tracer A), and the second tracer was over 70% dimers and trimers (^{14}C-Tracer B). A Beckman 1801 liquid scintillation counter was used to measure the activity of each sample. Fisher Scintiverse II was the scintillation cocktail used for the developer/resist solutions collected from the HD cell. The H-number quenching calibration for both the labeled solvents and labeled polymer is described elsewhere.[3] A small amount of each tracer (less than 7 wt%) was added to a separate novolac/PGMEA/PAC resist formulation. The spin speed was adjusted to obtain ~1.5 μm thick films. The PAB was 90^{o}C for 90s. The HD technique was then applied with the protocol discussed previously[26] in Chapter 5 to determine the concentration versus thickness of the radio-labeled low MW species.

The results of this experiment are shown in Figure 6.3. The distribution of the low MW species (both tracers) are constant throughout the thickness of the resist. Note the slightly positive y-intercept, indicating a higher than average concentration at the surface. If this theory were correct, there should be should be a depletion of low MW chains (the labeled species) near the surface of the resist. It appears that while the migration theory is plausible, the timescale necessary for this migration to occur is not present in the experiment or in a typical lithographic process.

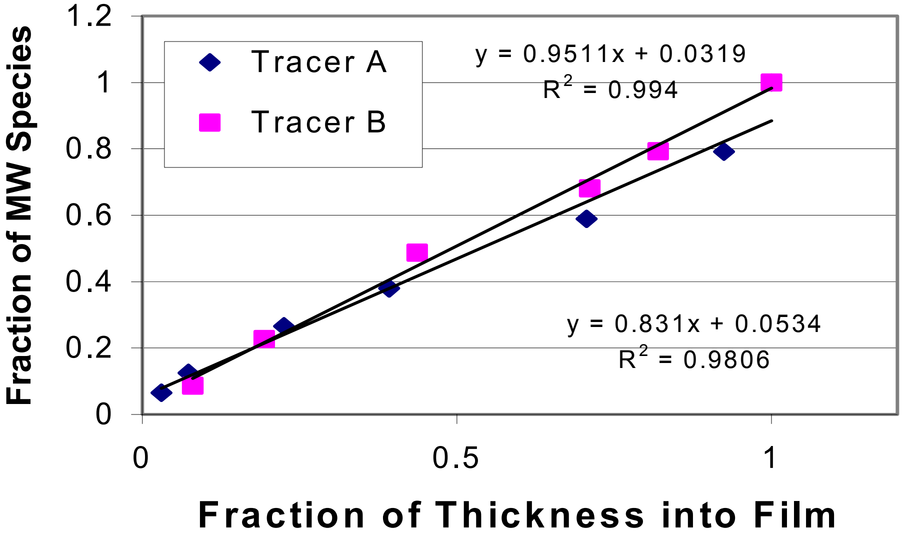

Figure 6.3 Low MW concentration throughout thickness in a novolac film

There is also indirect, empirical evidence that suggests low MW chain migration is *not* occurring. For example, a 1.0 μm film consisting of only the monodisperse novolac of Mn = 2130, Pd = 1.26, cast from PGMEA and baked at 150°C shows a considerable amount of surface inhibition. A blend of this resin and the polydisperse novolac (Mn = 9330, Pd = 4.9) showed no increase in surface inhibition, but a general decrease in the bulk dissolution rate – the expected result if the low MW chains were dispersed evenly throughout the film. If the low MW chain migration theory were correct, one would expect surface inhibition to be strongly dependent on the polydispersity, decreasing considerably at values of Pd close to unity. In our experiments, the extent of surface inhibition did not depend on polydispersity. Moreau reports that using higher MW narrow-dispersity novolac resin is a method of *increasing* the extent of surface inhibition,[9] although Dammel presents contrary data that show increasing surface inhibition with increasing polydispersity.[8] In summary, a variety of experiments provide both direct and indirect evidence suggesting that the migration of low MW chains away from the film surface is not an adequate explanation for surface inhibition in the novolac resin under investigation.

6.2.2 Investigating Density and PAC gradients by Halt Development

The HD technique was used to determine the gradient of novolac density and PAC concentration. In this case no resist components were specifically labeled. Rather, the characteristic UV-Vis absorbance of both the novolac (298 nm) and PAC (343 nm) was measured with a Hewlett Packard 8452A UV-Vis spectrophotometer to determine the concentration at specific depths throughout the film. Concentration standards were prepared of novolac and PAC, and their UV-Vis absorbance spectra were measured to verify that Beer's Law was applicable in the concentration region of interest. Films of Novolac/PGMEA/PAC were spun at 2500 rpm for 30s to achieve a film thickness of ~1.2μm. The PAB was 90°C for 90s. The films were not exposed. The HD technique was used to obtain specific fractions of the film in solution. Relative concentrations were determined at a specific thickness by normalizing the absorbance at the proper wavelength to the absorbance of a completely dissolved film. The results of this experiment are shown in Figure 6.4.

The concentration of novolac (density) and PAC were found to be constant throughout thickness within the resolution of the experiment. Thus, the film did not preferentially densify near the surface during the post apply bake (PAB), and the photoactive compound did not preferentially segregate towards (or away from) the surface. Furthermore, if there was a concentration gradient in residual solvent or density, one would expect a gradient in the index of refraction over thickness. Ficner *et al.* studied index of refraction gradients in novolac resists with a Metricon Prism coupler.[27] They observed gradients in the index of refraction for thick films (32μm), indicating a significant residual solvent gradient. But with thinner films (4-8 μm), the index gradient was "too small to lead to observable bent light modes", and any index gradient was not detectable.[27] This is consistent with our results. Based on these results, the solvent, density, and PAC gradient theories are not viable explanations for surface inhibition for this novolac resin.

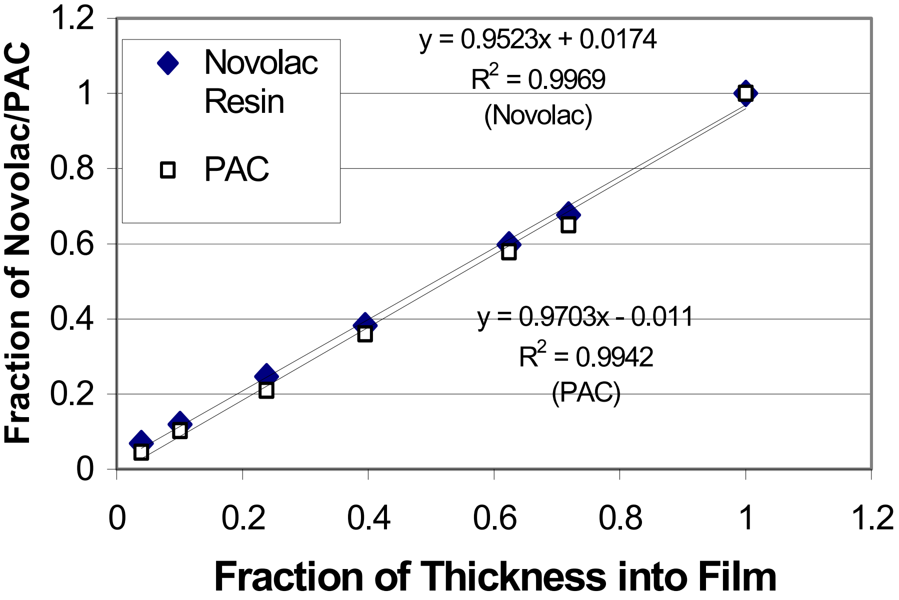

Figure 6.4 Overall polymer and PAC concentration throughout thickness in a novolac film

Note that the UV-Vis density experiment of Figure 6.4 is identical to the HD verification experiment performed in section 5.6.2. In Chapter 5, it was assumed that the density was linear (no gradients) such that the UV-Vis experiment proved that the HD technique was valid, and that no nonlinearities in the data could be attributed to the technique. In this chapter, it is assumed the technique is valid, and the experimental results prove that a density gradient does not exist in the photoresist film studied. Admittedly, this logic train is somewhat circular. However, the wide variety of data from the HD technique (Figures 6.4, 6.5, 5.10, 5.12, 5.13) with each photoresist component all yield identical, linear results. This wide array of results suggests that the HD technique itself does not introduce any nonlinearities into the data.

6.3 OXIDATION EFFECTS DURING PAB

6.3.1 Empirical Observations of Oxidation During PAB

The crosslinking reaction caused by heat (or light) and oxygen is reported by Moreau[9] and Dammel[8] and reproduced in Figure 6.2. This reaction has been studied in the context of understanding the post develop bake used to harden novolac resist features. In the presence of oxygen, chain scission is thought to occur at the methylene bridges followed by cross-linking to a nearby chain. One method of detecting the reaction is by monitoring the growth of the carbonyl peak by Fourier Transform Infrared (FTIR) spectroscopy. Dammel and Moreau point out that this reaction has been observed in an atmosphere with no oxygen, suggesting that oxygen was previously absorbed into the film or "self-oxidation" of the novolac occurred.[8,9] The oxidation theory for surface inhibition was first suggested due to the strong influence of PAB temperature upon the extent of surface inhibition. The dissolution rate of the novolac used in this study is shown over a range of PAB temperatures (60-150°C) in Figure 6.5. (Note that the initial film thickness varied with PAB temperature. To avoid confusion, the initial film thickness has been normalized to the average thickness of 1.25 μm for each experiment). The bulk dissolution rate slows as the temperature is increased, due to the known decrease in residual casting solvent.[8,9] There is also a dramatic change in the extent of surface inhibition. However, the HD experiments,[26] the model by Mack[28] and the results of Ficner[27] suggest that the change in surface inhibition is not related to a residual solvent concentration gradient in the film. Therefore the oxidation theory deserves close examination for the novolac resin studied in this work.

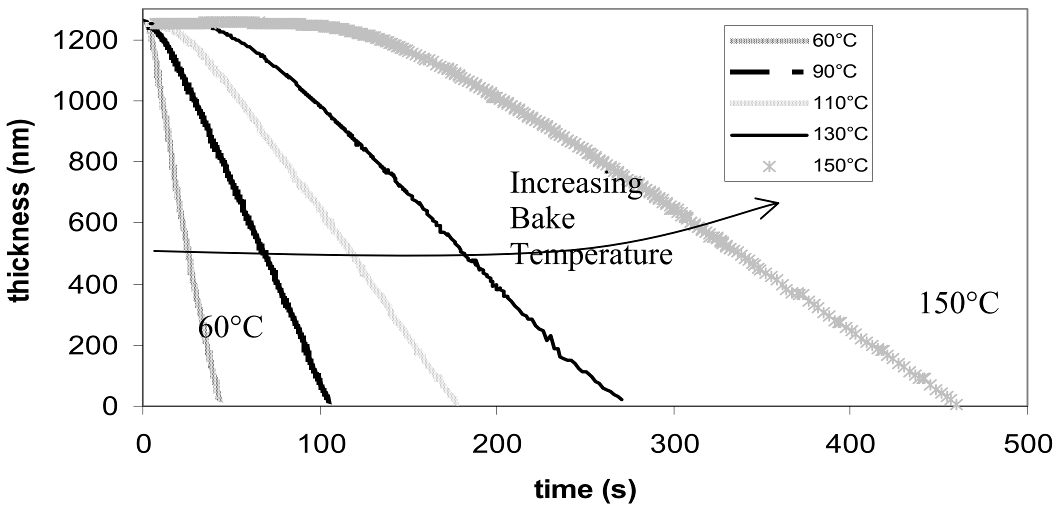

Figure 6.5 Response of dissolution rate to PAB temperature for novolac resin coated from PGMEA.

One approach is to perform the PAB in an oxygen free environment. This was done by purging the film with industrial grade nitrogen (purchased from PraxAir) at a high flow rate (~ 30 mL/s) during the PAB. Novolac films were spun cast from PGMEA at 2500 rpm for 30s with a 150°C for 90s to achieve a film thickness of ~1.2 μm. Three films were baked under a nitrogen purge, while two films were not. A developer concentration of 55 % AZ300 MIF and 45% deionized water by volume was used for dissolution, which was monitored with multiwavelength interferometry. The results are shown in Figure 6.6. The dissolution rate versus thickness is plotted for the five experiments. There is a slight decrease in the bulk dissolution rate for the films baked in an oxygen atmosphere, suggesting a small amount of cross-linking (due to oxidation) may be occurring. However, the extent of surface inhibition is the same for all films, suggesting that the crosslinking is not occurring preferentially at the surface, but rather uniformly throughout the bulk of the film.

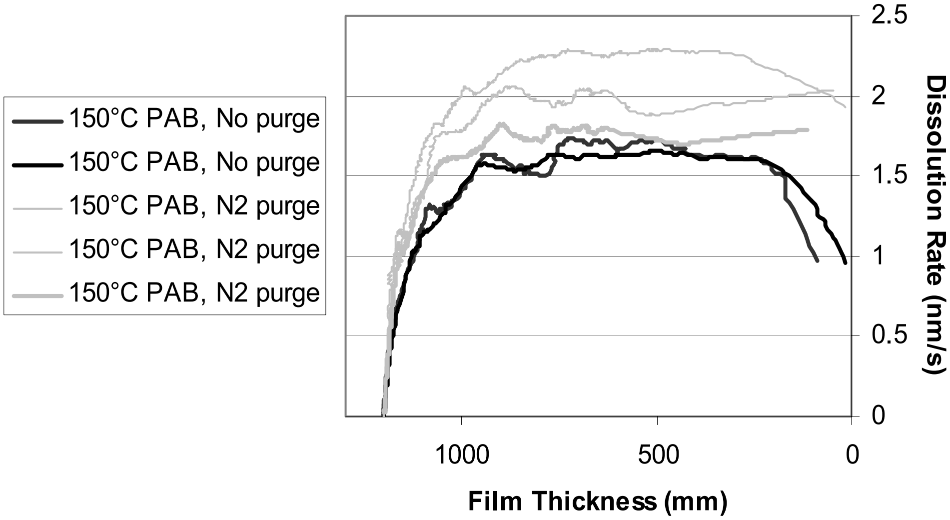

Figure 6.6 Dissolution rate versus film thickness of novolac with and without a nitrogen purge during a 150°C PAB.

FTIR spectra were taken for the novolac films baked over a range of times and temperatures (50-170°C). The films were cast from diglyme so that residual casting solvent would not contribute to the carbonyl peak. There was no observable increase in the carbonyl region (1550-1700 cm^{-1}) until the resin was baked for 30 minutes at 170°C. (But note the strong change in surface inhibition at moderate bake temperatures (90°C)).

However, only a few crosslinking events are needed in order to locally double the MW of the resin and drastically affect the dissolution properties -

possibly few enough events that the carbonyl band would not show a large increase. Also, oxygen may be absorbed during the spin coating of the polymer resin, which may account for observed surface inhibition even during a PAB purged with nitrogen. The main issue then is the sorption behavior of oxygen into the film during spin coating and baking. An assumption of the oxidation theory is that a concentration gradient of oxygen is present throughout the film thickness that would lead to a concentration gradient in MW as the cross-linking reaction occurs.

The mass transfer problem of sorption of small penetrant molecules into a flat slab from one side is trivial if Fickian diffusion is assumed and diffusivity data is known.[29] If the diffusion coefficient is known, it is possible to simulate the relative mass uptake and the time dependent concentration gradient of oxygen in the novolac film during spin coating and PAB. For these reasons, the diffusivity of oxygen in novolac was measured with a combination of permeation and equilibrium sorption experiments. These techniques were chosen for their availability and because their use is well documented for studying gaseous transport through polymer membranes.

6.3.2 Direct Measurement of Oxygen Diffusivity in Novolac

The diffusion coefficient of novolac was measured by a combination of permeation and sorption (solubility) experiments. The governing relationship is:

$$P = D \times S \tag{6.1}$$

where P is permeability, D is the diffusion coefficient, and S is the solubility. Thus, the diffusivity of oxygen in novolac can be calculated from measurements of permeability and solubility.

Novolac resin from Schenectady (Mn = 9320, Pd = 4.9) was used for these experiments. For the permeation measurements it was necessary to cast a free standing film. However, the adhesive nature of the resin did not lend itself to standard film formation techniques. A solution was prepared of novolac dissolved in PGMEA to saturation (~50 wt%), and spun coat on a Whatman Anopore Membrane Disc (0.02 μm, 47 mm) at 2000 rpm for 30 s. The film was then baked at 90°C for 1 hour. An identical film was cast on silicon, and the film thickness was measured to be 32 μm by a Tencor Instruments Alpha step 200 profilometer. The membrane disc provided a film support with a high rate of oxygen permeance. Thus, any resistance to oxygen was due to the polymer film. The sample geometry and experimental apparatus are shown in Figure 6.7. A detailed description of the technique can be found elsewhere.[30] Industrial grade oxygen (purchased from Praxair) was used as the pure gas feedstream at a pressure of 15 psia. The temperature of the apparatus was held at 35°C. The downstream pressure was recorded over time. The permeability of oxygen through novolac was measured to be 61.8 Barrers [10^{-10} cc(STP)-cm/(cm^2-s-cmHg)] at 35°C.

The powder form of the resin was used for the solubility (sorption) measurements. Novolac powder (~ 0.1 g) was loaded into a sorption cell, which was immersed in a temperature controlled water bath held at 35°C. The concentration of oxygen in the polymer was extracted over a range of pressures from 0-100 psi (Figure 6.8) by standard techniques.[31] The resulting curve was linear, with an R^2 close to 1, indicating Henry's law sorption in this range of pressures. The slope was fit to be 0.153 cc(STP)/cc polymer-psia.

Finally, the diffusion coefficient was calculated from equation (6.1) to be 3.1×10^{-11} cm^2/s. This value is slightly lower than the 10^{-7}-10^{-9} cm^2/s values reported for similar polymers.[29,32] During spin casting, it is possible that the novolac solution leaches into the porous support, creating a thicker film than previously thought. The net effect would be an increase in the measured permeability and a higher diffusivity. The measured diffusivity value can therefore be considered to be a conservative, lower bound estimate of the diffusivity. Assuming Fickian diffusion into a slab from an infinite reservoir, the calculated concentration profile of oxygen in a 1μm film of novolac over time is shown in Figure 6.9.

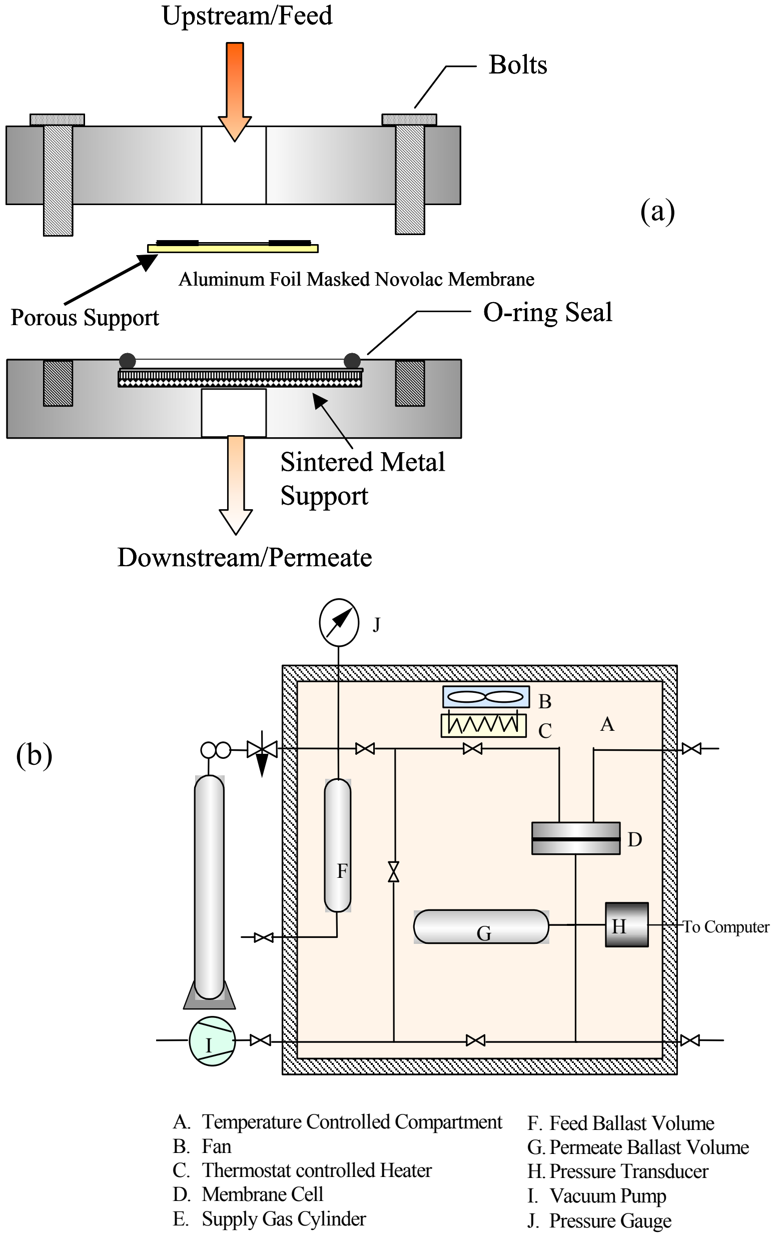

Figure 6.7 (a) Sample schematic and geometry (b) Schematic of the permeation cell used for O_2 permeance measurements through novolac.[30]

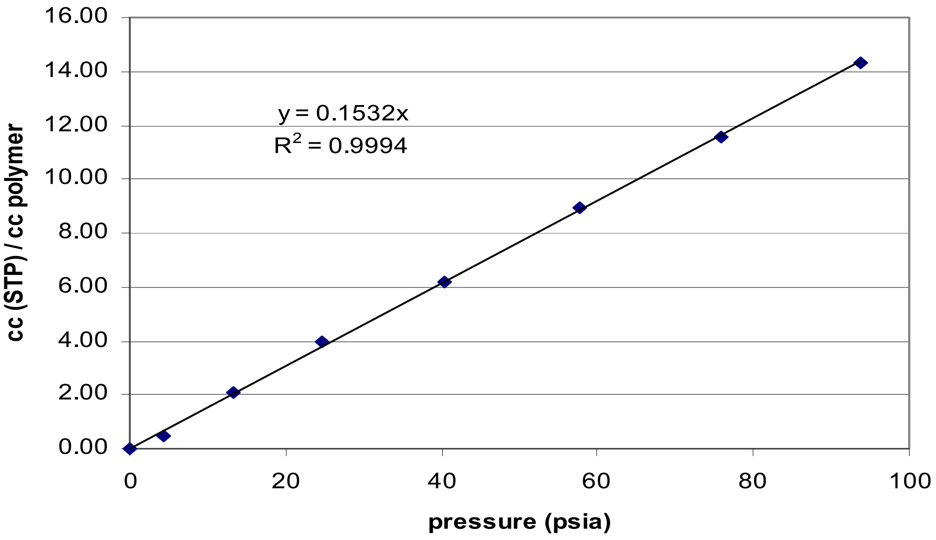

Figure 6.8 Sorption isotherm of oxygen in novolac at 35°C

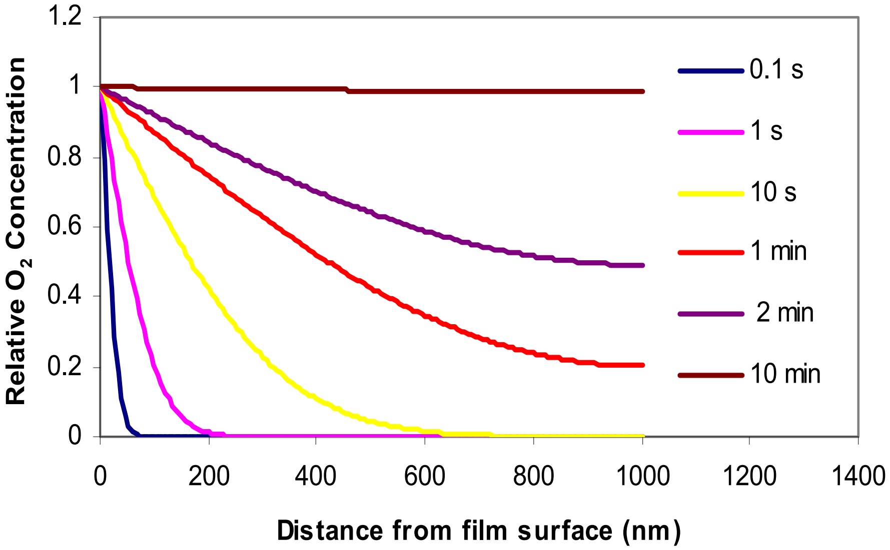

Figure 6.9 Simulated Fickian transport of oxygen through a 1 µm novolac film

Within 10 minutes, the film has completely sorbed the oxygen, and the concentration profile is flat. Since typical post apply bakes are on the order of 2 minutes, one might argue that oxidation of the top regions of the film is a plausible explanation for surface inhibition. However, the value of diffusivity is for 35°C (close to room temperature) and represents the sorption of oxygen into novolac during normal air exposure, spin casting, cooling, *etc*. The transport of oxygen into novolac during the PAB (at ~90°C) can be considered to be at least an order of magnitude faster. It is therefore highly unlikely that a concentration gradient of oxygen exists in the resist film during PAB.

One might also argue that oxidation of the film surface (top few nanometers) is possible if a higher concentration of oxygen exists in the surrounding environment due to the partitioning coefficient. In this scenario, oxidation of the top surface is more likely due to the high concentration of oxygen near the surface (compared to the bulk of the film) because of the equilibrium sorption properties of the polymer. However, the data from Figure 6.8 indicate that the equilibrium concentration of oxygen in novolac polymer is a factor of 10 higher than in air (at 35 C). Thus, there is no specific reason why oxidation should occur preferentially at the film surface.

6.3.3 Summary of Oxidation Effects in Novolac

Experiments in which the effect of bake temperature and ambient atmosphere on dissolution rate were determined provide empirical evidence that oxidation of the surface is a viable theory for the cause of surface inhibition. However, the N_2 purge experiments indicated only that the bulk dissolution rate was affected at high temperatures, and FTIR experiments indicated that observable amounts of oxidation (crosslinking) only occurs 50-80^{o}C above common PAB temperatures. Measurements of permeability and sorption of oxygen into a novolac film, combined with Fickian diffusion simulations suggest that the transport of oxygen into novolac is too rapid to result in a significant concentration gradient (which is consistent with the N_2 purge experiments). For all these reasons, it is highly unlikely that oxidation of the film surface is the fundamental mechanism that governs surface rate inhibition.

6.4 NOVOLAC AUTO-DISSOLUTION ENHANCEMENT

The premise of the dissolution enhancement theory is that dissolved novolac near the undissolved film acts as a dissolution promoter.[8] (For the moment, the exact mechanism of this enhancement is not considered). The simplest method for determining if dissolved novolac alters the dissolution rate (for the sample under consideration) is to perform the immersion tank experiment that was the origin of the theory. The experiment involves adding novolac to the developer prior to dissolution, and measuring the effect on the bulk dissolution rate. In this case, the experiment was done in puddle mode.

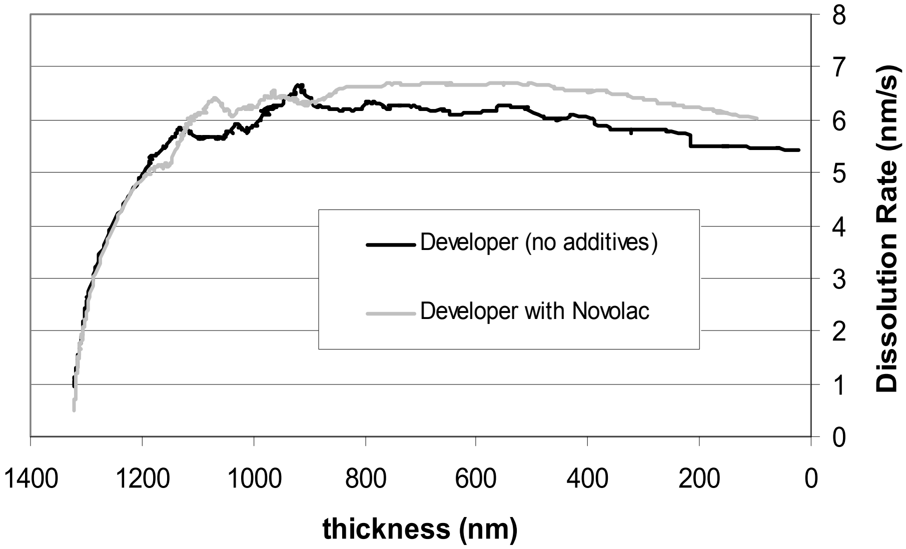

Figure 6.10 Dissolution rate versus thickness of a novolac film with and without adding novolac to the developer

The developer solution used was 55:45 AZ300MIF to deionized water (by volume). Aliquots of the developer were chosen and novolac was added in various ratios to the developer, up to 1% by weight. The novolac/developer solutions were stirred for up to an hour. At higher concentrations, not all of the added novolac dissolved. Films of novolac were cast from PGMEA at a spin speed of 2500 rpm for 30s with a PAB of 90°C for 90s. The films were dissolved with the various developer solutions, and the dissolution was monitored with multiwavelength interferometry. A typical result is shown in Figure 6.10. No change was observed in the bulk dissolution rate with the various developer solutions. Also, there was no change in the extent of surface inhibition. The novolac used in this work does not enhance or inhibit the bulk dissolution rate when added *a priori* to the developer. These empirical results suggest that novolac auto-dissolution enhancement is not an adequate explanation for surface inhibition in the photoresist studied.

6.5 SURFACE ROUGHNESS EFFECTS DURING DISSOLUTION

The roughness experiments were performed using the Schenectady novolac resin and PHOST (Mn = 8770, Pd = 1.11, obtained from Nippon Soda) resin coated from PGMEA. The spin speed was adjusted to obtain ~ 1 μm films, which were baked at 90^{o}C for 90s. In this case, the HD technique was used, although it was not necessary to collect the effluent. The development was quenched with water and the films were blown dry with nitrogen. The surface roughness was calculated from images taken on a Park Scientific Instruments Autoprobe AFM. It was assumed that quenching development with water and drying does not significantly alter the surface roughness.

The results of this experiment are shown in Figure 6.11. The average surface roughness and dissolution rate are plotted versus thickness. For each resin, the roughness trend is similar. Novolac and PHOST were smooth when first spun cast (under 1 nm of roughness), but as dissolution proceeded the roughness increased, reaching a bulk value of 2-3 nm. The roughness behavior is consistent with similar experiments performed by Reynolds and Taylor on APEX-E,[13] and is qualitatively consistent with observed roughness behavior from latticed-based simulation.[11,12]

For novolac, there is a strong correlation between the roughness curve and the dissolution rate. However, for PHOST, there is *no* correlation between surface roughness and dissolution rate. It is difficult to argue that surface roughness effects alone are responsible for surface inhibition when the same roughness trends are observed in materials with a wide range of dissolution rate profiles. That is, if only roughness effects were responsible for surface inhibition, one would expect to see surface inhibition in PHOST and APEX-E. However, the CI model offers an explanation for this strange paradox based upon the pKa of each resin material.

6.6 A NEW EXPLANATION FOR SURFACE INHIBITION – A COMBINATION OF PKA AND ROUGHNESS EFFECTS

The novolac resin studied in this work has been shown to have no significant concentration gradients of residual solvent, low MW chains, PAC or overall density over a 1 μm film. Furthermore, there is no evidence of preferential oxidation near the surface, or auto-dissolution enhancement occurring. The increase in roughness during dissolution may partially explain the observed surface inhibition in novolac, but lends no explanation to the dissolution profile of PHOST. Any theory offered to explain the dissolution behavior of both materials must incorporate the different chemistries of the two materials. (The oxidation theory and the auto-dissolution enhancement theory are candidates, but both have been disproved for the novolac resin of interest.) The CI model proposed by our research group has provided some insight into the issue. The main input parameters to the model are the fraction of ionized surface sites (α) and the critical fraction of sites necessary to render a polymer chain insoluble (f_{crit}). The latter value, f_{crit}, is assumed to change little from polymer to polymer. However, α is very dependent upon the structure and acidity of a given polymer. In Chapter 2 it was shown that the equilibrium of the deprotonation reaction dictates that α is related to the pH of the developer near the surface of the film (pH_o) and the pK_a of the polymer by:[33]

$$\alpha = \frac{10^{pH_o - pKa}}{1 + 10^{pH_o - pKa}} \tag{6.2}$$

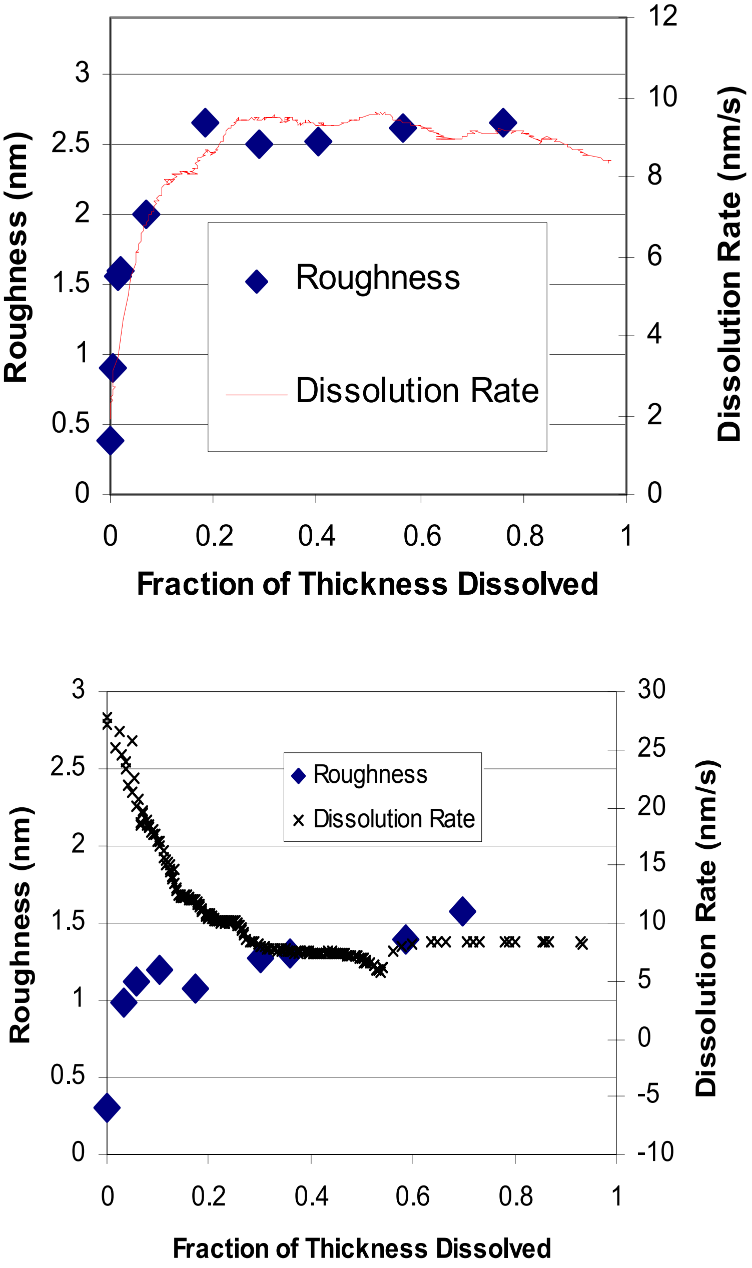

Figure 6.11 (a) Surface roughness and dissolution rate versus thickness for a novolac resin. (b) Surface roughness and dissolution rate versus thickness for a PHOST resin.

The acidity function of the polymer dictates that α is related to the pKa of the film[33]:

$$pK_a = f(\alpha) \tag{6.3}$$

where Equation (6.2) is the acidity function of the polymer. Our recent modeling efforts[34,35] (see Chapter 4) have included a third effect[34,35],

$$pH_o = f(pH_{bulk},\alpha) \tag{6.4}$$

in which the surface pH of the developer (pH_o) is lower than that of the bulk due to electrostatic repulsion of the negative hydroxide ions by the overall negative surface charge of the dissolving polymer (formation of an electric double layer). The solution to the Poisson-Boltzmann equation to determine Equation (6.3) and the calculation of α (for both novolac and PHOST) is reported in Chapter 4 and elsewhere.[35] For this discussion, the effect of surface forces is included to place a lower bound on the value of α for a given polymer. The values of α reported are for a developer concentration of 0.26 N. For PHOST, the calculated values of α are between 0.8 - 0.99. For novolac, the calculated value of α is in the range 0.5 - 0.8. The overall result is that α is considerably lower for novolac than for PHOST. This result was used to explain why PHOST dissolved much faster than novolac if all relevant conditions are equal.[33] Here, this result is used to provide insight into surface inhibition.

A new addition to the CI model has been ionization equilibrium. Previously, a fraction of surface sites (α) would ionize in a given time step.[11,36,37] For an undissolved chain, the same sites remained ionized for the remainder of the simulation (dissolution of the film). However, the equilibrium of the deprotonation reaction is known to be quite fast. The new algorithm assumes that a time step in the simulation is greater than the time needed for equilibrium, and that ionized sites on undissolved chains can reprotonate. The ionized sites are randomly redistributed in each time step while keeping the overall fraction of ionized sites constant. The system is then able to sample many more configurations, and also follows the principle of microscopic reversibility. At high values of α ($\alpha > f_{crit}$), this added change has little effect on the simulations. However, at low values of α ($\alpha \sim f_{crit}$), the effect is quite significant. Previously, when α approached f_{crit}, the system would often become "stuck" in a state where no chains would dissolve. Now, a new configuration is sampled in each time step, sometimes going through several time steps until the system becomes "unstuck". This effect is important at the surface, where the film starts smooth , and then the roughness increases as dissolution proceeds.

To illustrate, consider a lattice of monodisperse chains of degree of polymerization equal to 30 and a void fraction of 0.2. In this example, f_{crit} is set to 0.6. PHOST and novolac can be examined in the simulation simply by changing the value of α. (Larger values of α are correlated with PHOST, while smaller values are correlated with novolac). The thickness versus time in the simulations is shown for a range of $\alpha = 0.7 - 0.9$ in Figure 6.12(a). First, note that the bulk dissolution rate is slower at smaller values of α, as would be expected by experimentally comparing PHOST with novolac (Figure 6.12b). It is also evident that higher values of α result in only a slight amount of surface inhibition. Conversely, lower values of α result in a large extent of surface inhibition. At $\alpha = 0.7$, over 300 time steps elapse before a bulk dissolution rate is reached. The total time to clear is just over 800 time steps. Over 1/3 of the dissolution time is during the "inhibited" period at the beginning of dissolution. This comparison suggests that surface inhibition is due to a combination of two things. Most importantly, the increased pK_a, (and thus decreased α) of novolac. However, the increase in roughness during dissolution also plays a big role. If the initial spin coated film started out as rough as a dissolving film, then surface inhibition (as observed in the simulations) would also not be present. Thus, the simulations suggest that surface inhibition is a combination of pK_a and roughness effects, and provide an explanation for the general observation that novolac films show surface inhibition whereas PHOST films do not.

The simulations were compared to an experiment, shown in Figure 6.12(b). The dissolution profile of PHOST (Mn = 8770, Pd = 1.11) and novolac (Mn = 9300, Pd = 4.9) were compared. All other formulation parameters, developer concentraton, *etc*. were kept constant. Qualitatively, the simulations capture the correct trend. The most obvious difference is that the surface inhibition observed in the simulations is always "sharp". That is, the dissolution rate changes abruptly from near zero to the bulk dissolution rate over only a few nanometers. Experimentally, a more curved profile is usually observed over as much as 100 nm. (Figure 6.12(b)). The difference may be due to subtle mass transfer effects that are not considered in the model.

Another interesting trend emerges from the model. Figure 6.13 shows a simulation in which the void fraction of the lattice is varied between 0.05 and 0.3. In the lattice model, voids are considered to be either void fraction or residual casting solvent, so a void fraction of 0.3 is not an unreasonable value at low PAB temperatures. The other simulation parameters are kept constant at f_{crit}=0.6, α=0.8, and degree of polymerization of 30. The decrease in void fraction decreases the initial surface roughness, which has a large effect on the inhibition period. At a void fraction of 0.3 there is almost no surface inhibition, but at a void fraction of 0.05 there is considerable surface inhibition, over a depth of ~8 nm. This is an interesting trend when compared to the change in surface inhibition with PAB temperature shown in Figure 6.13. At low PAB temperatures, considerable amounts of PGMEA are present in the film. As much as 20 wt% has been reported to be present after a 70°C PAB for 90 seconds.[3] At higher PAB temperatures, nearly all the solvent is baked off, and the film is annealed, reducing the intrinsic void volume to ~3%.[27] The CI lattice model

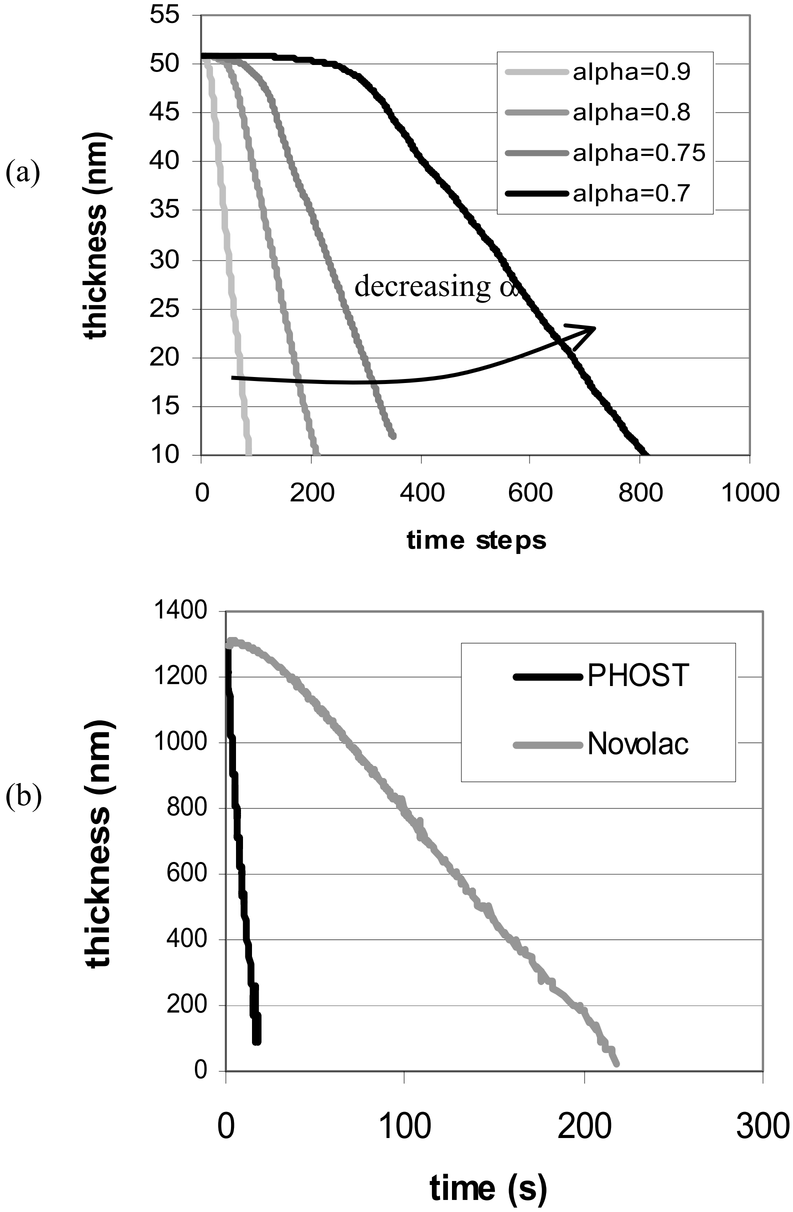

Figure 6.12 (a) Critical Ionization Dissolution Simulation showing effect of changing the fraction of ionized surface sites, α. (cell height is equal to 0.7 nm) (b) Dissolution of PHOST (Mn=8770, Pd=1.1) and novolac (Mn=9370, Pd=4.9) under identical conditions.

predicts the roughness to increase from 0.21 to 0.36 nm over the range of void volume presented. This small increase in roughness is difficult to confirm experimentally, and it should be noted that many other effects may contribute to the change in surface inhibition with temperatue. Again, the depth of the inhibition predicted in the model is smaller than observed experimentally. However, the simulation results qualitatively provide mechanistic explanations for every experimental result reported in this chapter.

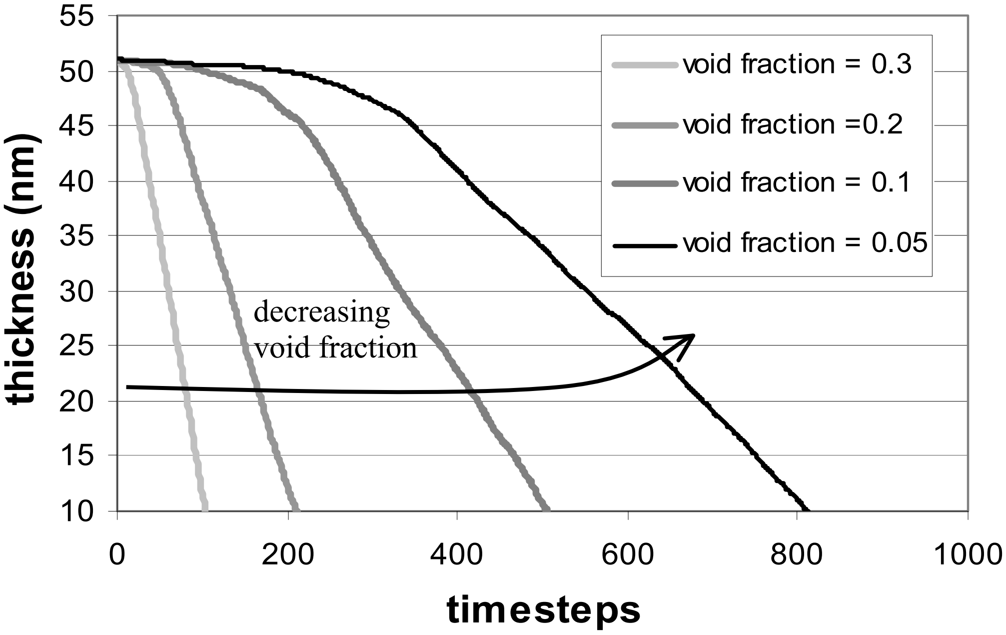

Figure 6.13 Critical Ionization Dissolution Simulation showing effect of changing the lattice void fraction. (dp=30, α=0.8, f_{crit}=0.6)

6.7 SUMMARY AND CONCLUSIONS

In this chapter, a wide variety of theories were explored to explain the phenomenon of surface inhibition observed during aqueous base dissolution of novolac films. The HD technique was used to measure the concentration gradient of residual casting solvent (Chapter 5), low molecular weight chains, photoactive component, and polymer density. Each component was found to be evenly distributed throughout the thickness of a novolac film. Several other theories were tested, including oxidation of the novolac surface, auto-dissolution enhancement, and surface roughness evolution. Close examination of these theories did not yield a single, satisfying explanation for surface rate inhibition.

The CI model has led some insight into surface inhibition by considering both roughness and pKa effects. The lattice dissolution model predicts that surface rate inhibition increases when the fraction of ionized surface sites (α) is lowered. This is qualitatively consistent with observed dissolution behavior of PHOST and novolac, and the fact that PHOST is more acidic than novolac (and thus will have a larger fraction of ionized sites at equilibrium). The result explains why surface roughness influences the dissolution rate of novolac, but not the dissolution rate of PHOST. Finally, simulations show changes in surface inhibition with changes in void fraction of the lattice sites. This is qualitatively consistent with the observation that higher PAB temperatures lead to increased surface inhibition. In the next chapter, the gel layer theory for surface inhibition is considered in detail.

6.8 REFERENCES

(1) Allen, R. D. e. a. *Proc. SPIE* **1995**, *2438*, 250.

(2) Tsiartas, P. C.; Simpson, L. L.; Qin, A.; Allen, R. D.; Krukonis, V. J.; Wetmore, P. M.; Willson, C. G. *Proc. SPIE* **1995**, *2438*.

(3) Gardiner, A. *PhD Dissertation*; The University of Texas at Austin: Austin TX, 1999.

(4) Hong, P. P.; Boerio, F. J. *Macromolecules* **1994**, *27*, 596-605.

(5) Harihan, A. e. a. *J. Chem. Phys.* **1993**, *99*, 656-663.

(6) Toukhy, M. A. *Proc. SPIE* **1987**, *771*, 263.

(7) Bowden, M.; Thompson, L.; Farenholtz, S.; Doerries, E. *J. Electrochem. Soc.* **1981**, *128*, 1304.

(8) Dammel, R. *Diazonapthoquinone-based Resists*; SPIE Optical Engineering Press: Bellingham, Washington, 1993.

(9) Moreau, W. M. *Semiconductor Lithography: Principles, Practices, and Materials*; Plenum Publishing: New York, 1988.

(10) Dill, F. H.; Shaw, J. *IBM J. Res. Dev.* **1977**, *21*, 210.

(11) Flanagin, L. W.; Singh, V. K.; Willson, C. G. *Journal of Vacuum Science & Technology B* **1999**, *17*, 1371-1379.

(12) Trefonas, P. *Proc. SPIE* **1989**, *1086*, 484.

(13) Reynolds, G. W.; Taylor, J. W. *J. Vac. Sci. Technol. B* **1999**, *17*, 334-344.

(14) Narasimhan, B.; Peppas, N. A. *Macromolecules* **1996**, *29*, 3283-3291.

(15) Kim, M. S.; Reiser, A. *Macromolecules* **1997**, *30*, 3860-3866.

(16) Kim, M. S.; Reiser, A. *Macromolecules* **1997**, *30*, 4652-4655.

(17) Reiser, A.; Huang, J. P.; He, X.; Yeh, T. F.; Jha, S.; Shih, H. Y.; Kim, M. S.; Han, Y. K.; Yan, K. *European Polymer Journal* **2002**, *38*, 619-629.

(18) Reiser, A.; Yan, Z. L.; Han, Y. K.; Kim, M. S. *Journal of Vacuum Science & Technology B* **2000**, *18*, 1288-1293.

(19) Shih, H. Y.; Reiser, A. *Macromolecules* **1994**, *27*, 3330-3336.

(20) Shih, H. Y.; Reiser, A. *Macromolecules* **1995**, *28*, 5595-5600.

(21) Shih, H. Y.; Reiser, A. *Macromolecules* **1997**, *30*, 4353-4356.

(22) Shih, H. Y.; Zhuang, H.; Reiser, A.; Teraoka, I.; Goodman, J.; Gallagher-Wetmore, P. M. *Macromolecules* **1998**, *31*, 1208-1213.

(23) Shih, H. Y.; Reiser, A. *Macromolecules* **1997**, *30*, 3855-3859.

(24) Hinsberg, W. D., et. al. *Presented at EIPBN, 2002; private communications with Dr. W.D. Hinsberg* **August, 2002**.

(25) Burns, S. D.; Gardiner, A.; Krukonis, V. J.; Wetmore, P. M.; Qin, A.; Willson, C. G. *Proc. Amer. Chem. Soc., PMSE* **1999**, *81*, 81-84.

(26) Gardiner, A.; Burns, S. D.; Qin, A.; Willson, C. G. *J. Vac. Sci. Technol. B* **2001**, *19*, 136.

(27) Ficner, S.; Dammel, R.; Perez, Y.; Gardiner, A. B.; Willson, C. G. *Proc. SPIE* **1997**, *3049*, 838.

(28) Mack, C.; Mueller, K. E.; Gardiner, A. B.; Sagan, J. P.; Dammel, R.; Willson, C. G. *J. Vac. Sci. Technol.* **1998**, *16*, 3779.

(29) Hines, A. L.; Maddox, R. N. *Mass Transfer: Fundamentals and Applications*; Prentice Hall: Englewood Cliffs, New Jersey, 1985.

(30) Obrien, K. C.; Koros, W. J.; Barbari, T. A.; Sanders, E. S. *J. Membrane Science* **1986**, *29*, 229-238.

(31) Koros, W. J.; Paul, D. R. *J. Polymer Sci. B - Polymer Physics* **1976**, *14*, 1903-1907.

(32) *Encyclopedia of Polymer Science and Engineering, Supplement Volume, 2nd Ed*; John Wiley & Sons: New York, 1989.

(33) Flanagin, L. W.; McAdams, C. L.; Hinsberg, W. D.; Sanchez, I. C.; Willson, C. G. *Proc. SPIE* **1999**, *3049*, 838.

(34) Schmid, G. M.; Burns, S. D.; Tsiartas, P. C.; Willson, C. G. *Journal of Vacuum Science & Technology B* **2002**, *20*, 2913.

(35) Burns, S. D.; Schmid, G. M.; Tsiartas, P. C.; Willson, C. G.; Flanagin, L. *Journal of Vacuum Science & Technology B* **2002**, *20*, 537-543.

(36) Flanagin, L. W. *Ph.D. Dissertation, University of Texas at Austin*, 1999.

(37) Flanagin, L. W.; Singh, V. K.; Willson, C. G. *Journal of Polymer Science Part B-Polymer Physics* **1999**, *37*, 2103-2113.

CHAPTER 7: INVESTIGATING INTERFACIAL GEL LAYER FORMATION IN PHENOLIC POLYMERS*

7.1 THE THEORY OF GEL LAYER FORMATION

In Chapter 2, the theory of gel layer formation during phenolic polymer dissolution in aqueous base was introduced. This theory was discussed briefly in Chapter 6 with regards to surface rate inhibition. The theory suggests that the first step in the dissolution process is solvent penetration into the polymer film (Figure 7.1). An intermediate phase, or zone, is proposed to form consisting of a mixture of solvent and polymer. A steady state thickness of the gel layer is reached in which the kinetics of dissolution match the mass transfer resistance across the intermediate zone. The polymer film then dissolves at a constant rate, with a constant gel layer thickness. Nearly all of the proposed theories concerning gel layer formation suggest that the process is rate limited by mass transport resistance, either by solvent diffusion or the disentanglement of polymer chains.[1-4]

*Reproduced in part with permission from S.D. Burns *et al.*, Proc SPIE, Copyright 2003, in press

7.2 REVIEW OF PREVIOUS GEL LAYER STUDIES IN PHOTORESISTS

Many resist dissolution models incorporate formation of an interfacial gel layer within the proposed dissolution mechanism. Models incorporating a gel layer have been developed by Arcus,[5]Reiser *et al.,*[6,7] Choi *et al.,*[8,9] and recently by Houle *et al.*[10] (although the specifics of the models are somewhat different). In contrast, the CI model proposed by our research group assumes that the dissolution of low molecular weight phenolic polymers in aqueous base can be described without significant formation of a gel/transition layer,[11] and this model has been quite successful at explaining many commonly observed dissolution trends.[11-15]

A recent work by Hunek and Cussler reported the change in dissolution rate of a novolac resin with the flow rate of developer. The conclusion of their analysis was that "the dissolution of low molecular weight phenolic resin is controlled by a combination of solute release and solute mass transfer, without the formation of any significant intermediate gel phase."[16] However, the models described above do not provide *direct* experimental evidence for the presence or absence of a gel layer in phenolic polymers. In this chapter, the question of gel layer is probed experimentally with the use of real time spectroscopic inteferometry and ellipsometry.

Interferometry has been used extensively to examine formation of gel layers during dissolution of thin (~ 1 μm) polymer films. Rodriguez *et al.* used single wavelength interferometry to examine interfacial layers primarily in poly(methylmethacrylate) (PMMA) dissolving in a variety of organic solvents.[17-19] An important result was that gel layers were observed in PMMA with molecular weight larger than Mn ~ 70,000. Above this value, the gel layer thickness was observed to increase with increasing chain length.[18] Poly(dimethylitaconate) with Mn ~ 400,000 did not show significant gel layer formation in a variety of organic solvents. Winnik *et al.* used the same technique

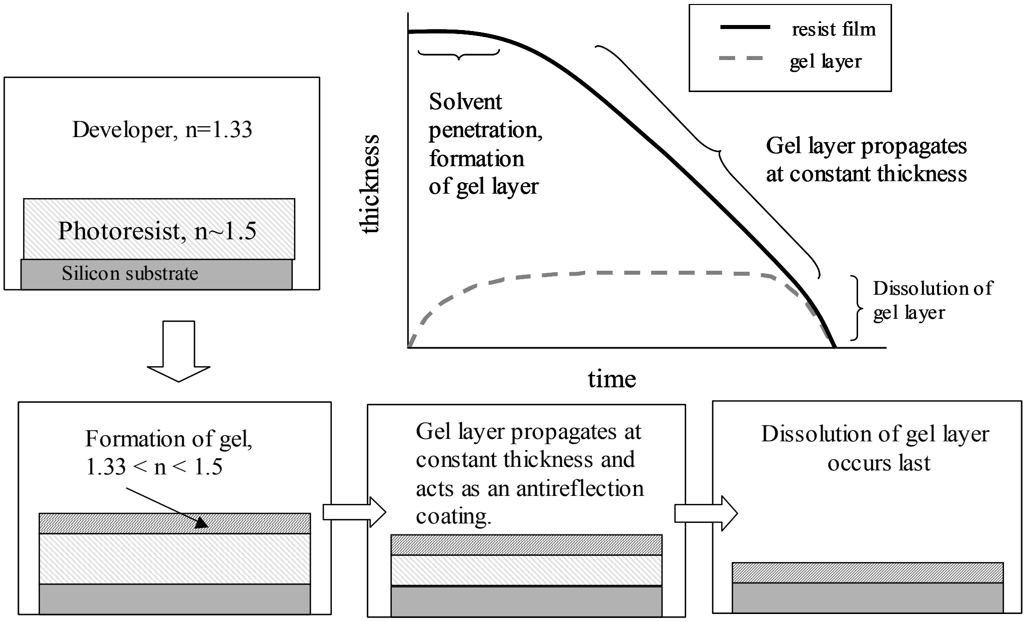

Figure 7.1 Description of 4-layer optical model used for both interferometry and ellipsometry analysis of polymer film dissolution. A description of gel layer formation is shown.

and report that a gel layer (~ 44 nm thick) is present in the dissolution of PMMA in a 2:1 mixture of methyl ethyl ketone and isopropyl alcohol.[20] In recent years, both interferometry and ellipsometry have been improved such that spectroscopic data can be obtained with a fast rate of acquisition. The work presented in this chapter may be considered an extension of that of Rodriguez,[17] Winnik[20] and Papanu[21] (who all used single wavelength techniques) in which spectroscopic data was used to quantitatively study dissolution and gel layer formation of thin polymer films.

Arcus presented the first experimental evidence of a gel layer during phenolic polymer dissolution with a single wavelength interferometry experiment performed on a high molecular weight novolac.[5] However, careful examination of the interferometry data leads to the conclusion that it was misinterpreted, and does not provide evidence of gel layer formation. This topic will be revisited as interferometry models for gel layer formation are presented in Section 7.3.1.

Hinsberg *et al*. have developed a quartz crystal microbalance technique that measures frequency changes as well as impedance changes during film dissolution.[22-24] The latter value is related to the polymer modulus and it is possible to examine swelling of polymer films during dissolution as well as interfacial gel layer formation. Using this technique (along with multiwavelength interferometry, in some cases) they have demonstrated that films of poly(norbornane carbonate-co-norbornanecarboxylic acid) (70:30) undergo swelling in aqueous base, and copolymers of poly(methyl methacrylate-co-methylacrylic acid) dissolve with significant interfacial layer formation. With regards to phenolic polymers, it was reported that a thin metacresol novolac film dissolved without an increase in resistance consistent with formation of an interfacial layer.[22] However, in a recent work it was reported that a Varcum 6006 novolac resin forms a ~60 nm gel layer when dissolved in 0.26 N tetramethylammonium hydroxide (TMAH) developer.[25] The thickness of the gel layer was determined by inteferometry. The QCM technique has also been used by Toriumi *et al.* to examine swelling behavior in photoresists.[26]

In this work, the formation of interfacial layers during aqueous base dissolution of a variety of photoresist resins was investigated with ellipsometry and interferometry. The focus was phenolic polymers, specifically novolac and poly(hydroxystyrene) (PHOST). The theory of multiwavelength interferometry is well understood, and the reader is referred to literature that describes the model equations for single and multilayered stacks.[27,28] Ellipsometry has also been used extensively as a thin film characterization technique, and the reader is referred to literature that describes the theory and fundamental model calculations.[27] Spectroscopic ellipsometry provides a complementary technique to interferometry to examine formation of interfacial layers during polymer dissolution.

It is expected that the thickness of a gel layer would be related to many parameters, most notably molecular weight.[4] In order to examine a wide range of cases, phenolic polymers of molecular weight up to Mn ~ 70,000 were examined. Also, the formation of a gel layer may be expected to be concurrent with surface rate inhibition,[4] which is observed primarily in novolac resins. In this work, a novolac film was processed with a high temperature PAB in order to induce as much surface inhibition as possible,[29] and thus increase the probability of observing a gel layer. These cases are examples of phenolic polymer dissolution that are beyond normal lithographic processing conditions, but they are cases in which formation of a gel layer would be expected to be amplified and observable during dissolution.

7.3 MEASURING GEL LAYERS WITH INTEFEROMETRY AND ELLIPSOMETRY

Interferometry and ellipsometry are both model-based techniques. The instrument does not directly measure the parameters of interest (thickness and optical constants). Rather, quantities such as reflectivity or ellipsometric parameters are directly measured. A model is then created to determine the expected values of these experimentally measured quantities, based on guessed (or fitted) model parameters (thickness and optical constants). If the model calculations compare well (judged by a merit function), the model parameters are considered to be correct. With this procedure, care must be taken to ensure that a reasonable model is assumed, that correct regression algorithms are used, and that acceptable correlations exist between model parameters. For a single layer consisting of a polymer film coated onto a silicon substrate, the techniques are straight forward and have been applied successfully to a variety of materials.[27] As additional layers are added to the model, the technique becomes more complicated. (This is especially true for the formation of a gel layer, which is only expected to be observed during a dynamic dissolution process.) The model film stack used in this work is shown in Figure 7.1. The model consists of 4 layers: the silicon wafer, the polymer film, the transition, or “gel” layer, and the developer ambient. The film stack is identical to that used in previous works.[18,20,25]

It is instructive to perform *a priori* model calculations of the expected change in interferometry and ellipsometry data when a gel layer forms. The calculations presented are for gel layers of varying thickness and composition. Because the composition of the gel layer is a mixture of the polymer film and the developer (materials with known optical constants), effective medium approximations (EMAs) can be used to relate the composition of the gel layer to the optical constants of the gel layer. The composition of the gel layer then becomes a fitted parameter, which reduces the number of parameters used in the model.[19,20] Throughout this chapter, the Cauchy equation[27] (defined in Chapter 3) has been used to describe the dispersion of index of refraction with wavelength.

7.3.1 Reflectance Calculations

In Figure 7.2, the calculated spectroscopic reflectance of a film (with optical constants typical of novolac) is shown for a 1000 nm film with no gel layer, a 970 nm film with a hypothetical 60 nm gel layer, and for intermediate cases. A 50% composition of the gel layer has been assumed. These calculations represent the beginning of dissolution when base may (or may not) penetrate the film and the gel layer grows, but significant dissolution has not yet occurred. This

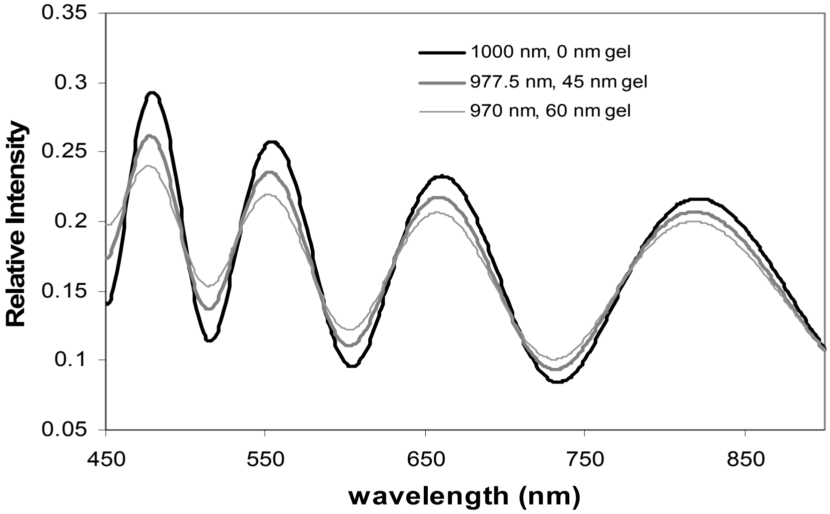

Figure 7.2 Spectral reflectivity calculations of a 1 mm novolac film (with Cauchy coefficients: A=1.62, B=0.01, C=0) and with formation of a thin gel layer, assuming no mass loss and a 50% gel layer composition, with a flat profile and the gel index calculated with a linear EMA.

is consistent with the theory of gel layer formation, although in a real system some dissolution may occur before the gel layer reaches a steady state value. The gel layer effectively acts as an antireflection coating,[19,25] and the overall amplitude of reflection (peak to valley ratio) is reduced.

In Figure 7.3, model calculations of single wavelength data are presented for a similar film in which a hypothetical 60 nm gel layer forms during the beginning of dissolution. The gel layer remains at constant thickness as the polymer dissolves, and the last event is the dissolution of the gel layer. Again, the

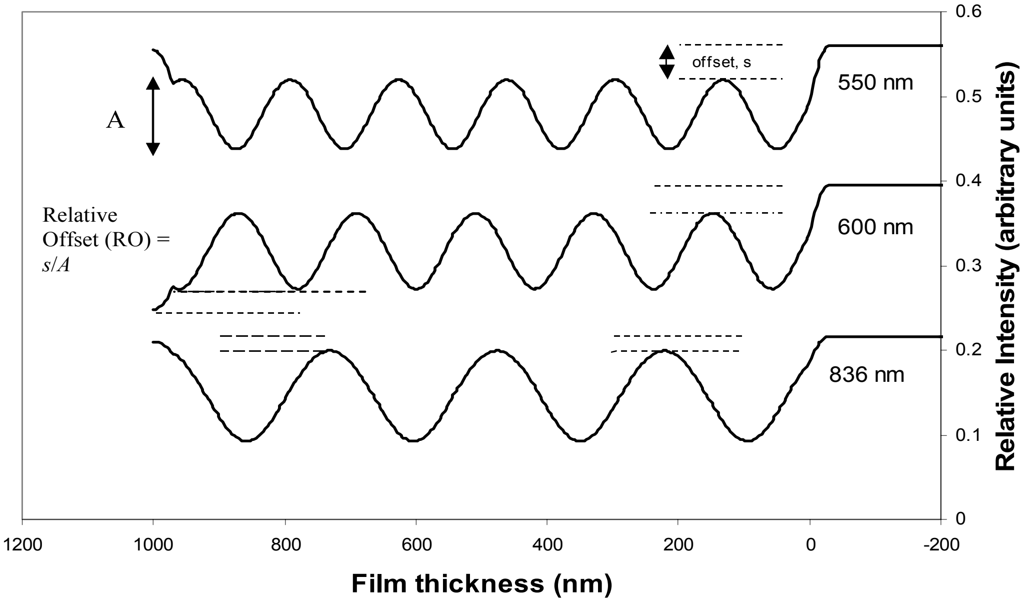

Figure 7.3 Single wavelength reflectance calculations for dissolution of a 1 mm novolac film with formation and depletion of a 60 nm gel layer (50% solvent). Note the beginning and end offset effects. The relative offset is defined as the offset, s, normalized by the amplitude of the interferogram.

gel layer acts as an antireflection coating, and the peak to valley ratio of the reflectance data is reduced. The most obvious trend is that at the end of dissolution, the antireflection coating dissolves last and the reflectivity increases substantially, resulting in an offset, *s*, between the final reflectivity and the peak reflectivity during dissolution. This concept was first used by Rodriguez[18] and then Winnik[20] to measure gel layers in polymer films with single wavelength interferometry. The relative offset (RO) is defined as the offset, *s*, normalized by the amplitude of the interferogram. The RO is a function of the gel layer composition and the gel layer thickness, which is demonstrated in Figure 7.4. The largest offset occurs for a gel composition of 50%, as this represents the largest contrast between optical constants of adjacent layers. Thus, it is more difficult to measure a gel layer with a composition close to 0 or 100%. Of course, near the extremes the layer is not accurately described as a gel layer. In Figure 7.3, the assumption has been made that the intermediate layer propagates at constant thickness and then dissolves at the end of dissolution. While this assumption is consistent with the theory of gel layer formation, some films may not behave in such an idealized manner. For example, the gel layer may dissipate near the end of dissolution before the entire bulk film has dissolved. However, if the gel layer propagates for most of the film dissolution, an offset will be observed between the final reflectivity and peak reflectivity during dissolution. Thus, the offset analysis is valid even if the gel layer formation and propagation are not 'ideal'. Other factors may affect the interferometry data in a similar manner to a gel layer. Surface roughness, non uniformities, and the formation of striations during dissolution may have similar effects on the reflectance data as an intermediate gel layer, which is demonstrated in Appendix D[30,31] It is useful to examine partially dissolved films with both AFM and profilometry to differentiate between the above effects. Formations of striations is known to occur during dissolution of some novolac films cast from PGMEA, and their effect on reflectivity has been

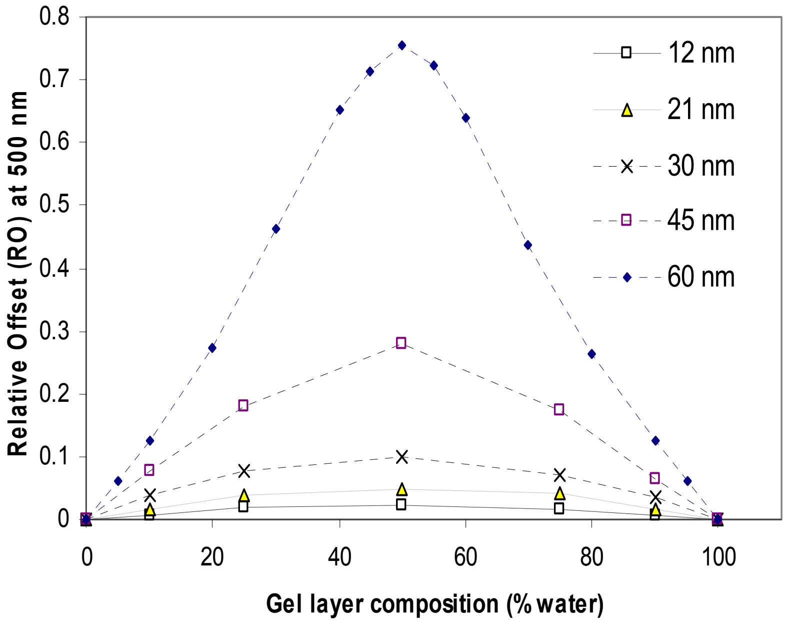

Figure 7.4 Calculation of the offset, *s*, as a function of gel layer thickness and composition with 500 nm incident light. A flat composition profile has been assumed, along with Cauchy coefficients of A=1.62, B=0.01.

shown to be somewhat similar to that of a gel layer.[30] Addition of surfactants to the mixture, or changing the casting solvent (diglyme was used for one novolac polymer in this work) has been shown to remove the striations.[30]

7.3.2 Calculating the Offset with Varying Thickness and Composition Profiles

Thus far, the gel layer has been modeled as an intermediate layer with a flat composition profile. That is, the change in composition at the interfaces is sharp. While existing models for gel layer formation may lend insight into the composition profile, there is little agreement about the shape of this profile.[19,20,25] One goal is to determine the ultimate resolution of the experimental techniques, so different profiles need to be considered for completeness. For this reason, a broad composition profile across the gel layer was also considered in our model calculations.

Determining the offset for a flat composition profile is a straight forward calculation.[27] However, to calculate the effect on reflectivity for a linear profile, the calculations become more difficult because the most rigorous approach is to consider a large number of very small layer slices. However, there have been two simplified mathematical approaches for calculating the offset based on a linear profile reported in the literature. These approaches are reviewed and compared to a more rigorous approach to the identical problem.

Recall equation (3.4), which gives the reflectivity from a single layer on a substrate as a function of the layer thickness, and the optical constants of the substrate, film, and ambient medium:

$$\boldsymbol{R}\,(\lambda,d) = |R|^2 = \frac{r_{12}^2 + 2r_{12}r_{23}\cos 2\delta + r_{23}^2}{1 + 2r_{12}r_{23}\cos 2\delta + r_{12}^2 r_{23}^2} \tag{7.1}$$

Rodriguez *et al*. state that if the polymer-solvent interface is not sharp, and is expanded into a continuous transition, the appropriate expression for the reflectivity becomes:

$$\boldsymbol{R}\,(\lambda,d) = \; = \frac{r_{12}^2 + 2r_{12}r_{23}f\cos 2\delta + f^2 r_{23}^2}{1 + 2r_{12}r_{23}f\cos 2\delta + f^2 r_{12}^2 r_{23}^2} \tag{7.2}$$

where *f* is a positive factor less than unity which depends on the thickness and concentration profile of the transition layer. Rodriguez *et al*. show that *f* is related to the relative offset (RO) by:

$$f = \frac{1}{1 + 2RO} \tag{7.3}$$

It was stated that the value of *f* is somewhat insensitive to the shape of the profile, however a linear profile was assumed for simplicity. Rodriguez *et al*. relate the value of *f* to the thickness of the intermediate layer (d_t). They state “optical theory gives as a good approximation”:

$$f = \frac{\sin\left(\frac{\alpha}{2}\right)}{\frac{\alpha}{2}} \tag{7.4}$$

where $$\alpha = \frac{4d_t \pi n_t}{\lambda} \quad , \quad n_t = \frac{n_1 + n_2}{2} \tag{7.5}$$

and n_1 and n_2 are the wavelength dependent index of refraction of the ambient medium and polymer film, respectively. However, no reference was provided for equation (7.4) and its origin remains unclear. Nevertheless, the expression is compared to that of Winnick *et al*. and the calculations of this work in Figure 7.5.

Winnik *et al*. provide another technique in order to determine the thickness of a gel layer with a composition profile of arbitrary shape, n(z), based upon the relative offset, RO. Winnik *et al*. begin by presenting the characteristic matrix theory developed by Abeles.[32] This theory seeks to describe the optical properties of a stratified medium by a 2 x 2 "characteristic" matrix:

$$M = \begin{bmatrix} m_{11} & m_{12} \\ m_{21} & m_{22} \end{bmatrix} \tag{7.6}$$

$$r = \frac{(m_{11} + n_s m_{12})n_1 - (m_{21} + n_s m_{22})}{(m_{11} + n_s m_{12})n_1 + (m_{21} + n_s m_{22})} \tag{7.7}$$

where n_1 is the refractive index of the first layer, n_s is the refractive index of the substrate, and *r* is the overall reflectivity. The physical reflectivity, R, is given by:

$$R = |r|^2 \tag{7.8}$$

For the case of a stratified medium of *n* homogeneous layers (each characterized by a matrix, M_i), it can be shown that the characteristic matrix M is the product of the individual matrices:

$$M = M_1 M_2 \ldots M_n \tag{7.9}$$

Winnik *et al.* use this method to determine a different expression for *f* (as defined in equation 7.2), based on a derivation that ignores second order terms in the matrix product:

$$f = \left[\frac{\left(1 + \frac{\left(\frac{2\pi}{\lambda}\right)^2}{(n_1 - n_2)^2} \beta^2 \right)}{\left(1 + \frac{\left(\frac{2\pi}{\lambda}\right)^2}{(n_1 + n_2)^2} \alpha^2 \right)} \right] \tag{7.10}$$

where

$$\alpha = \int n^2(z) dz + n_1 n_2 d_t \ , \qquad \beta = \int n^2(z) dz - n_1 n_2 d_t \tag{7.11}$$

and n_1 and n_2 are the wavelength dependent refractive index of the ambient medium and polymer film, respectively. In this work, only linear and constant index profiles have been considered. For a linear profile, the function *n*(*z*) becomes:

$$n(z) = n_1 + z \frac{(n_2 - n_1)}{d_t} \tag{7.12}$$

Using this technique, the relative offset has been calculated as a function of the gel layer thickness for a hypothetical novolac film (A=1.62, B=0.01). The results of this calculation are plotted in Figure 7.5 and compared to the technique of Rodriguez *et al*. and the calculations made in this work.

Our approach was also to utilize the characteristic matrix method described above. Our approach differed from that of Winnik *et al*. because the second order terms were not neglected. Rather, a Matlab algorithm was used to rigorously calculate the reflectivity for a stratified layer based upon the characteristic matrix method. Ideally, an infinite number of layers would be used in the calculation. It was determined that for a gel thickness of 100 nm, 100 strata were adequate to yield accurate results. This technique is preferred over the other methods, because no simplifying assumptions have to be made. This method was also used to calculate the relative offset as a function of gel layer thickness assuming a novolac film and a linear profile, and the results are plotted in Figure 7.5.

Several conclusions can be made from Figure 7.5. First, the two different profile shapes do lead to significantly different results. For example, if a relative offset of 0.3 is measured, that could indicate a 45 nm thick gel layer, with a flat, 50% composition profile. Or, it could indicate an 80 nm gel layer, with a linear composition profile. Unfortunately there is no way to distinguish what the profile shape is by only measuring the relative offset. However, the goal of this plot (for the purposes of this work) is to establish the minimum resolution that can be obtained using interferometry to measure the interfacial layer. For example, the relative offset for a 5 nm interfacial layer is barely above the baseline. It is almost impossible to distinguish this case from experimental noise, depending upon the precision of the experiment. However, a 15 nm gel layer is above the baseline

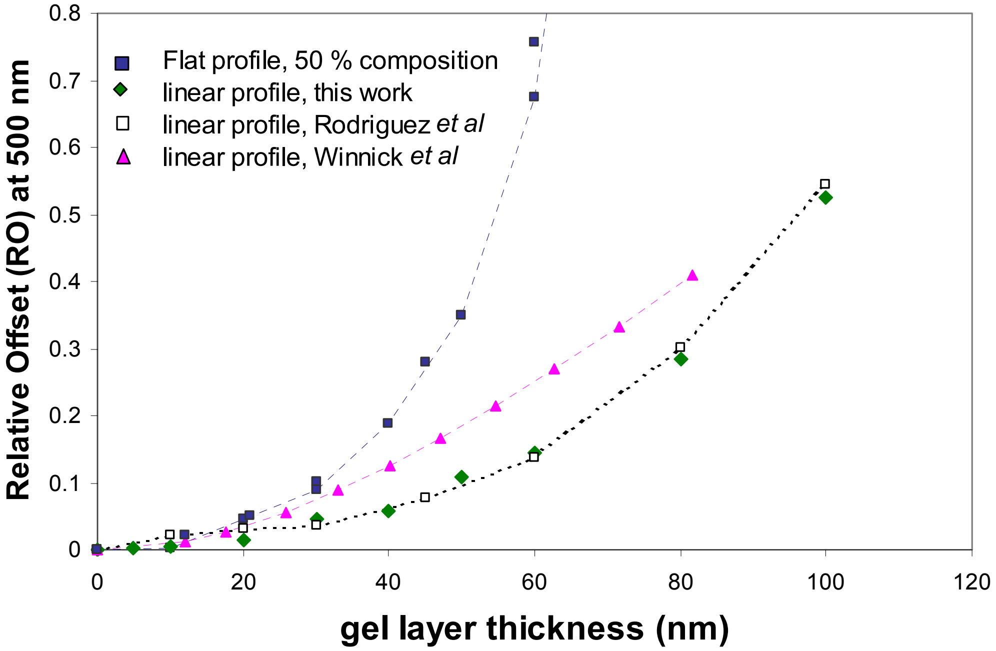

Figure 7.5 Calculation of the relative offset at 500 nm as a function of gel layer thickness and the shape of the composition profile (flat or linear)

and should be measurable (assuming 50 % composition and a flat profile). For a linear profile, the resolution is worse – the same relative offset corresponds to a 20 nm gel layer. These calculations provide a bound for the best resolution for detecting a gel layer.

7.3.3 Review of a Previous Gel Layer Study by Arcus

At this point in the modeling discussion, it should be noted that the single wavelength data presented by Arcus[5] as evidence of gel layer formation is not consistent with the single wavelength model calculations presented in this work or elsewhere.[18,20] Arcus' data is reproduced in Figure 7.6 and 7.7. The overlapping interferograms shown are *not* expected to occur during the formation of a gel layer that propagates at a steady state value. (Intuition suggests they might be expected, but model calculations do not.) Additionally, the only evidence of a gel layer in this previous work is in the first 5 seconds of the data (out of a total of ~ 40 s of film dissolution). However, the data in this time period are much more consistent with the water rippling effect (experimental noise) known to occur during puddle development,[33] and were most likely misinterpreted as evidence of a gel layer. If one chooses to argue that the initial data (5s) is not due to water rippling, then a standard interferometry analysis suggests the first half of the film dissolves faster than the bottom half by a factor of 4, with an abrupt transition – a highly improbable result for a novolac film. Therefore, our research group is

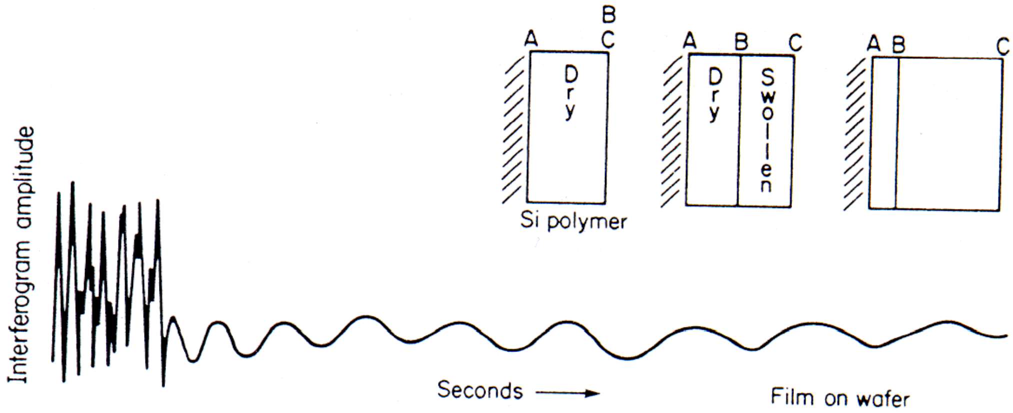

Figure 7.6 Reproduction of single wavelength interferogram of high MW novolac dissolution from Arcus.

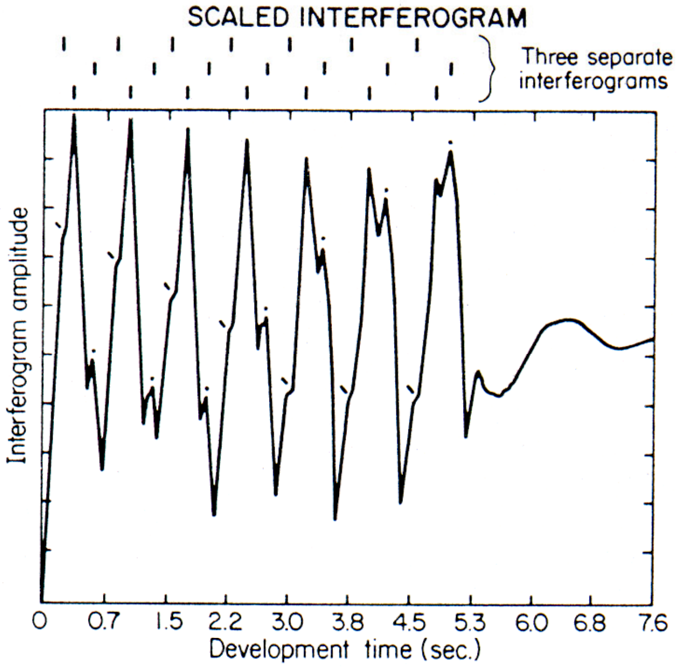

Figure 7.7 An enlargement of early time data in Figure 7.6. The 3 separate interferograms have been interpreted to represent gel layer formation. It is now believed that interpretation is incorrect.

confident that this previous work does not represent conclusive evidence of interfacial layer formation during dissolution of phenolic polymers.

7.3.4 Ellipsometry Calculations

The data obtained by ellipsometry are two ellipsometric parameters, ψ and Δ, which represent a change in the polarization state of the light. The reader is referred elsewhere for the theory behind the model calculation of these parameters.[27] The changes in ψ and Δ that occur during formation of a gel layer are significant, but are not as qualitatively intuitive as the changes that occur with reflectometry shown in Figures 7.2 and 7.3. Therefore, the focus in this section is not on the qualitative trends of the ellipsometric parameters during gel layer formation, but rather the uniqueness of the ellipsometry model fits for the case in which a gel layer is formed. The overall goal is the same – to determine the minimum resolution (gel layer thickness) that an ellipsometer will be capable of detecting. ψ and Δ were calculated (using WVASE32 by J. A. Woollam) for the case of a 1 μm novolac film and a gel layer of varying thickness (0-50 nm), and varying composition (0-100%). These data were then fit using the software regression algorithms for the case of a single layer model in which the thickness and optical constants were allowed to vary. (We thus posed the question: "*If an ideal gel layer is present, how thick does it have to be before a single layer model no longer provides an adequate fit to the data?")* The metric by which WVASE32 determines the best model fit is the mean-squared error (MSE), which is defined elsewhere.[27] Figure 7.8 shows the calculated MSE for a single layer fit to gel layer models with varying composition and thickness of the gel layer. At the extreme ends (0 and 100 % composition), the gel layer model is, of course, well represented by a single layer model and the MSE is low. As with reflectivity, the highest MSE is found for intermediate compositions, a case for which there is high contrast between the ambient medium (water), the intermediate layer, and the underlying polymer film. As the thickness of the gel is increased, the MSE increases substantially.

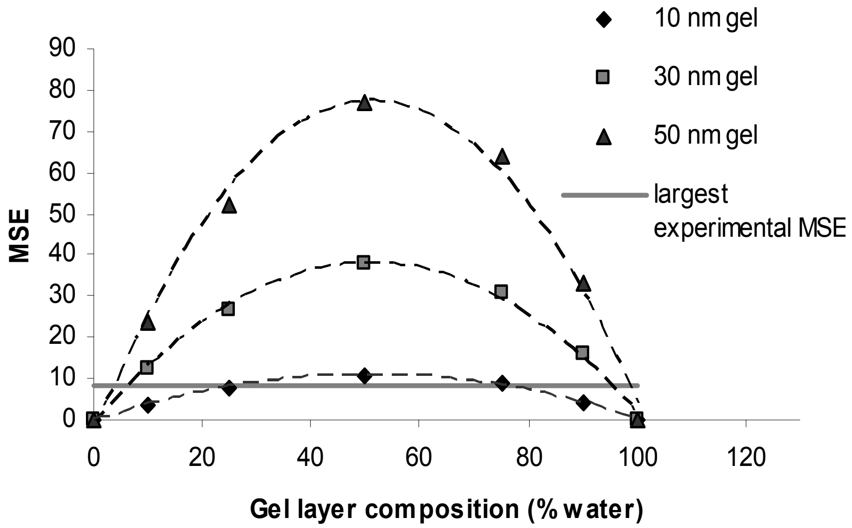

Figure 7.8 MSE of a single layer ellipsometry model fitted to an ideal gel layer (2 layer) model using WVASE32, shown as a function of gel layer composition and thickness. The base film was 1 μm thick, with optical constants of a typical novolac film. The dotted lines are included only for clarity. The solid gray line represents the largest experimental MSE observed for phenolic polymers (see Table I.)

The measurement of a 1 μm static novolac film may produce a MSE between 1-15, depending upon the quality of the film. Thus, a gel layer as thin as 10 nm cannot be uniquely distinguished with ellipsometry. However, a very large MSE would be obtained if, for example, a 50 nm gel layer of intermediate composition was present, and it would be clear that a single layer model was not adequate to describe the experimental data. This plot will be discussed further in Section 5.5.

7.4 EXPERIMENTAL RESULTS

7.4.1 Materials and Sample Preparation

Three novolac resins were used in this work. The first was from Schenectady (Mn=9330, Pd=4.9). The second was G2 novolac from Shipley, and the third was Varcum novolac resin (6001) obtained from IBM. Poly(hydroxystyrene) (PHOST) of various chain length was used. PHOST resin (Mn=72k, Pd = 2.89) was obtained from Chemfirst (Dallas, TX). PHOST resin (Mn=21k, Pd=1.9) was obtained from Hoechst Celanese. Poly (norbornane hexafluoroalcohol) (pNHFA) was obtained from BF Goodrich. The casting solvents used were propylene glycol methyl ether acetate (PGMEA) and methoxyethylether (diglyme), which were obtained from Aldrich Co. (Milwaukee, Wisconsin) and used as received. Aqueous solutions of TMAH were obtained from SACHEM (Austin, TX) and diluted as needed. Microposit

CD-26 developer was obtained from Shipley. Films were spin coated onto silicon wafers at 2500 rpm for 30s, and baked at 90°C for 90s, unless otherwise noted.

7.4.2 Reflectance Interferometry Results

Figure 7.9(a) shows the thickness plotted against time for a novolac (Schenectady) film cast from diglyme (measured by interferometry). The PAB (in this case) was 150°C for 90 s. The film was developed in 0.216 N TMAH. Note the large amount of surface rate inhibition – the initial thickness does not decrease at all for the first few seconds. Thickness versus time plots of PHOST and pNHFA dissolution are shown in Figure 7.9(b,c), also obtained by interferometry. Surface rate enhancement is observed for these polymers, and this observation has been reported previously for PHOST.[34] Dissolution is expected to be slow during the formation of the gel, resulting in the opposite effect (surface inhibition). Cases in which surface enhancement are observed are empirically inconsistent with the theory of gel layer formation. Our research group has observed that PHOST dissolves with surface rate enhancement over a wide range of molecular weights (Mn=3k-70k) and PAB temperatures (50-185°C). Surface rate enhancement has been observed with PHOST produced by four different companies (Nippon Soda, Hoechst Celanese, ChemFirst, and ShinEtsu), or formed by the acid catalyzed deprotection of tBOC (although pure PHOST is not formed in this case).[35] In our previous dissolution rate studies of a wide range of photoresist resins, our research group has consistently observed significant surface rate inhibition primarily in novolac resins.

Another metric for measuring gel layers from reflectance data is the offset, *s*, that occurs at the end of dissolution.[18] Figure 7.10 shows an interferogram (at λ=600 nm) of G2 novolac resin dissolving in 0.26 N TMAH. A significant offset is not present at the end of dissolution, and the peak to valley ratio has not been decreased by the presence of an antireflective gel layer. The calculated relative offset for this case is 0.0026, presented in Table 7.1. This low offset is characteristic of phenolic polymers dissolving in aqueous base, and represents (at most) a very thin (< 10 nm) transition layer between the developer solution and the dissolving polymer. Offset values for other polymers resins are also presented in Table 7.1. In all cases (except high MW PHOST), the measured offset is immeasurably small, and the data are not consistent with the formation of an interfacial layer.

Figure 7.11 shows a single wavelength interferogram of high MW PMMA (Mn = 960k) dissolving in acetone. A relative offset of 0.105 is measureable, and indicative of a ~36 nm interfacial layer during dissolution. The goal of this experiment was to demonstrate that the experimental measurement technique was capable of measuring interfacial layer formation for a polymer dissolving in an organic solvent. Also note that the molecular weight of the PMMA used was two orders of magnitude larger than a typical low molecular weight photoresist resin.

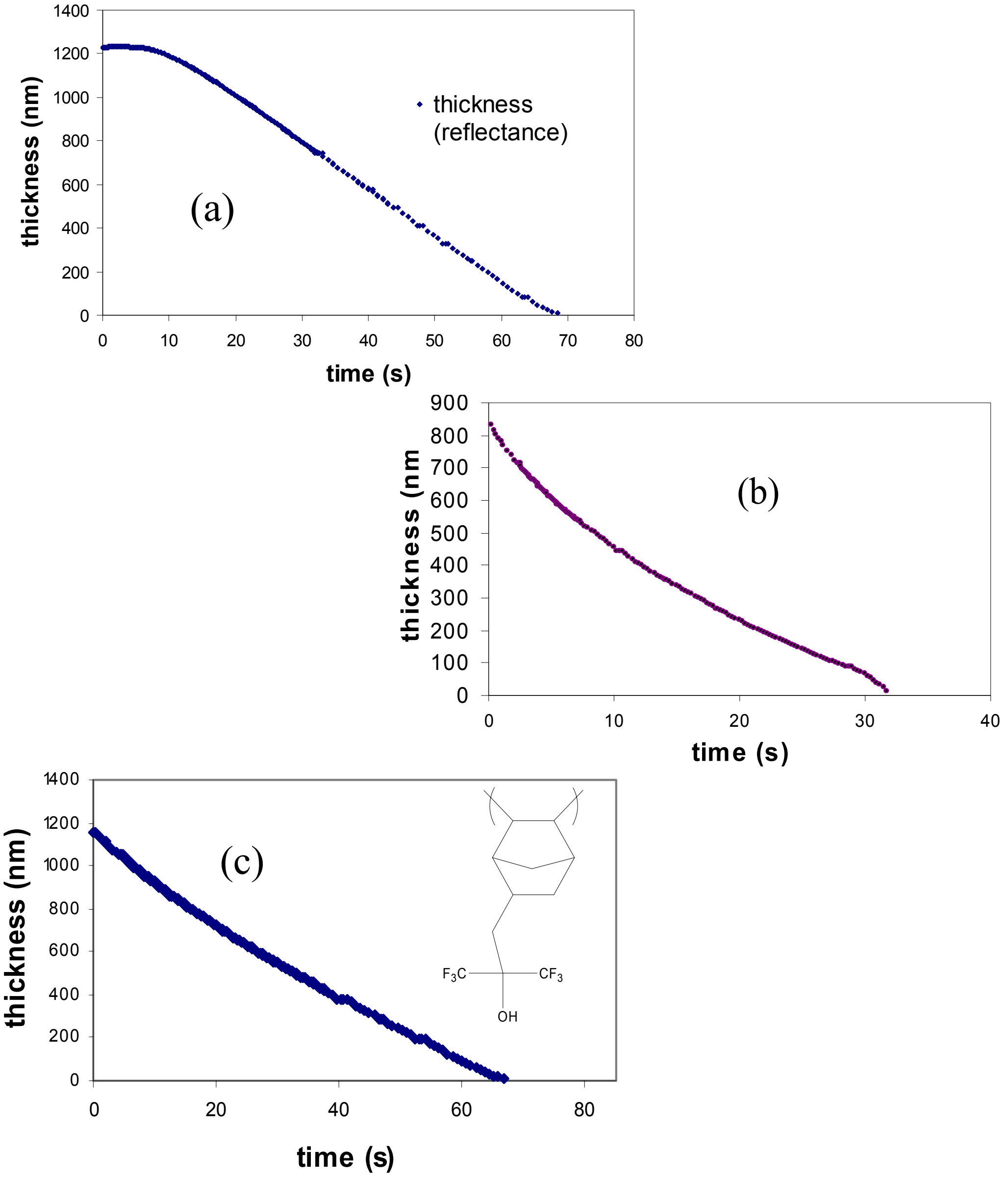

Figure 7.9 (a) Dissolution profile of novolac (Schenectady resin), baked at 150°C. A significant amount of surface rate inhibition is observed. (b) Dissolution profile of PHOST, Mn~70,000 in 0.15 N TMAH, and (c) pNHFA in 0.16 N TMAH. Slight surface rate enhancement is observed.

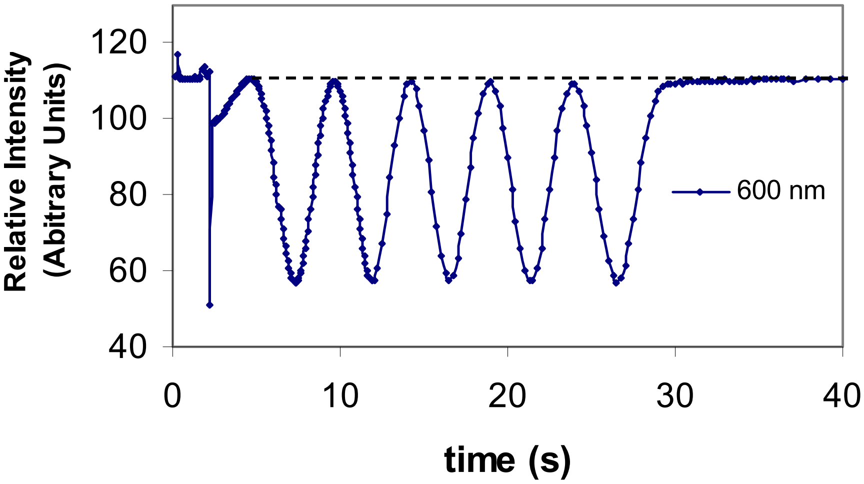

Figure 7.10 Experimental interferometry data showing the relative intensity at 600 nm during the dissolution of G2 novolac resin dissolving in 0.26 N TMAH. An offset is not measureable.

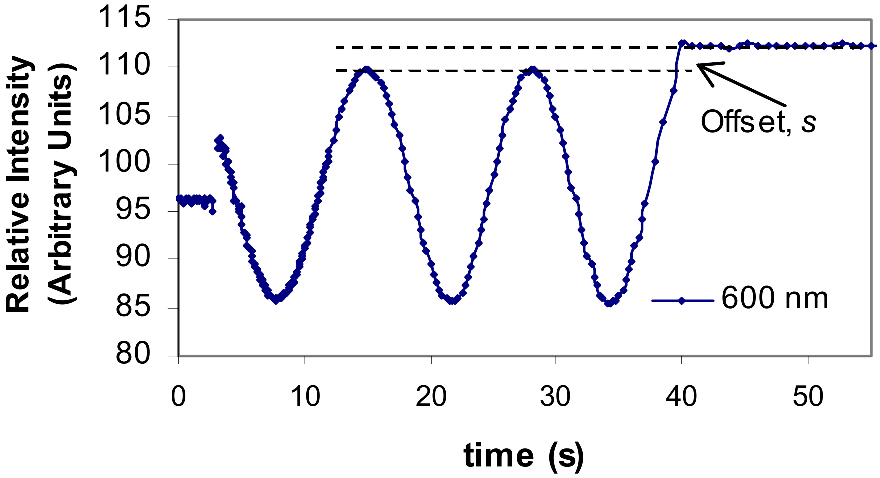

Figure 7.11 Experimental interferometry data showing the reflectance at 600 nm during the dissolution of high molecular weight (Mn ~ 960k) PMMA in acetone. An offset is observed, indicative of a gel layer.

7.4.3 Ellipsometry Results

Spectroscopic ellipsometry is not a standard technique for measuring polymer dissolution, so the initial experiments were control experiments to demonstrate the feasibility of the technique. The spectroscopic ellipsometer used in this work was a J.A. Woollam model M-2000, with a wavelength range of 193-1000 nm. For most experiments, the spectral range of 450-950 nm was used. The maximum data acquisition rate of this ellipsometer is 10 Hz. Because the angle of incidence is oblique to the surface (70°, in this case), a teflon cell was constructed with fused silica windows, which was modeled after similar cells.[21,36] The cell geometry is shown in Figure 7.12. The cell volume was ~2.5 ml, and developer was completely injected within ~ 2 s in most experiments.

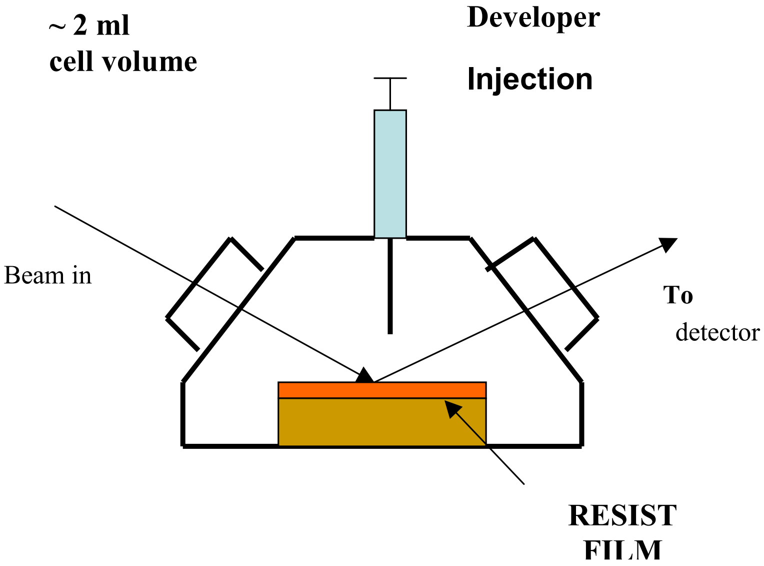

Figure 7.12 Geometry of dissolution cell for *in situ* spectroscopic ellipsometry experiments

Figure 7.13 and 7.14 shows the change in the measured ellipsometric parameters ψ and Δ during dissolution of a novolac film of ~ 1 μm film thickness. Intitially, ψ and Δ do not change because data is collected before dissolution begins. After enough data is obtained to determine the dry film thickness, developer (~ 2.5 mL) is injected into the dissolution cell. A few data points are noisy during the transient injection time. Then, ψ and Δ begin to oscillate in a predictable manner as the film thickness decreases. Dissolution is considered to be complete when ψ and Δ become constant.

Typical model fits to the data are also shown in Figures 7.13 and 7.14. WVASE32 software, supplied by J.A. Woollam was used to fit optical models to the ellipsometric data, a process described in Chapter 3. The fitting procedure was as follows: first, 4 parameters (thickness, and the 3 Cauchy coefficients) were fit to the dry film. Second, the first useable scan during dissolution was refit with all 4 parameters. Typically, the index of refraction would decrease slightly due to water sorption. Then, the Cauchy parameters were held constant, and the thickness was varied to fit the remainder of the dissolution curves. Cases in which the Cauchy parameters were allowed to vary during dissolution did not yield significantly different results. That is, the Cauchy parameters were found to be constant during dissolution. Using this technique, the mean squared error of the fits (defined elsewhere) was always maintained at acceptable levels. The quality of the fits is also apparent from Figure 7.13 and 7.14.

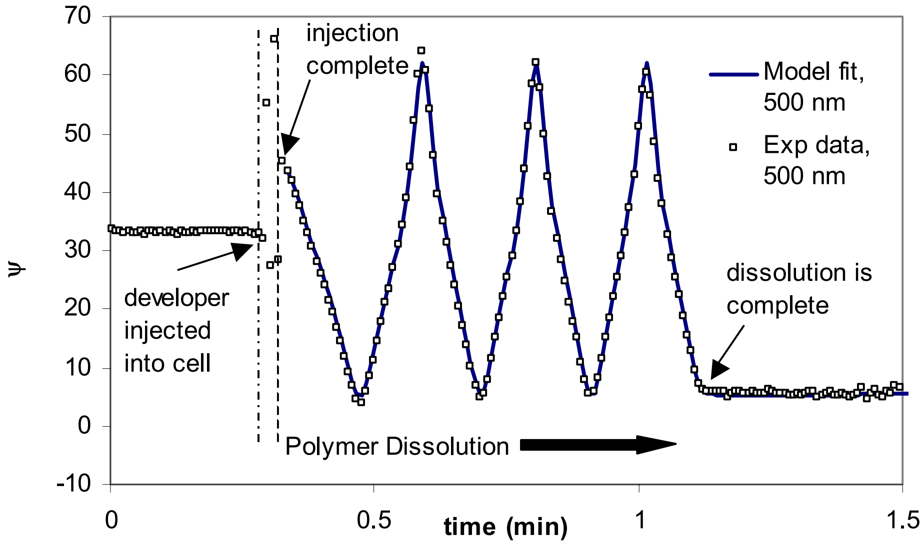

Figure 7.13 The measured value of the ellipsometric parameter ψ during aqueous base dissolution of a novolac film. The model fit (varying only film thickness) is also shown.

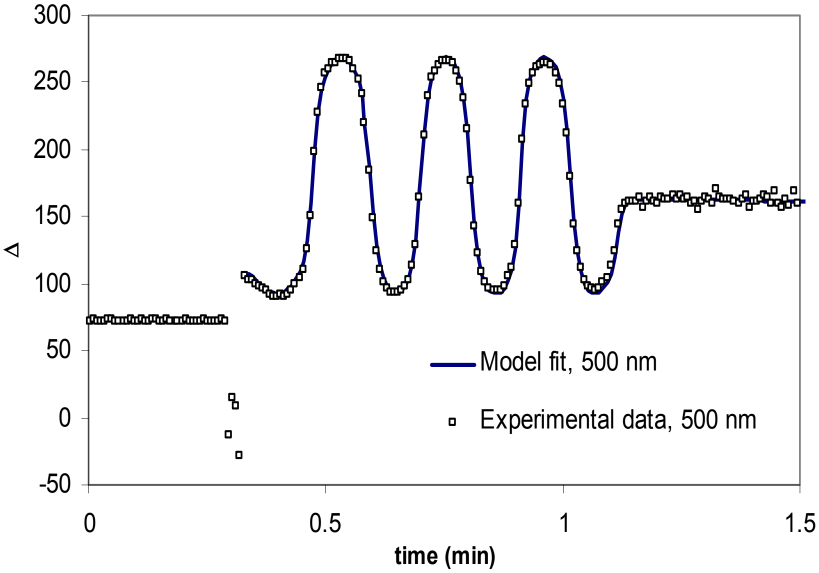

Figure 7.14. The measured value of the ellipsometric parameter Δ during aqueous base dissolution of a novolac film. The model fit (varying only film thickness) is also shown. Fits of similar quality were obtained for Δ over the visible spectral range.

This procedure resulted in a plot of thickness versus time, an example of which is shown in Figure 7.15. This case was compared to an identical novolac polymer/developer solution in which the dissolution was also measured by interferometry, which is a standard technique for measuring dissolution rates. There is very good comparison between the two techniques. The previous analysis demonstrates the feasibility of using real time ellipsometry as a photoresist dissolution rate monitor.

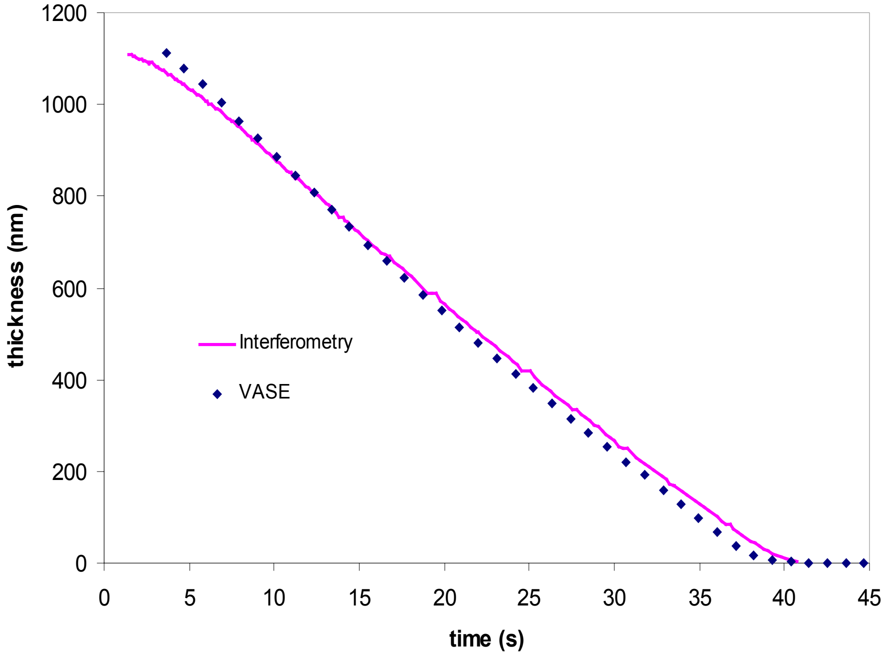

Figure 7.15 Comparison of dissolution rate results for a novolac polymer using both spectroscopic ellipsometry (VASE) and interferometry

For gel layer studies, identical polymer films and developer solutions were tested with ellipsometry as with interferometry (section 7.4.2). The average MSE during dissolution is presented in Table 7.2 for single layer models. The average MSE values are between 4-8. All fits are considered to be very good. Referring to Figure 7.8, it is clear that if a significant interfacial gel layer were present (at any point during dissolution) the MSE for a single layer model would be considerably higher. The conclusion from simple, single layer model fits is that no detectable interfacial layer forms during dissolution of any of the polymer resins shown in Table 7.1 (within the ~ 10 nm resolution of the experiment).

Although excellent model fits were obtained by a single layer model, other models were considered in order to explore many possible scenarios. Models with a gel layer having an intermediate composition were tested by allowing the thickness of the underlying polymer and the gel layer to vary with time. In most cases, a range of intermediate compositions for the gel layer were tested in separate analyses (usually 25-75%). The MSE was not lowered substantially in any case. However, the confidence intervals became significantly *larger*. This counterintuitive result occurs because the confidence intervals (as calculated by WVASE32) are related to both the MSE and to the extent of correlation of the fitted parameters. In the case of the two-layer model, the thickness of the gel layer and the thickness of the underlying film are strongly correlated (for thin gel layers), resulting in larger confidence intervals of the fitted parameters. This result represents a disadvantage in using spectroscopic ellipsometry to probe for gel layer formation in thin polymer films. For thin gel layers, the thickness of each layer in the stack will be highly correlated, and it will be challenging to uniquely determine the thickness of each layer. This result suggests that it may be possible to "miss" a gel layer in the data. However, the analysis shown in Figure 7.8 demonstrates that a single layer model would not be adequate for an ideal, interfacial gel layer thicker than ~ 10-15 nm. Therefore, the parameter correlation issue is only a concern in cases for which a single layer model does not provide an adequate fit to the data.

Table 7.1 Summary of Processing Conditions and Results of Gel Layer Analysis

Polymer Resin	TMAH Developer Concentration (N)	Dissolution Rate (nm/s)	Relative Offset (from Interferometry, 600 nm)	Gel layer thickness* (nm) {from Interferometry}	Average SE Mean Squared Error (Single layer model)	Gel layer thickness* (nm) {from SE}
Novolac (Schnectady)	0.216	18.2	0.016$	< 10 nm	5.2	< 10 nm
Varcum novolac	0.26 (CD-26)	13.6	0.011$	< 10 nm	5.6	< 10 nm
G2 novolac resin	0.26	32.4	0.0024	< 10 nm	5	< 10 nm
PHOST (Mn~70,000)	0.15	26.1	0.07	< 27 nm	8	< 10 nm
pNHFA	0.16	30.3	0.013	< 12 nm	3.2	< 10 nm

*assuming a gel layer with a constant index of refraction profile and 50 % solvent composition

$ RO at 700 nm

7.5 CONCLUSIONS

Spectroscopic ellipsometry was used in conjunction with interferometry to study interfacial layer formation during photoresist dissolution in aqueous base. For a variety of phenolic polymers and a 157 nm resin, no evidence of interfacial layer formation was found within the resolution limits (~ 10-15 nm) of the techniques. The one exception was high molecular weight (Mn=72k) PHOST. For this case, a slight offset was observed with interferometry, indicative of a ~ 27 nm gel layer. However, the ellipsometry results indicated that the interfacial layer was below the 10 nm resolution of the technique. This experiment will be repeated to determine if consistent results can be obtained.

The experimental work in this chapter validates the original assumption of the CI dissolution model that dissolution of low molecular weight phenolic polymers can be described without the formation of any significant intermediate gel layer. 100% of the phenolic polymer data collected in this work is consistent with that conclusion. Furthermore, it was possible to demonstrate that previous work of Arcus was not consistent with gel layer formation, and it follows that the large body of resist dissolution models that are based upon this experimental data (primarily the percolation model of Reiser) must be thoroughly reexamined.

Of course, a realistic picture of polymer dissolution does not involve an atomically sharp interface. That is, even if a separate "gel" phase does not form, there still must be a transition between the developer solution and the thin polymer film. The evidence suggests the length scale of this transition for phenolic polymers is below 10 nm, and probably on the length scale of the surface roughness, radius of gyration of the polymer chains, and coulombic forces (discussed in Chapter 4). That is, the length scale of this transition is probably 3-8 nm. Note that some previous gel layer models assume a small transition zone (10 nm, and 2-4 nm, respectively). Such a thin transition zone cannot be experimentally refuted, and in fact the current lattice CI model is completely consistent with a transition zone on this order of magnitude. However, the CI model does not consider this region to be a separate phase, or a region in which significant mass transport resistance is present. Rather, the thin transition arises from polymer morphology (surface roughness) and the expected concentration gradient of reaction species that is present anytime a reaction occurs at an interface, as well as Coulombic forces. This picture of dissolution is consistent with the wide array of experimental data that is consistent with the reaction limited CI model.

However, it is noted that the CI model assumptions, and the focus of this work, was on phenolic polymers that are used for 365 nm and 248 nm photoresists. There now exists a significant amount of data that suggests that 193 nm photoresist resists (at least, model 193 nm resins) undergo swelling and/or interfacial layer formation during aqueous base dissolution. This is primarily because the acidic group of 193 nm photoresists is a carboxylic acid, having a pKa ~ 5, which makes the dissolution behavior of these resists considerably different from that of 365, 248, and 157 nm photoresists, in which the pKa of the acidic group is ~9-10. 193 nm photoresists tend to dissolve faster than other photoresists, as discussed in Chapter 2. Also, since the pKa is below 7, water acts as a base to these 193 nm materials, and causes some amount of deprotonation to occur. This leads to greater hydrophilicity, larger water/developer solution sorption, and swelling of the polymer chains. In practice, the blocking fraction of 193 nm resists is reduced, and dissolution inhibitors are added to help control unwanted swelling and rapid dissolution, such that commercial 193 nm photoresists do have similar dissolution behavior to their larger wavelength predecessors. In principle, it should be possible to add these complex swelling and inhibitor effects to the CI lattice model, but this is currently a topic for future research.

7.6 REFERENCES

1) Arcus, R. A. *Proc. SPIE* **1986**, *631*, 124-131.

2) de Gennes, P. G. *Scaling Concepts in Polymer Physics*; Cornell University Press: Ithaca, NY, 1979.

3) Herman, M. F.; Edwards, S. F. *Macromolecules* **1990**, *23*, 3662-3671.

4) Peppas, N. A.; Wu, J. C.; Vonmeerwall, E. D. *Macromolecules* **1994**, *27*, 5626-5638.

5) Arcus, R. A. *Proc. SPIE-Int. Soc. Opt. Eng.* **1986**, *631*, 124-134.

6) Shih, H. Y.; Reiser, A. *Macromolecules* **1997**, *30*, 4353-4356.

7) Shih, H. Y.; Zhuang, H. F.; Reiser, A.; Teraoka, I.; Goodman, J.; Gallagher-Wetmore, P. M. *Macromolecules* **1998**, *31*, 1208-1213.

8) Choi, S.; Cho, J. Y. *Proc. SPIE* **2001**, *4345*, 952-962.

9) Cho, J. Y., Choi, S. *Proc. SPIE* **2002**, *4690*, 912-910.

10) Houle, F. A.; Hinsberg, W. D.; Sanchez, M. I. *Macromolecules* **2002**, *25*, 8591-8600.

11) Tsiartas, P. C.; Flanagin, L. W.; Henderson, C. L.; Hinsberg, W. D.; Sanchez, I. C.; Bonnecaze, R. T.; Willson, C. G. *Macromolecules* **1997**, *30*, 4656-4664.

12) Flanagin, L. W.; Singh, V. K.; Willson, C. G. *Journal of Polymer Science Part B-Polymer Physics* **1999**, *37*, 2103-2113.

13) Flanagin, L. W.; McAdams, C. L.; Hinsberg, W. D.; Sanchez, I. C.; Willson, C. G. *Abstracts of Papers of the American Chemical Society* **1999**, *218*, 112-PMSE.

14) Flanagin, L. W.; Singh, V. K.; Willson, C. G. *Journal of Vacuum Science & Technology B* **1999**, *17*, 1371-1379.

15) Burns, S. D.; Schmid, G. M.; Tsiartas, P. C.; Willson, C. G.; Flanagin, L. *Journal of Vacuum Science & Technology B* **2002**, *20*, 537-543.

16) Hunek, B.; Cussler, E. L. *Aiche Journal* **2002**, *48*, 661-672.

17) Krasicky, P. D.; Groele, R. J.; Rodriguez, F. *Chemical Engineering Communications* **1987**, *54*, 279-299.

18) Krasicky, P. D.; Groele, R. J.; Jubinsky, J. A.; Rodriguez, F.; Namaste, Y. M. N.; Obendorf, S. K. *Polymer Engineering and Science* **1987**, *27*, 282-285.

19) Krasicky, P. D.; Groele, R. J.; Rodriguez, F. *Journal of Applied Polymer Science* **1988**, *35*, 641-651.

20) Nivaggioli, T.; Winnik, M. A. *Chemistry of Materials* **1993**, *5*, 658-660.

21) Papanu, J. S.; Hess, D. W.; Bell, A. T.; Soane, D. S. *Journal of the Electrochemical Society* **1989**, *136*, 1195-1200.

22) Hinsberg, W. D.; Lee, S.-W.; Ito, H.; Horne, D. E.; Kanazawa, K. K. *Proceedings of SPIE-The International Society for Optical Engineering* **2001**, *4345*, 1-9.

23) Lee, S.; Hinsberg, W. *Anal. Chem.* **2002**, *74*, 125-131.

24) Wallow, T.; Chan, W.; Hinsberg, W.; Lee, S. *Proc. SPIE* **2002**, *4690*, 299.

25) Hinsberg, W. D., et. al. *Presented at EIPBN, 2002; private communications with Dr. W.D. Hinsberg* **August, 2002**.

26) Toriumi, M.; Itani, T. *Proc. SPIE-Int. Soc. Opt. Eng.* **2002**, *4690*, 904-911.

27) Tompkins, H. G.; McGahan, W. A. *Spectroscopic Ellipsometry and Reflectometry: A User's Guide*; John Wiley & Sons: New York, 1999.

28) Rancourt, J. D. *Optical Thin Films: User Handbood*; SPIE Optical Engineering Press: Bellingham, WA, 1996.

29) Burns, S. D.; Gardiner, A. B.; Krukonis, V. J.; Wetmore, P. M.; Lutkenhaus, J.; Schmid, G. M.; Flanagin, L. W.; Willson, C. G. *Proceedings of SPIE-The International Society for Optical Engineering* **2001**, *4345*, 37-49.

30) Chen, K. R.; Jordhamo, G.; Moreau, W. M. *Proc SPIE* **1996**, *2724*, 553-562.

31) Szmanda, C. R.; Yu, J.; Barclay, G.; Cameron, J.; Kavanagh, R. J.; Blacksmith, R.; Trefonas, P.; Taylor, G. N. *Proc SPIE* **1997**, *3049*, 65.

32) Abeles, F. *Ann. Phys.* **1950**, *5*, 596.

33) Scheer, S. A.; Brodsky, C. J.; Robertson, S. A.; Kang, D. *Proc SPIE* **2002**, *4689*, 937-948.

34) Burns, S. D.; Gardiner, A. B.; Lutkenhaus, J.; Krukonis, V. J.; Wetmore, P. M.; Schmid, G. M.; Willson, C. G. *Proc SPIE* **2001**, *4345*, 37.

35) Ito, H.; Sherwood, M. *J. Photopolymer Science & Technology* **1999**, *12*, 625.

36) Sirard, S. M.; Green, P. F.; Johnston, K. P. *J. Physical Chemistry B* **2001**, *105*, 766-772.

CHAPTER 8: SURFACE ROUGHNESS – COMPARING THE CI MODEL TO EXPERIMENTAL VALUES

8.1 AN INTRODUCTION TO LINE EDGE ROUGHNESS

As the miniaturization of electronic devices continues, line edge roughness (LER) is becoming an increasingly important problem to understand and control. LER is defined as the variation in CD (critical dimension) along a feature edge. There are generally two types of line edge roughness encountered: low frequency and high frequency roughness, shown in Figure 8.1. In this case the labels are obvious, but there are no strict definitions for these two cases. Currently, processes exist in semiconductor manufacturing that use 193 nm light to produce 130 nm structures with ~7 nm of line edge roughness (LER). The International Roadmap for Semiconductors (2001) states that by 2005, 90 nm features with 4 nm of LER will be required. By 2016, 25 nm features with 1 nm of LER will be needed.[1] There are currently no known solutions for reducing LER, and a large amount of research has recently been invested into determining the fundamental causes of LER and potential solutions.[2-10] Note that the future LER requirement (1 nm) is *smaller* than the characteristic polymer size (3-7 nm) in the photoresist film!

It's important to note that LER of the resist image does not directly affect any property of the final device; rather, it is the LER of the etch-transferred feature that matters. If an etch process could be developed to "smooth out" LER of the resist during the etch transfer, then it would not be necessary to significantly minimize (nor to understand) LER formation in the resist image. However, it is expected that etch transfer processes will not be capable of smoothing large amounts of LER, and that all efforts must be made to minimize LER during initial lithography imaging, but research into etch transferred LER is ongoing.[11]

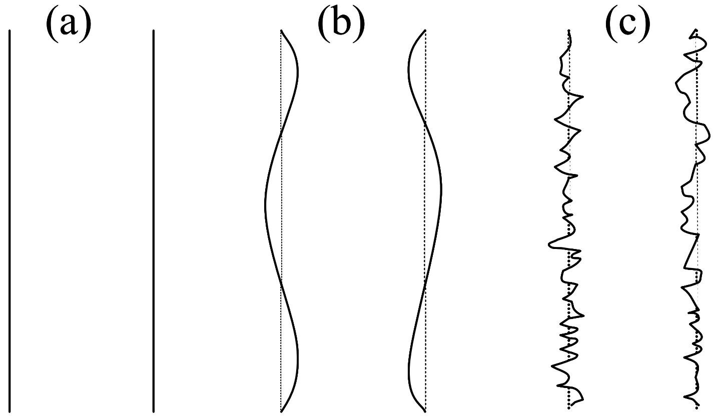

Figure 8.1 Top down diagram of line edge roughness (LER). (a) smooth feature, (b) low frequency LER, (c) high frequency LER

8.2 FUNDAMENTAL CAUSES OF LINE EDGE ROUGHNESS

LER has a broad definition (statistical variation in characteristic dimension across a feature) and it can be caused by any statistical or systematic fluctuation in the imaging process. For example, statistical transport effects of the catalytic acid, resist contamination, shot noise from the aerial image, photomask

LER or defects, the morphology of the polymer, *etc*. may all contribute to LER. The challenge is to isolate those variables or mechanisms that have the largest contribution to roughness. Many imaging experiments have been performed in which specific variables are isolated, and their effect on LER is measured.[8,9,11-14] This approach is certainly valid and provides knowledge that is ultimately necessary to solve this problem. However, it is often difficult to properly isolate individual variables in an experiment. For example, if the polymer molecular weight is increased, the developer concentration must also be increased.[9] For these reasons, it is equally valuable to approach the LER problem from a simulation perspective. Our research group, through the work of Flanagin *et al*.,[6] has previously used the lattice based CI dissolution model to quantitatively simulate the formation of surface roughness during dissolution as a function of development time, polymer molecular weight, polymer polydispersity, and exposure dose (polymer blocking fraction). However, at the time of this work there was only a scattered amount of literature data with which to compare the model predictions. The focus of this chapter was a series of AFM experiments in which the bulk surface roughness of partially dissolved photoresist resins was measured and compared with model predictions. The goal was to validate the model (or determine the areas in which the model failed). First, a review of other LER literature is presented.

8.2.1 REVIEW OF LINE EDGE ROUGHNESS STUDIES

The lithography process is very complicated, and many approaches have been proposed to minimize LER. These approaches can be lumped into two categories: processing solutions and materials solutions. For example, a processing solution might be changing a bake temperature, spin speed, or dissolution time. A materials solution might involve changing the photoresist resin, or photoactive component. Recent studies by Intel suggest that a processing solution will not be adequate to minimize LER[12,14] and a materials solution will be needed. Thus, it is important to understand the contribution of each component of the photoresist to line edge roughness.

He and Cerrina produced one of the first studies of surface roughness in CA photoresists.[5] Their experiment consisted of blanket exposing films of APEX-E (a PHOST-co-tBOC photoresist) with varying doses, performing a post exposure bake at 85°C for various times, dissolving the films in 0.26 N TMAH for 20s, and measuring the surface roughness of the remaining film by AFM. They found that surface roughness plotted against exposure dose resulted in curves with a maximum surface roughness (Figure 8.2). Their main conclusion was that equal degrees of deprotection yield similar surface morphologies, but that the standard deviation of the roughness can be different, and process (or path) dependent.[5] A fundamental mechanism for surface roughness formation was not explicitly proposed.

In Flanagin's work, surface roughness was simulated during dissolution of PHOST polymers with various blocking fractions (this is very similar to the effect of varying exposure dose).[6] The result of this work is shown in Figure 8.3 and is qualitatively consistent with that of He and Cerrina. That is, a maximum was observed in the plot of surface roughness versus blocking fraction (Figure 8.3). This behavior is undesirable, because at the resolution limit the exposure dose (and/or blocking fraction) that is present at a photoresist line edge will inevitably be in an intermediate range near the maximum of these roughness versus dose curves.

The mechanism of this "maximum" trend can be understood in the following way. At low exposure doses (or high blocking fractions), the polymer remains insoluble, and the roughness does not increase from that of the smooth, spun cast film. At high doses, the polymer is rendered completely soluble. In this case, the film dissolves fairly uniformly, so the roughness also remains low. This idea is represented in a simple cartoon in Figure 8.4, in which polymer chains are represented by spheres on a lattice. (Note that this is not the way polymers are represented in the actual CI simulations – this figure is simply an illustration.) For the case of a partially soluble film, statistical variations in the solubility of each chain will lead to an increased roughness. Thus, a maximum is observed in a plot of roughness versus blocking fraction or exposure dose. This mechanism

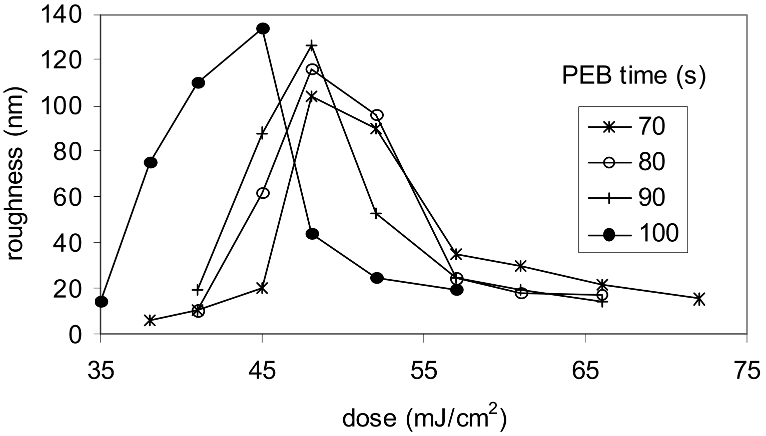

Figure 8.2 Experimental results of He and Cerrina: Formation of surface roughness versus dose for APEX-E films in which the PEB time was varied.

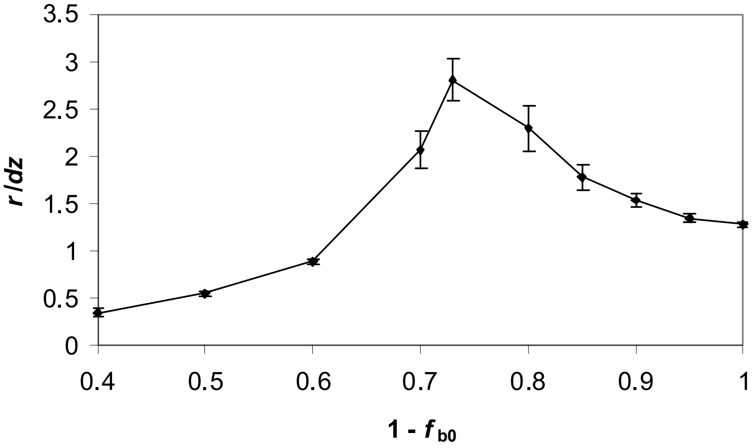

Figure 8.3 Simulation results of Flanagin for surface roughness plotted against the blocking fraction of polymer chains. The y-axis is the roughness (r) normalized to the height of a cell (dz), which for PHOST is ~ 0.7 nm.

explains the formation of roughness in the simulations (Figure 8.3), but may not completely describe the experimentally observed roughness in Figure 8.2.

For example, there is another way to interpret Figure 8.3. Instead of assuming that each sphere is an individual polymer chain, one may assume that each sphere is the region that is deprotected by a catalytic acid during the post exposure bake. It is unknown exactly how large these regions might be, but estimates of the catalytic chain length or "sphere of influence" of a photogenerated acid are approximately a sphere with a diameter of 5 nm.[15-17] The volume of this region may be larger in regions of low acid concentration.[18] If Figure 8.4 is viewed in this way, the mechanism of roughness formation is very similar (statistical variation in soluble regions), but the size of the roughness

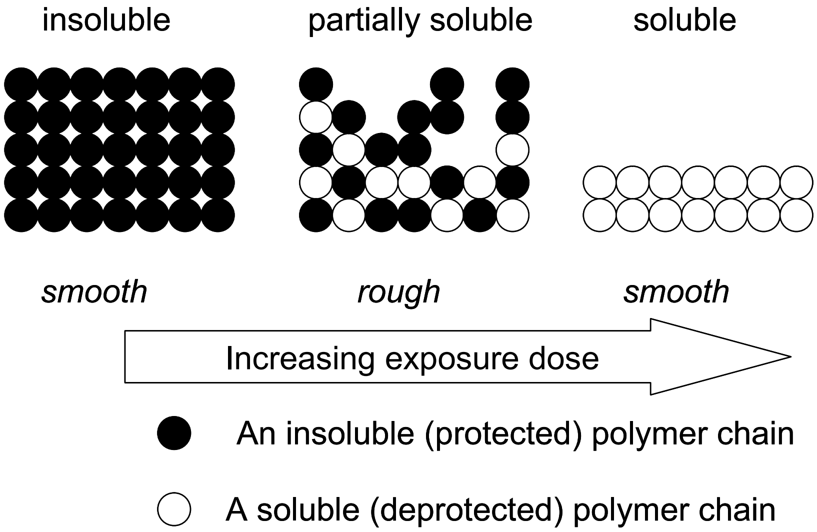

Figure 8.4 A cartoon explanation of a roughness maximum when plotted against blocking fraction, or exposure dose.

becomes much larger. Instead of individual chains that are insoluble, there are microscopic aggregates of chains that are insoluble, thus the roughness is larger.

Lin *et al*. have proposed a phase separation mechanism for line edge roughness formation in chemically amplified photoresists.[2,3] The basic premise of the theory is similar to the mechanism proposed above. However, an addition to the theory is that in the composition regions that are mixed (near the line edge), phase separation of the various polymer species occurs during the post exposure bake. Presumably phase separation would increase the measured line edge roughness. Lin *et al*. measured the surface roughness after bake and development of polymer blends of ESCAP type photoresists, which are copolymers of poly(hydroxystyrene) and poly(t-butyl acrylate). Increased roughness was observed in blend films after bake and development, with a maximum roughness of ~30 nm at a polymer blend content of 50 wt %. In non blend polymer films of various blocking fraction, little roughness (< 2 nm) was formed after development, regardless of the deprotection level. Lin *et al*. conclude that phase separation causes higher roughness in the blend films than the non blend films.[2,3] However, it is unknown whether or not this phase separation occurs in the resist solution, during spin coating, or during baking. It is unknown whether or not an equal degree of phase separation would occur during/after the post exposure bake, which is only a brief anneal below the glass transition of the polymer. Phase separation of different polymer species is an interesting explanation for line edge roughness, but more studies need to be performed to quantitatively determine the contribution of phase separation over other effects, such as the stochastic nature of the acid transport described above.

Lin *et al*. also presented some other notable results.[2,3] Recall the AFM experiments shown in Figure 6.11 in which films of novolac, PHOST, and APEX-E (~ 20% protected PHOST) were dissolved for varying times in aqueous base developer. The general trend was that the films started smooth and then the roughness increased to a constant bulk value (of 1-3 nm). Lin *et al*. performed a similar experiment with PHOST films of various levels of protection (10-20 wt %), in which each sample was partially dissolved in 0.14 N TMAH. The results of this experiment are shown in Figure 8.5. The results are very similar to the results of this work shown in Figures 6.11, and previous results of Reynolds and Taylor (shown in Figure 8.6). The films start smooth and the roughness then increases to a constant bulk value of 1-2 nm during dissolution. The notable result is that the protection level does not influence the bulk value of the surface roughness, and this bulk value is relatively low. Compare these results to those of He and Cerrina[5] (Figure 8.2), in which roughness in excess of 100 nm is observed during dissolution of partially deprotected APEX-E. In this case, the deprotection has occured because of acid transport and reaction during PEB. Note that APEX-E is partially protected (~ 20%) PHOST, therefore the average % of deprotection

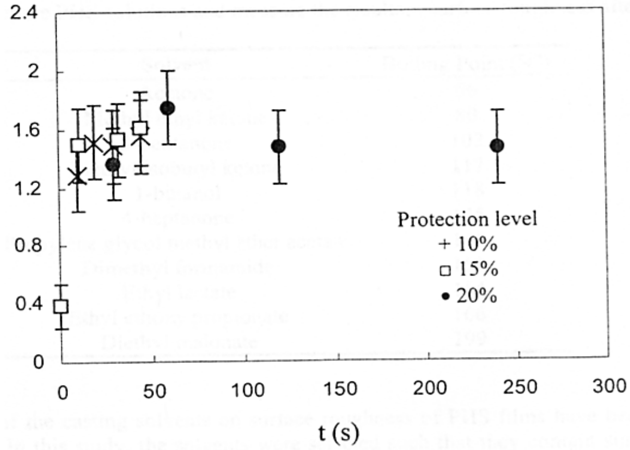

Figure 8.5 Results of Lin *et al*. showing roughness formation during aqueous base dissolution of partially protected PHOST films.

must lie between 0-20 % for this resin, with the fraction of deprotection depending on the exposure dose and thermal conditions of the PEB. Also note that the roughness results of He and Cerrina seem excessively large – results shown later in this chapter for an identical photoresist show roughness values an order of magnitude lower.

Regardless of this discrepancy, there is (at least) an order of magnitude increase in the roughness of partially deprotected APEX-E films over that of neat, partially protected PHOST films. Note that the pure films will have a distribution of blocking fraction from chain to chain, very similar to the random, Gaussian distribution of blocking fraction created by Flanagin in his simulations (Figure 8.3). Thus, the mechanism of statistical variations in polymer solubility (of individual chains) is not adequate to describe roughness formation observed in the experiments of He and Cerrina.[5] One would have to (at minimum) invoke the mechanism of statistical variations in the larger regions of acid catalyzed deprotection events. This explanation is consistent with the simulations of Schmid *et al.*, in which an acid molecule in a region of low concentration (low exposure dose) has a statistically larger effect than an acid in a high concentration region.[18] Also, the acid will have statistical fluctuations of its path, which cause relatively large regions of insoluble/soluble material. This mechanism could explain the larger values of roughness observed by He and Cerrina.[5]

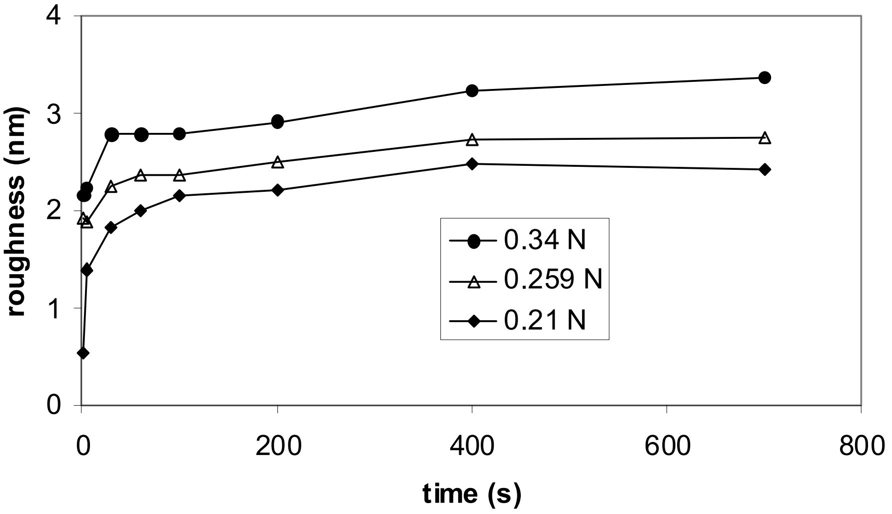

Figure 8.6 Experimental results of Reynolds and Taylor showing the surface roughness formation during aqueous base dissolution of APEX-E at various developer concentrations

8.2.3 Trade Offs between LER and Sensitivity

Photoresists are often characterized by their sensitivity, which can be defined in many ways. Perhaps the simplest definition is that sensitivity (S) is the incident input energy (E) per unit area (A) (or dose) required to achieve the desired chemical response in the photoresist[19]:

$$S = E/A \tag{8.1}$$

A low value for S is desired, because this reduces the time of the wafer in the exposure tool and improves the throughput of the lithography process. It is terribly confusing that photoresists with a low value of S (a low sensitivity) are said to be "high sensitivity" photoresists. The latter description is not consistent with the definition provided in Equation 8.1, yet is commonly used in everyday discussion. Chemically amplified photoresists have much lower value of S than non-chemically amplified resists, due to the catalytic nature of the imaging mechanism. Unfortunately, this "high sensitivity" results in greater statistical fluctuations in acid reaction and transport described above, which is thought to lead to roughness formation. Thus, there is expected to be a tradeoff between photoresist sensitivity and LER.[13,18]

A recent study by Intel confirms that a tradeoff exists between sensitivity and line edge roughness. Cao *et al*. performed a large study of a number of candidate EUV resists, and determined both LER and sensitivity for a number of resists and processing conditions.[12] It was confirmed that an inverse relationship exists between sensitivity and LER – it was not possible to find a photoresist and processing conditions that simultaneously provided low sensitivity and low LER.

8.2.4 LER Studies by Interferometric Lithography

Sanchez *et al*. used interferometric lithography to study the effect of aerial image contrast upon line edge roughness in a wide variety of photoresists.[9] This technique allows the unique ability to control exposure dose, aerial image contrast, and line spacing (pitch) independently. Their study was very important because aerial image contrast is diminished at low resolution (feature size). However, controlled LER is most important at small feature size, where aerial image contrast is limited. Thus, it is important to establish a relationship between aerial image contrast and roughness formation. The general result was that LER increased as aerial image contrast was decreased. This was observed for a wide variety of photoresists, including non-chemically amplified, chemically amplified, positive tone, and negative tone photoresists. The comparisons led to the conclusion that there was not a single isolated factor that led to LER formation. For example, it was postulated above (and elsewhere) that statistical variations of acid catalyzed transport and reaction may lead to nanoscopic regions of solubility variations. These, in turn, may lead to line edge roughness during dissolution. However, it was also shown that a non-chemically amplified photoresist (in which the imaging mechanism is entirely different) also shows increasing LER with decreasing aerial image contrast. Therefore, statistical variations in the chemically amplification mechanism are not the sole cause of LER.[9]

The other major example cited by Sanchez was that of two negative tone photoresists: one that was aqueous base soluble, and the other was soluble in an organic solvent.[9] It has been postulated that statistical effects due to the deprotonation reaction during dissolution may lead to line edge roughness. However, the organic soluble resist showed similar trends with decreasing aerial image contrast. Thus, it was not possible to isolate statistical variations in the aqueous base dissolution process as the major contributor to LER. The overall conclusion was that no specific type of photoresist chemistry had a particular advantage in minimizing LER over a range of aerial image contrasts.[9]

Another important result by Sanchez *et al.* was the influence of polymer molecular weight on line edge roughness. In their study, the molecular weight of a negative tone photoresist was varied between 2,500-15,000. At 100% aerial image contrast, all 3 samples showed little LER (~ 1 nm). At 60% contrast, the LER increased significantly with increased molecular weight, to the point that microbridges formed between neighboring lines for the Mn = 15,000 photoresist.[9] This observation is consistent with that of Yoshimura *et al.*, who observed the general trend that surface roughness increased with increasing molecular weight.[7] However, Yoshimura *et al.* only studied two PHOST samples, of Mn = 2,300 and Mn = 6800, and quantitative results were not presented. Flanagin presented simulations that showed increasing surface roughness with increasing molecular weight, which was consistent with these previous literature results, but a quantitative comparison could not be made between Flanagin's simulations and previous experiments.[6]

In this work, the surface roughness was measured after partial dissolution of several monodisperse PHOST samples over a range of molecular weights. These experiments were compared to CI lattice simulations, in order to quantitatively compare the model to simulation. Also, surface roughness was measured as a function of time, developer concentration, and exposure dose (for both a chemically amplified and non chemically amplified photoresist).

8.3 SURFACE ROUGHNESS VARIATION WITH POLYMER SIZE

The polymers used in this study are monodisperse polyhydroxystyrene, donated from Nippon Soda. A range of molecular weights between 3,000 and 15,000 were used. Films were spun cast on silicon wafers from solutions of 20% solids in PGMEA (propylene glycol methyl ether acetate) at a spin speed of 2500 rpm for 30 seconds. The post apply bake was 90°C for 90s. A range of film thickness from 1-1.6 μm resulted. The films were dissolved in 0.11 N KOH until approximately half the film dissolved. The surface roughness was measured with a Park Scientific Instruments Autoprobe AFM. The force used was 2 nN at a scan rate of 1 Hz and a gain of 0.2. The roughness values are averages of several scans on the wafer surface.

The algorithm used by the CI model to calculate surface roughness has been previously discussed. The surface roughness was calculated for the same simulations used in Figure 2.8, with the same simulation conditions. Figure 8.7 shows the average surface roughness plotted against degree of polymerization, determined by simulation and experiment. The surface roughness was found to increase linearly with increasing molecular weight, which is consistent with the results reported by Yoshimura *et al.*[12] There is surprisingly good agreement between the CI model prediction of surface roughness and the experimentally observed roughness over a MW range of 3,000 to 15,000.

It may be intuitive that smaller polymer chains will pack easier (with less entanglement) and the resulting polymer morphology will have smaller roughness. This simple idea is illustrated in Figure 8.8, again assuming that a polymer chain may be represented by a sphere. This simple idea has been quantitatively verified by a comparison between simulation and experiment. This exercise suggests that the lattice equilibration techniques used by Flanagin *et al.*[6]

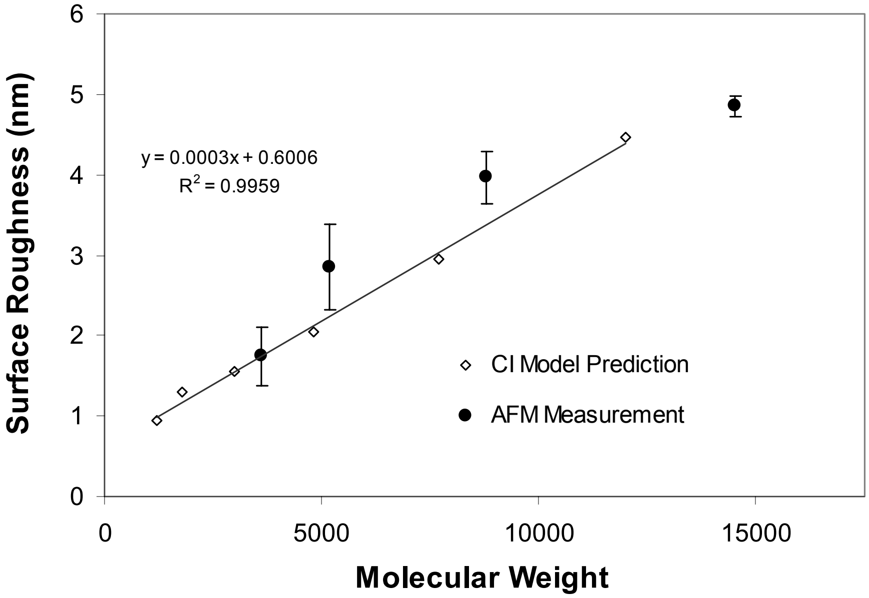

Figure 8.7 Average surface roughness as a function of degree of polymerization for PHOST determined by the CI lattice model and by AFM.

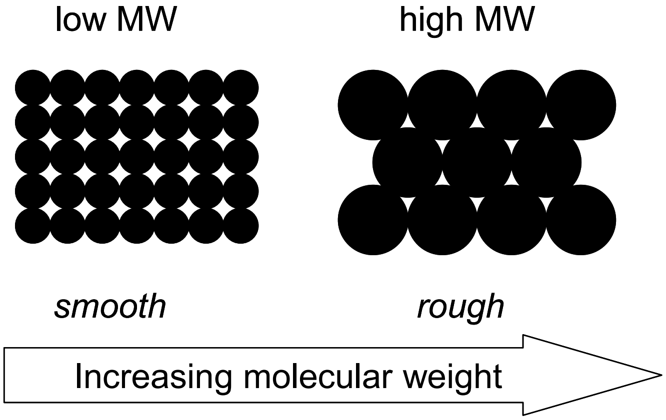

Figure 8.8 Idealized explanation for the observed trend that surface roughness increases with increasing molecular weight

and Schmid *et al.*[18] provide a valid representation of the polymer surface morphology. It also empirically suggests that the dissolution algorithm (the CI mechanism) is qualitatively correct. The most important result of Figure 8.7 is that a quantitative determination has been isolated and established between polymer size and surface roughness. Since LER must be reduced to ~1-2 nm over the next 10-15 years, it is envisioned that future photoresists may be composed of even lower molecular weight resins.

8.4 SURFACE ROUGHNESS VARIATION WITH FILM THICKNESS

AFM experiments have been presented in which the dissolution time (or thickness into the film) was varied and the surface roughness was measured. In each case (Figures 6.11, 8.5, and 8.6), the surface roughness was initially smooth (~0.5 nm) but then increased to a bulk value of 1–5 nm as dissolution occurred. These results are consistent with the lattice simulations discussed in Chapter 6, and are now presented here. The simulation results shown here are significantly different from those of Flanagin *et al.*,[6] because of subtle changes in the CI lattice model that have been applied. A typical simulation result is shown in Figure 8.9 and 8.10. The roughness starts smooth (< 0.5 nm) and then increases to a bulk value of ~1.5 nm. In the simulations, the dissolution rate tracks with the surface area of ionizeable sites, and thus increases with increasing roughness, which is also plotted in Figure 8.9.

It's important to understand the reasons for this behavior in the simulation. In the equilibration step of the polymer chains on the lattice, periodic boundary conditions are employed in the *x* and *y* direction, and physical boundaries are placed on the *z* planes (the top and bottom of the lattice). During equilibration, the polymer chains are forced into a relatively smooth configuration near the film surface and substrate, which results in a relatively smooth film surface (depicted in Figure 8.10 and 8.11). As the film dissolves over a distance equal to approximately the radius of gyration of the polymer chains, the roughness increases to a bulk value, which is also related to the radius of gyration of the polymer chains.

The fact that the roughness behavior over time is consistent between both the simulations and experiments may be considered a fortuitous effect. After all, there is no physical, excluded volume boundary at the film surface during spin casting that is comparable to the boundary imposed in the lattice simulations. The initially smooth films are probably caused by centrifugal and surface tension forces during spin casting that result in a similar gradient in polymer structure (and therefore roughness). This is probably the reason that the increase in surface roughness in experiments happens over a longer length scale than that of the simulations. It may be possible to consider the film formation more rigorously

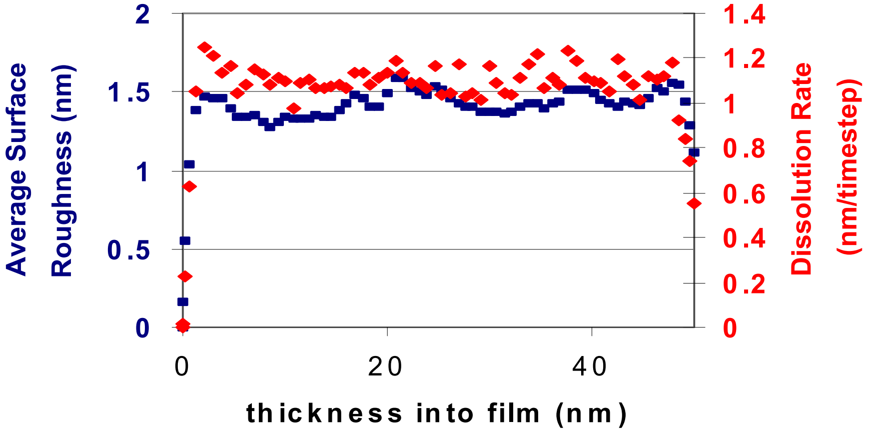

Figure 8.9 Roughness and dissolution rate versus film thickness during a typical CI lattice simulation.

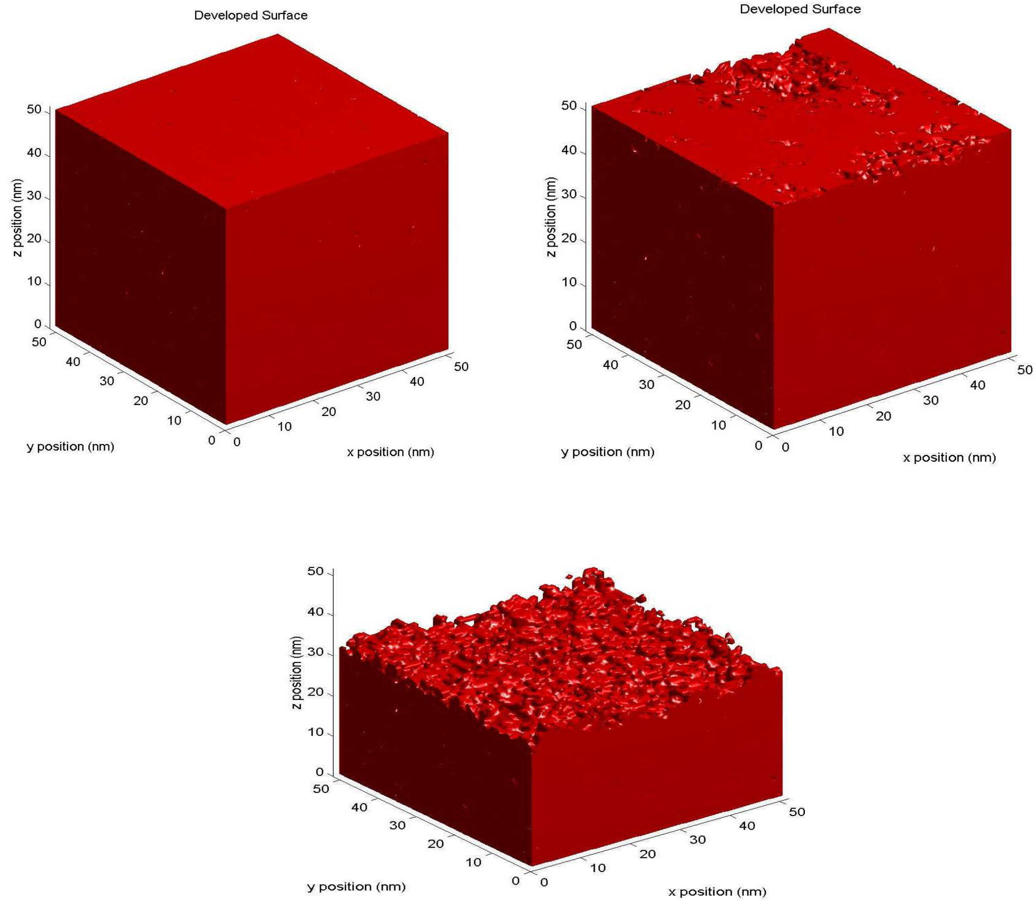

Developed Surface

Developed Surface

Figure 8.10 3-D lattice CI simulations showing the formation of roughness during dissolution.

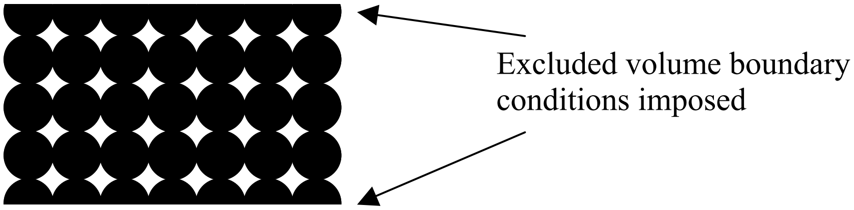

Figure 8.11 A cartoon description of polymer structure on a lattice with boundary conditions at the top and bottom. The film is forced to be smooth at the surface.

in order to quantitatively describe the increase in roughness over time, but this is not considered to be a large priority for improving the rigor of the lattice simulations.

8.5 SURFACE ROUGHNESS VARIATION WITH DEVELOPER PH

Few studies have been performed in which the variation in surface roughness has been measured with variation in aqueous base developer concentration. Reynolds and Taylor[10] varied the developer concentration in their AFM experiments (Figure 8.6), and those results indicate that roughness increases with increasing developer concentration. However, Flanagin plotted their data versus remaining film thickness (instead of time) and the result was that no difference in bulk roughness was observed with increasing base concentration.

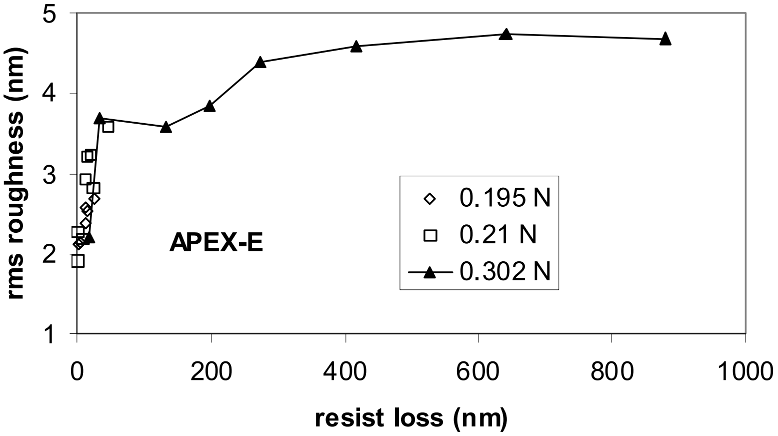

Figure 8.12 Experimental results of Reynolds and Taylor. The experimental data is identical to that of Figure 8.6, but the roughness is plotted versus film thickness as opposed to time.

These results were consistent with the original form of the CI model, in which roughness did not vary with developer concentration. Specifically, roughness did not vary with the fraction of ionized surface sites, α.

In this work, the roughness was measured for a series of identical PHOST films that were partially dissolved by various concentrations of KOH. Films were spun cast onto silicon substrates from a solution of 20 wt % PHOST (Mn=29,000 Pd~1.1) dissolved in PGMEA. The spin conditions were 2500 rpm for 30s and the films were baked at 170°C for 10 minutes, resulting in ~1.6 μm films. The films were dissolved until approximately ½ of the film remained. The developer used was potassium hydroxide (KOH) at concentrations varying between 0.11-0.19 N. The surface roughness of the partially dissolved films were measured on a Park Scientific Instruments AFM. The results of these experiments are shown in Figure 8.13. At low developer concentrations, the average surface roughness is high (~8.5 nm). As the developer concentration is increased, the average surface roughness decreases considerably, reaching a plateau value of 0.6 nm at 0.15 N KOH.

These results are not expected. The CI model does not predict any change in surface roughness with increasing pH of the developer. While the chains will dissolve faster with a higher developer concentration, the surface morphology does not change, and therefore there is no change in roughness predicted. Also, the results of this experiment are inconsistent with some literature results. Recent results of Stewart *et al*. suggest that roughness may increase with increasing developer concentration.[20] The results of Reynolds and Taylor suggest the same trend.[10] However, these latter results are ultimately inconclusive because bulk thicknesses were reached in only one case. At low developer concentrations, the films did not dissolve past the surface region, where the roughness is known to be smoother than that of the bulk.

In the experiment reported in Figure 8.13, each film was dissolved until a bulk thickness was reached. Thus, the film thickness loss remained constant, but the dissolution time was varied. It is unknown what effect, if any, this might have upon the experimental results. Also, it is unknown why a higher developer concentration would lead to decreased roughness. A higher base concentration does lead to increased ionization. Perhaps greater ionization leads to larger hydration near the film surface. If the surface of the film is "fluid like" then surface tension forces would be more likely to smooth the surface of the film. The experiment presented in this section shows an interesting trend with surface roughness, but should be reproduced in other photoresist systems before it is accepted as a general result.

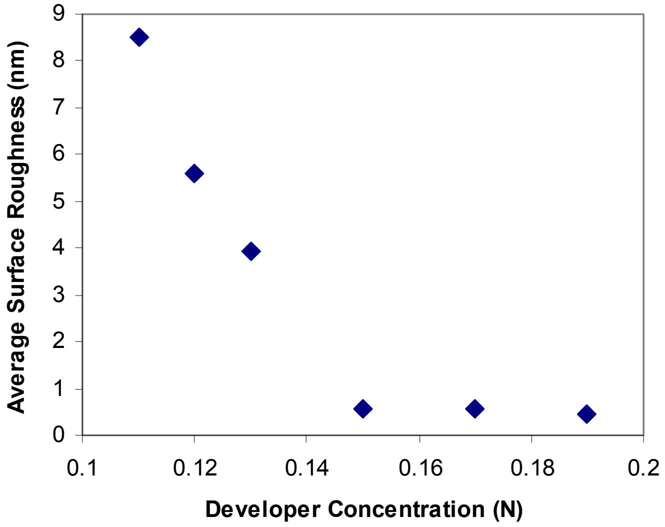

Figure 8.13 Variation in surface roughness of a PHOST film with varying developer concentration.

8.6 SURFACE ROUGHNESS VARIATION WITH EXPOSURE DOSE

In section 8.2, exposure dose was reported to have a large impact upon formation of surface roughness, and this trend was linked to the change in concentration of photogenerated acid. In this section, an experiment identical in form to that of He and Cerrina[5] was performed on both a chemically amplified and non chemically amplified photoresist (a traditional DNQ-novolac resist). It may seem unnecessary to test a NCA photoresist that does not have the resolution capabilities to necessitate low line edge roughness. However, recent results from our research group have shown that a 157 nm resin is capable of functioning as a non chemically amplified photoresist.[21,22] That is, it is possible to create a high resolution photoresist that operates via a NCA mechanism. For this reason, it is useful to determine if either mechanism (NCA or CA) offers an advantage in minimizing line edge roughness.

8.6.1 Chemically Amplified Resists – Roughness versus Dose

The experiment of He and Cerrina[5] was repeated here with only subtle changes. APEX-E was used as the photoresist, and spun cast onto silicon wafers at a speed of 2500 rpm (30 s) and a post apply bake temperature of 90°C, for 90 s. Individual films were flood exposed with an Oriel Mercury Arc Lamp through a 248 nm optical filter with varying doses. All films were post exposure baked at 90°C for 90 s, and then developed in 0.26 N aqueous base (TMAH) developer for

20 seconds. The surface roughness of the partially dissolved films was measured by AFM, as described in Chapter 3. The results of this experiment are shown in Figure 8.14.

The results of this experiment are qualitatively consistent with He and Cerrina, and the mechanism described in Section 8.2. At low exposure dose, small amounts of catalytic acid are generated and the film does not dissolve, leaving a smooth surface. At high exposure dose, large amounts of acid are generated, and the film completely dissolves. At intermediate doses, the film is rendered partially soluble, and a rougher surface forms during dissolution. Thus, the results of this experiment support the mechanism described in section 8.2.

However, the results are quantitatively different from those of He and Cerrina.[5] The maximum roughness in this experiment was ~ 5 nm, compared to a maximum roughness of ~ 130 nm in the experiment of He and Cerrina. This is a fairly large discrepancy considering that the exposure wavelength was the only significant difference in each experiment. The experimental results presented in this work are consistent with the order of roughness commonly observed at a line edge in 248 and 193 nm photoresists. The reason for the order of magnitude difference remains unknown.

8.6.2 Non Chemically Amplified Resists – Roughness versus Dose

An identical experiment was performed with a NCA photoresist formulation (consisting of a novolac resin from Schenectady Co. and 12 wt % DNQ photoactive compound). The resin and PAC were dissolved in PGMEA, and films were spun coated onto silicon wafers at 2500 rpm, for 30 s. The post apply bake was 90°C, for 90s. Films were flood exposed with varying doses of 365 nm light, and a post exposure bake was performed at 110°C for 90 s. The purpose of the post exposure bake was to blur standing waves. The films were then dissolved in 0.26 N aqueous base for 20 s, rinsed immediately with DI water, and the roughness was measured with an AFM as described previously. The result of this experiment is also shown in Figure 8.14.

The surface roughness of the initial film and the completely dissolved film (the substrate) are both less than 0.5 nm, while the roughness of the partially dissolved film is ~ 2.3 nm. With the exception of the beginning and end effects, the surface roughness of the NCA photoresist remains constant with exposure dose.

A control experiment was conducted in which unexposed films of the identical novolac resin (with no added PAC) were dissolved for varying times. In this case, the measured surface roughness was plotted against the remaining film thickness, and compared to the initial NCA experiment (Figure 8.15). The measured surface roughness is identical (within experimental error) in both experiments, suggesting that the roughness is caused only by the size and morphology of the polymer chains, and is independent of exposure dose and photoactive compound in NCA photoresists.

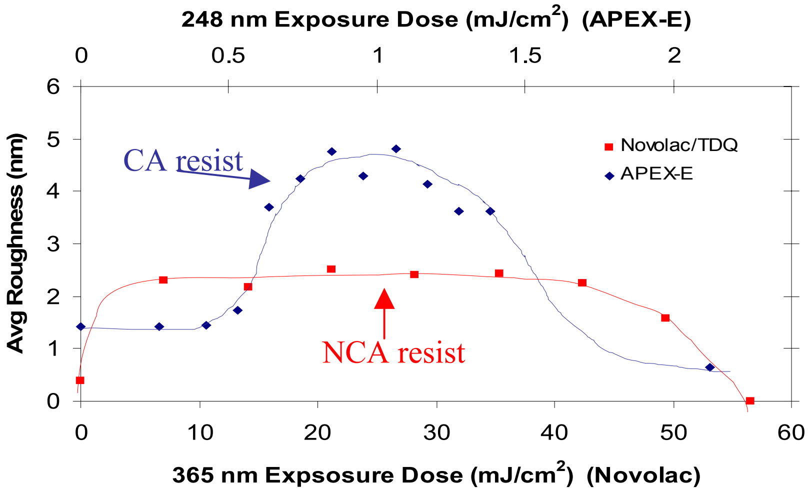

Figure 8.14 Measured bulk surface roughness as a function of exposure dose for a chemically amplified and non chemically amplified photoresist.

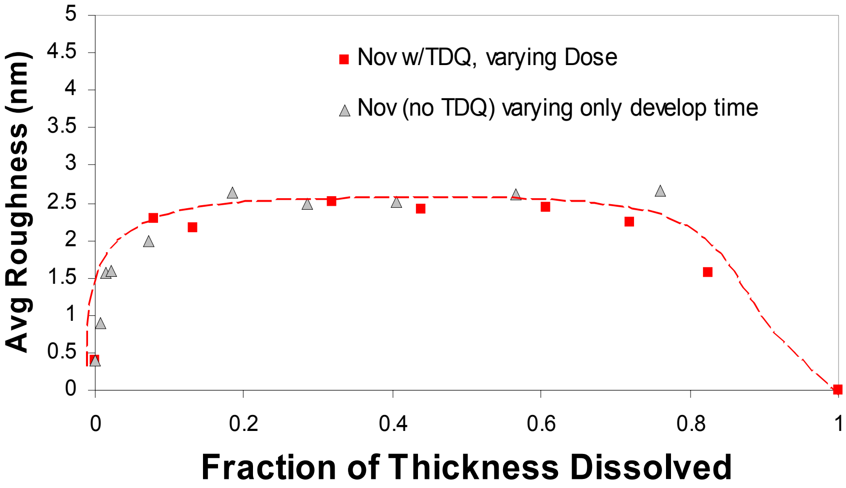

Figure 8.15 Measured bulk surface roughness as a function of film thickness for a non chemically amplified resin and photoresist formulation.

The explanation for this result is thought to be as follows: in a non chemically amplified photoresist, the base polymer resin is completely soluble. The interactions with the photoactive compound change the local pKa and reduce the dissolution rate considerably, but the polymer chains can never be considered to be insoluble. Thus, the mechanism of roughness formation described in section 8.2 for chemically amplified photoresists does not apply to non chemically amplified photoresists. CA resists operate by a gradient in solubility of individual chains, but NCA resists operate by a gradient in the dissolution rate of individual chains. One might argue that there would still be statistical differences in the dissolution rate of individual chains. However, the author proposes that the PAC-resin interactions of NCA resists are longer range and statistically "smoother" than the PAG-resin interactions of CA resists.

Consider Figure 8.16, in which a cartoon description is provided of the line edge of both a NCA and CA photoresist. The interaction of a PAC molecule in a NCA photoresist is usually thought to involve hydrogen bonding with neighboring chains.[23] If the PAC is multifunctional, the interactions might be viewed as a sphere surrounding the PAC molecule, in which the center of the sphere has the lowest dissolution rate with a gradient in dissolution rate outwards. In contrast, a PAG molecule of a CA resist carves out a tortuous path, in which deprotection of polymer blocking groups occurs haphazardly. Polymer chains located adjacent to one another (or even entangled together) might have extremely different solubilities at the end of the PEB. It is envisioned that the result of these effects is a line edge that is rougher in a CA resist than a NCA resist. The root cause is that PAC interactions are longer range, and thus may overlap with one another, resulting in a smooth gradient of pKa (dissolution rate) near the feature edge. The implication of this proposal (and the experimental results of Figure 8.15) is that surface roughness in NCA photoresists is independent of the imaging mechanism, and can be minimized by tuning parameters of the photoresist formulation such as polymer chain length.

8.6.3 A Non Chemically Amplified Solution to LER?

The previous discussion should be considered with two caveats. First, there exists very little data concerning LER formation in NCA photoresists. This work presents only initial data that suggests NCA resists may offer an advantage in minimizing LER. However, Sanchez *et al*. presented one case in which a NCA resist did not offer a significant advantage over CA photoresists (at least, not for reduced aerial image contrast).[9] Significant work remains to be done on 157 nm NCA photoresists to determine if this platform truly offers a significant reduction in LER over a traditional CA platform.

The second caveat is the tradeoff between LER and sensitivity. NCA photoresists traditionally have much larger sensitivity than CA photoresists. For example, notice in Figure 8.14 that the exposure dose of the NCA resist was much larger that that of the CA photoresist. Thus, one might expect that NCA photoresists do not offer any signficant advantage – even if LER is improved, it will be at the cost of increased exposure dose and throughput. However, there are two reasons this may not be a problem. First, the results of Chambers *et al*. show the pNHFA has a greater inhibition response to added PAC than a typical novolac film.[21,22] It is possible to attain adequate inhibition levels with much less added PAC. The sensitivity is expected to be better than a traditional NCA photoresist

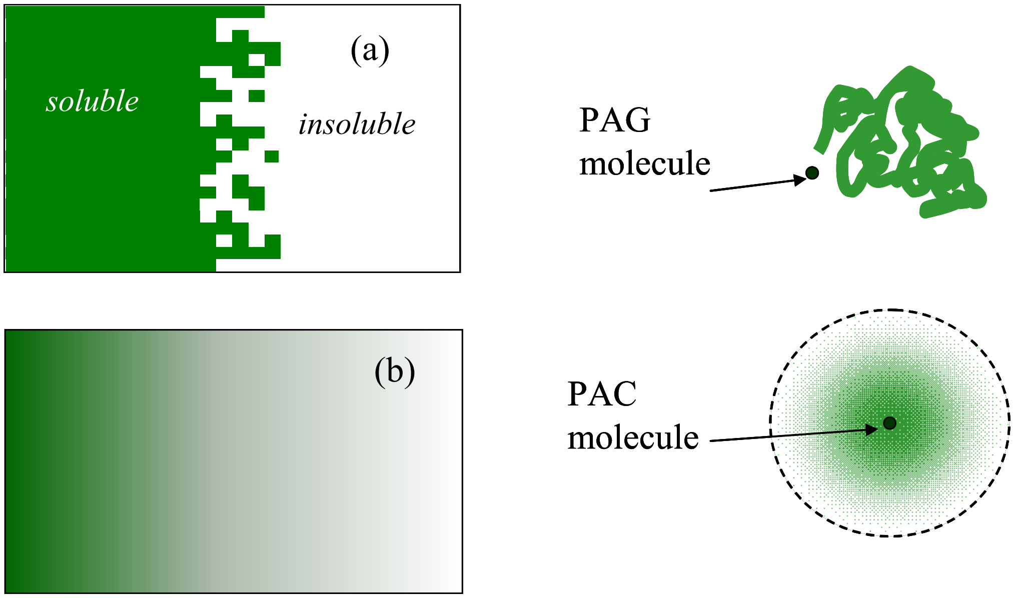

Figure 8.16 Illustration of a feature edge in both a (a) chemically amplified and (b) non chemically amplified photoresist. A PAG molecule leaves a tortuous path of soluble areas, creating a rough sidewall. However, a PAC molecule possibly creates a smooth gradient in resin pKa and dissolution rate, which would result in a smoother sidewall.

by a factor of ~3. Second, Chambers *et al.* are considering the use of hybrid CA-NCA photoresists.[22] That is, the dissolution inhibitors (usually the photoactive components) will be designed to undergo a solubility switch by an acid catalyzed reaction, and not with light. Thus, the exposure step can be used to create a small number of acid catalysts, which then cause a series of solubility switching reactions in a few dissolution inhibitor molecules. The sensitivity of a chemically amplified system is preserved, but the imaging mechanism is that of a non-chemically amplified photoresist. Hopefully, the advantages of both systems will be retained and adequate low levels of sensitivity and LER can be simultaneously achieved. The initial results are encouraging.[22]

8.7 CONCLUSIONS

In this chapter, several theories for line edge roughness formation were discussed. It was reasoned that the statistical nature of acid transport and reaction during PEB had a larger effect upon roughness formation than statistical variations in the dissolution rate of individual polymer chains. Furthermore, it was concluded that roughness increases with increasing molecular weight (and experimental results were found to be in good agreement with simulation results). Roughness was found to decrease with increasing developer concentration, a result which is inconsistent with the current CI lattice model and other literature results.

Exposure dose (photogenerated acid concentration) was found to have a large effect upon bulk surface roughness formation in CA photoresists, which is consistent with literature results. However, exposure dose was found to not have any effect upon the roughness formation in a NCA photoresist. It is envisioned that hybrid, 157 nm CA-NCA photoresists may have improved LER and sensitivity, along with extremely high resolution.

8.8 REFERENCES

1) *International Roadmap for Semiconductors, available at: http://public.itrs.net/Files/2002Update/2001ITRS/Home.htm* **2001**.

2) Lin, Q.; Goldfarb, D. L.; Angelopoulos, M.; Sriram, S. R.; Moore, J. S. *Proc SPIE* **2001**, *4345*, 78.

3) Lin, Q.; Sooriyakumaran, R.; Huang, W.-S. *Proc SPIE* **2000**, *3999*, 230.

4) Houle, F. A.; Hinsberg, W. D.; Sanchez, I. C. *Macromolecules* **2002**, *35*, 8591-8600.

5) He, D.; Cerrina, F. *J. Vac. Sci. & Tech. B* **1998**, *16*, 3748.

6) Flanagin, L. W.; Singh, V. K.; Willson, C. G. *J. Vac. Sci. Technol. B* **1999**, *17*, 1371-1379.

7) Yoshimura, T.; Shiraishi, H.; Yamamoto, J.; Okazaki, S. *Appl. Phys. Lett.* **1993**, *63*, 764-766.

8) Somervell, M.; Fryer, D.; Osborn, B.; Patterson, K.; Byers, J.; Willson, C. G. *J. Vac. Sci. & Tech. B* **2000**, *18*, 2251-2559.

9) Sanchez, M. I.; Hinsberg, W. D.; Houle, F. A.; Hoffnagle, J. A.; Ito, H.; Nguyen, C. *Proc SPIE* **1999**, *3678*, 160.

10) Reynolds, G.; Taylor, J. *J. Vac. Sci. & Tech. B* **1999**, *17*.

11) Mahorwala, A. P.; Goldfarb, D. L.; Petrillo, K. E.; Pfeiffer, D.; Babich, K.; Angelopoulos, M.; Gallatin, G.; Lawson, M. C.; Kwong, R. W.; Chen, K.; Li, W.; Varanasi, P. R. *Proc SPIE* **2003**.

12) Cao, H.; Roberts, J. M.; Meagley, R. P.; Panning, E. M.; Dalin, J.; Chandok, M.; Holl, S. M.; Shell, M. K. *Proc SPIE* **2003**.

13) Hinsberg, W. D.; Houle, F. A.; Sanchez, M. I.; Hoffnagle, J. A.; Wallraff, G. M.; Medeiros, D. M. *Proc SPIE* **2003**.

14) Rice, B. J.; Cao, H.; Chandok, M.; Meagley, R. P. *Proc SPIE* **2003**.

15) Hinsberg, W. D.; Houle, F. A.; Sanchez, M. I.; Wallraff, G. M. *Ibm Journal of Research and Development* **2001**, *45*, 667-682.

16) Hinsberg, W. D.; Houle, F. A.; Poliskie, G. M.; Pearson, D.; Sanchez, M. I.; Ito, H. *Journal of Physical Chemistry A* **2002**, *106*, 9776-9787.

17) Houle, F. A.; Hinsberg, W. D.; Morrison, M.; Sanchez, M. I.; Wallraff, G. M.; Larson, C. E.; Hoffnagle, J. *J. Vac. Sci. & Tech. B* **2000**, *18*, 1874.

18) Schmid, G. M.; M.S., S.; Singh, V. K.; Willson, C. G. *J. Vac. Sci. & Tech. B* **2002**, *20*, 185-190.

19) Thompson, L. F.; Willson, C. G.; Bowden, M. J. *Introduction to Microlithography*; 2nd ed.; American Chemical Society: Washington D.C., 1994.

20) Stewart, M.; Goldfarb, D. L.; Schmid, G. M.; Angelopoulos, M.; Willson, C. G. *Proc SPIE* **2003**.

21) Conley, W.; Miller, D. A.; Chambers, C. R.; Osborn, B. P.; Hung, R. J.; Tran, H. V.; Trinque, B. C.; Pinnow, M. J.; Chiba, T.; MacDonald, S.; Zimmerman, P.; Dammel, R.; Romano, A. R.; Willson, C. G. *Proc SPIE* **2002**, *4690*, 69-75.

22) Chambers, C. R.; Kusumoto, S.; Lee, G. S.; Vasudev, A.; Walthal, L.; Osborn, B.; Zimmerman, P.; Conley, W. *Proc SPIE* **2003**.

23) Dammel, R. *Diazonapthoquinone-based Resists*; SPIE Optical Engineering Press: Bellingham, Washington, 1993.

CHAPTER 9: CONCLUSIONS AND FUTURE WORK

9.1 THE CRITICAL IONIZATION MODEL - CONCLUSIONS

The CI dissolution model has now been used in many forms, with increasing levels of success. It has successfully explained experimentally observed trends such as the increase (and decrease) in dissolution rate with added salts, the decrease in dissolution rate with molecular weight, the increase in dissolution rate with increasing developer concentration, and many others.[1-10] In a parallel work, it has been included with lattice simulations of other lithography steps as a part of a full scale, lithographic simulation tool.[11]

In this work, the model was improved by considering Coulombic forces. These were incorporated in the model by solving the Poisson-Boltzmann equation and combining the results with previously derived equations to determine the fraction of ionized surface sites (α) as a function of polymer pKa and aqueous base developer concentration. This continuum approach was disregarded in favor of a stochastic approach, because the assumptions of a flat profile and infinitely small ions were not valid with the continuum model. In this work, a simple excluded volume, stochastic approach was used to model developer ions. In a parallel work, a rigorous stochastic analysis (in which excluded volume and Coulombic forces were considered) was used in combination with the CI model to simulate photoresist dissolution. Initial results of this model have been presented, and additional results are forthcoming.[3]

9.2 SURFACE RATE INHIBITION – CONCLUSIONS

Several theories were tested in an attempt to explain the surface rate inhibition that is observed during dissolution of novolac resin. The first set of theories involved concentration gradients of resist components throughout the thickness of the film. An experiment termed the "Halt-Development" technique was used to separate and analyze individual layers of a resist film. The results of these experiments indicated that no significant concentration gradients of residual casting solvent, polymer density, PAC, or low molecular weight polymer species were present in the novolac films that were studied. It was therefore concluded that a concentration gradient in photoresist components was not responsible for observed surface rate inhibition.

Several other theories were tested for surface inhibition including surface roughness effects, surface oxidation, an auto enhancement theory, a gel layer theory, *etc*. These theories alone did not account for the observed surface inhibition in the novolac polymer studied. For example, roughness effects could explain novolac surface inhibition, but similar roughness effects are apparent in many films that do not exhibit surface inhibition during dissolution. In the novolac system studied, a significant interfacial layer was not observed by interferometry or ellipsometry, so this was also ruled out as the cause of surface inhibition in this system, although the results of other polymer films vary.[4,12]

The best explanation for surface inhibition was a combination of pKa and roughness effects. The CI lattice model, through a combination of roughness and structure-property relationships, qualitatively describes the common observation that novolac films dissolve faster and with observable surface inhibition, whereas PHOST films generally dissolve slower and do not exhibit surface inhibition.[10]

9.3 SURFACE AND LINE EDGE ROUGHNESS – CONCLUSIONS

AFM experiments were performed on partially dissolved films and the results of these experiments indicate that surface roughness increased with increasing molecular weight, and decreased with increasing developer concentration. The former result was in excellent agreement with CI lattice model predictions, whereas the latter result was not predicted by the CI model. Also, surface roughness was measured as a function of residual film thickness (dissolution time) for phenolic polymers and it was demonstrated that roughness increased and then plateaued to a bulk value. This observation is consistent with studies of other polymer systems. Also, surface roughness was measured as a function of exposure dose for both a chemically amplified and non-chemically amplified photoresist. It was found that surface roughness was not a function of exposure dose for a non-chemically amplified photoresist, but this should be considered a preliminary result.

9.4 FUTURE WORK

9.4.1 The CI Dissolution Model – Future Work

Although many hours have been expended to determine the critical ionization fraction, f_{crit}, a clear experimental determination of this parameter remains elusive. It is clear that f_{crit} varies for different polymer systems. For example, it is apparently lower for 193 nm photoresist resins, in which much larger blocking fractions are used in practical photoresists. This can be understood in terms of the discussion provided in Section 2.5, but experimental verification of this idea would be preferable, both in terms of understanding the dissolution process and in determining an input parameter to the model. It is envisioned that the CI model is extendable to 193 and 157 nm photoresists, but this assumption has not been rigorously tested.

9.4.2 Line Edge Roughness – Future Work

From a materials perspective, line edge roughness (LER) is one of the most important problems to solve for next generation patterning technologies. Despite a substantial amount of initial research, there is no clear agreement about the fundamental mechanisms that contribute to line edge roughness and no clear solutions to minimize LER. It is generally agreed upon that there is a trade-off between resist sensitivity (throughput) and LER,[11,13-15] but both resist properties need to be improved for next generation photoresists.

In this work, preliminary data suggests that a non chemically amplified photoresist platform may have advantages over a chemically amplified platform in minimizing line edge roughness. However, much future work needs to be done in this area. Some of this work is ongoing, as chemists in our research group synthesize functional dissolution inhibitors for 157 nm lithography, for hybrid CA-NCA photoresists.[16,17] As resist formulations and processing conditions are optimized, it may be possible to also optimize these systems for minimum LER formation.

However, many questions remain about the fundamental interactions of these dissolution inhibitors with the polymer resin, the impact of these interactions on line edge roughness, as well as the feasibility of these types of photoresists for low resolution, high throughput imaging. As a start, it would be useful to repeat the AFM, NCA resist experiments on a functional 157 nm photoresist to determine if the same trends were applicable to both systems. The number of potential material combinations to study is almost limitless.

9.4.3 Immersion Lithography – Future Work

Interest has recently increased in using immersion lithography to extend the resolution capabilities of current optical lithography technologies.[18,19] This process involves immersing a photoresist during exposure in a transparent fluid with a high index of refraction. Recall the Rayleigh criterion, equation 1.1:

$$R = k\frac{\lambda}{NA} = k\frac{\lambda}{n\sin\vartheta} \qquad (9.1)$$

where the numerical aperture (NA) is defined as $n\sin\theta$, where n is the index of refraction of the ambient medium between the photoresist and the optical lens element. By increasing the index of refraction, the resolution can be decreased without decreasing the exposure wavelength. Using water as the ambient medium at 193 nm (n~1.43), a significant increase in resolution can be obtained. There are many engineering challenges to implementing this technique, such as elimination of bubbles through the exposure medium, the liquid dispense, scanning, and recovery, as well as controlling the index of refraction with subtle temperature changes that occur during exposure.

From a materials perspective, immersing the photoresist in a fluid during exposure could have adverse consequences to the imaging process. For example, significant water sorption could plasticize the film, leading to transport of important resist additives out of the photoresist film, which could cause a change in processing conditions or complete image failure. One approach to characterizing this problem is to measure the amount of water sorption during immersion for a particular photoresist. One method for making this measurement is by ellipsometry, using the dissolution cell discussed in Chapter 7. The change in index of refraction upon water immersion can be easily determined, and a simple linear effective medium approximation has been used to estimate the amount of water sorption in a few photoresist materials. This technique may be useful in determining which photoresist materials would be likely candidates for immersion lithography photoresists.

Furthermore, the optical constants of a photoresist film must be known in order to properly simulate the exposure step. Because the optical constants will change slightly during fluid immersion, it is useful to have a technique to characterize this process. This is also an area in which the dissolution cell/ellipsometer may prove useful in characterizing immersion lithography photoresists.

9.5 UNEXPLAINED PHENOMENA

9.5.1 Thin Film Dissolution Effects

During the course of this investigation, some dissolution phenomena were encountered that have not been easily explained with simple models. For example, using the ellipsometer as a dissolution rate monitor, it has been possible to measure the dissolution rate of ultrathin films (< 50 nm). Films of novolac varying only in initial thickness (by varying the solvent composition, not spin speed) have been found to dissolve at varying rates. Specifically, thin films (<130 nm) have been found to dissolve much slower than bulk films.[20] One other literature study has been done on polymer resins that are based on an ESCAP type resin, with opposite results.[21] In this case, the dissolution rate of thin films increases with decreasing thickness. This change in dissolution rate with decreasing thickness may be related to the changes in thermal properties that are known to occur with decreasing polymer film thickness. However, this correlation has yet to be determined, and the fundamental reasons for changes in thermal properties are the topic of much debate. Now that ellipsometry has been demonstrated as a dissolution rate monitoring technique, it is possible to study thin film dissolution behavior of a variety of polymer resins, and to relate this behavior to changes in thermal properties of thin films.

9.5.2 Added Salt Effects

In chapter 2, Figure 2.3 shows the effect of added salts upon the dissolution rate of G2 novolac resin for both NaOH-NaCl, and TMAH-TMACl developer solutions. This figure has been reproduced as Figure 9.1. In each case, the hydroxide concentration has been held constant, and the concentration of chloride salts has been altered. In each case, the dissolution rate initially increases with increasing salt concentration, reaches a maximum, and then decreases with increasing salt concentration. However, the interesting feature of this plot is that the peak position is shifted by a salt concentration of ~ 2 M. All of the group I hydroxides and chloride salts show a peak at ~ 0.8 M, and several quaternary ammonium hydroxides and salts have been tested, all showing a peak at ~ 3 M. The details of these experiments are discussed in more detail in

Appendix B, along with possible explanations of the peak shift. A clear explanation for the peak shift has not yet been determined.

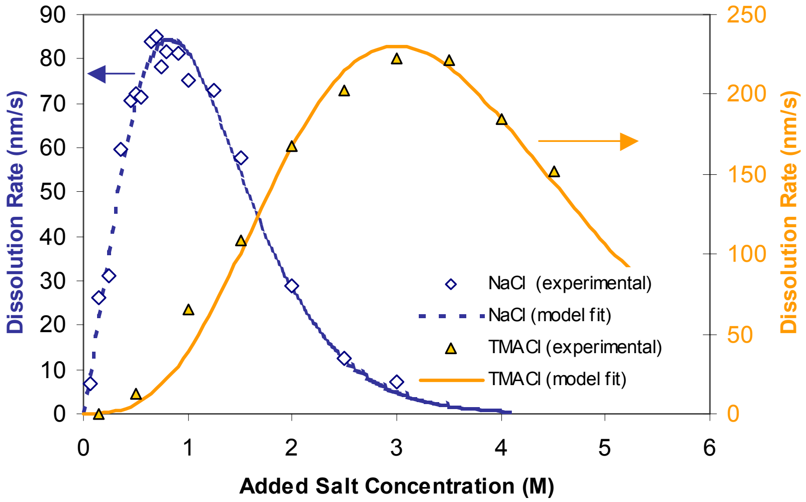

Figure 9.1 Dissolution rate of a novolac resin as a function of added chloride concentration for NaOH-NaCl and TMAH-TMACl solutions.

9.5.3 Other Unexplained Phenomena

Appendix C discusses two experiments that also do not have clear explanations. One is the change in developer flow rate with dissolution rate, and the other is poisoning of aqueous base developer with TMAH.

9.6 REFERENCES

(1) Tsiartas, P. C. *Ph. D. Thesis, The University of Texas at Austin* **1998**.

(2) Tsiartas, P. C.; Flanagin, L. W.; Henderson, C. L.; Hinsberg, W. D.; Sanchez, I. C.; Bonnecaze, R. T.; Willson, C. G. *Macromolecules* **1997**, *30*, 4656-4664.

(3) Schmid, G. M.; Burns, S. D.; Tsiartas, P. C.; Willson, C. G. *Journal of Vacuum Science & Technology B* **2002**, *20*, 2913.

(4) Houle, F. A.; Hinsberg, W. D.; Sanchez, M. I. *Macromolecules* **2002**, *35*, 8591-8600.

(5) Flanagin, L. W. *Ph.D. Dissertation, University of Texas at Austin*, 1999.

(6) Flanagin, L. W.; Singh, V. K.; Willson, C. G. *Journal of Vacuum Science & Technology B* **1999**, *17*, 1371-1379.

(7) Flanagin, L. W.; Singh, V. K.; Willson, C. G. *Journal of Polymer Science Part B-Polymer Physics* **1999**, *37*, 2103-2113.

(8) Flanagin, L. W.; McAdams, C. L.; Hinsberg, W. D.; Sanchez, I. C.; Willson, C. G. *Abstracts of Papers of the American Chemical Society* **1999**, *218*, 112-PMSE.

(9) Burns, S. D.; Schmid, G. M.; Tsiartas, P. C.; Willson, C. G.; Flanagin, L. *Journal of Vacuum Science & Technology B* **2002**, *20*, 537-543.

(10) Burns, S. D.; Gardiner, A. B.; Lutkenhaus, J.; Krukonis, V. J.; Wetmore, P. M.; Schmid, G. M.; Willson, C. G. *Proc SPIE* **2001**, *4345*, 37.

(11) Schmid, G. M.; M.S., S.; Singh, V. K.; Willson, C. G. *J. Vac. Sci. & Tech. B* **2002**, *20*, 185-190.

(12) Hinsberg, W. D., et. al. *Presented at EIPBN, 2002; private communications with Dr. W.D. Hinsberg* **August, 2002**.

(13) Cao, H.; Roberts, J. M.; Meagley, R. P.; Panning, E. M.; Dalin, J.; Chandok, M.; Holl, S. M.; Shell, M. K. *Proc SPIE* **2003**.

(14) Hinsberg, W. D.; Houle, F. A.; Sanchez, M. I.; Hoffnagle, J. A.; Wallraff, G. M.; Medeiros, D. M. *Proc SPIE* **2003**.

(15) Reynolds, G.; Taylor, J. *J. Vac. Sci. & Tech. B* **1999**, *17*.

(16) Chambers, C. R.; Kusumoto, S.; Lee, G. S.; Vasudev, A.; Walthal, L.; Osborn, B.; Zimmerman, P.; Conley, W. *Proc SPIE* **2003**.

(17) Conley, W.; Miller, D. A.; Chambers, C. R.; Osborn, B. P.; Hung, R. J.; Tran, H. V.; Trinque, B. C.; Pinnow, M. J.; Chiba, T.; MacDonald, S.; Zimmerman, P.; Dammel, R.; Romano, A. R.; Willson, C. G. *Proc SPIE* **2002**, *4690*, 69-75.

(18) Hoffnagle, J.; Hinsberg, W. D.; Sanchez, M. I.; Houle, F. A. *J. Vac. Sci. & Tech. B* **1999**, *17*, 3306.

(19) Switkes, M.; Rothschild, M. *J. Vac. Sci. & Tech. B* **2001**, *19*, 2353.

(20) Burns, S. D.; Schmid, G. M.; Trinque, B. C.; Willson, J.; Taylor, J. C.; Tsiartas, P. C.; Burns, R. L.; Willson, C. G. *Proc SPIE* **2003**.

(21) Robertson, S. A.; Kang, D.; Scheer, S. A.; Brodsky, C. In *Proc. SPIE*, 2002.

APPENDIX A

A.1 DERIVATION OF EQUATION 4.5

The following equation is derived by Israelachvili (p.233) for the total concentration of ions at an isolated surface of charge density σ:

$$\sum_i \rho_{oi} = \sum_i \rho_{\infty i} + \frac{\sigma^2}{2\varepsilon\varepsilon_o kT} \qquad \text{(in numbers per m}^3\text{)} \qquad \text{(A.1)}$$

where *i* is the total number of ions, ρ is the number density of ions, and the subscripts "o" and "∞" indicate the surface and bulk, respectively. ε is the dielectric constant of the medium, ε_o is the permitivity of free space, *k* is Boltzmann's constant, and *T* is absolute temperature. Converting equation A.1 to moles/L:

$$\left[R^+\right]_o + \left[OH^-\right]_o = 2\left[ROH\right]_{BULK} + \frac{\sigma^2}{2\varepsilon\varepsilon_o kT} \times (A_N \times 10^3)^{-1} \qquad \text{(M)} \qquad \text{(A.2)}$$

where A_N is Avogadro's number.

The Boltzmann distribution states that

$$\rho_{oi} = \rho_{\infty i} e^{\frac{-e\varphi_o}{kT}} \qquad \text{(A.3)}$$

Therefore,

$$\left[R^+\right]_o = \left[R^+\right]_\infty e^{\frac{e\psi_o}{kT}}, \quad \left[OH^-\right]_o = \left[OH^-\right]_\infty e^{\frac{-e\psi_o}{kT}} \qquad \text{(A.4)}$$

Rearranging equation A.2 and substituting equation A.4:

$$\sigma^2 = 2\varepsilon\varepsilon_o kTA_N \times 10^3 \left\{ \left[R^+\right]_{BULK} e^{\frac{-e\varphi_o}{kT}} + \left[OH^-\right]_{BULK} e^{\frac{+e\varphi_o}{kT}} - \left[R^+\right]_{BULK} - \left[OH^-\right]_{BULK} \right\} \tag{A.5}$$

Since,

$$\left[R^+\right]_{BULK} = \left[OH^-\right]_{BULK} = \left[ROH\right]_{BULK} \tag{A.6}$$

It follows that

$$\sigma^2 = 2\varepsilon\varepsilon_o kTA_N \times 10^3 \left[ROH\right]_{BULK} \left\{ e^{\frac{-e\varphi_o}{kT}} + e^{\frac{e\varphi_o}{kT}} - 2 \right\} \tag{A.7}$$

Recognizing that

$$\sinh^2 x = \left(\frac{e^x - e^{-x}}{x} \right)^2 = \frac{e^{2x} - e^{-2x} - 2}{4} \tag{A.8}$$

Then:

$$\sigma^2 = 8\varepsilon\varepsilon_o kTA_N \times 10^3 \left[NaOH\right] \sinh^2 \left(\frac{e\varphi_o}{2kT} \right) \tag{A.9}$$

Rearranging terms gives

$$\varphi_o = \frac{2kT}{e} \sinh^{-1} \left(\frac{\sigma^2}{\varepsilon\varepsilon_o kT\left[ROH\right] \times A_N \times 10^3} \right) \tag{A.10}$$

If the above analysis is done considering an inert electrolyte, AS (for added salt):

$$\varphi_o = \frac{2kT}{e} \sinh^{-1} \left(\frac{\sigma^2}{\varepsilon\varepsilon_o kT \left\{ \left[ROH\right] + \left[AS\right] \right\} \times A_N \times 10^3} \right) \tag{A.11}$$

APPENDIX B: VARIATION IN DISSOLUTION RATE WITH ADDED SALTS

B.1 INTRODUCTION

It has been previously observed that the dissolution rate of phenolic polymers changes significantly if salts are added to the aqueous base developer solution. These studies have been performed primarily with group I cations and their chloride salts by Tsiartas[1] and Henderson.[2] The results of these studies were that the dissolution rate could be described by relating the dissolution rate to the fraction of ionized surface sites (Equation 2), invoking a common model for the activity of strong electrolytes (Equation 3).[3,4]

$$\frac{\left[A^-\right]}{\left[HA\right]} = \frac{K\left[OH^-\right]\gamma_{OH^-}}{\gamma_{A^-}} = k \cdot 10^{Ac^{1/3}-Bc} = R \qquad \text{(B.1)}$$

$$\log \gamma_{\pm} = -Ac^{1/3} + Bc \qquad \text{(B.2)}$$

Few experiments have been performed with tetramethylammonium hydroxide or other quaternary ammonium developers. Henderson has performed a limited number of experiments, in which it was evident that this class of developers showed a significant peak shift with added salts (Figure 9.1). The peak in the dissolution rate versus added salt curve was shifted by more than 2 M from group I hydroxides to quarternary ammonium hydroxides. The goal of this work was to characterize the effect of added salts of this common class of developers on phenolic polymers, in order to lend insight to the fundamental mechanism of dissolution.

B.2 EXPERIMENTAL

The polymer used for these experiments was novolac G2 resin from Shipley Co. dissolved in PGMEA at 10 wt %. The solution was spin coated on silicon wafer chips at 2500 rpm for 30s, and the post apply bake was 90°C for 90 s, resulting in a film thickness of ~ 1μm. The developers used were TMAH, ETMAH, and TEAH in which the corresponding chloride salts (TMACl, ETMACl and TEACl) were added in various concentrations up to ~ 4.5 M. The hydroxide concentration was adjusted from developer to developer, in order to maintain measurable dissolution rates. The dissolution rates of the films were measured by multiwavelength interferometry in puddle development mode.

B.3 RESULTS

The results of these experiments are shown in Figure B.1. Initially, the dissolution rate increases with increasing salt concentration, but then reaches a maximum near 3 N, after which the dissolution rate decreases with increasing salt concentration. The trend is very similar to the group I hydroxides and their chloride salts, with the exception that the peak is significantly shifted to the right (by over 2 N). The TMAH-TMACl data obtained in this work very similar to the data obtained by Henderson *et al.*[2]

Table B.1 Added Salt Model Parameters

salt added	[OH-]	k	A	B	Bare cation radius (nm)	Hydrated radius (nm)	Hydration number (+/- 1)
LiCl	0.07	0.5628	3.869	1.703	0.068	0.38	5 or 6
NaCl	0.07	0.3236	3.869	1.47	0.095	0.36	4 or 5
KCl	0.07	0.2359	3.869	1.483	0.133	0.33	3 or 4
RbCl	0.07	0.0904	3.869	1.474	-	0.33	2 or 3
TMACl	0.14	0.0001881	6.333	1.014	0.347	0.37	0
ETMACl	0.14	0.000136	6.333	1.027	-	-	0
TEACl	0.3	0.0001312	6.333	1	-	-	0

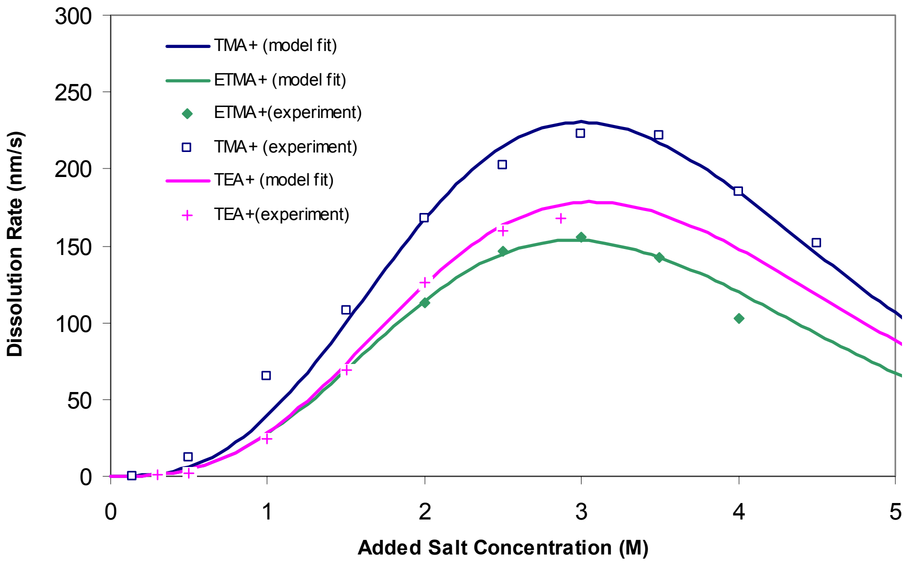

Figure B.1 Dissolution Rate versus concentration of quarternary ammonium added salts

Also shown in Figure B.1 are the model fits to the data, using equation (B.1), and allowing *A*, *B*, and *k* to vary. However, the parameter *A* is held constant for the family of curves. Note that the model fits are quite adequate, and that the CI model was once again successful at explaining a wide range of added salt curves. However, the parameters have changed significantly from the group I study. To gain insight into these changes (into why the peak shifts by ~ 2M), we review the group I study and reinvestigate the fundamental origins of equation (B.2) from Bahe's analysis.[3,4]

In the group I study, A was held constant at 3.89 for all the model fits, as the value of A should not change unless the charge on the cation changes. While *A* has a theoretical value of 0.289 for 1:1 electrolytes, and 0.641 for 2:1 electrolytes, the solutions under study are mixtures of salt, hydroxide, and polyions, so *A* was expected to be a different value. Since the quarternary ammonium cations all have a charge of $^{+}1$, one might expect that the value of *A* should be identical to the group I metals. However, the best-fit value of A is 6.33 (a factor of 1.6 larger than that for the group I cations). Note that change of the value of *A* represents the peak shift between the two developer families. The parameter *k* is simply a scaling factor, and the *B* parameter is much more empirical, and has not changed significantly. If one can understand the fundamental reason that value of *A* is changing, one can completely understand

Figures B.1 and 9.1, and probably gain useful insight into the dissolution mechanism with the industry's most common developer, TMAH.

The *A* parameter can be theoretically determined based on known information about the electrolyte soluton:[3,4]

$$A = \frac{A''\mathrm{z}_+\mathrm{z}_- N^{\frac{4}{3}} a_{A''}}{23\upsilon RTk} \tag{B.3}$$

where z_+ is the charge on the cation, z_- is the charge on the anion, *N* is Avogadro's number, υ_+ and υ_- ($\upsilon_+ + \upsilon_- = \upsilon$) are the number of positive and negative ions, respectively; *R* is the gas constant, *T* is the temperature, *k* is Boltzmann's constant, $a_{A''}$ is a value found from the particular structure under consideration and *A"* is given by:

$$A'' = \frac{\nu_+}{2}\left(\sum_{j+} \frac{1}{a_{j+'}}\right) + \frac{\nu_-}{2}\left(\sum_{j-} \frac{1}{a_{j-'}}\right) \tag{B.4}$$

where a_j is the distance between the central ion (arbitrarily chosen) and the *j*th ion. a_j has been normalized by the unit distance *R*, and has no units.

In equation (B.3) and (B.4), the only variables are z_+, z_-, and $a_{A''}$. The number of ions in solution, υ, is not expected to change from NaCl to TMACl, since it should remain constant for a given concentration. Similarly, a_j should not change, since the value is normalized to the unit distance between atoms. Thus *A''* should remain constant. The other values are all universal or experimental constants. The main variables to consider are the charge on the ions (z_+, z_-), and the structural differences of the "lattice" formed by the concentrated electrolyte solutions ($a_{A''}$). First, we must define the parameter $a_{A''}$.

Unfortunately, $a_{A''}$ is not defined well by Bahe. Bahe defines R to be the shortest distance between cation and anion, where:

$$R^{-1} = a_{A''}\left(\frac{N}{1000}\right)^{\frac{1}{3}}(c)^{\frac{1}{3}} \tag{B.5}$$

and the other variables have been previously defined. Bahe then gives an example of how to determine $a_{A''}$ for a particular structure. The structure he chose is a fluorite lattice, which is common for 2:1 electrolytes and is shown in Figure 6. Bahe states that "in this case, $R^{-1}= (2/3^{1/2})(2Nc/1000)^{1/3}$ and therefore $a_{A''}$…has the value $(2/3^{1/2})(2)^{1/3}$." Note the factor of 2 that has been introduced…it represents a correction factor for the number of different ions in solution. For example, 1 M NaCl represents 1 mol of Na^+ and 1 mol of Cl^- ions, for a total of 2 moles of ions per liter of solution. But how does the factor of $(2/3^{1/2})$ arise? If one examines the fluorite lattice structure shown below and defines d to be the distance of the nearest cation and anion and U to be the distance of the unit cell, then by geometric arguments it can be shown:

$$\frac{d}{U} = \frac{\sqrt{3}}{2} \Rightarrow a_{A''} = \frac{U}{d}(2)^{\frac{1}{3}} \tag{B.6}$$

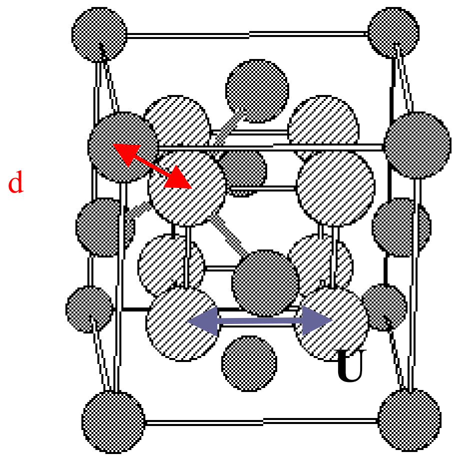

Figure B.2 Fluorite lattice structure that is common for 2:1 electrolytes

Table B.2 Values of a_A" for common lattice structures

Lattice Structure	$a_{A''}$
BCC	0.7274
FCC	1.78
Fluorite	1.4548
Halite (NaCl)	1.26

With the definition of $a_{A''}$ in Equation (B.6), $a_{A''}$ can be calculated for any lattice structure of interest. Table II shows the value of $a_{A''}$ calculated for four common lattice structures. The purpose of these calculations is to determine the extent that $a_{A''}$ will change with common structures, and to determine if these values may account for the difference in the *A* parameter for group I cations

(3.833) and quaternary ammonium cations (6.33). Thus, $a_{A''}$ would have to change by a factor of 1.6 to account for the peak shift observed in Figure 4. From Table II, the largest factor change is from FCC to BCC (a factor of 2.5). However, the crystalline structure of NaCl is a Halite structure with an $a_{A''}$ value of 1.26 and the FCC lattice is only a factor of 1.4 times as large. But, this is close to the value of 1.6 needed to explain the peak shift, and it also does not represent the structure of NaCl in an aqueous solution…it's possible that the structures in solution are significantly different. Another approach would be to measure the dissolution rate with added $CaCl_2$ in $Ca(OH)_2$. The added salt experiment has never been attempted with a 2:1 electrolyte. The structure is different than that of 1:1 electrolytes, and the change in the A parameter should be predictable. This will provide some empirical data indicating whether the structure factor is responsible for the peak shift observed in Figure 9.1.

The other explanation is that the quaternary ammonium hydroxides produce a different number of charges on the dissolved polymer, which would also account for a change in the value of A (by changing z_-). This is suggesting that the value of f_{crit} is different for TMAH than for NaOH, and unfortunately brings us back to the question of "How do we measure f_{crit}?" With no clear way to do this, we instead decided to change the molecular weight of the polymer…assuming that the fraction of ionized sites would remain constant and the charge per ion would change. If the theory is correct, a peak shift would be evident in the dissolution rate curve. For this study, KOH and KCl were used because the 'natural' peak occurs at ~1M, and this range of concentrations is more convenient. Also, KOH/KCl is the simplest experiment, and the resin had never been varied in previous work. Initially, PHS from Nippon Soda was used as the resin because a wide range of molecular weight was available (3k-30k) with a similar polydispersity (~1.0) and the samples were synthesized in the same manner.

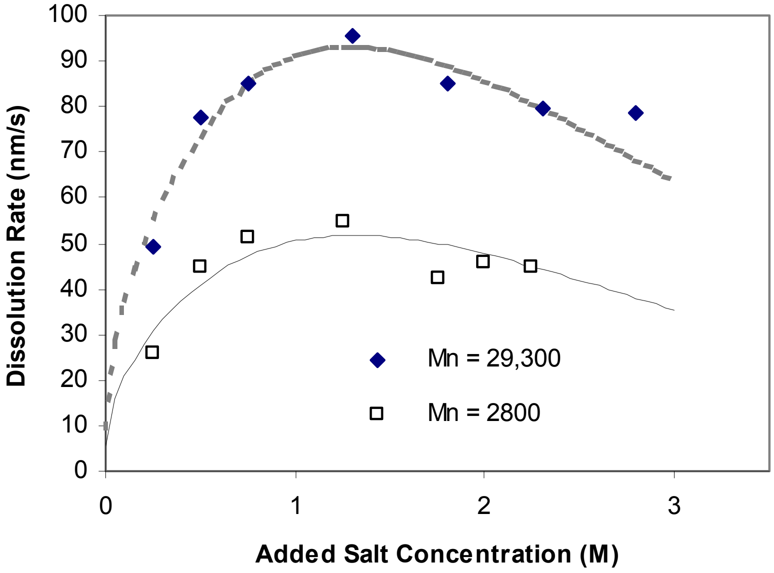

Figure B.3 Dissolution rate versus added K^+ concentration for KOH/KCl developer and PHS resin of varying molecular weight. No peak shift is observed.

Table B.3 Model parameters for added salt experiments with PHS resins of varying molecular weight.

	PHS, Mn=2800	PHS, Mn=29300
k	5.36	9.643
A	1.3502	1.3502
B	0.376	0.376

The PHS resins were dissolved in PGMEA at a given weight percent to yield a 1μm film after spin coating at 2500 rpm for 30s and a 90°C, 90s PAB. The base hydroxide concentration was varied such that the dissolution rates would fall in a measurable range. (It was not possible to investigate such a large range of molecular weight with the same hydroxide concentration.) It has been previously shown that adjusting the hydroxide concentration changes only the scale of the curve (the k parameter) and does not affect the peak position.[5] The results of the PHS resin with KOH/KCl developer are shown in Figure B.3. The model fits are shown, and the model parameters are shown in Table B.3. For both curves, the peak occurs at ~ 1.3 M. The curves are adequately fit with the CI model (Equation B.1) with the same *A* and *B* parameters. The k parameter is only a scaling factor, and is expected to change. By adjusting the hydroxide concentration, it would be possible to obtain identical *k* parameters for both curves. This experiment indicates that the length of the polymer (and hence, the charge on the polymer) does not change the A parameter or shift the peak in the dissolution curve (for PHOST).

Another interesting result is that the overall shape of the curve for PHS is different from that of novolac, and the *A* and *B* parameters are correspondingly different. At this time the reasons for this change are unknown, but we note that the model (Equation B.1) still provides a good fit to the data. We attempted the experiment with varying molecular weight novolac, but the experiments were were not practical due to adhesion problems.

Ralph Dammel recently suggested that the hydration number of the ions (5 or 6 for Li^+, 0 for TMA^+) might explain the peak shift observed in Figure 9.1. The theory is that the effective concentration is changed, and that if the hydration number is accounted for, the curves would overlap. However, correction for the hydration number results in only a minor shift in the curve, and cannot be the sole cause of the observed peak shift.

B.4 REFERENCES

(1) Tsiartas, P. C.; Flanagin, L. W.; Henderson, C. L.; Hinsberg, W. D.; Sanchez, I. C.; Bonnecaze, R. T.; Willson, C. G. *Macromolecules* **1997**, *30*, 4656-4664.

(2) Henderson, C. L., et al. *Proc. SPIE* **1996**, *2724*, 481.

(3) Bahe, L. W. *J. Am. Chem. Soc.* **1975**, *97*, 5664-5670.

(4) Bahe, L. W. *J. Phys. Chem.* **1972**, *76*, 1062-1071.

(5) Tsiartas, P. C. *Ph. D. Thesis, The University of Texas at Austin* **1998**.

APPENDIX C: UNEXPLAINED DISSOLUTION PHENOMENA

C.1 POISONING OF DEVELOPER SOLUTIONS (MIXING KOH AND TMAH)

C.1.1 Introduction

It has been anecdotally observed that the addition of small amounts of tetramethylammonium hydroxide (TMAH) to common group I metal hydroxides drastically reduces the dissolution rate of novolac polymers in the mixed aqueous base solution. This phenomenon has not been quantified, and few explanations exist as to the mechanism by which it occurs. Our goal was to quantify this phenomenon by measuring the dissolution rate of common phenolic resins in mixtures of TMAH and other group I hydroxides, and possibly to gain insight into the reason(s) for this behavior.

C.1.2 Experimental

G2 novolac resin from Shipley Co. was dissolved in PGMEA at 10 wt %. The solution was spun onto bare silicon wafers at 2500 rpm for 30s, and the post apply bake was 90°C for 90s, resulting in a film thickness of ~1μm. The developers used were mixtures of KOH, NaOH, TMAH, and TEAH. Solutions were prepared of 0.2 M hydroxide for the novolac experiment, and 0.13 N for the PHOST experiment. The cation concentration was varied from 100% group I metal to 100% TMAH or TEAH. The dissolution rate was measured by multiwavelength interferometry, in puddle development mode.

C.1.3 Results and Discussion

The results of these experiments are shown in Figures C.1-C.3. At 100 % KOH, the dissolution rate of the novolac resin is ~100 nm/s, while at 100% TMAH, the dissolution rate is ~ 7 nm/s. This is an expected trend, since TMA^+ is a much larger cation than K^+. As the two are mixed, one might expect that the dissolution rate could be predicted by a linear (or close to linear) rule of mixing. However, the anecdotal evidence was observed (Figure C.1). At very small concentrations of TMA^+, the dissolution rate drops dramatically. At 0.01 % (by volume), the dissolution rate drops to a small value that is not measurable. Not surprisingly, the same trend is observed with NaOH (Figure C.2). Figure C.3 shows the effect of mixing TMAH with TEAH. Surprisingly, the same trend is observed – TMAH also "poisons" TEAH!

Clearly, a small amount of TMAH interacts with novolac in such a way as to render the resin insoluble in aqueous base. Previous work by Garza *et al.*[1], Honda *et al.*,[2-4] and Dammel *et al.*[5] have suggested that a stable complex of TMAH forms with novolac that is insoluble in aqueous base.

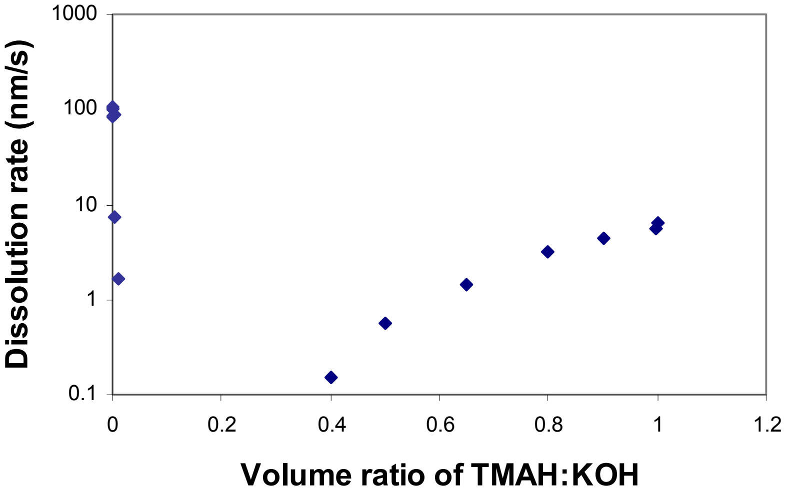

Figure C.1 Dissolution Rate versus the volume fraction of TMAH cation. 0.2 N hydroxide concentration, G2 novolac resin.

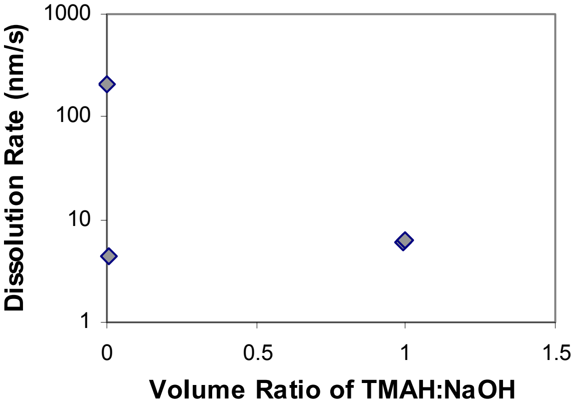

Figure C.2 Dissolution Rate versus volume fraction of TMAH cation. 0.2 N hydroxide concentration, G2 novolac resin.

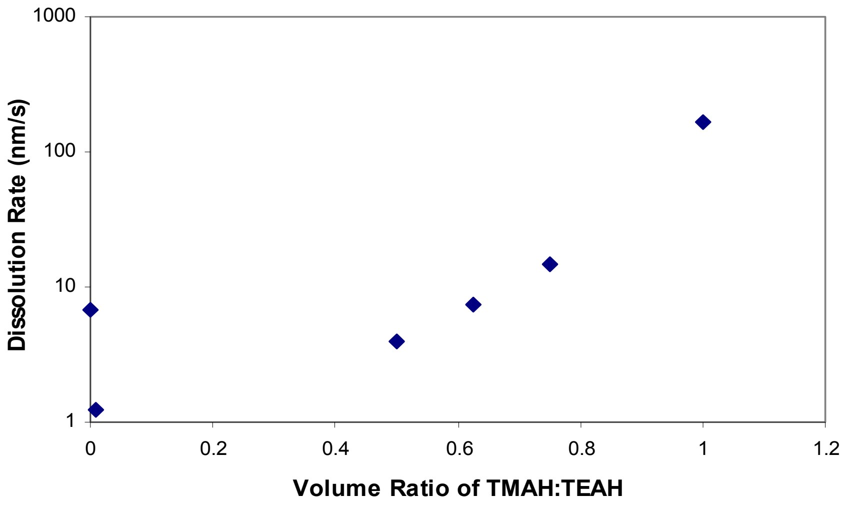

Figure C.3 Dissolution rate versus volume fraction of TMAH cation. 0.26 N hydroxide concentration, G2 novolac resin.

Garza *et al.*[1] report that the dissolution rate of novolac in TMAH decreases with increasing temperature (the opposite trend of metal-ion containing developers). They proposed that the deprotonation reaction of TMAH and novolac occurrs in two steps: first, a stable complex is formed in a very exothermic reaction followed by a rate determining deprotonation step. If the initial formation of the intermediate is sufficiently exothermic, the effective activation energy of the reaction sequence is negative, explaining the decrease in dissolution rate with increasing temperature. This is shown schematically by

Dammel, in which the relative reaction energy is plotted against the reaction coordinate. UV and FTIR spectroscopy evidence of such a complex have been provided by Honda *et al*.[2-4] This evidence may provide insight into the observed poisoning phenomenon, but this trend is still not fully understood.

C.2 VARIATION IN DISSOLUTION RATE WITH DEVELOPER FLOW RATE

A recent paper by Hunek and Cussler[6] examines the mechanism of phenolic polymer dissolution in aqueous base by carefully analyzing the change in dissolution rate with change in flow rate.[9] Their conclusion is that "*The dissolution of low molecular weight phenolic resin is controlled by a combination of solute release and solute mass transfer, without the formation of any significant gel phase*." They suggest that the rate limiting steps are the release of the polymer from the surface, and the subsequent transport of the polyion into the bulk of the solution. The general concept is that if flow rate has an effect on the dissolution rate, then mass transfer must play a role in the overall process. In order to explore this theory, measurements were made of changes in dissolution rate with varying flow rate using a flat plate geometry flow cell. The dissolution rate was measured by a mulitwavelength interferometer.

The resin used for these experiments was G2 novolac resin, dissolved in PGMEA at 15 wt % solids. The solution was filtered and spin coated onto 2" Si wafers at a spin speed of 2500 rpm for 30s. The post apply bake was 90°C for 90s. The wafers were loaded into the flow cell (described previously).[10] The developer used was AZ300 MIF (0.26 N TMAH). The gasket thickness (height of the flow channel) was 1/32 in. A flow controller was used to vary the flow velocity, and was calibrated between 10 and 140 ml/min. One data point (0 ml/min) was run in puddle development mode.

The results of this experiment are shown in Figure C.4. The dissolution rate varies from 35 nm/s at low flow rate to ~50 nm/s at high flow rate. The flow rates were chosen over a range of Reynold's number from 0 to 3.5 x 10^4. The theoretical change from laminar to turbulent flow occurs at Re = 2 x 10^4, although

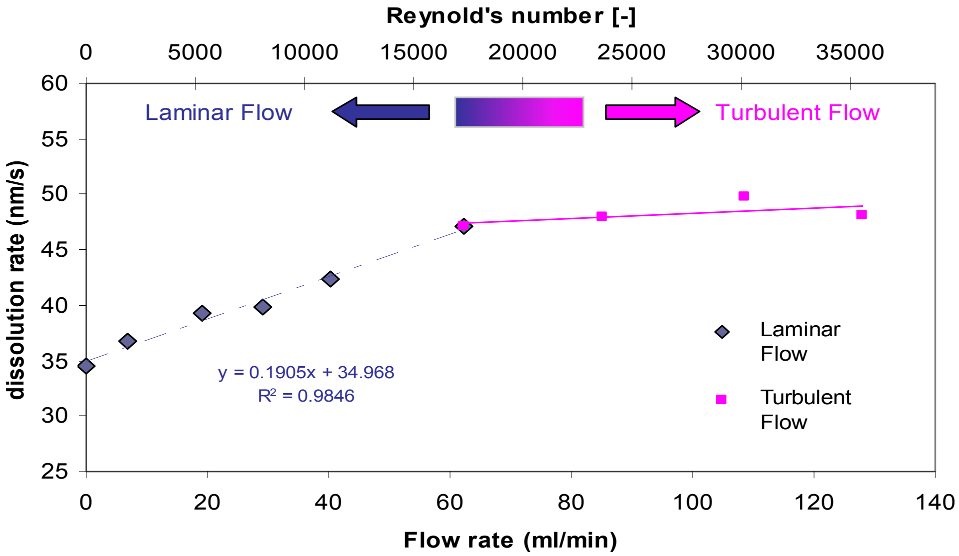

Figure C.4 Dissolution rate of G2 novolac with varying flow rates of 0.26 TMAH developer. The flow cell had a flat-plate geometry.

a range of Re is expected for this transition. In the laminar region, a linear increase in the dissolution rate is observed from 35 - 47 nm/s. At ~Re = 1.7×10^4, the dissolution rate levels off, becoming essentially constant with increase in flow rate and Reynold's number. This transition in slope occurs well within the theoretical prediction of the laminar to turbulent transition. The overall change in dissolution rate from puddle to turbulent flow is only a factor of 1.34. (One implication of this data is that industrial development processes should operate at turbulent flow rates to improve process control of the dissolution step.)

The current form of the CI model does not predict a change in photoresist dissolution rate with varying developer concentration. One possibility is that a LeChatlier mechanism is at work: when the reaction products (ionized polymer chains) are transported away from the interface at a faster rate by convective mass transfer, the reaction equilibrium may shift towards an ionized state, which would thus increase the dissolution rate of the polymer film as described by the CI model. However, it is also possible that the mass transport effects described by Hunek and Cussler also play a role in the dissolution mechanism. These data illustrate the difficulty in finding a single, simple model to describe each and every experimental phenomenon observed during photoresist dissolution.

C.3 DISSOLUTION BEHAVIOR AFTER INTERUPTED DEVELOPMENT

It has been reported that halting (and restarting) resist development results in a new inhibition profile. This observation was tested with 3 simple experiments: halting development of a novolac (Schenectady, Mn=9330, Pd = 4.9) film by quenching with water (with and without nitrogen drying afterwards), and halting development by only nitrogen drying (no water quench). The results of these experiments are shown in Figures C.5 and C.6. A related experiment was also performed. An identical film was prewashed with water to determine if the prewash had the same effect as quenching development with water. The results of this experiment are shown in Figure C.7. In each experiment, the thickness of the film was measured as a function of time with multiwavelength interferometry.

Quenching aqueous base dissolution of a novolac film with water leads to dramatic surface inhibition. In both cases (both the wet and dry experiments), quenching with water caused a very flat induction period for as much 40 seconds, after which the dissolution rate *immediately* returned to the bulk rate. The dissolution profile does not show "typical" surface inhibition, which is characterized by a gradual increase in dissolution rate. Rather, the rate change is abrupt, indicating that a separate mechanism may be causing the inhibition in this case. One theory for this mechanism is that low MW species at the surface have already dissolved, whereas the high MW species have not.[7] When development is halted and restarted, there is an induction period where the high MW species must be reionized and dissolve at a slower rate than the bulk of the film.

Figure C.6 shows the results of the experiment in which development was halted only by blow drying with nitrogen. When development was restarted, there was no inhibition period. The dissolution rate picked immediately where it left off. One hypothesis for this phenomenon is that without a water quench, the ionized sites at the surface remain charged. In order to maintain charge neutrality, some positive TMA^+ ions remain bonded to the resist surface when dissolution is halted. Then, when dissolution is restarted the ionic "salt" of TMA^+ ions and polyanions at the surface continue to dissolve as if the development was not interrupted. However, it still is unknown exactly why the inhibition period is so significant with a water washing.

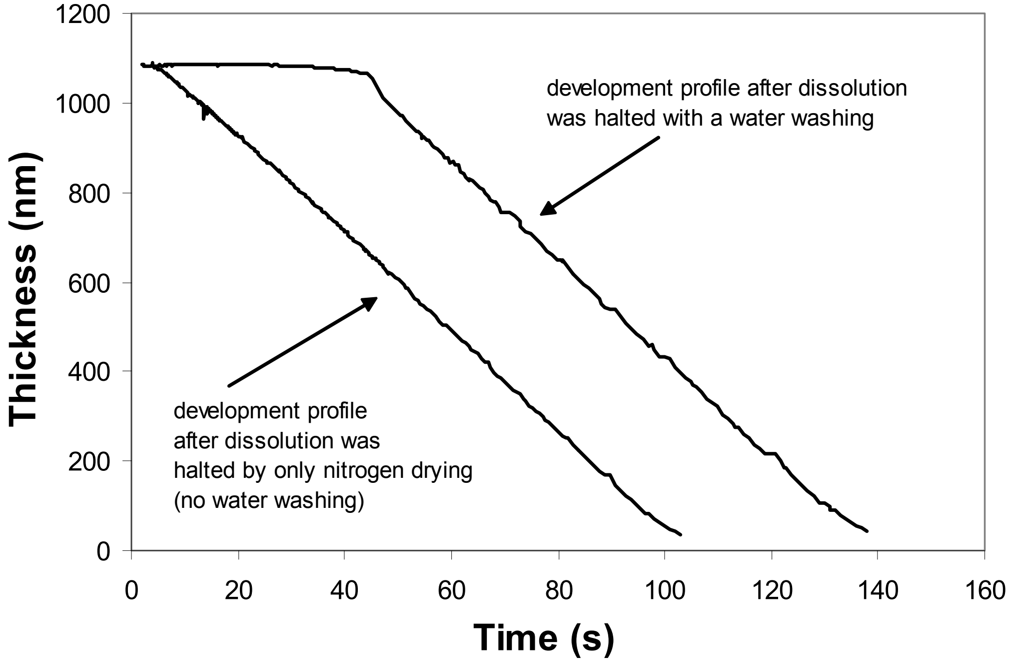

Figure C.5 Dissolution profiles of novolac films that have been partially dissolved. The dissolution was quenched by water washing (and subsequent nitrogen drying) and nitrogen drying only. Significant surface inhibition is observed in the film that was quenched with water.

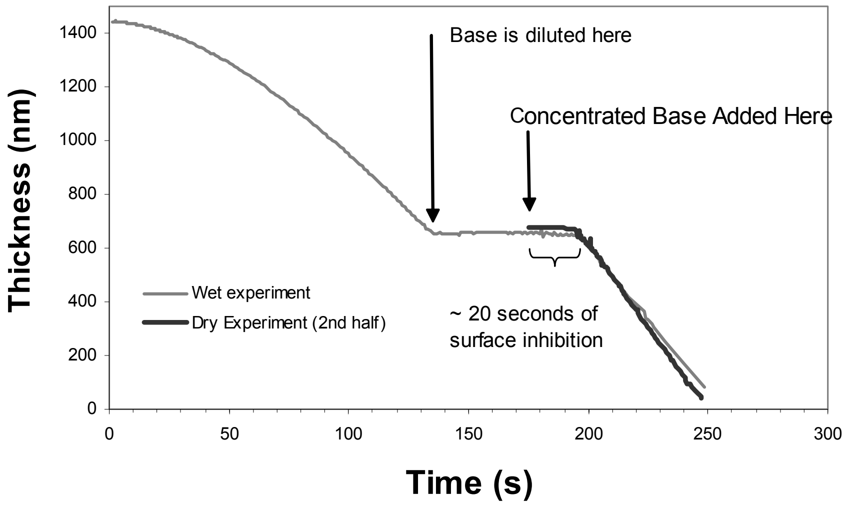

Figure C.6 Dissolution profiles of novolac films that have been dissolved, quenched with water, and redissolved. In one case, the film was kept wet (never exposed to air) and in the other case the film was blown dry with nitrogen. The dissolution behavior was identical in each case.

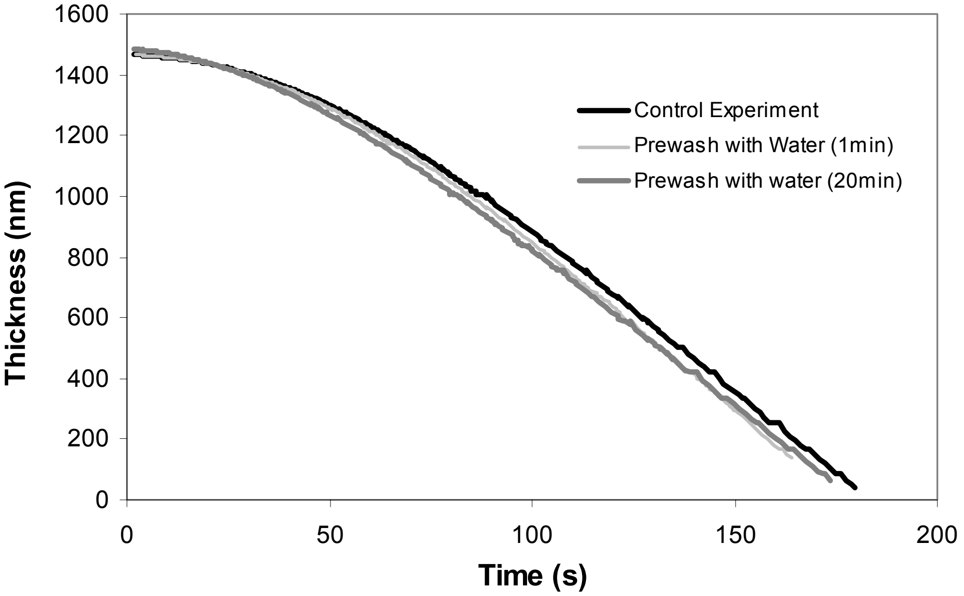

Figure C.7 Dissolution profile of a novolac film that was prewashed with water for 0,1 and 20 minutes. A prewash has no effect on the dissolution profile.

C.4 REFERENCES

1) Garza, C. M.; Szmanda, C. R.; Fisher, R. L. *Proc. SPIE* **1988**, *920*, 321-338.

2) Honda, K.; Beauchemin, B. T., Jr.; Hurditch, R. J.; Blakeney, A. J.; Kawabe, Y.; Kokubo, T. *Proc. SPIE* **1990**, *1262*, 493-500.

3) Honda, K.; Beauchemin, B. T., Jr.; Fitzgerald, E. A.; Jeffries, A. T. I.; Tadros, S. P.; Blakeney, A. J. *Proc. SPIE* **1991**, *1466*, 141-148.

4) Honda, K.; Beauchemin, B. T., Jr.; Hurditch, R. J.; Blakeney, A. J.; Kokubo, T. *Proc. SPIE* **1992**, *1672*, 297-304.

5) Dammel, R. *Diazonapthoquinone-based Resists*; SPIE Optical Engineering Press: Bellingham, Washington, 1993.

6) Hunek, B.; Cussler, E. L. *AIChE Journal: Fluid Mechanics and Transport Phenomena* **2002**, *48*, 661.

7) Hatzakis, M.; Canavello, B. J.; Shaw, J. M. *Ibm Journal of Research and Development* **1980**, *24*, 452.

BIBLIOGRAPHY

Abeles, F. *Ann. Phys.* **1950**, *5*, 596.

Allen, R. D.; Wallraff, G. M.; Hinsberg, W. D.; Conley, W. E.; Kunz, R. R. *J. Photopolymer Sci. Tech.* **1993**, *6*, 575.

Allen, R. D.; Wallraff, G. M.; Hofer, D. C.; Kunz, R. R. *Ibm Journal of Research and Development* **1997**, *41*, 95.

Allen, R. D. *et al*. *Proc. SPIE* **1995**, *2438*, 250.

Amblard, G.; Byers, J.; Domke, W.-D.; Rich, G.; Graffenburg, V.; Patel, S.; Miller, D.; Perez, G. *Proc. SPIE* **2000**, *3999*, 32.

Arcus, R. A. *Proc. SPIE* **1986**, *631*, 124-131.

Arcus, R. A. *Proc. SPIE-Int. Soc. Opt. Eng.* **1986**, *631*, 124-134.

Azzam, R. M. A.; Bashara, N. M. *Ellipsometry and Polarized Light* North-Holland, Amsterdam, 1988.

Bahe, L. W. *J. Am. Chem. Soc.* **1975**, *97*, 5664-5670.

Bahe, L. W. *J. Phys. Chem.* **1972**, *76*, 1062-1071.

Bailey, T. C.; Johnson, S. J.; Sreenivasan, S. V.; Ekerdt, J. G.; Willson, C. G. *J. Photopolymer Sci. Tech.* **2002**, *15*, 481.

Barclay, G. G.; Hawker, C. J.; Ito, H.; Orellana, A.; Malefant, P. R. L.; Sinta, R. F. *Proc. SPIE* **1996**, *2724*, 249-260.

Beauchemin, B. T.; Ebersole, C. E.; Daraktchiev, I. *Proc. SPIE* **1994**, *2195*, 610.

Bloomstein, T. M.; Horn, M. W.; Rothschild, M.; Kunz, R. R.; Palmacci, S. T.; Goodman, R. B. *J. Vac. Sci. & Tech. B* **1997**, *13*, 2112.

Bowden, M.; Thompson, L.; Farenholtz, S.; Doerries, E. *J. Electrochem. Soc.* **1981**, *128*, 1304.

Brochard, F.; Degennes, P. G. *Physicochemical Hydrodynamics* **1983**, *4*, 313-322.

Brodsky, C.; Byers, J.; Conley, W.; Hung, R.; Yamada, S.; Patterson, K.; Somervell, M.; Trinque, B.; Tran, H. V.; Cho, S.; Chiba, T.; Lin, S. H.; Jamieson, A.; Johnson, H.; Vander Heyden, T.; Willson, C. G. *Journal of Vacuum Science & Technology B* **2000**, *18*, 3396-3401.

Brodsky, C.; Trinque, B.; Johnson, H.; Willson, C. G. *Proc. SPIE* **2001**, *4343*, 415-420.

Burns, R. L.; Punsalan, D.; Towidjaja, M. C.; Koros, W. J. *J. Vac. Sci. & Tech. B* **2001**, *20*, 1954.

Burns, S. D.; Gardiner, A.; Krukonis, V.; Wetmore, P.; Schmid, G. M.; Lutkenhaus, J.; Flanagin, L. W.; Willson, C. G. *Proc. SPIE* **2001**, *4345*, 37-49.

Burns, S. D.; Gardiner, A.; Krukonis, V. J.; Wetmore, P. M.; Qin, A.; Willson, C. G. *Proc. Amer. Chem. Soc., PMSE* **1999**, *81*, 81-84.

Burns, S. D.; Gardiner, A. B.; Krukonis, V. J.; Wetmore, P. M.; Lutkenhaus, J.; Schmid, G. M.; Flanagin, L. W.; Willson, C. G. *Proceedings of SPIE-The International Society for Optical Engineering* **2001**, *4345*, 37-49.

Burns, S. D.; Gardiner, A. B.; Lutkenhaus, J.; Krukonis, V. J.; Wetmore, P. M.; Schmid, G. M.; Willson, C. G. *Proc SPIE* **2001**, *4345*, 37.

Burns, S. D.; Schmid, G. M.; Flanagin, L. W.; Tsiartas, P. C.; Willson, C. G. *J. Vac. Sci. & Tech. B* **2002**, *20*, 527.

Burns, S. D.; Schmid, G. M.; Trinque, B. C.; Willson, J.; Taylor, J. C.; Tsiartas, P. C.; Burns, R. L.; Willson, C. G. *Proc SPIE* **2003**.

Burns, S. D.; Schmid, G. M.; Tsiartas, P. C.; Flanagin, L. W.; Willson, C. G. *J. Vac. Sci. & Tech. B* **2002**, *20*, 537.

Burns, S. D.; Schmid, G. M.; Tsiartas, P. C.; Willson, C. G.; Flanagin, L. *Journal of Vacuum Science & Technology B* **2002**, *20*, 537-543.

Burns, S. D.; Stewart, M. D.; Hilfiker, J. N.; Synowicki, R. A.; Schmid, G. M.; Brodsky, C.; Willson, C. G. *Forefront of Lithographic Materials Research, Proc. of the 12th International Conference on Photopolymers* **2000**, 232-334.

Byers, J.; Patterson, K.; Cho, S.; McMallum, M.; Willson, C. G. *J. Photopolymer Sci. Tech.* **1998**, *11*, 465.

Campbell, S. A. *The Science and Engineering of Microelectronic Fabrication*; Oxford University Press: New York, 2001.

Cao, H.; Roberts, J. M.; Meagley, R. P.; Panning, E. M.; Dalin, J.; Chandok, M.; Holl, S. M.; Shell, M. K. *Proc SPIE* **2003**.

Chambers, C. R.; Kusumoto, S.; Lee, G. S.; Vasudev, A.; Walthal, L.; Osborn, B.; Zimmerman, P.; Conley, W. *Proc SPIE* **2003**.

Champman, H. N. e. a. *J. Vac. Sci. & Tech. B* **2001**, *19*, 2389.

Chen, K. R.; Jordhamo, G.; Moreau, W. M. *Proc SPIE* **1996**, *2724*, 553-562.

Cho, J. Y., Choi, S. *Proc. SPIE* **2002**, *4690*, 912-910.

Choi, S.; Cho, J. Y. *Proc. SPIE* **2001**, *4345*, 952-962.

Colburn, M.; Grot, A.; Amistoso, M.; Choi, B.; Bailey, T. C.; Ekerdt, J. G.; Sreenivasan, S. V.; Hollenhorst, J.; Willson, C. G. *Proc. SPIE* **2000**, *3999*, 453-457.

Conley, W.; Miller, D. A.; Chambers, C. R.; Osborn, B. P.; Hung, R. J.; Tran, H. V.; Trinque, B. C.; Pinnow, M. J.; Chiba, T.; MacDonald, S.; Zimmerman, P.; Dammel, R.; Romano, A. R.; Willson, C. G. *Proc SPIE* **2002**, *4690*, 69-75.

Dammel, R. *Diazonapthoquinone-based Resists*; SPIE Optical Engineering Press: Bellingham, Washington, 1993.

de Gennes, P. G. *Scaling Concepts in Polymer Physics*; Cornell University Press: Ithaca, NY, 1979.

Dill, F. H.; Shaw, J. *IBM J. Res. Dev.* **1977**, *21*, 210.

Ficner, S.; Dammel, R.; Perez, Y.; Gardiner, A. B.; Willson, C. G. *Proc. SPIE* **1997**, *3049*, 838.

Flanagin, L. W. *Ph.D. Dissertation, University of Texas at Austin*, 1999.

Flanagin, L. W.; McAdams, C. L.; Hinsberg, W. D.; Sanchez, I. C.; Willson, C. G. *Proc. SPIE* **1999**, *3049*, 838.

Flanagin, L. W.; McAdams, C. L.; Hinsberg, W. D.; Sanchez, I. C.; Willson, C. G. *Abstracts of Papers of the American Chemical Society* **1999**, *218*, 112-PMSE.

Flanagin, L. W.; Singh, V. K.; Willson, C. G. *Journal of Polymer Science Part B-Polymer Physics* **1999**, *37*, 2103-2113.

Flanagin, L. W.; Singh, V. K.; Willson, C. G. *Journal of Vacuum Science & Technology B* **1999**, *17*, 1371-1379.

Frechet, J. M. J.; Eichler, E.; Ito, H.; Willson, C. G. *Polymer* **1983**, *24*, 995-1000.

Furata, A.; Hanabata, M.; Uemura, Y. *Journal of Vacuum Science & Technology B* **1986**, *4*, 430-436.

Gardiner, A. *PhD Dissertation*; The University of Texas at Austin: Austin TX, 1999.

Gardiner, A.; Burns, S. D.; Qin, A.; Willson, C. G. *J. Vac. Sci. Technol. B* **2001**, *19*, 136.

Gardiner, A. B. *PhD Dissertation*; The University of Texas at Austin: Austin TX, 1999.

Garza, C. M.; Szmanda, C. R.; Fisher, R. L. *Proc. SPIE* **1988**, *920*, 321-338.

Gibson, J. A. B. *Liquid Scintillation Counting Recent Applications and Developments*; Academic Press: New York, 1980.

Goken, H.; Esho, S.; Ohnishi, Y. *J. Electrochem. Soc.* **1983**, *130*, 143.

Gwyn, C. W.; Stulen, R.; Sweeney, D.; Attwood, D. *J. Vac. Sci. & Tech. B* **1998**, *16*, 3142.

Hall, D.; Osborne, B.; Patterson, K.; Burns, S. D. *Proc. SPIE* **2001**, *4345*.

Hanabata, M.; Furata, A. *Proc. SPIE* **1990**, *1262*, 476-482.

Hanabata, M.; Furata, A.; Uemura, Y. *Proc. SPIE* **1986**, *631*, 76-82.

Hanabata, M.; Furata, A.; Uemura, Y. *Proc. SPIE* **1987**, *771*, 85-92.

Hanabata, M.; Uetani, Y.; Furata, A. *Proc. SPIE* **1988**, *920*, 349-354.

Harihan, A. e. a. *J. Chem. Phys.* **1993**, *99*, 656-663.

He, D.; Cerrina, F. *J. Vac. Sci. & Tech. B* **1998**, *16*, 3748.

Heavens, O. S. *Optical Properties of Thin Solid Films*; Dover Publications: New York, 1965.

Henderson, C. L. *PhD Dissertation, The University of Texas at Austin* **1998**.

Henderson, C. L. *Ph.D Dissertation*; The University of Texas at Austin: Austin, TX, 1998.

Henderson, C. L., et al. *Proc. SPIE* **1996**, *2724*, 481.

Herman, M. F.; Edwards, S. F. *Macromolecules* **1990**, *23*, 3662-3671.

Hines, A. L.; Maddox, R. N. *Mass Transfer: Fundamentals and Applications*; Prentice Hall: Englewood Cliffs, New Jersey, 1985.

Hinsberg, W. D., et. al. *Presented at EIPBN, 2002; private communications with Dr. W.D. Hinsberg* **August, 2002**.

Hinsberg, W. D.; Houle, F. A.; Poliskie, G. M.; Pearson, D.; Sanchez, M. I.; Ito, H. *Journal of Physical Chemistry A* **2002**, *106*, 9776-9787.

Hinsberg, W. D.; Houle, F. A.; Sanchez, M. I.; Hoffnagle, J. A.; Wallraff, G. M.; Medeiros, D. M. *Proc SPIE* **2003**.

Hinsberg, W. D.; Houle, F. A.; Sanchez, M. I.; Wallraff, G. M. *Ibm Journal of Research and Development* **2001**, *45*, 667-682.

Hinsberg, W. D.; Lee, S.-W.; Ito, H.; Horne, D. E.; Kanazawa, K. K. *Proceedings of SPIE-The International Society for Optical Engineering* **2001**, *4345*, 1-9.

Hinsberg, W. D.; MacDonald, S. A.; Snyder, C. D.; Ito, H.; Allen, R. D. *Polym. Mater. Sci. Eng.* **1992**, *66*, 52-53.

Hinsberg, W. D. e. a. *Chem. Mater.* **1994**, *6*, 481-488.

Hoffnagle, J.; Hinsberg, W. D.; Sanchez, M. I.; Houle, F. A. *J. Vac. Sci. & Tech. B* **1999**, *17*, 3306.

Honda, K.; Beauchemin, B. T., Jr.; Fitzgerald, E. A.; Jeffries, A. T. I.; Tadros, S. P.; Blakeney, A. J. *Proc. SPIE* **1991**, *1466*, 141-148.

Honda, K.; Beauchemin, B. T., Jr.; Hurditch, R. J.; Blakeney, A. J.; Kawabe, Y.; Kokubo, T. *Proc. SPIE* **1990**, *1262*, 493-500.

Honda, K.; Beauchemin, B. T., Jr.; Hurditch, R. J.; Blakeney, A. J.; Kokubo, T. *Proc. SPIE* **1992**, *1672*, 297-304.

Hong, P. P.; Boerio, F. J. *Macromolecules* **1994**, *27*, 596-605.

Horrocks, D. L. *Applications of Liquid Scintillation Counting*; Academic Press: New York, 1974.

Horrocks, D. L. *Liquid Scintillation Science and Technology*; Academic Press: New York, 1976.

Houle, F. A.; Hinsberg, W. D.; Morrison, M.; Sanchez, M. I.; Wallraff, G. M.; Larson, C. E.; Hoffnagle, J. *J. Vac. Sci. & Tech. B* **2000**, *18*, 1874.

Houle, F. A.; Hinsberg, W. D.; Sanchez, I. C. *Macromolecules* **2002**, *35*, 8591-8600.

Houle, F. A.; Hinsberg, W. D.; Sanchez, M. I. *Macromolecules* **2002**, *35*, 8591-8600.

Houlihan, F. M. J.; TI, W.; Nalamasu, O.; Reichmanis, E. *Macromolecules* **1997**, *30*, 6517.

Howard, P. L. *Basic Liquid Scintillation Counting*; American Society of Clinical Pathologists: Chicago, 1976.

Huggins, M. L. *J. Am. Chem. Soc.* **1931**, *53*, 3190-3191.

Hunek, B.; Cussler, E. L. *AIChE Journal: Fluid Mechanics and Transport Phenomena* **2002**, *48*, 661.

Israelachvili, J. *Intermolecular and Surface Forces, 2nd Ed*; Harcourt Brace & Company: London, 1992.

Ito, H. *IBM Journal of Research and Development* **2001**, *45*, 683.

Ito, H.; Allen, R. D.; Opitz, J.; Wallow, T. I.; Truong, H. D.; Hofer, D. C.; Varanasi, P. R.; Jordhamo, G. M.; Jayaraman, S.; Vicari, R. *Proc. SPIE* **2000**, *3999*, 2-12.

Ito, H.; Sherwood, M. *Proc. SPIE* **1999**, *3678*, 104.

Ito, H.; Wallraff, G. M.; Fender, N.; Brock, P. J.; Hinsberg, W. D.; Mahorwala, A.; Larson, C. E.; Truong, H. D.; Breyta, G.; Allen, R. D. *J. Vac. Sci. & Tech. B* **2001**, *19*, 2678.

Ito, H.; Willson, C. G. *Polymer Engineering and Science* **1983**, *23*, 1012-1018.

Kaimoto, Y.; Nozaki, K.; Takechi, S.; Abe, N. *Proc. SPIE* **1992**, *1672*.

Kim, M. S.; Reiser, A. *Macromolecules* **1997**, *30*, 3860-3866.

Kim, M. S.; Reiser, A. *Macromolecules* **1997**, *30*, 4652-4655.

Kong, B. S.; Kim, D. *Polymer-Korea* **1997**, *21*, 270-281.

Koros, W. J.; Paul, D. R. *J. Polymer Sci. B - Polymer Physics* **1976**, *14*, 1903-1907.

Krasicky, P. D.; Groele, R. J.; Jubinsky, J. A.; Rodriguez, F.; Namaste, Y. M. N.; Obendorf, S. K. *Polymer Engineering and Science* **1987**, *27*, 282-285.

Krasicky, P. D.; Groele, R. J.; Rodriguez, F. *Chemical Engineering Communications* **1987**, *54*, 279-299.

Krasicky, P. D.; Groele, R. J.; Rodriguez, F. *Journal of Applied Polymer Science* **1988**, *35*, 641-651.

Kunz, R. R.; Allen, R. D.; Hinsberg, W. D.; Wallraff, G. M. *Proc. SPIE* **1993**, *1672*, 66.

Kunz, R. R.; Bloomstein, T. M.; Hardy, D. E.; Goodman, R. B.; Downs, D. K.; Curtin, J. E. *Proc. SPIE* **1009**, *3768*, 13.

Lee, S.; Hinsberg, W. *Anal. Chem.* **2002**, *74*, 125-131.

Lin, E. K.; Soles, C. L.; Goldfarb, D. L.; Trinque, B.; Burns, S. D.; Jones, R. L.; Lenhart, J. L.; Angelopoulos, M.; Willson, C. G.; Satija, S. K.; Wu, W.-l. *Science* **2002**, *297*, 372.

Lin, Q.; Goldfarb, D. L.; Angelopoulos, M.; Sriram, S. R.; Moore, J. S. *Proc SPIE* **2001**, *4345*, 78.

Lin, Q.; Sooriyakumaran, R.; Huang, W.-S. *Proc SPIE* **2000**, *3999*, 230.

Long, T.; Rodriguez, F. *Proc. SPIE* **1991**, *1466*, 188-198.

Mack, C.; Mueller, K. E.; Gardiner, A. B.; Sagan, J. P.; Dammel, R.; Willson, C. G. *J. Vac. Sci. Technol.* **1998**, *16*, 3779.

Mack, C. A. *Inside Prolith: A Comprehensive Guide to Optical Lithography Simulation*; FINLE Technologies: Austin, TX, 1997.

Mack, C. A. *Ph.D. Dissertation*; University of Texas at Austin: Austin, TX, 1998.

Mahorwala, A. P.; Goldfarb, D. L.; Petrillo, K. E.; Pfeiffer, D.; Babich, K.; Angelopoulos, M.; Gallatin, G.; Lawson, M. C.; Kwong, R. W.; Chen, K.; Li, W.; Varanasi, P. R. *Proc SPIE* **2003**.

Metropolis, N.; Rosenbluth, A. W.; Rosenbluth, M. N.; Teller, A. H.; Teller, E. *J. Chem. Phys.* **1953**, *21*, 1087.

Moreau, W. M. *Semiconductor Lithography: Principles, Practices, and Materials*; Plenum Publishing: New York, 1988.

Mueller, K. *Ph.D. Disseration*; The University of Texas at Austin: Austin, TX, 1998.

Narasimhan, B. *Advanced Drug Delivery Reviews* **2001**, *48*, 195-210.

Narasimhan, B.; Peppas, N. A. *Macromolecules* **1996**, *29*, 3283-3291.

Narasimhan, B.; Peppas, N. A. In *Polymer Analysis - Polymer Physics*, 1997; Vol. 128, pp 157-207.

Narasimhan, B.; Peppas, N. A. *Advances in Polymer Science* **1997**, *128*, 157-207.

Nivaggioli, T.; Winnik, M. A. *Chemistry of Materials* **1993**, *5*, 658-660.

Obrien, K. C.; Koros, W. J.; Barbari, T. A.; Sanders, E. S. *J. Membrane Science* **1986**, *29*, 229-238.

Okoroanyanwu, U.; Byers, J.; Shimokawa, T.; Willson, C. G. *Chemistry of Materials* **1998**, *10*, 3328-3333.

Okoroanyanwu, U.; Shimokawa, T.; Byers, J.; Willson, C. G. *Chemistry of Materials* **1998**, *10*, 3319-3327.

Okoroanyanwu, U.; Shimokawa, T.; Medeiros, D.; Willson, C. G.; Frechet, J. M. J.; J.Q., N.; Byers, J.; Allen, R. D. *Proc. SPIE* **1997**, *3049*, 92.

Ouana, A. C.; Carothers, J. A. *Polym. Eng. Sci.* **1980**, *20*, 160-166.

Papanu, J. S.; Hess, D. W.; Bell, A. T.; Soane, D. S. *Journal of the Electrochemical Society* **1989**, *136*, 1195-1200.

Papanu, J. S.; Hess, D. W.; Soane, D. S.; Bell, A. T. *Journal of the Electrochemical Society* **1989**, *136*, 3077-3083.

Papanu, J. S.; Hess, D. W.; Soane, D. S.; Bell, A. T. *Journal of Applied Polymer Science* **1990**, *39*, 803-823.

Papanu, J. S.; Soane, D. S.; Bell, A. T.; Hess, D. W. *J. Applied Polymer Science* **1989**, *38*, 859-885.

Patterson, K.; Okoroanyanwu, U.; Shimokawa, T.; Cho, S.; Byers, J.; Willson, C. G. *Proc. SPIE* **1998**, *3333*, 425-437.

Patterson, K.; Somervell, M.; Willson, C. G. *Solid State Technology* **2000**, *43*, 41-+.

Patterson, K.; Yamachika, M.; Hung, R.; Brodsky, C.; Yamada, S.; Somervell, M.; Osborn, B.; Hall, D.; Dukovic, G.; Byers, J.; Conley, W.; Willson, C. G. *Proc. SPIE* **2000**, *3999*.

Peppas, N. A.; Wu, J. C.; Vonmeerwall, E. D. *Macromolecules* **1994**, *27*, 5626-5638.

Perrin, D. D.; Dempsey, B.; Serjeant, E. P.; Chapman and Hall: London, 1981.

Pol, V.; Bennewitz, J. H.; Escher, G. C.; Feldman, M.; Firtion, V.; Jewell, T. E.; Wilcomb, B. E.; Clemens, J. T. *Proc. SPIE* **1986**, *633*, 6.

Postnikov, S.; Stewart, M. D.; Tran, H. V.; Nierode, M.; Medeiros, D.; Cao, T.; Byers, J.; Webber, S.; Willson, C. G. *J. Vac. Sci. & Tech. B* **1999**, *17*, 2965-2969.

Rancourt, J. D. *Optical Thin Films: User Handbood*; SPIE Optical Engineering Press: Bellingham, WA, 1996.

Rao, V.; Hinsberg, W. D.; Frank, C. W.; Pease, R. F. W. *Proc. SPIE* **1993**, *1925*, 538.

Reinhardt, M.; Pfeiffer, K.; Lorkowski, H. J. *Journal of Applied Polymer Science* **1994**, *51*, 297-301.

Reiser, A. *Photoreactive Polymers*; John Wiley & Sons: New York, 1989.

Reiser, A.; Huang, J. P.; He, X.; Yeh, T. F.; Jha, S.; Shih, H. Y.; Kim, M. S.; Han, Y. K.; Yan, K. *European Polymer Journal* **2002**, *38*, 619-629.

Reiser, A.; Yan, Z. L.; Han, Y. K.; Kim, M. S. *Journal of Vacuum Science & Technology B* **2000**, *18*, 1288-1293.

Reynolds, G.; Taylor, J. *J. Vac. Sci. & Tech. B* **1999**, *17*.

Reynolds, G. W.; Taylor, J. W. *J. Vac. Sci. Technol. B* **1999**, *17*, 334-344.

Rice, B. J.; Cao, H.; Chandok, M.; Meagley, R. P. *Proc SPIE* **2003**.

Robertson, S. A.; Kang, D.; Scheer, S. A.; Brodsky, C. In *Proc. SPIE*, 2002.

Robertson, S. A.; Kang, D.; Scheer, S. A.; Brodsky, C. J. *Proc. SPIE* **2002**, *4689*, 213-222.

Sanchez, M. I.; Hinsberg, W. D.; Houle, F. A.; Hoffnagle, J. A.; Ito, H.; Nguyen, C. *Proc SPIE* **1999**, *3678*, 160.

Scheer, S. A. *MS Thesis: Design of Development Rate Monitoring Software and Measurement of Photoacid Concentration in Chemically Amplified Resists*; The University of Texas at Austin, 2001.

Scheer, S. A.; Brodsky, C. J.; Robertson, S. A.; Kang, D. *Proc SPIE* **2002**, *4689*, 937-948.

Schmid, G. M.; Burns, S. D.; Tsiartas, P. C.; Willson, C. G. *J. Vac. Sci. & Tech. B* **2002**, *20*, 2193-2199.

Schmid, G. M.; Burns, S. D.; Tsiartas, P. C.; Willson, C. G. *J. Vac. Sci. & Tech. B* **2002**, *20*, 2913.

Schmid, G. M.; M.S., S.; Singh, V. K.; Willson, C. G. *J. Vac. Sci. & Tech. B* **2002**, *20*, 185-190.

Serjeant, E. P.; Dempsey, B. *Ionisation Constants of Organic Acids in Aqueous Solution* Pergamon: Oxford, 1979.

Shih, H. Y.; Reiser, A. *Macromolecules* **1997**, *30*, 4353-4356.

Shih, H. Y.; Reiser, A. *Macromolecules* **1997**, *30*, 4353-4356.

Shih, H. Y.; Reiser, A. *Macromolecules* **1994**, *27*, 3330-3336.

Shih, H. Y.; Reiser, A. *Macromolecules* **1995**, *28*, 5595-5600.

Shih, H. Y.; Reiser, A. *Macromolecules* **1997**, *30*, 3855-3859.

Shih, H.-Y.; Reiser, A. *Macromolecules* **1996**, *29*, 2082-2087.

Shih, H. Y.; Zhuang, H.; Reiser, A.; Teraoka, I.; Goodman, J.; Gallagher-Wetmore, P. M. *Macromolecules* **1998**, *31*, 1208-1213.

Shih, H. Y.; Zhuang, H. F.; Reiser, A.; Teraoka, I.; Goodman, J.; Gallagher-Wetmore, P. M. *Macromolecules* **1998**, *31*, 1208-1213.

Sirard, S. M.; Green, P. F.; Johnston, K. P. *J. Physical Chemistry B* **2001**, *105*, 766-772.

Somervell, M.; Fryer, D.; Osborn, B.; Patterson, K.; Byers, J.; Willson, C. G. *J. Vac. Sci. & Tech. B* **2000**, *18*, 2251-2559.

Stewart, M.; Goldfarb, D. L.; Schmid, G. M.; Angelopoulos, M.; Willson, C. G. *Proc SPIE* **2003**.

Stewart, M. D.; Patterson, K.; Somervell, M.; Willson, C. G. *J. Physical Organic Chemistry* **2000**, *13*, 767-764.

Stewart, M. D.; Schmid, G. M.; Postnikov, S.; Willson, C. G. *Proc. SPIE* **2001**, *4345*, 10-18.

Stewart, M. D.; Tran, H. V.; Schmid, G. M.; Stachowiak, T.; Becker, D. J.; Willson, C. G. *J. Vac. Sci. & Tech. B* **2002**, *20*, 2946.

Styrkas, D.; Doran, S. J.; Gilchrist, V.; Keddie, J. L.; Lu, J. R.; Murphy, E.; Sackin, R.; Su, T.-J.; Tzitzinou, A. *Application of Ellipsometry to Polymers at Interfaces and Thin Films*; John Wiley & Sons: New York, 1999; Vol. III.

Switkes, M.; Rothschild, M. *J. Vac. Sci. & Tech. B* **2001**, *19*, 2353.

Szmanda, C. R.; Yu, J.; Barclay, G.; Cameron, J.; Kavanagh, R. J.; Blacksmith, R.; Trefonas, P.; Taylor, G. N. *Proc SPIE* **1997**, *3049*, 65.

Thompson, L. F.; Willson, C. G.; Bowden, M. J. *Introduction to Microlithography*; 2nd ed.; American Chemical Society: Washington D.C., 1994.

Tompkins, H. G.; McGahan, W. A. *Spectroscopic Ellipsometry and Reflectometry: A User's Guide*; Wiley: New York, 1999.

Toriumi, M.; Itani, T. *Proc. SPIE-Int. Soc. Opt. Eng.* **2002**, *4690*, 904-911.

Toriumi, M.; Yamazaki, T.; Furukawa, S.; Irie, S.; Ishikawa, S.; Itani, T. *J. Vac. Sci. & Tech. B* **2002**, *20*, 2909.

Toukhy, M. A. *Proc. SPIE* **1987**, *771*, 263.

Tran, H. V.; Hung, R.; Loy, D. A.; Wheeler, D. R.; Byers, J.; Conley, W.; Willson, C. G. *Polymeric Materials: Science and Engineering* **2001**, *84*.

Trefonas, P. *Proc. SPIE* **1989**, *1086*, 484.

Trinque, B.; Chiba, T.; Hung, R.; Chambers, C.; Pinnow, M.; Tran, H. V.; Wunderlich, J.; Hsieh, Y.; Thomas, B.; Shafer, G.; Shafer, D.; DesMartequ, D.; Conley, W.; Willson, C. G. *J. Vac. Sci. & Tech. B* **2002**, *20*, 531-536.

Tsiartas, P. C. *Ph. D. Thesis, The University of Texas at Austin* **1998**.

Tsiartas, P. C.; Flanagin, L. W.; Henderson, C. L.; Hinsberg, W. D.; Sanchez, I. C.; Bonnecaze, R. T.; Willson, C. G. *Macromolecules* **1997**, *30*, 4656-4664.

Tsiartas, P. C.; Simpson, L. L.; Qin, A.; Allen, R. D.; Krukonis, V. J.; Wetmore, P. M.; Willson, C. G. *Proc. SPIE* **1995**, *2438*, 261.

Ueberreiter, K.; Asmussen, F. *Journal of Polymer Science* **1957**, *23*, 75-81.

Umbach, C. P.; Broers, A. N.; Willson, C. G.; Koch, R.; Laibowitz, R. B. *Journal of Vacuum Science & Technology B* **1988**, *6*, 319-322.

Vrentas, J. S.; Vrentas, C. M. *Journal of Polymer Science Part B-Polymer Physics* **1998**, *36*, 2607-2614.

Wallow, T.; Chan, W.; Hinsberg, W.; Lee, S. *Proc. SPIE* **2002**, *4690*, 299.

Willson, C. G. *Acs Symposium Series* **1983**, *219*, 87-159.

Wunderlich, J.; Schmid, G. M. *Unpublished data - available on request from C. Grant Willson, willson@che.utexas.edu* **2002**.

Yamachika, M.; Patterson, K.; Cho, S.; Rager, T.; Yamada, S.; Byers, J.; Paniez, P. J.; Mortini, B.; Gally, S.; Sassoulas, P.; Willson, C. G. *J. Photopolymer Sci. Tech.* **1999**, *12*, 553.

Yeh, T. F.; Shih, H. Y.; Reiser, A. *Macromolecules* **1992**, *25*, 5345-5352.

Yoshimura, T.; Shiraishi, H.; Yamamoto, J.; Okazaki, S. *Appl. Phys. Lett.* **1993**, *63*, 764-766.

Vita

Sean David Burns was born in New Port Richey, Florida on June 21st, 1976 as the son of Philip Lance Burns and Marguerite Linda Burns. After graduating from Gulf High School in New Port Richey, Florida in June of 1994 he entered the Georgia Institute of Technology and graduated with a Bachelor of Science degree in Chemical Engineering in June of 1998. In August of 1998 he entered graduate school at the University of Texas at Austin as a Ph.D. student working under the supervision of Dr. C. Grant Willson. After completion of his degree, he has accepted a position as a Research Staff Member at IBM T.J. Watson Research Center in Yorktown Heights, New York.

Permanent address: 4015 Speedway #2
Austin TX 78751

This dissertation was typed by the author